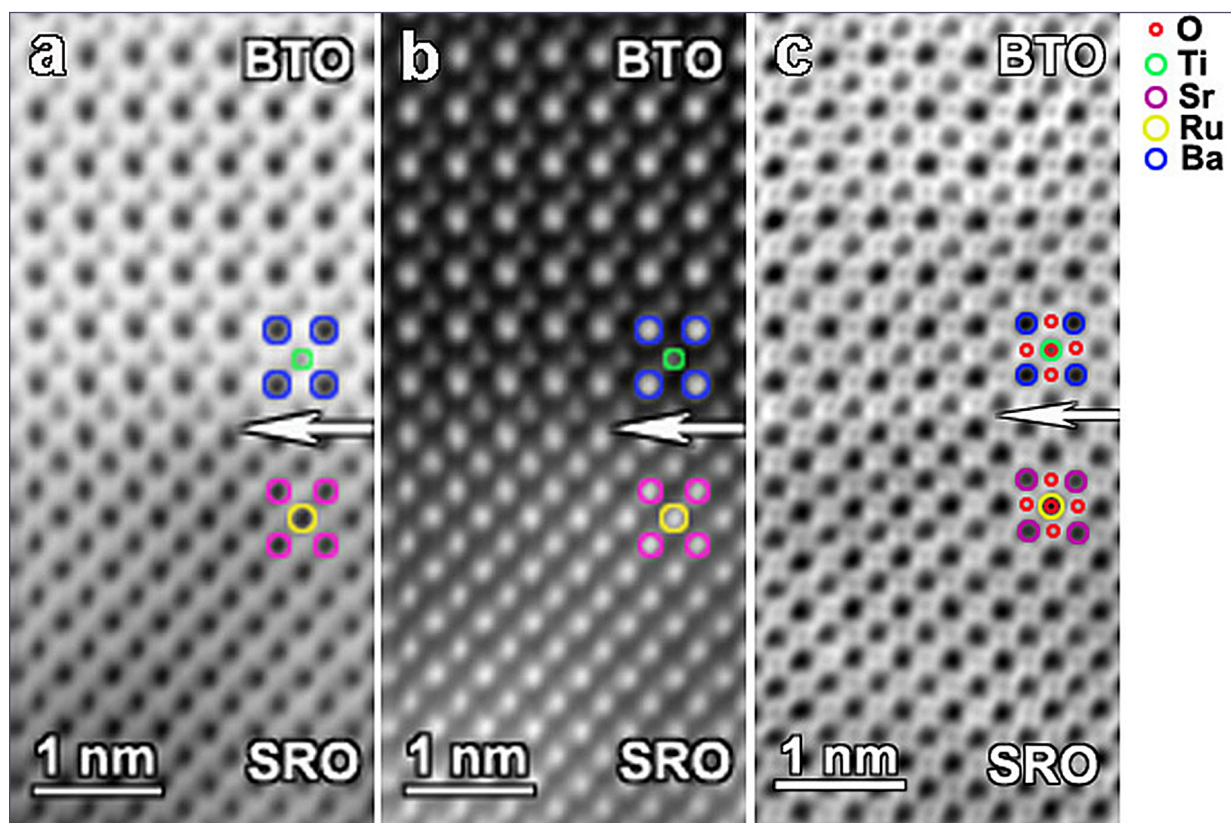


NATIONAL INSTITUTE OF MATERIALS PHYSICS



ANNUAL REPORT 2015

20th Edition (1996-2015)

National Institute of Materials Physics

(Institutul Național de Cercetare-Dezvoltare pentru Fizica Materialelor)

National Institute of Materials Physics

(Institutul Național de Cercetare-Dezvoltare pentru Fizica Materialelor)

DIRECTORATE

Director: Dr. Ionut Enculescu

Scientific Director: Dr. Florin Vasiliu

ADDRESS

P.O. BOX MG – 7

Bucharest – Magurele / ROMANIA

Tel. (+4) 021 369 01 85

Fax (+4) 021 369 01 77

E-Mail

I. Enculescu: encu@infim.ro

F. Vasiliu: fvasiliu@infim.ro

WWW

[http: // www.infim.ro](http://www.infim.ro)

Contents

Preface	5
Laboratories	9
Personnel	15
List of Personnel	16
Visiting Guests	23
Ph. D. Theses	25
Awards	26
Honorary Membership	28
Publications and Presentations	31
Book Chapters	32
Journals	33
Conference Proceedings	51
Contributed Presentations	53
Invited Lectures	73
Selected Results	75
Condensed Matter Physics at Mesoscale	75
Nanoscale Physics	111
Potential Applications	127
Patents and Patent Requests	149
Events	153
International Cooperation	159
Funding	169

Cover image: *Atomic-resolution STEM images at the SRO - BTO interface: (a) BF image (b) HAADF image and (c) ABF image. The arrow marks the interface.*

R. F. Negrea, V. S. Teodorescu, C. Ghica, *Appl. Surf. Sci.* 315, 250-255 (2015).

Foreword

NIMP is a highly regarded research and development organization having a national and international reputation. This report contains examples of NIMP's applied expertise in the materials physics along with notable facts and figures from the past year.

In **2015**, NIMP published **174** papers in ISI journals which correspond to a cumulated impact factor of about 400 and a total AIS of about 100, values comparable to the ones in the previous year (Fig. 1). **The cumulative impact factors from the 2010-2015 period show a consolidation of the scientific performance, given that there was initially a continuous increase, the last two years showing a stabilization of this parameter.**

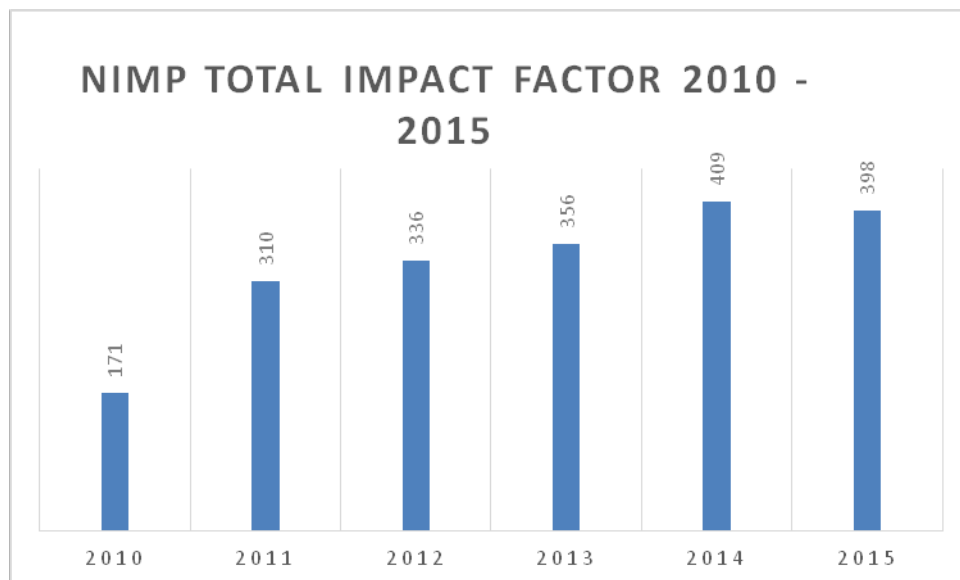


Fig.1- Cummulated impact factors of NIMP papers published in 2010-2015

In 2015 a downward trend of articles with impact factor between 1 and 2 was recorded, while the number of those with an impact factor between 3 and 4 remained the same. A previously observed increase of the works between 4 -5 is continuing, as well as those exceeding the value of 5. We can also observe an increase in the number of works belonging to the lower area of impact factor.

The number of citations in 2015 in ISI journals for articles published during 1990-2015 was about 2620 (according to Web of Science).

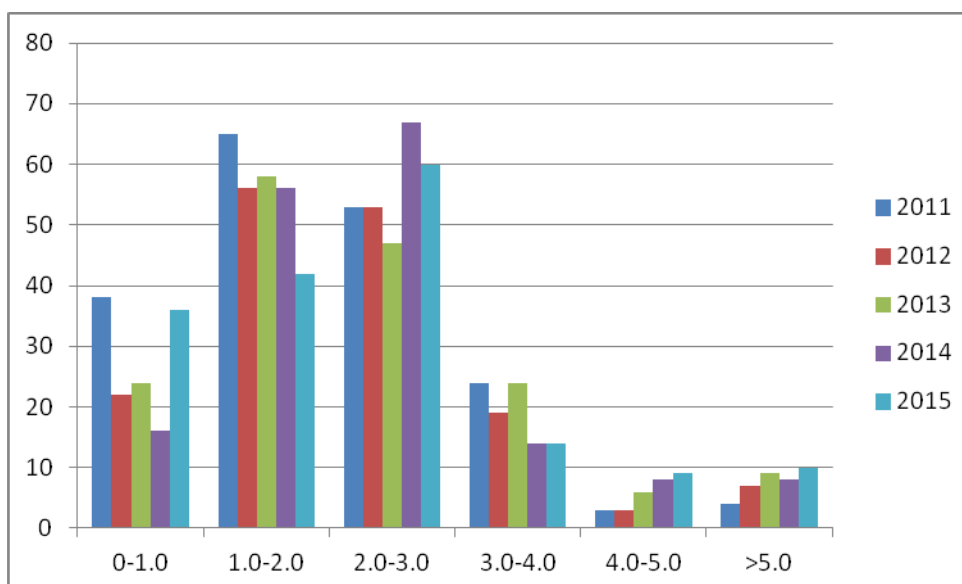


Fig. 2-NIMP distribution of published works based on impact factor in the period 2011-2015

183 scientific communications were presented in prestigious international conferences.

In 2015 the numbers of patents (4) and patent requests (12) have also increased. A total of 10 products and 15 technologies resulted from the conducted research, and 9 services were contracted to economical agents.

An important section of this annual report highlights the major selected results representing scientific accomplishments of the past year.

The most important event of the year was the **conclusion of the "Centre for Research, Innovation and Technologies for New Materials"**, SMIS-CSNR 49185 code, co-financed by the European Regional Development Fund, based on contract 654/07.08.2014, signed with the Ministry of National Education (MEN), in the framework of the Sectorial Operational Programme "Increase of Economic Competitiveness". Total value of the project was 43.248.955 lei from which 35.000.000 lei were nonrefundable financial assistance.

On December 4th, 2015, at 10:30, NIMP held at its headquarters the conference on the conclusion of the project. The event was inaugurated by the General Director Ionut Enculescu's speech, followed by the presentation of the three laboratories of the Center.

RITecC 01 Laboratory (Laboratory for production, processing and analyzing of functional materials for high-technology applications) and RITecC 02 Laboratory (Laboratory for production, processing and analyzing materials for increasing life quality) were presented by Dr. Lucian Pintilie, and RITecC Laboratory 03 (Laboratory for production, processing and analyzing materials for extreme conditions) was presented by Dr. Andrei Galatanu.

NIMP was co-organizer of the following conferences:

7th International Conference on Amorphous and Nanostructured Chalcogenides

<http://www.infim.ro/events/amorphous-and-nanostructured-chalcogenides-anc-7-conference>

8th International Conference on Advanced Materials (ROCAM), Bucharest, 7-10 July 2015

<http://rocam.unibuc.ro/rocam2015/>

Workshop “Advances in Nanophysics and Nanophotonics”, Bucharest, 31.08.-2.09.2015

<http://www.infim.ro/nanophysics-solar/>

Conference “Lights of the World”, Bucharest, House of Parliament, 30.10-1.11.2015

<http://iyl2015.infim.ro/>

Between 5th and 10th of July 2015, NIMP organized in Cluj-Napoca, the **7th Edition of the Amorphous and Nanostructured Chalcogenides Conference, ANC-7**. The aim of the conference was the presentation of the latest results in the field and to promote the exchange of ideas in associated topics, including applications of the chalcogenides materials.

The **8th edition of the International Conference on Advanced Materials** took place in Bucharest between 7th to 10th of July, 2015. The purpose of the conference was to present a synthesis of the latest developments in some areas of advanced materials theory, modeling, processing, characterization and applications. The scientific works were conducted in eight sections, as follows:

1. Advanced Materials for solar energy conversion
2. Carbon-based Nanomaterials and Applications
3. Thin films and nanostructures of functional materials
4. Advanced Biomaterials, Bio-devices and Biotechnology
5. Advances in surface science and engineering
6. Advanced ceramics: synthesis, properties, and applications
7. Ferroelectrics, Nonlinear Optical and Luminescent Materials, Properties and Application
8. Advanced Materials Characterization and Modeling

NIMP was co-organizer of this conference and one of the chairmen of the Organizing Committee was Dr. Lucian Pintilie. The Romanian Scientific Committee counted six researchers from NIMP. Dr. M. L. Ciurea and Dr. C. M. Teodorescu held presentations as Key Speakers.

A large number of highly prestigious professors and researchers from a large number of countries around the world (Germany, France, Italy, Sweden, Spain, Belgium, The Netherlands, Portugal, USA, Japan, South Africa, etc.) participated with invited lectures and oral presentations.

The management team believes that 2015 was an important year by erecting the RITecC center and strengthening and preserving of the academic level reached by researchers from NIMP.

Dr. Ionut Enculescu

General Director

Laboratories

10. Laboratory of Multifunctional Materials and Structures

The laboratory is divided into two research groups:

- **The group of functional nanostructures**, which includes teams with research interests in the field of preparation and characterization of different nano-objects (nanoparticles, nanotubes, nanowires or nano-strips) with potential applications in micro- and nano-optoelectronics (field effect transistors, hybrid LED or photodiodes), advanced sensors (with a focus on bio-sensors), renewable energy and medicine (biocompatible and / or biofunctional materials).
- **The group of complex heterostructures and perovskite oxides**, which includes teams working with research interests in the preparation and characterization of oxide materials with dielectric, ferroelectric, multiferroic properties or semiconductors for applications in micro- and nano-electronics (non-volatile memories, transparent electronics), telecommunications and security (devices for emitting-receiving of microwaves), advanced sensors (pyroelectric sensing and photoconductor), solar cells (based on the photovoltaic effect in ferroelectrics or other perovskites), medicine (2D and 3D coatings with biocompatible / biofunctional oxides).

Teams working in the laboratory carry out both fundamental research related to identifying and explaining the physical and chemical phenomena that occur in the obtained materials and structures (in particular size effect, interfaces, doping/stoichiometry) , as well as development activities of various applications such as sensors, field effect transistors, photovoltaic cells, apparatus for processing materials. Research topics are generally multidisciplinary, requiring collaboration between physicists, chemists and engineers.

The human resources of the laboratory consist of 8 CS1, 4 CS2, 8 CS3, 4 CS, 14 ACS, two sub-engineers, five technicians and two workers. The laboratory infrastructure includes modern equipment for preparing and characterizing including: systems of pulsed laser deposition (PLD and MAPLE); sputter deposition systems in magnetron (RF and DC); scanning electron microscope (SEM); microfluorescence microscope; cryoprobes with vertical and horizontal magnetic fields and illumination facilities with UV radiation; vector analyzer for networks up to 325 GHz ; THz spectrometer (up to 7 THz); spectroscopic ellipsometer; FTIR spectrometers and UV-Vis; fluorescence spectrometer; magnetic circular dichroism spectrometer.

20. Laboratory of Magnetism and Superconductivity

The laboratory is devoted to research in the field of materials with magnetic or superconducting properties. The research process covers all stages from preparation (bulk materials, thin films and nanostructures) to structural and electronic characterization, completed by thorough analysis of magnetic and superconducting properties. The research is focused mainly on the study of nanostructures, especially nanoparticle systems and multilayer magnetic materials for colossal magnetoresistance (CMR), giant magnetoresistance (GMR) and tunneling magnetoresistance (TMR), soft and hard magnetic materials, magnetic diluted semiconductors, etc. In the case of superconducting materials, superconductors of high critical temperatures are especially targeted, as thin films with nanometric inclusions for pinning, MgB_2 (bulk and strip), superconductors in the class of Fe-based pnictides ($\text{FeSmAsF}_x\text{O}_{1-x}$), new superconducting materials, etc.

Among the most important research equipment, targeting both the infrastructure of preparation and characterization, we mention the following: spark plasma sintering equipment, microwave sintering installation, melt spinning installation, system for preparing nanoparticles by hydrothermal/solvothermal synthesis in autoclave and centrifugation for separation by size, laser ablation deposition (PLD) system, magnetic multilayer deposition system by RF and DC sputtering with 4 sources and vacuum based in the 10^{-9} mbar domain, radiofrequency thermal transfer facility to determine SAR in magnetic nanoparticles systems, systems for thermo-gravimetric determination, Vibrating Sample Magnetometer systems (VSM) for up to 9 Tesla magnetic fields, Mossbauer systems with various accessories to carry out measurements at variable temperatures (4.5 K - 1000 K) also in applied fields by detection of radiation gamma / X-ray / conversion electrons, a complex system of measuring the physical properties (PPMS) with magnetic fields up to 14 Tesla, a SQUID type magnetometer system (Superconducting Quantum Interference Device) and a liquid He production unit (18 l / 24 h).

For the high temperatures field, the laboratory has a Laser Flash Analyzer system which enables the defining of thermal diffusivity, specific heat and thermal conductivity of the bulk or multi-layer (3-layer, including liquids) materials in the range of 25-1100 C, a dilatometer (Netzsch C 402, 2015) for determining the coefficients of thermal expansion (25-1600 C) and an equipment (Netzsch, Nemesis 2015) for determining electrical conductivity and the Seebeck coefficient (25-800 C).



Spark Plasma Sintering

30. Laboratory of Nanoscale Condensed Matter

The subjects of experimental investigation are directed towards the properties and the specific processes of the low dimensional systems, supplemented by modeling of the morphology, structure and composition, electric transport and phototransport, of the ferroic properties, chemical activity and surface/interface processes, as well as the phenomena of capture and storage of charge carriers for memory effects. Various types of nanostructured materials (e.g. nanostructures and nanocomposites, surfaces and interfaces with different features, especially magnetic, ferroelectric and catalytic properties) are prepared through advanced cleaning and deposition by physical methods (evaporation, sputtering).

An important part of the research that is done in the laboratory is aimed at applications in micro- and nanoelectronics, optoelectronics, spintronics, advanced sensors, photocatalysis and heterogenous catalysis.

Theoretical investigations are largely motivated by recent results and aim at: the spectral properties of the Lieb optical networks and of the topological insulators, charge transport of the bidimensional materials (e.g. graphene, phosphorene), the dynamics of excitons in optically active quantum dots including magnetic impurities, artificial nanomagnets.

In the laboratory there are two "clusters" dedicated to the study of in-situ surfaces, which operate in ultra-vacuum (UHV $10^{-10} - 10^{-11}$ mbar). Each system is comprised of a preparation chamber by molecular beam epitaxy (MBE), a photoelectron spectroscopy characterization (XPS, UPS) chamber and a characterization by scanning tunneling microscopy (STM) chamber. In MBE systems there also the following in-situ characterization processes: fast and slow electron diffraction RHEED, LEED, thermal desorption by mass spectrometry studies, Auger electron spectroscopy. The XPS-UPS chambers permit spectroscopy measurements with angular resolution (photoelectron diffraction, dispersion laws in the valence band) and, in the case of one of the two clusters, also spin. Thus one can determine the atomic composition, the nature of chemical bonds, the structure at a nanoscopic scale, band structure.

Currently, one of the two clusters is located at Elettra synchrotron in Trieste. The LEEM-PEEM microscope (Low-Energy Electron Microscopy- Photoelectron Electron Microscopy) allows the investigation of samples with nanometer resolution using slow electrons (hence ideal for sensitive or insulating samples) as well as photoelectron spectroscopy studies with spatial resolution in the order of 20 nm. A third XPS automatic equipment allows investigation of several samples simultaneously and XPS analysis with spatial resolution in the order of 200 μm , coupled with the possibility of in situ thermal treatment at high values of pressure (4 bar) and temperature (1000° C). The magnetron sputtering equipment (10^{-8} torr high vacuum) for deposition of thin films and multi-layer structures is equipped with in situ analysis techniques consisting of Auger electron surface spectroscopy and diffraction low-energy electron diffraction – LEED, as well as real time in situ ellipsometric monitoring. For thermal processing under controlled conditions, there is a rapid heat treatment equipment (RTA) in inert gas, oxidation - RTO and nitriding RTN.

Lab 30 carries out also complex experimental studies of the surfaces, interfaces (ferromagnetism, ferroelectrics, catalysis) of certain thin layers and multi- layer structures based on nanocrystals from the GeSiSn system (correlated with modeling studies), and studies of certain 2D semiconductor materials based on chalcogenides of (2D-TMD) transition metals.

For experimental studies, the laboratory is equipped with three chains for electrical and photoelectric, Hall effect and magnetoresistance measurements.

40. Laboratory of Optical Process in Nanostructured Materials

This laboratory is almost entirely dedicated to optical investigative methods applied to materials and focusing on nanostructures and nanocomposites. Other research topics are related to : the preparation and characterization of nanoscale semiconducting polymers with special properties, electrochemistry and production and characterization of chalcogenide glasses. The main equipments used for optical characterization of investigated materials are: UV-Vis-NIR and FTIR absorption spectrophotometry, FTIR imaging microscope, FTRaman equipped with a YAG: Nd laser, confocal Raman spectrophotometer equipped with Ar and Kr lasers, SNOM (Scanning Near Field Optical Microscope) coupled with AFM (Atomic Force Microscope), systems for photoluminescence in VIS and NIR and thermoluminescence, and experimental setups for solar simulator and photoconductivity.



Fluorolog-3, model FL3-22, Horiba Jobin Yvon

Other equipments used in the characterization and / or preparation of the studied materials are: broadband dielectric spectroscopy system, drop shape analysis for estimation of contact angle, equipment for deposition by vacuum evaporation of organic materials, Langmuir-Blodgett film deposition systems and potentiostats/galvanostats for the synthesis of composite materials and their testing as electrode materials in battery and supercapacitors.

50. Laboratory of Atomic Structures and Defects in Advanced Materials

This laboratory is mainly committed to structural investigations by advanced characterization methods such as analytical transmission electron microscopy (TEM) and scanning electron microscopy (SEM), electron paramagnetic resonance (EPR), Mössbauer spectroscopy, evaluation of physical properties in controlled environments (gas sensors, photocatalysis). The research activity includes, also, synthesis of nanostructured materials by the hydrothermal or co-precipitation methods.

Among the important research equipments we mention: a high resolution analytical electron microscope; a conventional transmission electron microscopy which allows working in the temperature range 77-1300 K ; preparation equipments of TEM/SEM specimens; a SEM-FIB dual analytical system, five EPR spectrometers operating in several microwave bands and working modes in continuous wave or in pulsed regime, down to liquid He temperature; He liquefaction station; three Mössbauer spectrometers in the temperature range 4-1000 K ; XRD diffractometers for powders and thin films; specialized equipments for hydrothermal and co-precipitation synthesis.

The high resolution electron microscope is provided with probe Cs corrector of the spherical aberration and EDS and EELS microanalytical facilities, allowing the obtaining of a spatial resolution under 1 Å and atomic elemental mapping. The SEM-FIB dual system which has been installed in a cleanroom is used for morphostructural and microanalytical investigations (SEM, EDS, EBSD) and for the processing of advanced materials at micro and nanometric scale by means of ion beams and nanomanipulators. Electron microscopy and RES spectroscopy facilities are included in the European network of research infrastructures C-ERIC (<http://www.c-eric.eu/>).



- a. High resolution analytical transmission electron microscope (0.08 nm in mode STEM HAADF);
- b. Analytical SEM-FIB dual system;
- c. RES spectrometer in X band (9.7 GHz) in pulsed regime with accessories ENDOR;
- d. Mossbauer spectrometer with cryostat for high magnetic fields (7 T) and cryogenic temperatures
- e. Setup for electrical measurements in controlled atmosphere gas mixing station.

The research activity of the scientists working in this laboratory is focused on the physical properties of advanced materials (structure, optical, electrical properties), resulting either as size effects (nanostructures, thin films) or by structural defect engineering. The scientific concerns are mainly directed towards the discovery, investigation and manipulation of physical properties at nanometric and atomic scale for the development and characterization of new materials (dielectrics, semiconductors, alloys, ceramics) to be used in various applications (semiconductor technology, gas sensing, radiation detectors, telecommunications, aerospace technologies).

Personnel

List of Personnel

Lab. 10 – Laboratory of Multifunctional Materials and Structures

HEAD: Dr. Lucian PINTILIE
E-mail: pintilie@infim.ro
Tel : (+4) 021 369 01 85
Fax: (+4) 021 369 01 77

1. Dr. Ioana PINTILIE	senior researcher I
2. Dr. Corneliu Florin MICLEA	senior researcher I
3. Dr. Daniela PREDOI	senior researcher I
4. Dr. Aurelian GALCA	senior researcher I
5. Dr. Cornel MICLEA	senior researcher I
6. Dr. Gabriel BANCIU	senior researcher I
7. Dr. Silviu POLOSAN	senior researcher I
8. Dr. Monica ENCULESCU	senior researcher I
9. Dr. Elena MATEI	senior researcher II
10. Dr. George STAN	senior researcher II
11. Dr. Liviu NEDELCU	senior researcher II
12. Dr. Nicoleta PREDA	senior researcher II
13. Dr. Victor-Constantin DICULESCU	senior researcher III
14. Lucian-Dragos FILIP	senior researcher III
15. Dr. Luminita HRIB	senior researcher III
16. Dr. Viorica STANCU	senior researcher III
17. Dr. Luminita AMARANDE	senior researcher III
18. Dr. Alin IUGA	senior researcher III
19. Dr. Lucian TRUPINA	senior researcher III
20. Dr. Iuliana PASUK	senior researcher III
21. Dr. Cristina CHIRILA	senior researcher III
22. Dr. Carmen CIOBANU	researcher
23. Cristina BESLEAGA STAN	researcher
24. Dr. Marius CIOANGHER	researcher
25. Georgia BONI	researcher
26. Liliana-Marinela TRINCA	assistant researcher
27. Camelia FLORICA	assistant researcher
28. Roxana RADU	assistant researcher
29. Alexandru EVANGHELIDES	assistant researcher
30. Constantin CIOBOTARU	assistant researcher
31. Mihaela BEREGOI	assistant researcher
32. Cristina POPA	assistant researcher
33. Andrei TOMULESCU	assistant researcher
34. Mihai GRIGOROSCU	assistant researcher
35. Mihaela BOTEA	assistant researcher

36. Dorin RUSU	assistant researcher
37. Irina GHITA	assistant researcher
38. Corina CIOBOTARU	assistant researcher
39. Claudiu POPA	assistant researcher
40. Andrei CATRINA	assistant researcher
41. Simona ICONARU	assistant researcher
42. Daniela DOGARU	assistant researcher
43. Anamaria TRANDAFIR	assistant researcher
44. Vasilica TOMA	engineer
45. Alexandru GAVRILA	engineer

Lab. 20 – Laboratory of Magnetism and Superconductivity

HEAD: Dr. Victor Eugen KUNCSEER

E-mail: kuncser@infim.ro

Tel.: (+4) 021 369 01 85

Fax: (+4) 021 369 01 77

- | | |
|-------------------------------------|--|
| 1. Dr. Gheorghe Virgil ALDICA | senior researcher I |
| 2. Dr. Petre BADICA | senior researcher I |
| 3. Dr. Adrian Ioan CRISAN | senior researcher I |
| 4. Dr. Ovidiu CRISAN | senior researcher I |
| 5. Dr. George FILOTI | senior researcher I (associate collaborator) |
| 6. Dr. Andrei GALATANU | senior researcher I |
| 7. Dr. Lucica MIU | senior researcher I |
| 8. Dr. Neculai PLUGARU | senior researcher I |
| 9. Dr. Viorel Constantin SANDU | senior researcher I |
| 10. Dr. Mihaela VALEANU | senior researcher I |
| 11. Dr. Petru PALADE | senior researcher II |
| 12. Dr. Gabriel SCHINTEIE | senior researcher II |
| 13. Dr. Alina CRISAN | senior researcher III |
| 14. Dr. Valentina MIHALACHE | senior researcher III |
| 15. Dr. Ancuta BARSAN | researcher |
| 16. Dr. Ion IVAN | researcher |
| 17. Dr. Bogdan POPESCU | researcher |
| 18. Dr. Mihaela SOFRONIE | researcher |
| 19. Dr. Felicia TOLEA | researcher |
| 20. Dr. Maria-Cristina BARTHA | researcher |
| 21. Mihai Burdusel | assistant researcher |
| 22. Cezar-Catalin COMANESCU | assistant researcher |
| 23. Magda GALATANU | assistant researcher |
| 24. Simona Gabriela GRECULEASA | assistant researcher |
| 25. Marilena Alina IONESCU | assistant researcher |
| 26. Anda STANCIU | assistant researcher |
| 27. Dr. Carmen PLAPCIANU | chemist |
| 28. Aurel LECA | engineer |
| 29. Dr. Adrian JIANU ¹ | senior researcher I |
| 30. Dr. Marilena TOMUT ² | senior researcher III |

¹ Institute for Pulsed Power and Microwave Technology, Forschungszentrum Karlsruhe.

² GSI / KP2 Nuclear Structure and Nuclear Chemistry, Darmstadt.

Lab. 30 – Laboratory of Nanoscale Condensed Matter**HEAD:** Dr. Valeriu MOLDOVEANU

E-mail: valim@infim.ro

Tel.: (+4) 021 369 01 85

Fax: (+4) 021 369 01 77

1. Dr. Alexandru Emil ALDEA	senior researcher I
2. Dr. Magdalena Lidia CIUREA	senior researcher I
3. Dr. Paul GARTNER	senior researcher I
4. Dr. Sorina LAZANU	senior researcher I
5. Dr. Dan MACOVEI	senior researcher I
6. Dr. Nicolae POPA	senior researcher I
7. Dr. Toma STOICA	senior researcher I
8. Dr. Cristian-Mihail TEODORESCU	senior researcher I
9. Dr. Gheorghe IORDACHE	senior researcher II
10. Dr. Rodica GHITA	senior researcher II
11. Dr. Nicoleta APOSTOL	senior researcher III
12. Dr. Bogdana BORCA	senior researcher III
13. Dr. Maria-Ruxandra COSTESCU	senior researcher III
14. Dr. Marius Adrian HUSANU	senior researcher III
15. Dr. Ana Maria LEPADATU	senior researcher III
16. Dr. Stefan NEATU	senior researcher III
17. Dr. Constantin Catalin NEGRILA	senior researcher III
18. Dr. Marian NITA	senior researcher III
19. Dr. Ionel STAVARACHE	senior researcher III
20. Dr. Mugurel TOLEA	senior researcher III
21. Dr. George-Adrian LUNGU	researcher
22. Dr. Dana Georgeta POPESCU	researcher
23. Adrian SLAV	researcher
24. Dr. Mihaela STEGARESCU	researcher
25. Ion Viorel DINU	researcher
26. Laura Elena ABRAMIUC	assistant researcher
27. Amelia Elena BOCARNEA	assistant researcher
28. Radu DRAGOMIR	assistant researcher
29. Bogdan OSTAHIE	assistant researcher
30. Catalin PALADE	assistant researcher
31. Nicoleta RADUTOIU	assistant researcher
32. Liviu Cristian TANASE	assistant researcher
33. Ioana Cristina BUCUR	engineer
34. Cristian TACHE	engineer
35. Dr. Nicolae BARSAN ¹	senior researcher I
36. Dr. Andrei MANOLESCU ²	senior researcher I

¹ Institute of Physical and Theoretical Chemistry, University of Tübingen² School of Science and Engineering, Reykjavik, Iceland

Lab. 40 – Laboratory of Optical Processes in Nanostructured Materials

HEAD: Dr. Mihaela BAIBARAC
E-mail: barac@infim.ro
Tel.: (+4) 021 369 01 77
Fax: (+4) 021 369 01 77

1. Dr. Ioan BALTOG	senior researcher I
2. Dr. Ligia FRUNZA	senior researcher I
3. Dr. Mihai POPESCU	senior researcher I
4. Dr. Mihai SECU	senior researcher I
5. Dr. Marian SIMA	senior researcher II
6. Dr. Anca STANCULESCU	senior researcher II
7. Dr. Adam LORINCZI	senior researcher III
8. Lucian MIHUT	senior researcher III
9. Dr. Corina SECU	senior researcher III
10. Dr. Mariana SIMA	senior researcher III
11. Dr. Marcela SOCOL	senior researcher III
12. Dr. Alin VELEA	senior researcher III
13. Dr. Irina Ionela ZGURA	senior researcher III
14. Dr. Florin COTOROBAI	physicist
15. Dr. Paul Constantin GANEA	researcher
16. Dr. Oana RASOGA	researcher
17. Dr. Florinel SAVA	researcher
18. Carmen BREAZU	assistant researcher
19. Monica DAESCU	assistant researcher
20. Ioana DUMITRESCU	assistant researcher
21. Mirela ILIE	assistant researcher
22. Adelina MATEA	assistant researcher
23. Andreea NILA	assistant researcher
24. Daniel-Iosif SIMANDAN	assistant researcher
25. Ion SMARANDA	assistant researcher
26. Malvina STROE	assistant researcher

Lab. 50 – Laboratory of Atomic Structures and Defects in Advanced Materials

HEAD: Dr. Corneliu GHICA
E-mail: cghica@infim.ro
Tel.: (+4) 021 369 01 85
Fax: (+4) 021 369 01 77

- | | |
|-----------------------------------|-----------------------|
| 1. Dr. Lucian DIAMANDESCU | senior researcher I |
| 2. Dr. Leona Cristina NISTOR | senior researcher I |
| 3. Dr. Sergiu Vasile NISTOR | senior researcher I |
| 4. Dr. Valentin Serban TEODORESCU | senior researcher I |
| 5. Dr. Marin CERNEA | senior researcher II |
| 6. Dr. Adelina STANOIU | senior researcher II |
| 7. Dr. Mariana STEFAN | senior researcher II |
| 8. Dr. Alina BANUTA | senior researcher III |
| 9. Dr. Daniela GHICA | senior researcher III |
| 10. Dr. Mihai VLAICU | senior researcher III |
| 11. Dr. Cristian Eugen SIMION | researcher |
| 12. Alexandra Camelia JOITA | assistant researcher |
| 13. Andrei Cristian KUNC SER | assistant researcher |
| 14. Raluca NEGREA | assistant researcher |
| 15. Dr. Traian POPESCU | assistant researcher |
| 16. Ioana VLAICU | assistant researcher, |
| 17. Dr. Valentin Adrian MARALOIU | assistant researcher |
| 18. Dr. Ionel Florinel MERCIONIU | assistant researcher |
| 19. Dr. Manuela STIR | assistant researcher |
| 20. Dr. Marcel FEDER | chemist |
| 21. Stefan BULAT | engineer |
| 22. Gheorghe STERIAN | assistant engineer |

MAAS Laboratory for X-Ray Photoelectron Spectroscopy (XPS) Analysis

- | | |
|---------------------------------|-----------------------|
| 1. Dr. Mihail Florin LAZARESCU | senior researcher I |
| 3. Dr. Constantin LOGOFATU | senior researcher III |
| 4. Dr. Costel COTIRLAN-SIMIONUC | assistant researcher |
| 5. Dr. Florica FRUMOSU | assistant researcher |

Visiting Guests

Professor Dr. Marin Alexe

Department of Physics, University of Warwick, Coventry, United Kingdom

Spintronic functionalities in multiferroic BiFeO_3

18.06.2015

Professor José M.F. Ferreira

Department of Materials Engineering and Ceramics, CICECO, University of Aveiro, Portugal

Synthetic multifunctional bone grafts for advanced therapies in dentistry and orthopaedic applications

6.07.2015

Dr. Eren Karsu

Celal Bayar Üniversitesi, Manisa, Turkey

Luminescence properties of novel $\text{CaLa}_4(\text{SiO}_4)_3\text{O}:\text{Ln}^{2+}, \text{Ln}^{3+}$ (Ln= Ce, Nd, Eu, Tb, Dy) phosphor

21.07.2015

Dr. Mihai Irimia-Vladu

Joanneum Research Forschungsgesellschaft mbH, Graz, Austria

Circuite electronice cu materiale organice de origine naturala

13.08.2015

Professor Antonio H. Castro Neto

Department of Materials Science Engineering,, National University of Singapore

Centre for Advanced 2D Materials and Graphene

2D Materials: A revolution in progress

10.09.2015

Professor Yoshio Sakka

Managing Director of the Materials Processing Unit within National Institute for Materials Science, Tsukuba, Japan

Brief introduction of National Institute for Materials Science (NIMS), Japan and Fabrication of innovative ceramics through advanced nanoparticle processing 2.11.2015

Working Stages

Dr. Zoltan Imre DUDAS

Magyar Tudományos Akadémia Wigner Fizikai Kutatóközpont - Wigner RCP, Budapest, Ungaria

Morphologic and spectroscopic characterization of methyl substituted hybrid silica gels

Consortium C-ERIC, 22-27.02.2015, Lab. 50 electron microscopy group (invitation Dr. C. Ghica)

Dr. Daniel MAZUR & Dr. Jaroslava LAVKOVA

Elettra - Sincrotrone Trieste S.C.p.A., Italia & Charles University of Prague - Department of Electronics and Vacuum Physics, Praga, Cehia

Platinum-Cobalt alloy GLAD film for Carbon-free PEMFC cathodes

Consortium C-ERIC, 15-24.03.2015, Lab. 50 electron microscopy group (invitation Dr. C. Ghica)

Dr. Heinz Wilfried AMENITSCH & Barbara SARTORI

Graz University of Technology Institute of Inorganic Chemistry, Graz, Austria

Controlling the morphology of the meso/microstructure during the evaporation induced self-assembly process in the aerosol route with ammonium sulphate

Consortium C-ERIC, 14-19.06.2015, Lab. 50 electron microscopy group (invitation Dr. C. Ghica)

Dr. Jaroslava LAVKOVA & Dr. Ivan KHALAKHAN

Charles University of Prague - Department of Electronics and Vacuum Physics, Praga, Cehia

Electrochemically shape-controlled synthesis of Pt nanostructures with high index facets

Consortium C-ERIC, 15-20.09.2015, Lab. 50 electron microscopy group (invitation Dr. C. Ghica)

Dr. Zoltan Imre DUDAS

Magyar Tudományos Akadémia Wigner Fizikai Kutatóközpont - Wigner RCP, Budapest, Ungaria

Vinyl substituted hybrid silica gels textural, morphological and spectroscopic characterization

Consortium C-ERIC, 21-25.09.2015, Lab. 50 electron microscopy group (invitation Dr. C. Ghica)

Dr. Giovanni DE GIUDICI & Claudia PUSCEDDU

Università degli Studi di Cagliari - Dipartimento di Scienze della Terra, Cagliari, Italia

Biosphere - geosphere interaction and environmental implications for heavy metals mobility

Consortium C-ERIC, 04-10.10.2015, Lab. 50 electron microscopy group (invitation Dr. C. Ghica)

Dr. Marco CAMPANINI

C.N.R.-I.M.E.M. Parma, Italia

Electronic, chemical, magnetic and microstructural properties of semiconductive and ferroelectric nanowires for gas sensing applications

Consortium C-ERIC, 22-28.11.2015, Lab. 50 electron microscopy group (invitation Dr. C. Ghica)

Dr. Matteo FERRONI, Angela BERTUNA

Università degli Studi di Brescia - Dipartimento di Chimica e Fisica per i Materiali, Brescia, Italia

Electronic, chemical, magnetic and microstructural properties of semiconductive and ferroelectric nanowires for gas sensing applications

Consortium C-ERIC, 22-28.11.2015, Lab. 50 electron microscopy group (invitation Dr. C. Ghica)

Ph. D. Theses

Roxana Radu

Radiation induced defects in silicon: from point defects to defect clusters

Mai 2015

Ioana Mihaela Ene (Botea)

Nanoprocessing and characterization of oxide and nitride structures with applications in micro- and optoelectronics

September 2015

Andra-Georgia Ibanescu (Boni)

Charge transport in oxides and nitrides structures having ferroelectric and/or multiferroic properties

September 2015

Andreea-Liliana Costas

Optical, electrical and magnetic properties of unidimensional nanostructures

September 2015

Simona-Gabriela Greculeasa

Magnetic phases and interfacial couplings in bidimensional heterogeneous structures

September 2015

Raluca Florentina Negrea

High Resolution Analytical Transmission Electron Microscopy: atomic structure of interfaces and extended defects in heterogeneous crystalline systems

October 2015

Ancuta Birsan

New systems having high spin polarization for spintronics applications

December 2015

Abilitare**Cristian M. Teodorescu**

Ferromagnetic and ferroelectric surfaces and interfaces

June 2015

Awards

Teodorescu C M: Romanian Academy Prize "Radu Grigorovici" for the group of papers entitled "Study of ferroelectric surfaces and interfaces of type magnetic metals/semiconductors" awarded in December 2015

Awards at International Fairs and Exhibitions

XIII International Inventics Salon PRO INVENT, Cluj-Napoca

Cristina Busuioc, Alexandru Ionut Evanghelidis, Monica Maria Enculescu, Elena Matei, Nicoleta Preda, Florina Camelia Florica, Liliana Andreea Costas, Mihaela Oancea, Ionut Marius Enculescu

Thermochromic device based on flexible transparent electrodes obtained by electrospinning
DIPLOME OF EXCELLENCE and GOLD MEDAL with special mention

Magdalena Galatanu, Monica Enculescu, Mihai Cioca, Andrei Galatanu

SPS technology for achievement of W-Cu component of divertor for ITER fusion reactor
DIPLOME OF EXCELLENCE and GOLD MEDAL with special mention

Camelia Florina Florica, Nicoleta Preda, Monica Maria Enculescu, Alexandru Ionut Evanghelidis, Liliana Andreea Costas, Mihaela Oancea, Cristina Busuioc, Elena Matei, Ionut Marius Enculescu

Preparation procedure by autocatalytic deposition of some predefined micronic areas formed from ZnO structures
DIPLOME OF EXCELLENCE and GOLD MEDAL

Gheorghe Aldica, Mihail Burdusel, Vladimir Cioca, Petre Badica

MgB₂ based machinable superconducting material and magnetic field concentrator/storer
DIPLOME OF EXCELLENCE and GOLD MEDAL

Lucian Pintilie, Mihai Cioca, Gabriel Dobrescu, Liviu Culea, Petre Soare

Installation for rapid thermal treatment of oxidic thin films
BRONZE MEDAL for inventics of Stefan cel Mare Suceava University

European Exhibition of Creativity and Innovation EUROINVENT, IASI 14-16 MAI, 2015

Lucian Pintilie, Mihai Cioca, Gabriel Dobrescu, Liviu Culea, Petre Soare

Installation for rapid thermal treatment of oxidic thin films
GOLD MEDAL

Cernea Marin, Ghita Rodica, Negrilă Constantin Catalin

Method for preparing a photosensitive structure of TiO₂/GaAs.
GOLD MEDAL

Matei Elena, Busuioc Cristina, Evanghelidis Alexandru, Enculescu Maria Monica, Preda Nicoleta Roxana, Florica Camelia Florina, Oancea Mihaela, Enculescu Ionut Marius

Electrochromic device based of transparent and flexible electrodes obtained through electrospinning and polyaniline electrodes deposition.
GOLD MEDAL

Galatanu Magdalena, Ruiu George, Enculescu Maria Monica, Cioca Mihai, Galatanu Andrei
W-metals laminates by FAST
SILVER MEDAL

Aldica Gheorghe Virgil, Burdusel Mihail, Cioca Vladimir, Badica Petre
A MgB₂-based superconducting material machinable by cutting tools and a magnetic field concentrator/storage device.
SILVER MEDAL

Cotarlan Simioniuc Constantin, A.S.Manea, C.Logofatu
Structure of electro-optical superlens performed with micro- or nanostructured plasmonic guide for imaging with resolution below the diffraction limit.
SILVER MEDAL

Steluta Carmen Ciobanu
Nanoparticles with luminescent properties.
SILVER MEDAL

Florica Camelia Florica, Preda Nicoleta Roxana, Enculescu Maria Monica, Evanghelidis Alexandru Ionut, Costas Liliana Andreea, Oancea Mihaela, Busuioc Cristina, Matei Elena, Enculescu Ionut Marius
Process for obtaining predefined micronic areas of zinc oxide structures through autocatalytic deposition.
BRONZE MEDAL

Cristina Liliana Popa, Stefan Antohe, Mousif Echcherif Elkettani
Physico-chemical and ultrasonic characterization of ceramic materials used for biomedical applications
DIPLOME OF EXCELLENCE (Valahia University) and BRONZE MEDAL

Aldica GV, Burdusel M, Cioca EM, Badica P
Machinable superconducting material and magnetic field concentrator/storer made of superconducting material based on MgB₂, machinable by chip removal, Patent No: RO130252-A2, Published 29 May 2015
Participation at TIB, Bucharest, 14-17 Oct. 2015.

Honorary Membership

NIMP is present in following databases:

- The **CEEC IST NET** portal (www.eu-istcommunity.net) – is a support instrument for partners search and consortia creation in the field of research and innovation concerning the information society technologies
- **Europartners Search** (www.europartnersearch.net)
- **Resource Guide to Nanotechnology and Nanomaterials Services** (denumit NanoPerspective)

This guide includes a list of more 1000 organizations active in the field of Nanotechnology and Nanomaterials.

- <http://wikimapia.org/19116027/INCDFM-National-RD-Institute-of-Materials-Physics-NIMP>
- http://cercetare.ccib.ro/intranetHTML/infoFILES/infoHTML/File/2012_03_22_prezentareINCDFM.pdf
- <http://www.ancs.ro/ro/articol/1325/de-cercetare-incd-institute-nationale-de-cercetare-dezvoltare-incd-in-coordonarea-ancs-institutul-national-de-cercetare-dezvoltare-pentru-fizica-materialelor-incdfm-bucuresti>
- http://www.infocercetare.ro/ro/Listeaza-Institutie/Ilfov-84_Localitate_Magurele-86_Institutie_INCDFM-pentru-Fizica-Materialelor-INCDFM-253
- <http://ro-ro.facebook.com/pages/INCDFM/122100527823931>
- <http://wikimapia.org/19116027/ro/Institutul-National-de-Cercetare-Dezvoltare-pentru-Fizica-Materialelor-INCDFM>
- <http://site.roinno.ro/data/pdf/ca/369.pdf>

INCDFM is membership of C-ERIC (Central European Research Infrastructure Consortium) **Consortium** (<http://www.ceric-eric.eu>). C-ERIC is a distributed research facility, set up as an ERIC, by *Austria, Czech Republic, Italy, Romania, Croatia, Polonia, Slovenia, Serbia*, and *Hungary* and open to other interested countries.

The specific scope of this ERIC concerns the offer as an integrated service to external researchers of the access to *synchrotron light and other microscopic probes for analytical and modification techniques* notably for materials preparation and characterization, structural investigations and imaging in Life Sciences, Nanoscience and Nanotechnology, Cultural Heritage, Environment and Materials Sciences and to their various technological and industrial outcomes ranging from energy to biomedical and of interest to most manufacturing industries.

CERIC's mission is to bring the integrated service to world-level quality thus contributing to the attractiveness of the European Research Area and stimulating a beneficial impact on the scientific and economic development of the entire region, also helping to introduce a strong interchange between scientists and technicians and attraction of scientists from other regions.

Membership in Other International Organizations

Badica Petre: member of American Chemical Society and German Physical Society

Banciu Marian Gabriel: member of IEEE: Microwave Theory and Techniques Society, Antennas and Propagation Society; founding member of Romanian Society for Non-Ionizing Radiation Safety (SRPRNI)

Bibicu Ion: member of European Physical Society; titular member of Romanian Academy of Technical Sciences, secretary of Section Electronics and Automatics

Ciurea Magdalena Lidia: member of European Physical Society

Costas Liliana Andreea: member of European Physical Society ; member of European Microscopy Society; member of Romanian Society of Electron Microscopy

Crisan Ovidiu: member of Institute of Nanotechnology, UK; member of Materials Research Society

Diamandescu Lucian: member of “American Nano Science”
- Romanian Representative in International Board on the Applications of Mössbauer Effect - IBAME (2011-2017)
- member in Editorial Board of “ISRN Nanomaterials” (SUA)

Frunza Ligia: member of American Chemical Society and of Romanian Society of Catalysis

Ghica Corneliu: member of European Materials Research Society; member of European Microscopy Society; member in Directory Council of Romanian Society of Electron Microscopy

Ghica Daniela: member of European Materials Research Society

Kuncser Andrei Cristian: member of European Microscopy Society; member of Romanian Society of Electron Microscopy

Lepadatu Ana Maria: member of European Physical Society

Maraloiu Valentin Adrian: member of Société Française des Microscopies ; member of Romanian Society of Electron Microscopy

Mercioniu Ionel Florinel: member of European Microscopy Society; member of Romanian Society of Electron Microscopy

Negrea Raluca Florentina: member of European Microscopy Society; member of Romanian Society of Electron Microscopy

Nistor Leona Cristina: member of European Microscopy Society; vicepresident of Romanian Society of Electron Microscopy

Nistor Sergiu Vasile: member of American Physical Society

Pintilie Lucian: member of European Physical Society; honorary member of Romanian Society of Electron Microscopy

Popescu Mihai: member of NACNOG (North Atlantic Consortium on Non-Oxide Glasses, 19 countries from Europe, Canada și SUA)
- member of VIP (Virtual Institute of Physics): <http://www.infim.ro/~inst>

Predoi Daniela: member of Romanian Society of Catalysis

Sandu Viorel: member of American Physical Society and Material Research Society Singapore

Sarbu Corneliu: member of Microscopical Society of America

Socol Marcela: member of International Organization on Crystal Growth

Stanculescu Anca: member of International Organization on Crystal Growth
- member of SPIE

Teodorescu Valentin Șerban: member of European Microscopy Society; general secretary
of Romanian Society of Electron Microscopy

Vasiliu Florin: member of European Microscopy Society; member of Romanian Society of Electron
Microscopy

Vlaicu Aurel Mihai: member of European Microscopy Society; member of Romanian Society
of Electron Microscopy

Publications and Presentations

BOOK CHAPTERS

- **Badica P**, Endo K, *Substrate-Film lattice engineering for the growth by spin coating of c-axis and non c-axis BSCCO HTS epitaxial thin films*, Chapter 2 in **Oxide Thin films, Multilayers, and Nanocomposites**, eds. P. Mele, S. Arisawa, C. Li, T. Tsuchiya, Springer International Publishing, pp. 27-38, ISBN 978-3-319-14477-1 (doi 10.1007/978-3-319-14478-8).
- Batalu D, **Aldica G**, **Badica P**, *Nanocompozite supraconductoare de MgB₂ cu adaosuri pe baza de pamanturi rare obtinute prin metoda "Spark Plasma Sintering"*, Chapter 4 in **Tratat de Stiinta si Ingineria Materialelor Metalice vol 6** – Proiectare-Calitatea Produselor- Materiale Speciale-Inginerie Economica Metalurgica, Eds. M.O. Cojocaru, N. Ghiban, AGIR, 2015, pp. 1041-1063 (ISBN 978-973-720-533-9 (vol 6)).
- Miculescu F, Maidaniuc A, **Stan GE**, Miculescu M, Voicu SI, Ciocan LT, *Thermal degradation and morphological characteristics of bone products*, pp. 393-410, in: **Reactions and Mechanisms in Thermal Analysis of Advanced Materials**, A. Tiwari and B. Raj (Eds.), John Wiley & Sons Inc., Toronto, Canada, 2015, ISBN: 978-1-119-11757-5.
- Mu G, **Sandu V**, Li W, Shen B, *Exotic superconductivity in correlated electron systems*, in **Exotic Superconductivity in Correlated Electron Systems**, Editors Gang Mu, **V. Sandu**, Wei Li, Bing Shen, Advances in Condensed Matter Physics, Hindawi Publ. House, 2015.
- **Pintilie I**, **Badica P**, Bulinski M, **Kuncser V**, *Shapes and patterns in matter and fields: inter-related microscopic and macroscopic physical properties*, Chapter 10 in **On Form and Pattern**, Ed. Vasilescu C, Flonta ML, Craciun I, Editura Academiei Romane, Humboldt Symposium, Bucharest 29-31 May, 2014, pp. 101-139, 2015, ISBN 978-973-27-2531-3.
- Primo A, **Neatu S**, Garcia H, *Photocatalytic CO₂ reduction*, in **Advanced Materials for Clean Energy**, CRC Press Taylor & Francis Group (2015), ISBN: 9781482205787, URL: <http://www.crcpress.com/product/isbn/9781482205787>.

Stanculescu A, Stanculescu F, *Organic semiconductors for non-linear optical applications*, pp. 235-273 in the book **Optoelectronics - Materials and Devices** edited by Sergei L. Pyshkin and John Ballato, ed. Intech, Rijeka, Croatia - EUROPEAN UNION, ISBN 978-953-51-2174-9 (2015).

JOURNALS

Papers in ISI Ranked Journals (with Impact Factor and AIS)

1. Ac sente T, **Negrea RF**, **Nistor LC**, **Logofatu C**, **Matei E**, Birjega R, Grisolia C, Dinescu G
Synthesis of flower-like tungsten nanoparticles by magnetron sputtering combined with gas aggregation
EUROPEAN PHYSICAL JOURNAL D, (2015),69, 161, **1.228**, **0.454**
2. **Aldica G**, **Burdusel M**, **Popa S**, **Enculescu M**, **Pasuk I**, **Badica P**
The influence of heating rate on superconducting characteristics of MgB₂ obtained by spark plasma sintering technique
PHYSICA C-SUPERCONDUCTIVITY AND ITS APPLICATIONS, (2015),519, pp.184-189, **0.942**, **0.297**
3. Alegre D, Ac sente T, Martin-Rojo AB, Oyarzabal E, Tabares FL, Dinescu G, De Temmerman G, Birjega R, **Logofatu C**, Kovac J, Mozetic M
Characterisation of tungsten nitride layers and their erosion under plasma exposure in NANO-PSI
ROMANIAN REPORTS IN PHYSICS, (2015),67, pp.532-546, **1.517**, **0.21**
4. Anastasescu C, Spataru N, Culita D, Atkinson I, Spataru T, Bratan V, Munteanu C, Anastasescu M, **Negrila CC**, Balint I
Chemically assembled light harvesting CuO_x-TiO₂ p-n heterostructures
CHEMICAL ENGINEERING JOURNAL, (2015),281, pp.303-311, **4.321**, **0.945**
5. Andronescu E, Iordache FM, **Ciobanu CS**, Badea ML, Costescu A, Prodan AM
Optical properties of bioactive europium doped hydroxyapatite (HAp:Eu³⁺)
OPTOELECTRONICS AND ADVANCED MATERIALS-RAPID COMMUNICATIONS, (2015), 9, pp.1155-1159, **0.394**, **0.07**
6. **Apostol NG**, Stoflea LE, **Tanase LC**, Bucur IC, **Chirila C**, **Negrea RF**, **Teodorescu CM**
Band bending at copper and gold interfaces with ferroelectric Pb(Zr,Ti)O₃ investigated by photoelectron spectroscopy
APPLIED SURFACE SCIENCE, (2015),354, pp.459-468, **2.711**, **0.549**
7. Avram D, Cojocaru B, Florea M, **Teodorescu VS**, Tiseanu I, Tiseanu C
NIR to Vis - NIR up - conversion and X-ray excited emission of Er doped high Z BiOCl
OPTICAL MATERIALS EXPRESS, (2015),5, pp.951-962, **2.844**, **0.863**
8. **Badica P**, Tiseanu I, **Aldica G**, Craciunescu T, **Sandu V**, Jakob G, Rindfleisch M
Qualitative comparative analysis of MgB₂ powder-in-tube wires: superconductivity and X-ray cone-beam microtomography
JOURNAL OF OPTOELECTRONICS AND ADVANCED MATERIALS, (2015),17, pp.1636-1649, **0.429**, **0.089**
9. **Baibarac M**, **Baltog I**, **Matea A**, Lefrant S
Raman scattering and photoluminescence studies of ZnO nanowhiskers assembled as flowers in the presence of fullerene
JOURNAL OF CRYSTAL GROWTH, (2015),419, pp.158-164, **1.698**, **0.401**

10. **Baibarac M, Baltog I, Matea A, Mihut L, Lefrant S**
Anti-Stokes Raman spectroscopy as a method to identify the metallic and semiconducting configurations of double-walled carbon nanotubes
JOURNAL OF RAMAN SPECTROSCOPY, (2015),46, pp.32-38, **2.671**, **0.575**
11. **Baibarac M, Baltog I, Smaranda I, Magrez A**
Photochemical processes developed in composite based on highly separated metallic and semiconducting SWCNTs functionalized with polydiphenylamine
CARBON, (2015),81, pp.426-438, **6.196**, **1.463**
12. **Baibarac M, Matea A, Ilie M, Baltog I, Magrez A**
Anti-Stokes Raman spectroscopy as a method to identify metallic and mixed metallic/semiconducting configurations of multi-walled carbon nanotubes
ANALYTICAL METHODS, (2015),7, pp.6225-6230, **1.821**, **0.38**
13. **Baibarac M, Smaranda I, Scocioreanu M, Mitran RA, Enculescu M, Galatanu M, Baltog I**
Exciton-phonon interaction in PbI₂ revealed by Raman and photoluminescence studies using excitation light overlapping the fundamental absorption edge
MATERIALS RESEARCH BULLETIN, (2015),70, pp.762-772, **2.288**, **0.458**
14. **Balaceanu M, Parau AC, Braic M, Vladescu A, Luculescu CR, Logofatu C, Braic V**
Growth and characterization of arc evaporated TiSiC-Ni coatings
TRIBOLOGY LETTERS, (2015),58, 43, **1.739**, **0.666**
15. **Bartha C, Plapcianu C, Palade P, Vizman D**
Model-free kinetic analysis of Sr₂FeMoO₆ re-crystallization process used for double-perovskite monocrystals grown by bridgman method
TIM14 PHYSICS CONFERENCE: PHYSICS WITHOUT FRONTIERS, (2015),1694, UNSP 040006
16. **Batalu D, Aldica G, Burdusel M, Popa S, Enculescu M, Pasuk I, Miu D, Badica P**
Ge-Added MgB₂ superconductor obtained by Ex Situ Spark Plasma Sintering
JOURNAL OF SUPERCONDUCTIVITY AND NOVEL MAGNETISM, (2015),28, pp.531-534, **0.909**, **0.19**
17. **Batalu D, Aldica G, Popa S, Kuncser A, Mihalache V, Badica P**
GeO₂-added MgB₂ superconductor obtained by Spark Plasma Sintering
SOLID STATE SCIENCES, (2015),48, pp.23-30, **1.839**, **0.442**
18. **Birsan A, Kuncser V**
Theoretical investigations of electronic structure and magnetism in Zr₂CoSn full-Heusler compound
JOURNAL OF MAGNETISM AND MAGNETIC MATERIALS, (2015),388, pp.1-4, **1.97**, **0.483**
19. **Bjelajac A, Djokic V, Petrovic R, Stan GE, Socol G, Popescu-Pelin G, Mihailescu IN, Janackovic D**
Pulsed laser deposition method for fabrication of CdS/TiO₂ and PbS photoelectrodes for solar energy application
DIGEST JOURNAL OF NANOMATERIALS AND BIOSTRUCTURES, (2015),10, pp.1411-1418, **0.945**, **0.202**

20. **Boni AG, Chirila C, Hrib L, Pintilie I, Pintilie L**
Study of the leakage current in epitaxial ferroelectric $\text{Pb}(\text{Zr}_{0.52}\text{Ti}_{0.48})\text{O}_3$ layer with SrRuO_3 bottom electrode and different metals as top contacts
DIGEST JOURNAL OF NANOMATERIALS AND BIOSTRUCTURES, (2015),10, pp.1257-1265, **0.945**, **0.202**
21. **Boni AG, Chirila C, Pasuk I, Negrea RF, Trupina L, Le Rhun G, Vilquin B, Pintilie I, Pintilie L**
Electrode interface controlled electrical properties in epitaxial $\text{Pb}(\text{Zr}_{0.52}\text{Ti}_{0.48})\text{O}_3$ films grown on Si substrates with SrTiO_3 buffer layer
THIN SOLID FILMS, (2015),593, pp.124-130, **1.759**, **0.456**
22. **Borca B, Schendel V, Petuya R, Pentegov I, Michnowicz T, Kraft U, Klauk H, Arnau A, Wahl P, Schlickum U, Kern K**
Bipolar conductance switching of single anthradithiophene molecules
ACS NANO, (2015),9, pp.12506-12512, **12.881**, **3.979**
23. **Botea M, Pintilie L, Pintilie I, Stancu V**
Indirect amplification of the pyroelectric signal in $\text{Pb}(\text{Zr},\text{Ti})\text{O}_3$ thin films by the photo-generation of carriers in the Si substrates
DIGEST JOURNAL OF NANOMATERIALS AND BIOSTRUCTURES, (2015),10, pp.341-347, **0.945**, **0.202**
24. **Braic M, Zoita NC, Danila M, Grigorescu CEA, Logofatu C**
Hetero-epitaxial growth of TiC films on $\text{MgO}(001)$ at 100 degrees C by DC reactive magnetron sputtering
THIN SOLID FILMS, (2015),589, pp.590-596, **1.759**, **0.456**
25. **Breazu C, Stanculescu A, Socol M, Rasoga O**
Effect of cholesterol on the deposition of beta-amyloid 1-40 and 1-42 films
DIGEST JOURNAL OF NANOMATERIALS AND BIOSTRUCTURES, (2015),10, pp.299-313, **0.945**, **0.202**
26. **Bulai G, Diamandescu L, Dumitru I, Gurlui S, Feder M, Caltun OF**
Effect of rare earth substitution in cobalt ferrite bulk materials
JOURNAL OF MAGNETISM AND MAGNETIC MATERIALS, (2015),390, pp.123-131, **1.97**, **0.483**
27. **Burdusel M, Aldica G, Popa S, Enculescu M, Mihalache V, Kuncser A, Pasuk I, Badica P**
 B_4C in ex-situ spark plasma sintered MgB_2
CURRENT APPLIED PHYSICS, (2015),15, pp.1262-1270, **2.212**, **0.474**
28. **Burdusel M, Miu L, Zhao PH, Yan W, Han YL, Nie JC, Badica P**
Growth and characterization by STM of BiCo_{222} crystal objects: whiskers and bows
JOURNAL OF OPTOELECTRONICS AND ADVANCED MATERIALS, (2015),17, pp.426-430, **0.429**, **0.089**
29. **Burzo E, Balasz I, Valeanu M, Kozlenko DP, Kichanov SE, Rutkauskas AV, Savenko BN**
Magnetic and transport properties of $\text{Ca}_{1.5}\text{La}_{0.5}\text{FeMo}_{1-x}\text{W}_x\text{O}_6$ perovskites
JOURNAL OF ALLOYS AND COMPOUNDS, (2015),621, pp.71-77, **2.999**, **0.557**

30. **Busuioc C, Evanghelidis A, Enculescu M, Enculescu I**
optical and photocatalytic properties of electrospun ZnO fibers
DIGEST JOURNAL OF NANOMATERIALS AND BIOSTRUCTURES, (2015),10, pp.957-965, **0.945**, **0.202**
31. **Cernea M**, Vasile BS, Ciuchi IV, **Iuga A**, Alexandrescu E, Pinte J, Galassi C
Synthesis, structural and electrical properties of BNT-BTCe@SiO₂ Core-Shell Heterostructure
SCIENCE OF ADVANCED MATERIALS, (2015),7, pp.2297-2305, **2.598**, **0.375**
32. **Chirila C, Boni AG, Pasuk I, Negrea RF, Trupina L**, Le Rhun G, Yin S, Vilquin B, **Pintilie I, Pintilie L**
Comparison between the ferroelectric/electric properties of the PbZr_{0.52}Ti_{0.48}O₃ films grown on Si (100) and on STO (100) substrates
JOURNAL OF MATERIALS SCIENCE, (2015),50, pp.3883-3894, **2.371**, **0.592**
33. Chirita A, Prilepov V, **Popescu M**, Andries I, Caraman M, Jidcov IU
Effect of optical coating in the thin-film system of chalcogenide glassy semiconductor-dielectric when recording the holographic optical information
JOURNAL OF OPTOELECTRONICS AND ADVANCED MATERIALS, (2015),17, pp.925-929, **0.429**, **0.089**
34. Chirita A, Prilepov V, **Popescu M**, Corsac O, Chetrus P, Nasedchina, N
Electro-optical properties of As-Se-S-dielectric structure for optical information recording in real time
OPTOELECTRONICS AND ADVANCED MATERIALS-RAPID COMMUNICATIONS, (2015), 9, pp.919-923, **0.394**, **0.07**
35. Chirita P, Constantin CA, Badica CE, Duinea MI, Birsa LM, **Matei E, Baltog I**
Inhibition of troilite (FeS) oxidative dissolution in air-saturated acidic solutions by O-ethyl-S-2-(2-hydroxy-3,5-diiodophenyl)-2-oxoethylxantogenate
MATERIALS CHEMISTRY AND PHYSICS, (2015),157, pp.101-107, **2.259**, **0.543**
36. **Ciobanu CS**, Groza A, **Iconaru SL, Popa CL**, Chapon P, Chifiriuc MC, Hristu R, Stanciu GA, **Negrila CC, Ghita RV**, Ganciu M, **Predoi D**
Antimicrobial activity evaluation on silver doped hydroxyapatite/polydimethylsiloxane composite layer
BIOMED RESEARCH INTERNATIONAL, (2015), 926513, **1.579**, **0.367**
37. **Ciobanu CS, Iconaru SL, Popa CL**, Motelica-Heino M, **Predoi D**
Evaluation of samarium doped hydroxyapatite, ceramics for medical application: antimicrobial activity
JOURNAL OF NANOMATERIALS, (2015), 849216, **1.644**, **0.371**
38. **Ciurea ML, Lepadatu AM**
Tuning the properties of Ge and Si nanocrystals based structures by tailoring the preparation conditions Review
DIGEST JOURNAL OF NANOMATERIALS AND BIOSTRUCTURES, (2015),10, pp.59-87, **0.945**, **0.202**

39. Collazos JC, Guner SB, Celik ME, Oprea A, Gencer A, **Crisan IA**
High-field pinning potential in YBCO films with nanoengineered pinning centres
JOURNAL OF SUPERCONDUCTIVITY AND NOVEL MAGNETISM, (2015),28, pp.355-360, **0.909**, **0.19**
40. Coman SM, Verziu M, Tirsoaga A, Jurca B, **Teodorescu CM**, **Kuncser V**, Parvulescu VI, Scholz G, Kemnitz E
NbF₅-AIF(3) catalysts: design, synthesis, and application in lactic acid Synthesis from Cellulose
ACS CATALYSIS, (2015),5, pp.3013-3026, **9.312**, **2.283**
41. Comorosan S, Popescu I, **Polosan S**, Pirvu C, Ionescu E, Paslaru L, Apostol M
Conformational changes and metastable states induced in proteins by green light
EUROPEAN PHYSICAL JOURNAL B, (2015),88, 8, **1.345**, **0.538**
42. **Constantinescu G**, Rasekh S, Torres MA, Bosque P, Madre MA, Sotelo A, Diez JC
Thermoelectric doping effect in Ca₃Co_{4-x}Ni_xO₉ ceramics
BOLETIN DE LA SOCIEDAD ESPANOLA DE CERAMICA Y VIDRIO, (2015),54, pp.21-27, **0.29**, **0.07**
43. **Constantinescu G**, Rasekh S, Torres MA, Madre MA, Sotelo A, Diez JC
Improvement of thermoelectric properties in Ca₃Co₄O₉ ceramics by Ba doping
JOURNAL OF MATERIALS SCIENCE-MATERIALS IN ELECTRONICS, (2015),26, pp.3466-3473, **1.569**, **0.248**
44. **Costas A**, **Florica C**, **Evangelidis A**, **Enculescu M**, **Preda N**, **Enculescu I**
Electrospraying of ZnO microstructures for electrical contacting
DIGEST JOURNAL OF NANOMATERIALS AND BIOSTRUCTURES, (2015),10, pp.1181-1188, **0.945**, **0.202**
45. **Crisan O**, **Crisan AD**, **Mercioniu I**, Pantelica D, Pantelica A, Vaucher S, Nicula R, Stir M, **Vasiliu F**
Effect of Mn addition on the thermal stability and magnetic properties of rapidly-quenched L1(0) FePt alloys
INTERMETALLICS, (2015),65, pp.81-87, **2.131**, **0.673**
46. Cristescu R, Surdu AV, Grumezescu AM, Oprea AE, Trusca R, Vasile O, Dorcioman G, Visan A, Socol G, Mihailescu IN, Mihaiescu D, **Enculescu M**, Chifiriuc MC, Boehm RD, Narayan RJ, Chrisey DB
Microbial colonization of biopolymeric thin films containing natural compounds and antibiotics fabricated by MAPLE
APPLIED SURFACE SCIENCE, (2015),336, pp.234-239, **2.711**, **0.549**
47. Datcu A, Duta L, del Pino AP, **Logofatu C**, Luculescu C, Duta A, Perniu D, Gyorgy E
One-step preparation of nitrogen doped titanium oxide/Au/reduced graphene oxide composite thin films for photocatalytic applications
RSC ADVANCES, (2015),5, pp.49771-49779, **3.84**, **0.747**
48. del Pino AP, Gyorgy E, **Logofatu C**, Puigmarti-Luis J, Gao W
Laser-induced chemical transformation of graphene oxide-iron oxide nanoparticles composites deposited on polymer substrates
CARBON, (2015),93, pp.373-383, **6.196**, **1.463**

49. Deniz H, Preziosi D, Alexe M, Hesse D, Eisenschmidt C, Schmidt G, **Pintilie L**
Microstructure and properties of epitaxial Sr₂FeMoO₆ films containing SrMoO₄ precipitates
JOURNAL OF MATERIALS SCIENCE, (2015),50, pp.3131-3138, **2.371**, **0.592**
50. Dias M, Guerreiro F, Correia JB, **Galatanu A**, Rosinski M, Monge MA, Munoz A, Alves E, Carvalho PA
Consolidation of W-Ta composites: Hot isostatic pressing and spark and pulse plasma sintering
FUSION ENGINEERING AND DESIGN, (2015),98-99, pp.1950-1955, **1.152**, **0.358**
51. Dippong T, Levei EA, **Diamandescu L**, **Bibicu I**, Leostean C, Borodi G, Tudoran LB
Structural and magnetic properties of Co_xFe_{3-x}O₄ versus Co/Fe molar ratio
JOURNAL OF MAGNETISM AND MAGNETIC MATERIALS, (2015),394, pp.111-116, **1.97**, **0.483**
52. Donescu D, Ghiurea M, Spataru CI, Sting G, Anghel D, **Baibarac M**, **Baltog I**
1D-polyaniline starting from self-assembled systems
COLLOID AND POLYMER SCIENCE, (2015),293, pp.2515-2524, **1.865**, **0.406**
53. **Dragomir R**, **Moldoveanu V**, **Dinu IV**
Intraband relaxation of p-shell excitons in disk-shaped quantum dots
ROMANIAN JOURNAL OF PHYSICS, (2015),60, pp.686-690, **0.924**, **0.165**
54. Dragu A, Kinayyigit S, Garcia-Suarez EJ, Florea M, Stepan E, Velea S, **Tanase LC**, Colliere V, Philippot K, Granger P, Parvulescu VI
Deoxygenation of oleic acid: Influence of the synthesis route of Pd/mesoporous carbon nanocatalysts onto their activity and selectivity
APPLIED CATALYSIS A-GENERAL, (2015),504, pp.81-91, **3.942**, **0.883**
55. Dumbrava A, Olar R, Badea M, Maxim C, **Ghica D**, Andruh M
New coordination polymers with chromato bridges: (1)(infinity)[Ni(phen)(H₂O)(2)(mu-O₂CrO₂)] and (3)(infinity)[Mn(4,4'-bipy)(H₂O)(mu-O₃CrO)]center dot H₂O
INORGANICA CHIMICA ACTA, (2015),426, pp.50-54, **2.046**, **0.331**
56. **Filip LD**, **Pintilie L**, **Stancu V**, **Pintilie I**
Simulation of the capacitance-voltage characteristic in the case of epitaxial ferroelectric films with Schottky contacts
THIN SOLID FILMS, (2015),592, pp.200-206, **1.759**, **0.456**
57. Florea NM, Lungu A, **Badica P**, Craciun L, **Enculescu M**, Ghita DG, Ionescu C, Zgiran RG, Iovu H
Novel nanocomposites based on epoxy resin/epoxy-functionalized polydimethylsiloxane reinforced with POSS
COMPOSITES PART B-ENGINEERING, (2015),75, pp.226-234, **2.983**, **0.774**
58. **Florica C**, **Costas A**, **Boni AG**, **Negrea RF**, Ion L, **Preda N**, **Pintilie L**, **Enculescu I**
Electrical properties of single CuO nanowires for device fabrication: Diodes and field effect transistors
APPLIED PHYSICS LETTERS, (2015),106, 223501, **3.302**, **1.125**
59. **Ghica C**, Damian RF, Culita D, Turcu I, Ionita P
Silver azide nanoparticles embedded into silica as energetic nano-materials
MATERIALS SCIENCE-MEDZIAGOTYRA, (2015),21, pp.329-332, **0.51**, **0.151**

60. **Ghita RV**
Evolution of surface oxides on GaAs
JOURNAL OF OPTOELECTRONICS AND ADVANCED MATERIALS, (2015),17, pp.1703-1709, **0.429**, **0.089**
61. Gingasu D, Mindru I, Culita DC, Patron L, Calderon-Moreno JM, Osiceanu P, Preda S, Oprea O, Parvulescu V, **Teodorescu VS**, Walsh JPS
Structural, magnetic and catalytic properties of cobalt chromite obtained through precursor method
MATERIALS RESEARCH BULLETIN, (2015),62, pp.52-64, **2.288**, **0.458**
62. **Greculeasa SG**, **Miu L**, **Badica P**, Nie J, **Tolea M**, **Kuncser V**
Electron reconfiguration and enhanced phonon activation in the superconducting state of a FeSe_{0.3}Te_{0.7} single crystal, as evidenced by Mossbauer Spectroscopy
JOURNAL OF THE PHYSICAL SOCIETY OF JAPAN, (2015),84, 14701, **1.585**, **0.644**
63. Grumezescu AM, Cristescu R, Chifiriuc MC, Dorcioman G, Socol G, Mihailescu IN, Mihaiescu DE, Ficai A, Vasile OR, **Enculescu M**, Chrisey DB
Fabrication of magnetite-based core-shell coated nanoparticles with antibacterial properties
Biofabrication, (2015),7, 15014, **4.289**, **1.198**
64. Grumezescu V, Andronescu E, Holban AM, Mogoanta L, Mogosanu GD, Grumezescu AM, **Stanculescu A**, Socol G, Iordache F, Maniu H, Chifiriuc MC
MAPLE fabrication of thin films based on kanamycin functionalized magnetite nanoparticles with anti-pathogenic properties
APPLIED SURFACE SCIENCE, (2015),336, pp.188-195, **2.711**, **0.549**
65. Guerreiro F, Dias M, **Galatanu A**, Correia JB, Alves E, Carvalho PA
W-Ta composites consolidated by Spark Plasma Sintering.
MICROSCOPY AND MICROANALYSIS : THE OFFICIAL JOURNAL OF MICROSCOPY SOCIETY OF AMERICA, MICROBEAM ANALYSIS SOCIETY, MICROSCOPICAL SOCIETY OF CANADA, (2015),21, **1.872**, **0.793**
66. **Husanu MA**, **Ganea CP**, Anghel I, **Florica C**, **Rasoga O**, **Popescu DG**
Surface topography to reflectivity mapping in two-dimensional photonic crystals designed in germanium
APPLIED SURFACE SCIENCE, (2015),355, pp.1186-1191, **2.711**, **0.549**
67. **Husanu MA**, **Popescu DG**, **Ganea CP**, Anghel I, **Florica C**
Correlation of optical reflectivity with numerical calculations for a two-dimensional photonic crystal designed in Ge
EUROPEAN PHYSICAL JOURNAL D, (2015),69, 273, **1.228**, **0.454**
68. **Husanu MA**, **Popescu DG**, **Tache CA**, **Apostol NG**, Barinov A, Lizzit S, Lacovig P, **Teodorescu CM**
Photoelectron spectroscopy and spectro-microscopy of Pb(Zr,Ti)O₃ (111) thin layers: Imaging ferroelectric domains with binding energy contrast
APPLIED SURFACE SCIENCE, (2015),352, pp.73-81, **2.711**, **0.549**

69. Iacob N, **Schinteie G, Palade P, Kuncser V**
Approach for an improved experimental evaluation of the specific absorption rate in magnetic fluid hyperthermia
JOURNAL OF NANOPARTICLE RESEARCH, (2015),17, 190, **2.184**, **0.596**
70. Iacob N, **Schinteie G, Palade P**, Ticos CM, **Kuncser V**
Stepped heating procedure for experimental SAR evaluation of ferrofluids
EUROPEAN PHYSICAL JOURNAL E, (2015),38, 57, **1.757**, **0.782**
71. Ionascu AM, Raikova G, Mladenova E, **Mercioniu I**
ELECTRICAL CONDUCTIVITY STUDIES OF SCANDIA DOPED CERIA CERAMIC COMPOSITES
DIGEST JOURNAL OF NANOMATERIALS AND BIOSTRUCTURES, (2015),10, pp.1275-1280, **0.945**, **0.202**
72. Ivanov VG, Vlahov ES, **Stan GE**, Zamfirescu M, Albu C, Mihailescu N, Negut I, Luculescu C, **Socol M**, Ristoscu C, Mihailescu IN
Surface-enhanced Raman scattering activity of niobium surface after irradiation with femtosecond laser pulses
JOURNAL OF APPLIED PHYSICS, (2015),118, 203104, **2.183**, **0.682**
73. Ivekovic A, **Galatanu A**, Novak S
Low-activation W-Si-C composites for fusion application
FUSION ENGINEERING AND DESIGN, (2015),100, pp.638-645, **1.152**, **0.358**
74. Jankovic A, Erakovic S, Ristoscu C, Mihailescu N, Duta L, Visan A, **Stan GE, Popa AC, Husanu MA**, Luculescu CR, Srdic VV, Janackovic D, Miskovic-Stankovic V, Bleotu C, Chifiriuc MC, Mihailescu IN
Structural and biological evaluation of lignin addition to simple and silver-doped hydroxyapatite thin films synthesized by matrix-assisted pulsed laser evaporation
JOURNAL OF MATERIALS SCIENCE-MATERIALS IN MEDICINE, (2015),26, 17, **2.587**, **0.585**
75. **Kuncser A, Kuncser V**
Magnetization reversal via a Stoner-Wohlfarth model with bi-dimensional angular distribution of easy axis
JOURNAL OF MAGNETISM AND MAGNETIC MATERIALS, (2015),395, pp.34-40, **1.97**, **0.483**
76. **Kuncser A, Schinteie G, Ghica C**, Antohe S, **Kuncser V**
Applicability of the Stoner-Wohlfarth model for Ni-Fe graded thin films
JOURNAL OF SUPERCONDUCTIVITY AND NOVEL MAGNETISM, (2015),28, pp.965-969, **0.909**, **0.19**
77. **Kuncser V**, Coman SM, Kemnitz E, Parvulescu VI
Magnetic nanocomposites for an efficient valorization of biomass
JOURNAL OF APPLIED PHYSICS, (2015),117, 17D724, **2.183**, **0.682**

78. Kupka K, **Tomut M**, Simon P, Hubert C, Romanenko A, Lommel B, Trautmann C
Intense heavy ion beam-induced temperature effects in carbon-based stripper foils
JOURNAL OF RADIOANALYTICAL AND NUCLEAR CHEMISTRY, (2015),305, pp.875-882, **1.034**, **0.196**
79. Lazarescu V, Toader AM, Enache M, Preda L, Anastasescu M, Dobrescu G, **Negrila CC, Lazarescu MF**
Field - dipole interactions in L-cysteine-thiolate self assembled at p- and n-GaAs(100) electrodes
ELECTROCHIMICA ACTA, (2015),176, pp.112-124, **4.504**, **0.886**
80. Lazea-Stoyanova A, Vlad A, **Vlaicu AM, Teodorescu VS**, Dinescu G
Synthesis of Copper Particles by non-thermal atmospheric pressure plasma jet
PLASMA PROCESSES AND POLYMERS, (2015),12, pp.705-709, **2.453**, **0.568**
81. Limongelli J, **Tolea F, Valeanu M, Diamandescu L**, Xu TH, Sorescu M
Nanostructured iridium oxide-hematite magnetic ceramic semiconductors
CERAMICS INTERNATIONAL, (2015),41, pp.333-343, **2.605**, **0.452**
82. Abt M, Affolder A, Aleev A, Allport PP, Altenheiner S, Andricek L, Arcidiacono R, Artuso M, Barabash L, Barber T, Barcz A, Bartosik MR, Baselga M, Bates R, Battaglia M, Bellan R, Benitez V, Bernardini J, Betancourt C, Bhardwaj A, Bilei GM, Blue A, Bohm J, Bomben M, Borrello L, Bosma MJ, Bowcock TJV, Broz J, Bruzzi M, Brzozowski A, Buhmann P, Buttar C, Calderini G, Carna M, Cartiglia N, Casse G, Centis-Vignali M, Charron S, Chauveau J, Chren D, Cihangir S, Cindro V, Collins P, Cortina Gil E, Creanza D, Crescioli F, Curras Rivera E, Dalal R, De Boer W, De Palma M, Dervan P, Dierlamm A, Dobos D, Doherty F, Dolenc Kittelmann I, Dolezal Z, Dolgolenko A, Donegani E, Driewer A, Dutta S, Eber R, Eckstein D, Eichhorn T, Eklund L, Eremin I, Eremin V, Erfle J, Esteban S, Fadeeva N, Fadeyev V, Feigl S, Fernandez M, Fiori F, Flaschel N, Fleta C, Flores D, **Pintilie L, Pintilie I, Nistor LC, Nistor SV, Lazanu S, Radu R, Boni AG**
The RD50 activity in the context of future pixel detector systems
JOURNAL OF INSTRUMENTATION, (2015),10, C05020, **1.399**, **0.483**
83. Abt M, Affolder A, Aleev A, Allport PP, Altenheiner S, Andricek L, Arcidiacono R, Artuso M, Barabash L, Barber T, Barcz A, Bartosik MR, Baselga M, Bates R, Battaglia M, Bellan R, Benitez V, Bernardini J, Betancourt C, Bhardwaj A, Bilei GM, Blue A, Bohm J, Bomben M, Borrello L, Bosma MJ, Bowcock TJV, Broz J, Bruzzi M, Brzozowski A, Buhmann P, Buttar C, Calderini G, Carna M, Cartiglia N, Casse G, Centis-Vignali M, Charron S, Chauveau J, Chren D, Cihangir S, Cindro V, Collins P, Cortina Gil E, Creanza D, Crescioli F, Curras Rivera E, Dalal R, De Boer W, De Palma M, Dervan P, Dierlamm A, Dobos D, Doherty F, Dolenc Kittelmann I, Dolezal Z, Dolgolenko A, Donegani E, Driewer A, Dutta S, Eber R, Eckstein D, Eichhorn T, Eklund L, Eremin I, Eremin V, Erfle J, Esteban S, Fadeeva N, Fadeyev V, Feigl S, Fernandez M, Fiori F, Flaschel N, Fleta C, Flores D, **Pintilie L, Pintilie I, Nistor LC, Nistor SV, Lazanu S, Radu R, Boni AG**
Silicon sensors for trackers at high-luminosity environment
NUCLEAR INSTRUMENTS & METHODS IN PHYSICS RESEARCH SECTION A-ACCELERATORS SPECTROMETERS DETECTORS AND ASSOCIATED EQUIPMENT, (2015), 796, pp.74-79, **1.216**, **0.415**

84. **Matei E, Florica C, Costas A**, Toimil-Molares ME, **Enculescu I**
Electrical properties of single CdTe nanowires
BEILSTEIN JOURNAL OF NANOTECHNOLOGY, (2015),6, pp.444-450, **2.67**, **0.877**
85. Merigeon J, Maalej O, Boulard B, **Stanculescu A**, Leontie L, Mardare D, Girtan M
Studies on Pr³⁺-Yb³⁺ codoped ZBLA as rare earth down convertor glasses for solar cells encapsulation
OPTICAL MATERIALS, (2015),48, pp.243-246, **1.981**, **0.468**
86. Mezey RS, Mathe I, Shova S, **Greacu MN**, Rosu T
Synthesis, characterization and antimicrobial activity of copper(II) complexes with hydrazone derived from 3-hydroxy-5-(hydroxymethyl)-2-methylpyridine-4-carbaldehyde
POLYHEDRON, (2015),102, pp.684-692, **2.011**, **0.33**
87. **Miclea CC, Amarande L, Cioanher M**, Miclea CT, Mihailescu M, Radu C, Ivanov A
Nanostructured titanium doped iron oxide photoelectrodes for water splitting
ROMANIAN JOURNAL OF INFORMATION SCIENCE AND TECHNOLOGY, (2015),18, pp.93-105, **0.304**, **0.099**
88. Miculescu F, Jepu I, **Stan GE**, Miculescu M, Voicu SI, Cotrut C, Pisu TM, Ciuca S
Tailoring the electric and magnetic properties of submicron-sized metallic multilayered systems by TVA atomic inter-diffusion engineered processes
APPLIED SURFACE SCIENCE, (2015),358, pp.619-626, **2.711**, **0.549**
89. Mihaiu S, Toader A, Atkinson I, Mocioiu OC, Hornoiu C, **Teodorescu VS**, Zaharescu M
Advanced ceramics in the SnO₂-ZnO binary system
CERAMICS INTERNATIONAL, (2015),41, pp.4936-4945, **2.605**, **0.452**
90. Mindru I, Gingasu D, Patron L, Marinescu G, Calderon-Moreno JM, **Diamandescu L**, Preda S, Oprea O
Chromium substituted copper ferrites via gluconate precursor route
CERAMICS INTERNATIONAL, (2015),41, pp.5318-5330, **2.605**, **0.452**
91. Miroiu FM, Stefan N, Visan AI, Nita C, Luculescu CR, **Rasoga O, Socol M, Zgura I**, Cristescu R, Craciun D, Socol G
Composite biodegradable biopolymer coatings of silk fibroin - Poly(3-hydroxybutyric-acid-co-3-hydroxyvaleric-acid) for biomedical applications
APPLIED SURFACE SCIENCE, (2015),355, pp.1123-1131, **2.711**, **0.549**
92. Miu DN, Jinga SI, Vasile BS, **Miu L**
Out of plane superferromagnetic behavior of quasi two-dimensional Fe/Al₂O₃ multilayer nanocomposites
JOURNAL OF APPLIED PHYSICS, (2015),117, 74303, **2.183**, **0.682**
93. **Miu L, Ionescu AM, Ivan I**, Miu D, Adachi T, Omori K, Koike Y
Behaviour of the second magnetization peak in La_{2-x}Sr_xCuO₄ single crystals upon entering the doping domain of static stripe order
PHYSICA C-SUPERCONDUCTIVITY AND ITS APPLICATIONS, (2015),519, pp.79-84, **0.942**, **0.297**

94. **Miu L**, Mele P, **Ivan I**, **Ionescu AM**, Miu D
DC magnetization relaxation and the AC susceptibility of YBCO films with strong inlining
JOURNAL OF SUPERCONDUCTIVITY AND NOVEL MAGNETISM, (2015),28, pp.361-365, **0.909**, **0.19**
95. Miyazaki A, Matsuda K, Papa F, Scurtu M, **Negrila CC**, Dobrescu G, Balint I
Impact of particle size and metal-support interaction on denitration behavior of well-defined Pt-Cu nanoparticles
CATALYSIS SCIENCE & TECHNOLOGY, (2015),5, pp.492-503, **5.426**, **1.171**
96. **Moldoveanu V**, **Dinu IV**, Tanatar B
Non-equilibrium transport and spin dynamics in single-molecule magnets
SUPERLATTICES AND MICROSTRUCTURES, (2015),87, pp.71-76, **2.097**, **0.371**
97. **Moldoveanu V**, **Dinu IV**, Tanatar B, Moca CP
Quantum turnstile operation of single-molecule magnets
NEW JOURNAL OF PHYSICS, (2015),17, 83020, **3.558**, **1.982**
98. Moragues A, **Neatu F**, Parvulescu VI, Marcos MD, Amoros P, Michelet V
Heterogeneous gold catalyst: synthesis, characterization, and application in 1,4-addition of boronic acids to enones
ACS CATALYSIS, (2015),5, pp.5060-5067, **9.312**, **2.283**
99. **Neatu F**, Ciobanu M, Stoflea LE, **Frunza L**, Parvulescu VI, Michelet V
Arylation of alkynes over hydrotalcite docked Rh-m-TPPTC complex
CATALYSIS TODAY, (2015),247, pp.155-162, **3.893**, **0.9**
100. Necula C, Panaiotu C, **Schinteie G**, **Palade P**, **Kuncser V**
Reconstruction of superparamagnetic particle grain size distribution from Romanian loess using frequency dependent magnetic susceptibility and temperature dependent Mossbauer spectroscopy
GLOBAL AND PLANETARY CHANGE, (2015),131, pp.89-103, **2.766**, **1.395**
101. **Negrea RF**, **Teodorescu VS**, **Ghica C**
Atomic scale elemental mapping of light elements in multilayered perovskite coatings
APPLIED SURFACE SCIENCE, (2015),355, pp.250-255, **2.711**, **0.549**
102. Nemnes GA, Goehry C, Mitran TL, Nicolaev A, Ion L, Antohe S, **Plugaru N**, Manolescu A
Band alignment and charge transfer in rutile-TiO₂/CH₃NH₃PbI₃-xCl_x interfaces
PHYSICAL CHEMISTRY CHEMICAL PHYSICS, (2015),17, pp.30417-30423, **4.493**, **1.209**
103. Nicula R, **Crisan O**, **Crisan AD**, **Mercioniu I**, Stir M, **Vasiliu F**
Thermal stability, thermal expansion and grain-growth in exchange-coupled Fe-Pt-Ag-B bulk nanocomposite magnets
JOURNAL OF ALLOYS AND COMPOUNDS, (2015),622, pp.865-870, **2.999**, **0.557**
104. **Nila AA**, Nemnes GA, Manolescu A
AB initio investigation of optical properties in triangular graphene - boron nitride core-shell nanostructures
ROMANIAN JOURNAL OF PHYSICS, (2015),60, pp.696-700, **0.924**, **0.165**

105. **Nistor SV, Stefan M**, Goovaerts E, Ramaz F, Briat B
Revealing the Cu²⁺ ions localization at low symmetry Bi sites in photorefractive Bi₁₂GeO₂₀ crystals doped with Cu and V by high frequency EPR
JOURNAL OF MAGNETIC RESONANCE, (2015),259, pp.87-94, **2.51**, **0.826**
106. **Nistor SV, Stefan M, Nistor LC, Ghica D, Vlaicu ID, Joita AC**
Doping ultrasmall cubic ZnS nanocrystals with Mn²⁺ ions over a broad nominal concentration range
JOURNAL OF PHYSICAL CHEMISTRY C, (2015),119, pp.23781-23789, **4.772**, **1.234**
107. **Ostahie B, Nita M, Aldea A**
Electrical manipulation of edge states in graphene and the effect on quantum Hall transport
PHYSICAL REVIEW B, (2015),91, 155409, **3.736**, **1.331**
108. **Palade C, Lepadatu AM, Slav A, Ciurea ML, Lazanu S**
Strain driven changes of defect parameters in heavy ion implanted Si
DIGEST JOURNAL OF NANOMATERIALS AND BIOSTRUCTURES, (2015),10, pp.1373-1381, **0.945**, **0.202**
109. Pana A, Badea FL, Ilis M, Staicu T, Micutz M, **Pasuk I**, Circu V
Effect of counterion on the mesomorphic behavior and optical properties of columnar pyridinium ionic liquid crystals derived from 4-hydroxypyridine
JOURNAL OF MOLECULAR STRUCTURE, (2015),1083, pp.245-251, **1.602**, **0.295**
110. Pana A, Chiriac FL, **Secu M, Pasuk I**, Ferbinteanu M, Micutz M, Circu V
A new class of thermotropic lanthanidomesogens: Eu(III) nitrate complexes with mesogenic 4-pyridone ligands
DALTON TRANSACTIONS, (2015),44, pp.14196-14199, **4.197**, **0.824**
111. Pellemoine F, Avilov M, Bender M, Ewing RC, Fernandes S, Lang M, Li WX, Mittig W, Schein M, Severin D, **Tomut M**, Trautmann C, Zhang FX
Study on structural recovery of graphite irradiated with swift heavy ions at high temperature
NUCLEAR INSTRUMENTS & METHODS IN PHYSICS RESEARCH SECTION B-BEAM INTERACTIONS WITH MATERIALS AND ATOMS, (2015),235, pp.522-524, **1.124**, **0.407**
112. **Pintilie L, Ghica C, Teodorescu CM, Pintilie I, Chirila C, Pasuk I, Trupina L, Hrib L, Boni AG, Apostol NG, Abramiuc LE, Negrea RF, Stefan M, Ghica D**
Polarization induced self-doping in epitaxial Pb(Zr_{0.20}Ti_{0.80})O₃ thin films
SCIENTIFIC REPORTS, (2015),5, 149740, **5.578**, **2.075**
113. **Polosan S, Ciobotaru IC**, Tsuboi T
Absorption, phosphorescence and Raman spectra of IrQ(ppy)₂ organometallic compound
MATERIALS CHEMISTRY AND PHYSICS, (2015),162, pp.822-830, **2.259**, **0.543**
114. **Polosan S, Negrea RF, Ciobotaru IC, Schinteie G, Kuncser V**
Ferromagnetic behaviour of bismuth germanate oxides glass-ceramic materials
JOURNAL OF ALLOYS AND COMPOUNDS, (2015),623, pp.192-196, **2.999**, **0.557**

115. Popa A, **Stan GE, Enculescu M**, Tanase C, Tulyaganov DU, Ferreira JMF
Superior biofunctionality of dental implant fixtures uniformly coated with durable bioglass films by magnetron sputtering
JOURNAL OF THE MECHANICAL BEHAVIOR OF BIOMEDICAL MATERIALS, (2015),51, pp.313-327, **3.417**, **0.936**
116. **Popa CL**, Andronescu E, Turculet C, Beuran M, Le Coustomer P, Badea ML, Surugiu A, Prodan AM
Preliminary histological studies on the influence of glycerol-iron-oxide nanoparticles
JOURNAL OF OPTOELECTRONICS AND ADVANCED MATERIALS, (2015),17, pp.1572-1576, **0.429**, **0.089**
117. **Popa CL, Bartha CM**, Albu M, Guegan R, Motelica-Heino M, Chifiriuc MC, Bleotu C, Badea ML, Antohe S
Synthesis, characterization and cytotoxicity evaluation on zinc doped hydroxyapatite in collagen matrix
DIGEST JOURNAL OF NANOMATERIALS AND BIOSTRUCTURES, (2015),10, pp.681-691, **0.945**, **0.202**
118. **Popa CL, Ciobanu CS**, Voicu G, Vasile E, Chifiriuc MC, **Iconaru SL, Predoi D**
Influence of thermal treatment on the antimicrobial activity of silver-doped biological apatite
NANOSCALE RESEARCH LETTERS, (2015),10, 502, **2.779**, **0.677**
119. **Popa CL**, Groza A, Chapon P, **Ciobanu CS, Ghita RV**, Trusca R, Ganciu M, **Predoi D**
Physicochemical analysis of the polydimethylsiloxane interlayer influence on a hydroxyapatite doped with silver coating
JOURNAL OF NANOMATERIALS, (2015), 250617, **1.644**, **0.371**
120. **Popa CL**, Prodan AM, Chapon P, Turculet C, **Predoi D**
Inhibitory effect evaluation of glycerol-iron oxide thin films on methicillin-resistant staphylococcus aureus
JOURNAL OF NANOMATERIALS, (2015), 465034, **1.644**, **0.371**
121. Popescu AC, **Stan GE**, Duta L, Nita C, Popescu C, Surdu VA, **Husanu MA**, Bitu B, Ghisleni R, Himcinschi C, Craciun V
The role of ambient gas and pressure on the structuring of hard diamond-like carbon films synthesized by pulsed laser deposition
MATERIALS, (2015),8, pp.3284-3305, **2.651**, **0.796**
122. **Popescu DG**, Barrett N, **Chirila C, Pasuk I, Husanu MA**
Influence of hole depletion and depolarizing field on the BaTiO₃/La_{0.6}Sr_{0.4}MnO₃ interface electronic structure revealed by photoelectron spectroscopy and first-principles calculations
PHYSICAL REVIEW B, (2015),92, 235442, **3.736**, **1.331**
123. **Popescu DG, Husanu MA, Trupina L, Hrib L, Pintilie L**, Barinov A, Lizzit S, Lacovig P, **Teodorescu CM**
Spectro-microscopic photoemission evidence of charge uncompensated areas in Pb(Zr,Ti)O₃(001) layers
PHYSICAL CHEMISTRY CHEMICAL PHYSICS, (2015),17, pp.509-520, **4.493**, **1.209**

124. Popescu LM, Piticescu RM, Petriceanu M, Ottaviani MF, Cangiotti M, Vasile E, Dirtu MM, Wolff M, Garcia Y, **Schinteie G, Kuncser V**
Hydrothermal synthesis of nanostructured hybrids based on iron oxide and branched PEI polymers. Influence of high pressure on structure and morphology
MATERIALS CHEMISTRY AND PHYSICS, (2015),161, pp.84-95, **2.259, 0.543**
125. **Popescu M, Lorinczi A, Sava F, Velea A, Simandan ID, Badica P, Burdusel M, Galca AC**, Socol G, Jipa F, Zamfirescu M
Thin films of amorphous Ga₂S₃ and rare-earth sulphides
MATERIALS LETTERS, (2015),142, pp.229-231, **2.489, 0.476**
126. **Popescu M, Sava F, Lorinczi A, Velea A, Simandan ID, Badica P, Burdusel M, Galca A, Matei E, Preda N, Secu M**, Socol G, Jipa F, Zamfirescu M, Balan A
Ceramics and amorphous thin films based on gallium sulphide doped by rare-earth sulphides
SEMICONDUCTOR SCIENCE AND TECHNOLOGY, (2015),30, 44001, **2.19, 0.669**
127. **Popescu T**, Lupu AR, Raditoiu V, Purcar V, **Teodorescu VS**
On the photocatalytic reduction of MU tetrazolium salt on the surface of TiO₂ nanoparticles: Formazan production kinetics and mechanism
JOURNAL OF COLLOID AND INTERFACE SCIENCE, (2015),457, pp.108-120, **3.368, 0.827**
128. Popescu-Pelin G, Craciun D, Socol G, Cristea D, Floroian L, Badea M, **Socol M**, Craciun V
Investigations of pulsed laser deposited TiN thin films for titanium implants
ROMANIAN REPORTS IN PHYSICS, (2015),67, pp.1491-1502, **1.517, 0.21**
129. **Preda N, Evanghelidis A, Enculescu M, Florica C, Enculescu I**
Zinc oxide electroless deposition on electrospun PMMA fiber mats
MATERIALS LETTERS, (2015),138, pp.238-242, **2.489, 0.476**
130. Predoana L, Jitianu A, Voicescu M, **Apostol NG**, Zaharescu M
Study of formation of LiCoO₂ using a modified Pechini aqueous sol-gel process
JOURNAL OF SOL-GEL SCIENCE AND TECHNOLOGY, (2015),74, pp.406-418, **1.532, 0.339**
131. Prioteasa I, Porosnicu C, Lungu CP, Jepu I, **Schinteie G**, Ciupina V, Prodan G, Vasile E, Dinca P
GMR on CuNiCo thin layers deposited using tva method
DIGEST JOURNAL OF NANOMATERIALS AND BIOSTRUCTURES, (2015),10, pp.429-436, **0.945, 0.202**
132. Racu AV, Ursu DH, Kuliukova OV, **Logofatu C, Leca A**, Miclau M
Direct low temperature hydrothermal synthesis of YFeO₃ microcrystals
MATERIALS LETTERS, (2015),140, pp.107-110, **2.489, 0.476**
133. **Radu R, Pintilie I, Nistor LC**, Fretwurst E, Lindstroem G, Makarenko LF
Investigation of point and extended defects in electron irradiated silicon-Dependence on the particle energy
JOURNAL OF APPLIED PHYSICS, (2015),117, 164503, **2.183, 0.682**

134. Rusen E, Mocanu A, **Nistor LC**, Hudhomme P, Diacon A
Anionic polymerization by an electron transfer process from a CdSe quantum dot-perylenediimide (PDI) system
RSC ADVANCES, (2015),5, pp.28228-28232, **3.84**, **0.747**
135. Satulu V, Ion V, **Aldica G**, Mitu B, Dinescu G
In-situ iodine doped polythiophene-like thin films obtained by post-discharge rf plasma
ROMANIAN JOURNAL OF PHYSICS, (2015),60, pp.1550-1560, **0.924**, **0.165**
136. Scarisoreanu M, Morjan I, Fleaca CT, Morjan IP, Niculescu AM, Dutu E, Badoi A, Birjega R, Luculescu C, Vasile E, Danciu V, **Filoti G**
Synthesis and optical properties of TiO₂-based magnetic nanocomposites
APPLIED SURFACE SCIENCE, (2015),336, pp.335-342, **2.711**, **0.549**
137. Scarisoreanu ND, Craciun F, Moldovan A, Ion V, Birjega R, **Ghica C**, **Negrea RF**, Dinescu M
High permittivity (1-x)Ba(Zr_{0.2}Ti_{0.8})O₃ - x(Ba_{0.7}Ca_{0.3})TiO₃ (x=0.45) epitaxial thin films with nanoscale phase fluctuations
ACS APPLIED MATERIALS & INTERFACES, (2015),7, pp.23984-23992, **6.723**, **1.373**
138. **Schinteie G**, **Greculeasa SG**, **Palade P**, **Lungu GA**, Porosnicu C, Jepu I, Lungu CP, **Filoti G**, **Kuncser V**
Effects of annealing in Be/W and Be/C bilayers deposited on Si(001) substrates with Fe buffer layers
JOURNAL OF NUCLEAR MATERIALS, (2015),457, pp.220-226, **1.865**, **0.636**
139. **Secu CE**, **Secu M**
Luminescence properties of Eu³⁺-doped SiO₂-LiYF₄ glass-ceramic microrods
OPTICAL MATERIALS, (2015),47, pp.95-98, **1.981**, **0.468**
140. **Secu M**, **Cernea M**, **Secu CE**, Vasile BS
Structural and optical properties of fluorescent BaFBr-Eu²⁺@SiO₂ core/shell phosphor heterostructure
MATERIALS CHEMISTRY AND PHYSICS, (2015),151, pp.81-86, **2.259**, **0.543**
141. **Secu M**, **Secu CE**
Up-conversion luminescence of Er³⁺/Yb³⁺ co-doped LiYF₄ nanocrystals in sol-gel derived oxyfluoride glass-ceramics
JOURNAL OF NON-CRYSTALLINE SOLIDS, (2015),426, pp.78-82, **1.766**, **0.438**
142. **Sima M**, **Baibarac M**, Vasile E, **Sima AM**, **Mihut L**
Fabrication and Raman scattering of a core-shell structure based on Mn doped ZnO and barium titanate
APPLIED SURFACE SCIENCE, (2015),355, pp.1057-1062, **2.711**, **0.549**
143. **Sima M**, **Mihut L**, Vasile E, **Sima AM**, **Logofatu C**
Optical properties of Mn doped ZnO films and wires synthesized by thermal oxidation of ZnMn alloy
THIN SOLID FILMS, (2015),590, pp.141-147, **1.759**, **0.456**
144. **Sima M**, Vasile E, **Sima AM**
Organic-inorganic solar cell based on ZnO nanorod arrays

JOURNAL OF OPTOELECTRONICS AND ADVANCED MATERIALS, (2015),17, pp.1309-1313, **0.429**, **0.089**

145. **Simion CE**, Sackmann A, **Teodorescu VS**, Rusti CF, **Stanoiu A**
Room temperature ammonia sensing with barium strontium titanate under humid air background
SENSORS AND ACTUATORS B-CHEMICAL, (2015),220, pp.1241-1246, **4.097**, **0.754**
146. **Smaranda I**, **Baibarac M**, **Ilie M**, **Matea A**, **Baltog I**, Lefrant S
Optical properties of single-walled carbon nanotubes functionalized with poly(2,2'-bithiophene-co-pyrene) copolymer
CURRENT ORGANIC CHEMISTRY, (2015),19, pp.652-661, **2.157**, **0.589**
147. **Socol M**, **Rasoga O**, **Breazu C**, Socol G, **Preda N**, **Pasuk I**, Visan D, **Stavarache I**, Gherendi F, Girtan M, Sidwaba U
HETEROSTRUCTURES BASED ON SMALL MOLECULES ORGANIC COMPOUNDS
DIGEST JOURNAL OF NANOMATERIALS AND BIOSTRUCTURES, (2015),10, pp.1383-1392, **0.945**, **0.202**
148. **Sofronie M**, Elisa M, Sava BA, Boroica L, **Valeanu M**, **Kuncser V**
Rapid determination of Faraday rotation in optical glasses by means of secondary Faraday modulator
REVIEW OF SCIENTIFIC INSTRUMENTS, (2015),86, 53905, **1.614**, **0.586**
149. **Sofronie M**, **Tolea F**, **Kuncser V**, **Valeanu MC**, **Filoti G**
Magneto-structural properties and magnetic behavior of Fe-Pd ribbons
IEEE TRANSACTIONS ON MAGNETICS, (2015),51, 2500404, **1.386**, **0.403**
150. Somacescu S, Florea M, Osiceanu P, Calderon-Moreno JM, **Ghica C**, Serra JM
Ni-doped (CeO₂-delta)-YSZ mesoarchitectured with nanocrystalline framework: the effect of thermal treatment on structure, surface chemistry and catalytic properties in the partial oxidation of methane (CPOM)
JOURNAL OF NANOPARTICLE RESEARCH, (2015),17, 426, **2.184**, **0.596**
151. Sorescu M, **Diamandescu L**, DiGnazio J, Xu TH
Structural, thermal, Fe-57 and Eu-151 Mossbauer studies of Eu₂O₃-Fe₂O₃ ceramic nanostructures
CERAMICS INTERNATIONAL, (2015),41, pp.1579-1588, **2.605**, **0.452**
152. Staicu T, Circu V, Ionita G, **Ghica C**, Popa VT, Micutz M
Analysis of bimodal thermally-induced denaturation of type I collagen extracted from calfskin
RSC ADVANCES, (2015),5, pp.38391-38406, **3.84**, **0.747**
153. **Stan GE**, **Botea M**, **Boni GA**, **Pintilie I**, **Pintilie L**
Electric and pyroelectric properties of AlN thin films deposited by reactive magnetron sputtering on Si substrate
APPLIED SURFACE SCIENCE, (2015),353, pp.1195-1202, **2.711**, **0.549**

154. Stanculescu F, **Rasoga O**, Catargiu AM, Vacareanu L, **Socol M**, **Breazu C**, **Preda N**, Socol G, **Stanculescu A**
MAPLE prepared heterostructures with arylene based polymer active layer for photovoltaic applications
APPLIED SURFACE SCIENCE, (2015),336, pp.240-248, **2.711**, **0.549**
155. Stange D, Wirths S, den Driesch NV, Mussler G, **Stoica T**, Ikonc Z, Hartmann JM, Mantl S, Grutzmacher D, Buca D
Optical transitions in direct-bandgap Ge_{1-x}Sn_x alloys
ACS PHOTONICS, (2015),2, pp.1539-1545, **0**
156. Stratulat A, Serban BC, de Luca A, Avramescu V, Cobianu C, Brezeanu M, Buiu O, **Diamandescu L**, **Feder M**, Ali SZ, Udrea F
Low power resistive oxygen sensor based on sonochemical SrTi_{0.6}Fe_{0.4}O_{2.8} (STFO40)
SENSORS, (2015),15, pp.17495-17506, **2.245**, **0.566**
157. Stroh C, **Tolea F**, **Valeanu M**, **Diamandescu L**, Xu TH, Sorescu M
Ruthenium oxide-hematite magnetic ceramic nanostructures
CERAMICS INTERNATIONAL, (2015),41, pp.14367-14375, **2.605**, **0.452**
158. **Teodorescu CM**
Image molecular dipoles in surface enhanced Raman scattering
PHYSICAL CHEMISTRY CHEMICAL PHYSICS, (2015),17, pp.21302-21314, **4.493**, **1.209**
159. **Teodorescu VS**, **Ghica C**, **Maraloiu AV**, **Vlaicu M**, **Kuncser A**, **Ciurea ML**, **Stavarache I**, **Lepadatu AM**, Scarisoreanu ND, Andrei A, Ion V, Dinescu M
Nanostructuring of GeTiO amorphous films by pulsed laser irradiation
BEILSTEIN JOURNAL OF NANOTECHNOLOGY, (2015),6, pp.893-900, **2.67**, **0.877**
160. **Tolea F**, **Grecu MN**, **Kuncser V**, **Constantinescu SG**, **Ghica D**
On the role of Fe ions on magnetic properties of doped TiO₂ nanoparticles
APPLIED PHYSICS LETTERS, (2015),106, 142404, **3.302**, **1.125**
161. **Tolea F**, **Sofronie M**, **Crisan AD**, **Enculescu M**, **Kuncser V**, **Valeanu M**
Effect of thermal treatments on the structural and magnetic transitions in melt-spun Ni-Fe-Ga-(Co) ribbons
JOURNAL OF ALLOYS AND COMPOUNDS, (2015),650, pp.664-670, **2.999**, **0.557**
162. **Tolea F**, **Sofronie M**, **Tolea M**, **Kuncser V**, **Valeanu M**
Shape memory properties of FeNiCoTi ribbons evidenced by magnetic measurements
DIGEST JOURNAL OF NANOMATERIALS AND BIOSTRUCTURES, (2015),10, pp.567-575, **0.945**, **0.202**
163. **Tolea F**, **Tolea M**
Hearing shapes of few electrons quantum drums: A configuration-interaction study
PHYSICA B-CONDENSED MATTER, (2015),458, pp.85-91, **1.319**, **0.309**
164. **Tolea F**, **Tolea M**, **Sofronie M**, **Valeanu M**
Distribution of plates' sizes tell the thermal history in a simulated martensitic-like phase transition
SOLID STATE COMMUNICATIONS, (2015),213, pp.37-41, **1.897**, **0.54**

165. Tyunina M, **Pintilie I**, Levoska J, **Pintilie L**
Quasi-static electric field-temperature diagrams in epitaxial relaxor ferroelectric films
PHASE TRANSITIONS, (2015),88, pp.74-81, **0.954**, **0.266**
166. Ulmeanu M, Petkov P, Ursescu D, **Maraloiu AV**, Jipa F, Brousseau E, Ashfold MNR
Pattern formation on silicon by laser-initiated liquid-assisted colloidal lithography
NANOTECHNOLOGY, (2015),26, 455303, **3.821**, **1.041**
167. Vajda K, Kasa Z, Dombi A, Nemeth Z, Kovacs G, Danciu V, Radu T, **Ghica C**, Baia L, Hernadi K, Pap Z
Crystallographic holes: new insights for a beneficial structural feature for photocatalytic applications
NANOSCALE, (2015),7, pp.5776-5786, **7.394**, **1.74**
168. Vasilescu CA, **Trupina L**, Vasile BS, Trusca R, **Cernea M**, Ianculescu AC
Characteristics of 5 mol% Ce³⁺-doped barium titanate nanowires prepared by a combined route involving sol-gel chemistry and polycarbonate membrane-templated process
JOURNAL OF NANOPARTICLE RESEARCH, (2015),17, 434, **2.184**, **0.596**
169. **Velea A**, Socol G, **Popescu M**, **Galca AC**
In-situ characterization of the optical and electronic properties in GeTe and GaSb thin films
JOURNAL OF APPLIED PHYSICS, (2015),118, 135712, **2.183**, **0.682**
170. Visinescu D, Scurtu M, **Negrea RF**, Birjega R, Culita DC, Chifiriuc MC, Draghici C, Moreno JC, Musuc AM, Balint I, Carp O
Additive-free 1,4-butanediol mediated synthesis: a suitable route to obtain nanostructured, mesoporous spherical zinc oxide materials with multifunctional properties
RSC ADVANCES, (2015),5, pp.99976-99989, **3.84**, **0.747**
171. Voicescu M, Craciunescu O, Moldovan L, Anastasescu M, Angelescu DG, **Teodorescu VS**
Physicochemical characterization and in vitro cytotoxic effect of 3-hydroxyflavone in a silver nanoparticles complex
JOURNAL OF FLUORESCENCE, (2015),25, pp.1215-1223, **1.927**, **0.366**
172. von den Driesch N, Stange D, Wirths S, Mussler G, Hollander B, Ikonik Z, Hartmann JM, **Stoica T**, Mantl S, Grutzmacher D, Buca D
Direct bandgap group IV epitaxy on Si for laser applications
CHEMISTRY OF MATERIALS, (2015),27, pp.4693-4702, **8.354**, **2.2**
173. **Zgura I**, **Frunza S**, **Enculescu M**, **Florica C**, Cotorobai F
Deposition of titanium dioxide layers upon polyester textile materials: checking the adherence by ultra-sonication
ROMANIAN JOURNAL OF PHYSICS, (2015),60, pp.488-494, **0.924**, **0.165**
174. **Zgura I**, **Frunza S**, **Frunza L**, **Enculescu M**, **Florica C**, **Ganea CP**, **Negrila CC**, **Diamandescu L**
Titanium dioxide layer deposited at low temperature upon polyester fabrics
JOURNAL OF OPTOELECTRONICS AND ADVANCED MATERIALS, (2015),17, pp.1055-1063, **0.429**, **0.089**

Conference Proceedings

1. Miculescu F, Jepu I, Stan GE et al. **Tailoring the electric and magnetic properties of submicron-sized metallic multilayered systems by TVA atomic inter-diffusion engineered processes** In: Conference: 9th International Conference on Materials Science and Engineering (BRAMAT) Location: Transilvania Univ, Sergiu T Chiriacescu Aula, Brasov, ROMANIA Date: MAR 05-07, 2015 APPLIED SURFACE SCIENCE Volume: 358 Pages: 619-626 Part: B Published: DEC 15 2015
2. Husanu MA, Popescu DG, Tache CA et al. **Photoelectron spectroscopy and spectro-microscopy of Pb(Zr,Ti)O-3 (111) thin layers: Imaging ferroelectric domains with binding energy contrast** In: Conference: 10th International Conference on Physics of Advanced Materials (ICPAM) Location: Iasi, ROMANIA Sponsor(s): Romanian Minist Educ & Res; NanoAndMore; ExpressCredit; Amer Elements; ArcelorMittal Tubular Prod Iasi; Agilrom Sci; Schaefer SE Europe; PIM Copy; Histeresis; ApeLaser; Nitech; Technosteel LBR; Thorlabs GmbH; MaTeck; Sartorom; Antalis; Emfutur; Romanian Phys Soc Date: SEP 22-28, 2014, APPLIED SURFACE SCIENCE Volume: 352 Pages: 73-81 Published: OCT 15 2015
3. Dias M, Guerreiro F, Correia JB et al. **Consolidation of W-Ta composites: Hot isostatic pressing and spark and pulse plasma sintering** In: Conference: 28th Symposium on Fusion Technology (SOFT) Location: San Sebastian, SPAIN Sponsor(s): Spanish Res Ctr Energy Environm & Technol Date: SEP 29-OCT 03, 2014, FUSION ENGINEERING AND DESIGN Volume: 98-99 Pages: 1950-1955 Part: B Published: OCT 2015
4. Tolea F, Crisan AD, Sofronie M et al. **Magnetic and martensitic transformations in the bulk and melt spun ribbons of Ni_{57-x}Nd_xFe₁₈Ga₂₅ ferromagnetic shape memory alloys** In: Conference: 14th International Conference on Martensitic Transformations (ICOMAT) Location: Bilbao, SPAIN Sponsor(s): Univ Basque Country UPV EHU Date: JUL 06-11, 2014, MATERIALS TODAY-PROCEEDINGS Volume: 2 Supplement: 3 Pages: 875-878 Published: 2015

5. Tusa L, Nicolaescu I, Moni M et al. **Time-frequency domain radar cross section evaluation of an iar 99 scaled model aircraft** In: Conference: 7th International Conference on Electronics, Computers and Artificial Intelligence (ECAI) Location: Bucharest, ROMANIA
Sponsor(s): IEEE Romania section; IEEE Industry Applications Society; Univ Pitesti; Univ Europei Sud Est Lumina; Ministerul Educatiei Cercetarii Stiintifice
PROCEEDINGS OF THE 2015 7TH INTERNATIONAL CONFERENCE ON ELECTRONICS, COMPUTERS AND ARTIFICIAL INTELLIGENCE (ECAI) Book Series: International Conference on Electronics Computers and Artificial Intelligence
Date: JUN 25-27, 2015
Published: 2015

6. Bartha C, Plapcianu C, Palade P et al. **Model-free kinetic analysis of Sr₂FeMoO₆ Recrystallization process used for double-perovskite monocrystals grown by Bridgman Method**
Edited by: Vizman, D; Popescu, A In: Conference: TIM Physics Conference on Physics without Frontiers Location: W Univ Timisoara, Timisoara, ROMANIA
Sponsor(s): Cent European Initiat TIM14 PHYSICS CONFERENCE: PHYSICS WITHOUT FRONTIERS Book Series: AIP Conference Proceedings Volume: 1694 Article
Number: UNSP 040006
Date: NOV 20-22, 2014
Published: 2015

7. Dragomir R, Moldoveanu V, Dinu IV **Intraband relaxation of p-shell excitons in disk-shaped quantum dots** In: Conference: 2nd Conference on Advanced Many-Body and Statistical Methods in Mesoscopic Systems Location: Transilvania Univ Brasov, Brasov, ROMANIA
Sponsor(s): IFIN HH; Romanian Natl Author Sci Res ROMANIAN JOURNAL OF PHYSICS Volume: 60 Issue: 5-6 Pages: 686-690
Date: SEP 01-05, 2014
Published: 2015

8. Nila AA, Nemnes GA, Manolescu A
AB initio investigation of optical properties in triangular graphene - boron nitride core-shell nanostructures In: Conference: 2nd Conference on Advanced Many-Body and Statistical Methods in Mesoscopic Systems Location: Transilvania Univ Brasov, Brasov, ROMANIA
Sponsor(s): IFIN HH; Romanian Natl Author Sci Res ROMANIAN JOURNAL OF PHYSICS Volume: 60 Issue: 5-6 Pages: 696-700
Date: SEP 01-05, 2014
Published: 2015

Contributed Presentations

1. *Alexandru HV, Mindru C, **Ganea CP**, Vineticu N*
Dielectric spectroscopy in ferroelectric relaxation of TGS crystal
The 8th International Conference on Advanced Materials, Bucharest, Romania
7-10 July 2015, Talk
2. ***Aldica G, Sandu V, Popa S, Enculescu M, Badica P***
Bulk and tape MgB₂ superconductor co-added with SiC and Te processed by ex-situ spark plasma sintering
EUCAS 2015, Lyon, France
6-10 September 2015, Poster
3. ***Aldica G, Matei C, Paun A, Batalu D, Ferbinteanu M, Badica P***
Thermal analysis on C₆H₁₀Ge₂O₇ – doped MgB₂ superconductor
3rd Central and Eastern European Conference on Thermal Analysis and Calorimetry (CEEC-TAC3), Ljubljana, Slovenia
25-28 August 2015, Poster
4. ***Aldica G, Matei C, Paun A, Batalu D, Ferbinteanu M, Badica P***
Thermal decomposition of C₆H₁₀Ge₂O₇
3rd Central and Eastern European Conference on Thermal Analysis and Calorimetry (CEEC-TAC3) Ljubljana, Slovenia
25-28 August 2015, Poster
5. *Antonova K, Szekeeres A, Duta L, **Stan GE**, Mihailescu N, Mihailescu IN*
Orientation of the nanocrystallites in aluminum nitride thin films determined by Fourier Transform InfraRed spectroscopy
INERA Conference 2015, Hisarya, Bulgaria
20–22 October 2015, Poster
6. ***Banciu MG, Nedelcu L, Geambasu DC, Nicolaescu I***
Terahertz investigations of BST and KDP ferroelectric materials
COST-VISTA IC1102 workshop, Focus area B „mm waves, THz and nano-antennas”, Sofia, Bulgaria
18-20 May 2015, Talk
7. ***Banciu MG, Nedelcu L, Geambasu DC***
Method to improve the characteristics of dielectric resonator antennas
8th International Conference on Advanced Materials, ROCAM 2015, Bucharest, Romania
7-10 July 2015, Talk
8. ***Banciu MG, Nedelcu L, Alexandru HV, Furuya T, Tani M***
Investigations on dielectric parameters of some ferroelectric materials in Terahertz waves
Second International Symposium on Frontiers in THz Technology FTT 2015, Hamamatsu – Shizuoka, Japan
30 August – 02 September 2015, Poster

9. **Banciu MG, Nedelcu L, Geambasu DC**
Influence of the ferroelectric materials properties on the characteristics of the microwave antennas
COST-VISTA IC1102 meeting, Work Group 3, Villefranche-sur-Mer, France
21-23 October 2015, Talk
10. **Bartha C**
Heteronuclear oxides containing iron and lanthanides used for growing by Bridgman method of the monocrystals
EMRS Spring, Lille, France
10-15 May 2015, Poster
11. **Bartha C**
Thermokinetics and electronic properties of LaFeO_3 polycrystalline used for monocrystals processed by Bridgman method
14th International Conference - European Ceramic Society, Toledo, Spain
21-25 June 2015, Poster
12. **Batalu D, Burdusel M, Popa S, Enculescu M, Pasuk I, Aldica G, Badica P**
Enhancement of the critical current density by $\text{Ge}_2\text{C}_6\text{H}_{10}\text{O}_7$ addition into MgB_2 superconductor obtained by ex-situ Spark Plasma Sintering
EUCAS 2015, Lyon, France
6-10 September 2015, Poster
13. **Beregoi M, Busuioc C, Evanghelidis A, Matei E, Enculescu I**
Electrical activity and electrochromic properties of polyaniline-coated fiber networks for tissue engineering applications
The 8th International Conference on Advanced Materials, Bucharest, Romania
7-10 July 2015, Poster
14. **Beregoi M, Busuioc C, Evanghelidis A, Matei E, Enculescu I**
Polyaniline - coated electrospun fibers for electrochromic applications
6th International Conference on Nanotechnology: Fundamentals and Applications, Barcelona, Spain
14-18 July 2015, Talk
15. **Beregoi M, Iovu H, Busuioc C, Evanghelidis A, Matei E, Enculescu M, Enculescu I**
Synthesis of smart materials based on polyaniline coated fibers
17th International Conference on Materials Science and Engineering – ICMSE 2015 Londra, UK
22-25 October 2015, Poster
16. **Besleaga C, Stancu V, Tomulescu A, Sima M, Pintilie L, Pintilie I, Radu A, Iftimie S, Ion L, Antohe S**
Stability in perovskite solar cells
8th International Conference on Advanced Materials, ROCAM 2015, Bucharest, Romania
7–10 July 2015, Poster
17. **Besleaga C, Galca AC, Trinca LM**
Characterization of amorphous oxide semiconductor thin films by X-ray reflectivity
EMRS Spring Meeting, Lille, France
11-15 May 2015, Poster

18. **Besleaga C, Stancu V, Tomulescu AG, Sima M, Trinca LM, Stan GE, Galca AC, Pintilie L, Pintilie I, Radu A, Iftimie S, Ion L, Antohe S, Nemnes A, Goehry C, Manolescu A**
Hybrid perovskite solar cells: aging effects and reliability
8th International Conference on Advanced Materials, ROCAM 2015, Bucharest, Romania
7-10 July 2015, Poster
19. **Birsan A, Palade P, Kuncser V**
The stability of half-metallic properties for the Zr₂CoIn full-heusler compound
15th International Balkan Workshop on Applied Physics, Constanta, Romania
2-4 July 2015, Poster
20. **Birsan A**
The effect of the main group elements on the half metallic properties in scandium based heusler compounds
8th International Conference on Advanced Materials”, ROCAM, Bucharest, Romania
7-10 July 2015, Poster
21. **Birsan A, Palade P, Kuncser V**
Prediction of half-metallic ferromagnetism in zirconium based full-heusler compounds
8th International Conference on Advanced Materials”, ROCAM, Bucharest, Romania
7-10 July 2015, Talk
22. **Birzu M, Frunza L, Zgura I, Frunza S, Ganea CP, Diamandescu L, Cotorobai VF**
Complex treatment to make new surface functionalization of some wool textiles
The 8th International Conference on Advanced Materials, Bucharest, Romania
7-10 July 2015, Poster
23. **Boni AG, Chirila C, Pasuk I, Trupina L, Negrea R, Pintilie I, Pintilie L**
Investigation of the structural, magnetic and electrical/ferroelectric properties of Pb(Zr_{0.2}Ti_{0.8})O₃/CoFe₂O₄ multiferroic structures with two different metallic conductive bottom electrodes
EMRS Spring Meeting, Lille, France
11-15 May 2015, Talk
24. **Boni AG, Chirila C, Hrib L, Greculeasa S, Kuncser V, Pasuk I, Trupina L, Negrea R, Pintilie I, Pintilie L**
The study of structural, magnetic and electric/ferroelectric properties in epitaxial multiferroic heterostructures based on PZT/CFO grown by PLD
8th International Conference on Advanced Materials, ROCAM 2015, Bucharest, Romania
7-10 July 2015, Poster
25. **Botea M, Iuga A, Chirila C, Boni AG, Pintilie L**
Enhancing the pyroelectric effect of epitaxial Pb(Zr_{0.2}Ti_{0.8})O₃ structures
EMRS Spring Meeting, Lille, France
11-15 May 2015, Talk
26. **Botea M, Pintilie L, Pintilie I, Stancu V**
Silicon substrate influence on pyroelectric behavior of Pb(Zr,Ti)O₃ thin films
8th International Conference on Advanced Materials, ROCAM 2015, Bucharest, Romania
7-10 July 2015, Poster

27. **Breazu C, Dragoman D**
Transfer matrix scattering theory for optimization of plasmonic nanostructured organic solar cells,
The International Conference of Differential Geometry and Dynamical Systems (DGDS-2015),
University Politehnica of Bucharest, Romania
8-11 October 2015, Poster
28. **Breazu C, Socol M, Albu A-M, Girtan M, Stanculescu A, Stanculescu F**
Effect of maleic anhydride-aniline derivatives monomers buffer layer on the properties of
pentacene (rubrene)/ Pbd (TPyP) Bi-layer organic structures
The 8th International Conference on Advanced Materials, Bucharest, Romania
7-10 July 2015, Talk
29. **Burdusel M**
Superconducting composite materials based on MgB₂ obtained by Spark Plasma Sintering
ECERS Students speech contest, Toledo, Spain,
21-25 June 2015, Talk
30. **Ciobanu CS, Popa CL, Prodan AM, Turculeț C, Iconaru SL, Surugiu A, Le Coustumer P, Predoi D**
Photoluminescence and antimicrobial activity of Ag or Eu doped hydroxyapatite powders
15th European Conference on Solid State Chemistry, Viena, Austria
23-26 August 2015, Poster
31. **Ciobanu CS, Prodan AM, Turculeț C, Iordache F, Iconaru SL, Popa CL, Badea ML, Predoi D**
Optical properties and antimicrobial activity evaluation of europium/silver doped hydroxyapatite
nanoparticles
EUROTOX 2015, Porto, Portugal
13-16 September 2015, Poster
32. **Costas A, Florica C, Matei E, Enculescu M, Pintilie L, Pintilie I, Enculescu I**
Transport properties of templateless electrodeposited ZnO nanowires on metallic interdigitated
electrodes
3rd Euro-Mediterranean Conference on Materials and Renewable Energies, EMCMRE-3,
Marrakech, Morocco
2-6 November 2015, Talk
33. **Costas A, Florica C, Matei E, Enculescu M, Pintilie L, Pintilie I, Enculescu I**
Transport properties of templateless electrodeposited ZnO nanowires
The 8th International Conference on Advanced Materials, Bucharest, Romania
7-10 July 2015, Talk
34. **Crisan AD, Vasiliu F, Mercioniu I, Crisan O**
New trends in nanocomposite magnets based on FePt systems
Proceedings of the Workshop on Micro and Nanotechnology of Novel Devices and Scaling,
Colloque MINOS 2015
16-18 March 2015, Poster
35. **Crisan AD, Palade P, Vasiliu F, Mercioniu I, Crisan O**
Surface and morphology modification by high pressure nitriding of FePt
based nanocomposite magnets”
Proceedings of the European materials research society spring meeting E-MRS 2015
11-15 May 2015, Poster

36. **Diamandescu L, Feder M, Vasiliu F, Tanase L, Teodorescu CM, Popescu T, Dumitrescu I**
Hydrothermal route to (Fe, N) codoped titania photocatalysts with increased visible light activity;
7th Texteh International Conference, Bucharest, Romania
22-23 October 2015, Talk
37. **Dinescu M, Scarisoreanu ND, Andrei A, Teodorescu VS, Ghica C, Maraloiu AV, Lepadatu AM, Stavarache I, Ciurea ML**
Fast atomic diffusion in solid state amorphous thin films irradiated with low fluence laser pulse in UV
13th Conference on Laser Ablation COLA 2015, Australia
31 August - 4 September, Poster
38. **Dumitrescu I, Dinca L, Diamandescu L, Feder M, Iordache OG**
Enhanced photocatalytic degradation of textile fabrics coated with (Fe, N) codoped TiO₂;
7th Texteh international conference, Bucharest, Romania,
22-23 October 2015, Talk
39. **Duta L, Stan GE, Anastasescu M, Stroescu H, Gartner M, Fogarassy Zs, Mihailescu N, Szekeres A, Bakalova S, Mihailescu IN**
Structural and morphological characterization of Aluminum Nitride multi-layers synthesized by Pulsed Laser Deposition at different temperatures
7th International Workshop on “Advanced optical and X-ray characterization techniques of multifunctional materials for information and communication technologies, health and renewable energy applications”, Bucharest, Romania
16–18 September 2015, Talk
40. **Duta L, Stan GE, Anastasescu M, Stroescu H, Gartner M, Fogarassy Zs, Mihailescu N, Luculescu C, Bakalova S, Szekeres A, Mihailescu IN**
Structural, optical and vibrational properties of nanostructured aluminum nitride films synthesized by multi-stage pulsed laser deposition
VEIT Conference 2015, Sozopol, Bulgaria
21–25 September 2015, Poster
41. **Dutheil P, Dumas-Bouchiat F, Goldner-Constantinescu C, Quignon S, Marchet P, Champeaux C, Rammal M, Huitema L, Crunteanu A, Passerieux D, Cros D, Monédière T, Madrangeas V, Nedelcu L, Trupina L, Banciu G, Cernea M**
(Ba,Sr)TiO₃ thin films integrated in miniature antenna
EMRS Spring Meeting, Lille, France
11-15 May 2015, Poster
42. **Dutheil P, Dumas-Bouchiat F, Goldner-Constantinescu C, Quignon S, Marchet P, Champeaux C, Rammal M, Huitema L, Crunteanu A, Passerieux D, Cros D, Monédière T, Madrangeas V, Nedelcu L, Trupina L, Banciu G, Cernea M**
Tunable thin films (Ba,Sr)TiO₃ and multilayers for miniature antenna
14th International Conference of European Ceramic Society, Toledo, Spain
21-25 June 2015, Talk

43. *Dutheil P, Dumas-Bouchiat F, Goldner-Constantinescu C, Quignon S, Marchet P, Champeaux C, Rammal M, Huitema L, Crunteanu A, Passerieux D, Cros D, Monédière T, Madrangeas V, Nedelcu L, Trupina L, Banciu G, Cernea M*
Ferroelectric thin films deposited by PLD for tunable capacitors
20th International Colloquium on Plasma Processes, Saint –Etienne, France
1-5 June 2015, Poster
44. *Enculescu I, Matei E, Costas A, Florica C, Enculescu M*
Electronic devices based on electrodeposited nanowires
4th Zing Electrochemistry Conference, Tivoli Carvoeiro, Portugal
19-22 April 2015, Talk
45. *Enculescu I, Matei E, Costas A, Florica C*
CdTe nanowire channel field effect transistors
Third International Conference on Advanced Complex Inorganic Nanomaterials – ACIN 2015, Namur, Belgium
13-17 July 2015, Poster
46. *Enculescu M*
Optical properties of dye-doped nanostructures
The 8th International Conference on Advanced Materials – ROCAM 2015, Bucharest, Romania
7-10 July 2015, Talk
47. *Enculescu M*
Optical properties of dye-doped nanostructures
Lights of the World Conference, Bucharest, Romania
30 October – 1 November 2015, Poster
48. *Enculescu M, Evanghelidis A, Enculescu I*
Morphological and optical properties of doped electrospun nanofibers
Conference Science in Technology, SCinTE-2015, Athens, Greece
5-7 November 2015, Poster
49. *Endo K, Arisawa S, Yamasaki H, Tateno Y, Kawai S, Wada M, Tsuyumoto I, Kaneko T, Badica P*
Orientation engineering for the growth of c-axis and non c-axis epitaxial $\text{Bi}_2\text{Sr}_2\text{CaCu}_2\text{O}_{8+\delta}$ thin films by MOCVD
EUCAS 2015, Lyon, France
6-10 September 2015, Poster
50. *Evanghelidis A, Enculescu M, Galca A, Enculescu I*
Influence of doping nanoparticles on the optical properties of electrospun polymer nanofibers
The 8th International Conference on Advanced Materials – ROCAM 2015, Bucharest, Romania
7-10 July 2015, Poster
51. *Evanghelidis A, Preda N, Florica C, Costas A, Zgura I, Socol M, Enculescu M, Enculescu I*
Designing ZnO/polymer hybrid materials by electroless deposition and electrospinning
The 8th International Conference on Advanced Materials, Bucharest, Romania
7-10 July 2015, Talk

52. ***Evangelidis A, Preda N, Enculescu M, Zgura I, Socol M, Florica C, Costas A, Enculescu I***
Electroless deposition of ZnO nanostructures on natural and synthetic fibers
3rd Euro-Mediterranean Conference on Materials and Renewable Energies, Marrakech, Morocco
2-6 November, 2015, Talk
53. ***Evangelidis A, Enculescu M, Galca AC, Enculescu I***
Influence of doping nanoparticles on the optical properties of electrospun polymer nanofibers
8th International Conference on Advanced Materials, ROCAM 2015, Bucharest, Romania
7–10 July 2015, Poster
54. ***Evangelidis A, Preda N, Florica C, Costas A, Zgura I, Socol M, Enculescu M, Enculescu I***
Designing ZnO/polymer hybrid materials by electroless deposition and electrospinning *The 8th*
International Conference on Advanced Materials, Bucharest, Romania
7-10 July 2015, Talk
55. ***Evangelidis A, Preda N, Enculescu M, Zgura I, Socol M, Florica C, Costas A, Enculescu I***
Electroless deposition of ZnO nanostructures on natural and synthetic fibers
3rd Euro-Mediterranean Conference on Materials and Renewable Energies, Marrakech, Morocco
2-6 November 2015, Talk
56. ***Florica C, Preda N, Costas A, Evangelidis A, Zgura I, Socol M, Enculescu M, Enculescu I***
Electrical properties of chemically synthesized ZnO micro/nanostructures
The 8th International Conference on Advanced Materials, Bucharest, Romania
7-10 July 2015, Poster
57. ***Florica C, Costas A, Matei E, Ion L, Pintilie L, Preda N, Enculescu I***
Electrical properties of n-type and p-type single semiconductor nanowires
3rd Euro-Mediterranean Conference on Materials and Renewable Energies, EMCMRE-3,
Marrakech, Morocco
2-6 November 2015, Talk
58. ***Florica C, Costas A, Matei E, Toimil-Morales ME, Boni AG, Pintilie L, Preda N, Enculescu I***
Electrical properties of field effect transistors based on single nanowires
The 8th International Conference on Advanced Materials, Bucharest, Romania
7-10 July 2015, Talk
59. ***Florica C, Beregoi M, Costas A, Matei E, Eugenia M, Molares T, Enculescu I***
Single ZnO nanowire based transistors passivated with gelatin
International Conference “Science in Technology” – ScinTE 2015, Atena, Greece
5-8 November 2015, Talk
60. ***Florica C, Preda N, Costas A, Evangelidis A, Zgura I, Socol M, Enculescu M, Enculescu I***
Electrical properties of chemically synthesized ZnO micro/nanostructures
The 8th International Conference on Advanced Materials, Bucharest, Romania
7-10 July 2015, Poster
61. ***Frunza L, Negri CC, Zgura I, Căpăț C, Udrea I, Olaru EA, Bradu C, Balint I, State R, Papa F***
Interaction of some bimetallic catalyst nanoparticles deposited on support: XPS studies
The 8th International Conference on Advanced Materials, Bucharest, Romania
7-10 July 2015, Poster

62. **Frunza L, Zgura I, Enculescu M, Florica C, Cotorobai VF, Ganea CP, Diamandescu L, Frunza S**
Depuneri de particule amorfe de dioxid de titan pe materiale textile
Seminarul National de Nanostiinta si Nanotehnologie, Academia Romanaprezentare
26 March 2015, Talk
63. **Frunza L, Frunza S, Ganea CP, Neatu F, Parvulescu VI**
Dielectric behavior of some layered materials used as catalyst supports
10th International Conference Processes in Isotopes and Molecules PIM2015, Cluj Napoca
23-25 septembrie 2015, Poster
64. **Frunza L, Ganea P, Zgura I, Frunza S, Neatu F, Parvulescu VI**
Layered materials of LDH-type containing Zn ions: dielectric measurements show rotational
fluctuations of water molecules
The 38th International Semiconductor Conference (CAS 2015), Sinaia, Romania
12 - 14 October, 2015, Poster
65. **Galca AC, Tomulescu AG, Pintilie I**
On the structural and optical properties of hybrid perovskite thin films
8th International Conference on Advanced Materials, ROCAM 2015, Bucharest, Romania
7–10 July 2015, Talk
66. **Galca AC, Arayedh B, Oumezzine Ma, Oumezzine Mo, Enculescu M, Iuga A**
The structural and dielectric properties of zinc substituted nickel-cobalt ferrite nanoparticles
synthesized by citrate-gel combustion
8th International Conference on Advanced Materials, ROCAM 2015, Bucharest, Romania
7–10 July 2015, Talk
67. **Galca AC, Besleaga C, Stan GE, Ghica C, Pasuk I**
Out of plane coherence length and microstrain of rf sputtered ZnO thin films
8th International Conference on Advanced Materials, ROCAM 2015, Bucharest, Romania
7–10 July 2015, Talk
68. **Galca AC, Oumezzine Ma, Oumezzine Mo, Pasuk I, Chirila C, Leca A, Kuncser A, Ghica C,
Tanase LC, Teodorescu CM, Kuncser V**
Room temperature giant magnetoresistance in $\text{La}_{0.67}\text{Ba}_{0.33}\text{Ti}_{0.02}\text{Mn}_{0.98}\text{O}_3$ epilayers
8th International Conference on Advanced Materials, ROCAM 2015, Bucharest, Romania
7–10 July 2015, Talk
69. **Galca AC, Socol G, Trinca LM, Craciun V**
In-situ high temperature study of AOS optical and structural properties
EMRS fall meeting, Warsaw, Poland
15-18 September 2015, Poster
70. **Geambasu DC, Banciu MG, Nedelcu L**
Advanced microwave antennas using low-loss, high dielectric permittivity materials
International Balkan Workshop of Applied Physics and Materials Science, IBWAP 2015,
Constanta, Romania
2-4 July 2015, Poster

71. **Geambasu DC, Banciu MG, Nedelcu L, Ramer R**
New antennas with dielectric resonators of axial symmetry
International Semiconductor Conference, CAS 2015, Sinaia, Romania
12-14 October 2015, Talk
72. **Ghica D, Stefan M, Ghica C, Stan GE**
Mapping the paramagnetic impurities distribution in nanostructured films by EPR
8th International Conference on Advanced Materials, ROCAM 2015, Bucharest, Romania
7–10 July 2015, Talk
73. **Ghica C, Negrea RF, Teodorescu VS, Scarisoreanu N, Birjega R, Dinescu M**
QRTEM investigation on growth evolution of the residual strain in epitaxial films
European Congress and Exhibition on Advanced Materials and Processes EUROMAT 2015
Warsaw, Poland
20 – 24 September 2015, Poster
74. **Ghica D, Stefan M, Ghica C, Stan GE**
Mapping the Paramagnetic Impurities Distribution in Nanostructured Films by EPR
The 8th International Conference on Advanced Materials ROCAM-2015, Bucharest, Romania
7-10 July 2015, Talk
75. **Ghica D, Stefan M, Ghica C**
Evaluation of the Paramagnetic Impurities Segregation at Grain Boundaries in Nanostructured ZnO Films
European Congress and Exhibition on Advanced Materials and Processes EUROMAT 2015
Warsaw, Poland
20 – 24 September 2015 Talk
76. **Hussien M, Holban AM, Socol G, Popa M, Bleotu C, Mihailescu N, Duta L, Stan G, Lazar V, Hapenciuc C, Negut I, Ristoscu C, Mihailescu I, Chifiriuc MC**
Titanium surfaces coated with carbon and silver nanoparticles inhibit colonization and biofilm formation of Gram positive bacteria
The 6th EMBO Meeting, Birmingham, UK
6–8 September 2015, Poster
77. **Ilie M, Baibarac M, Baltog I**
Photoluminescence properties of composites based on poly(paraphenylene vinylene) and reduced graphene oxide
The 8th International Conference on Advanced Materials, , Bucharest, Romania
7-10 July 2015, Poster
78. **Ionescu M, Ivan I, Badica P, Aldica G, Miu L, Antohe S**
Magnetization relaxation in superconducting MgB2 bulk samples with improved vortex pinning
ICPS 2015, Zagreb, Croatia
12-19 August 2015, Talk
79. **Iordanescu C, Sofronie M, Galca AC, Tolea F, Kuncser V, Valeanu M, Elisa M, Feraru ID, Sava BA, Boroica L**
Magneto-optical and magnetic properties of doped alumino-phosphate glasses
20th International Conference on Magnetism, Barcelona, Spain
05-11 July 2014, Poster

80. *Iordanescu R, Feraru I, Elisa M, Sava B, Boroica L, Valeanu M, Kuncser V, Sofronie M*
Magnetic and magneto-optical properties of La, Y and Eu-doped phosphate glasses
20th International Conference on Magnetism, Barcelona-Spain,
5-10 July 2015, Poster
81. *Ivan I, Mele P, Miu D, Miu L*
DC magnetization relaxation and the frequency dependent AC magnetic response of $\text{YBa}_2\text{Cu}_3\text{O}_7$
films with embedded nanorods and nanoparticles
VORTEX IX – training school, Rhodes, Greece
12-17 September 2015, Poster
82. *Kuncser AC, Ghica C, Antohe S, Kuncser V*
Micromagnetic vs. multi-component Stoner-Wohlfarth interpretation of magnetization reversal in
magnetic nanosized systems
8th International Conference on Advanced Materials, ROCAM 2015, Bucharest, Romania
7-10 July 2015, Talk
83. *Lörinczi A, Sava F*
Non-crystalline As_2S_3 and Se - a new approach
Amorphous and Nanostructured Chalcogenides (ANC-7), Cluj-Napoca (Romania)
5-10 July 2015, Talk
84. *Majidian M, Grimaldi C, Baibarac M, Baltog I, Forró L, Magrez A*
U8-graphene: a new photo-patternable conductive polymer composite
EUPOC-Conducting polymeric materials, Gargnano, Italy
24-28 May 2015, Talk
85. *Matea A, Baibarac M, Baltog I, Lefrant S*
ZnO nanowhiskers transformed in flower-like type in the presence of C60 fullerene
The 8th International Conference on Advanced Materials, Bucharest, Romania
7-10 July 2015, Poster
86. *Matei E, Costas A, Florica C, Enculescu M, Enculescu I*
Transport properties of electrodeposited ZnO nanowires
4th Zing Electrochemistry Conference 2015, Tivoli Carvoeiro, Portugal
19-22 April 2015, Talk
87. *Matei E, Costas A, Florica C, Oancea M, Enculescu M, Enculescu I*
Co doped templateless electrodeposited ZnO nanowires
Third International Conference on Advanced Complex Inorganic Nanomaterials – ACIN 2015,
Namur, Belgium
13-17 July 2015, Poster
88. *Mercioniu I, Vlaicu AM, Kuncser AC, Negrea RF, Ghica C, Mihailescu A, Stefan A, Ionescu G,
Manoliu V*
HRTEM detailed analysis of oxides structures of Y and Ta doped NiCrAl compounds for TBC
European Congress and Exhibition on Advanced Materials and Processes EUROMAT 2015
Varsovia, Poland
20-24 September 2015, Poster

89. *Mîndru C, Vineticu N. **Ganea CP, Alexandru HV***
Down the ferroelectric transition
The 8th International Conference on Advanced Materials, Bucharest, Romania
7-10 July 2015, Poster
90. ***Miclea CF, Niclas M, Mota AC, Thomson JD, Movshovich R***
Possible signature of magnetic order inside superconducting state at low magnetic field in
CeCoIn₅
20th International Conference on Magnetism, Barcelona, Spain
05-11 July 2014, Poster
91. *Mihailescu N, Socol G, Hapenciuc C, **Stan GE, Negut I, Ristoscu C, Mihailescu IN, Chifriuc C***
Pulsed Laser Fabrication of Ag, Si:C thin films for antimicrobial coatings of implants
EMRS Spring Meeting, Lille, France
11–15 May 2015, Poster
92. *Moni MV, **Banciu MG, Tuta L***
Cylindrical dielectric resonator antenna for wireless application
23rd Telecommunications Forum (TELFOR), Belgrade, Serbia
24-26 November 2015, Talk
93. ***Neatu F, Ciobanu M, Stoflea L, Frunza L, Pârvulescu VI, Michelet V***
Nanostructured materials as efficient catalysts: characterization of hydrotalcite docked Rh complex
The 8th International Conference on Advanced Materials, Bucharest, Romania
7-10 July 2015, Poster
94. ***Nedelcu L, Trupina L, Ganea CP, Geambasu DC, Cioangher M, Banciu MG***
Ferroelectric transitions in Ba_{1-x}Sr_xTiO₃ solid solutions
International Balkan Workshop of Applied Physics and Materials Science, IBWAP 2015,
Constanta, Romania
2-4 July 2015, Poster
95. ***Nedelcu L, Geambasu CD, Banciu MG, Gugiu M, Ghenescu V, Preda T***
Dielectric properties of proton-irradiated Mg₄Nb₂O₉ ceramics
8th International Conference on Advanced Materials, ROCAM 2015, Bucharest, Romania
7-10 July 2015, Poster
96. ***Nedelcu L, Geambasu CD, Banciu MG, Iwamae A, Furuya T, Tani M***
Submillimeter-wave properties of Zn₂SiO₄ ceramics
40th International Conference on Infrared, Millimeter, and Terahertz Waves, IRMMW-THz
2015, Hong-Kong, China
24-28 August 2015, Poster
97. ***Nedelcu L, Geambasu CD, Banciu MG, Iwamae A, Furuya T, Tani M***
Terahertz absorption properties of Mg₂SiO₄ ceramics
Second International Symposium on Frontiers in THz Technology FTT 2015, Hamamatsu –
Shizuoka, Japan
30 Aug – 02 September 2015, Poster

98. **Negrea RF, Ghica C, Teodorescu VS**
Atomic scale elemental mapping of light elements in multilayered perovskite coatings
8th International Conference on Advanced Materials, ROCAM 2015, Bucharest, Romania
7-10 July 2015, Talk
99. **Negrea RF, Ghica C, Teodorescu VS, Chirila C**
Atomic scale characterization of interfaces in ferroelectric epitaxial multilayers by STEM and EELS
European Congress and Exhibition on Advanced Materials and Processes EUROMAT 2015
Warsaw, Poland
20 – 24 September 2015, Poster
100. **Niculescu AE, Bucur C, Galca AC, Besleaga C, Pasuk I**
Effect of structural properties on superconducting properties of Nb thin films
8th International Conference on Advanced Materials, ROCAM 2015, Bucharest, Romania
7-10 July 2015, Poster
101. **Nila A, Baibarac M, Baltog I**
Exciton-phonon interaction in PbI₂ layered crystals evidenced by photoluminescence and Raman studies
The 8th International Conference on Advanced Materials, Bucharest, Romania
7-10 July 2015, Poster
102. **Nistor LC, Negrea RF, Nistor SV, Vlaicu I**
Imaging impurities in Mn-doped cubic ZnS nanocrystals by EEL-spectroscopic methods
E-MRS Fall Meeting 2015, Symposium V, Warsaw, Poland
15– 18 September 2015, Poster
103. **Nistor SV, Stefan M, Nistor L C, Ghica D**
Unusual thermal decomposition of the Zn(OH)₂ surface phase of cubic ZnS quantum dots with core-shell structure
E-MRS Fall Meeting 2015, Symposium V, Warsaw, Poland
15– 18 September 2015, Talk
104. **Nita C, Visan A, Axente E, Rasoga O, Cristescu R, Stefan N, Miroiu M, Dorcioman G, Zgura I, Breazu CS, Chiritoiu M, Sima L, Socol G**
Characterization and deposition of lysozyme embedded into degradable coatings based on PLA/PCL blends
2015 E-MRS Spring Meeting, Advanced Materials Synthesis, Processing and Characterization Symposium, Lille, France
11 -15 May 2015, Poster
105. **Olaru EA, Capat C, Frunza L, Papa F, Munteanu C, Udrea I, Bradu C**
Pd-Cu catalysts supported on anion exchange resins for the simultaneous catalytic reduction of nitrate and reductive dehalogenation of 4-chlorophenol from water
12th European Congress on Catalysis – EuropaCat-XII, Kazan, Russia
30 August – 4 September 2015, Talk

106. *Orfanidou CM, Mihailescu CN, Mai VH, Nguyen VS, Schneegans O, Stan GE, Giapintzakis J*
Resistive switching in MIM devices based on Li_xCoO_2
EMRS Spring Meeting, Lille, France
11–15 May 2015, Talk
107. *Oumezzine Ma, Galca AC, Pasuk I, Chirila C, Leca A, Kuncser V, Kuncser A, Ghica C, Tanase LC, Oumezzine Mo*
Giant magnetoresistance and magnetic properties of epilayers-perovskite LBMT0
20th International Conference on Magnetism, Barcelona, Spain
05-11 July 2014, Poster
108. *Papa F, Balint I, Negriela C, Olaru EA, Munteanu C, Zgura I, Bradu C*
Pd-Cu nanostructured catalysts for water phase reduction of nitrates. Influence of the support and of the pH
12th European Congress on Catalysis – EuropaCat-XII, Kazan, Russia
30 August – 4 September 2015, Poster
109. *Pasuk I, Pintilie I, Chirila C, Pintilie L*
Epitaxial growth of ZnO thin films on square symmetry substrate plane
Second Balkan School on Fundamental Crystallography and Workshop on Magnetic Symmetry
Istanbul, Turkey
13-19 July 2015, Talk
110. *Pintilie I, Radu R, Lindstroem G, Fretwurst E, Makarenko L*
Defect generation and damage functions in electron irradiated silicon – dependence on particle energy
26th RD50 Workshop on radiation hard semiconductor devices for very high luminosity colliders, Santander, Spain
22-24 June 2015, Talk
111. *Pintilie L, Pintilie I, Botea M, Iuga A, Pasuk I, Boni AG, Chirila C, Hrib LM, Stancu V*
Pyroelectric/photovoltaic properties in polar thin films
2015 Joint IEEE International Symposium on Applications of Ferroelectric (ISAF), International Symposium on Integrated Functionalities (ISIF), and Piezoresponse Force Microscopy Workshop (PFM) (ISAF-ISIF-PFM 2015), Singapore
24-27 May 2015, Talk
112. *Plugaru N*
GGA+U study of RMn_2O_5 (R= Bi, Y, Gd, Tb, Dy, Ho, Er and Lu)
CECAM/Psi-k Research Conference: "Frontiers of first-principles simulations: materials design and discovery", Berlin, Germany
1-5 February 2015, Poster
113. *Plugaru N, Filip L, Valeanu M, Plugaru R, Campo J*
A study by neutron scattering and first principles calculations of the crystal structure and magnetism of $\text{Y}_3\text{Ni}_{13}\text{B}_2$, $\text{Y}_3\text{Co}_{13}\text{B}_2$, and $\text{Y}_3\text{Ni}_{10}\text{Co}_3\text{B}_2$
VI-th European Conference on Neutron Scattering (ECNS 2015), Zaragoza, Spain
30 August – 4 September 2015, Talk

114. **Plugaru N, Nemnes GA, Manolescu A**
Atomistic simulations of methylammonium lead halide layers on PbTiO₃
Psi-k 2015 Conference: "Ab initio (from the electronic structure) calculations of processes in materials" San Sebastian, Spain
6-10 September 2015, Poster
115. **Plugaru R, Filip L, Plugaru N**
Exchange interactions and magnetic structures of RMn₂O₅ by first-principles calculations
Psi-k 2015 Conference: "Ab initio (from the electronic structure) calculations of processes in materials", San Sebastian, Spain
6-10 September 2015, Poster
116. **Polosan S**
Organometallic materials for optoelectronic devices and their applications
Workshop - "Advances in Nanophysics and Nanophotonics", Magurele, Romania
1 August -02.09.2015, Talk
117. **Polosan S, Matei E, Ciobotaru C, Ciobotaru CC**
ZnO nanowires in organic light emitting diodes
The 15th International Balkan Workshop on Applied Physics and Materials Science, Constanta, Romania
2-4 July 2015, Talk
118. **Polosan S**
Charge transport optimization in OLED structures by using ZnO nanowires
The 8th International Symposium on Flexible Organic Electronics, Thessaloniki, Greece
6-9 July 2015, Talk
119. **Popa CL, Ciobanu CS, Badea ML, Chapon P, Ghita RV, Antohe S, Predoi D**
Structural characterization and bacterial inhibiting effect of zinc doped hydroxyapatite layer
The 8th International conference on advanced materials: ROCAM 2015, Bucharest, Romania
5-10 July 2015, Poster
120. **Popa CL, Ciobanu CS, Chapon P, Antohe S, Iconaru SL, Predoi D**
Evaluation of the antimicrobial activity of different antibiotics enhanced with silver doped hydroxyapatite thin solid films
The 8th International conference on advanced materials: ROCAM 2015, Bucharest, Romania
5-10 July 2015, Poster
121. **Popa CL, Ciobanu CS, Albu M, Motelica-Heino M, Predoi D**
Physico-chemical characterizations and cytotoxicity evaluation of novel zinc doped hydroxyapatite embedded in a collagen matrix
The 15th European Conference on Solid State Chemistry, Viena, Austria
23-26 August 2015, Poster
122. **Popa CL, Ciobanu CS, Prodan AM, Turculet C, Badea ML, Predoi D**
Antimicrobial activity of zinc doped hydroxyapatite prepared by co-precipitation method
EUROTOX 2015, Porto, Portugal
13-16 September 2015, Poster

123. **Popescu-Pelin G, Axente E, Sima F, Nita C, Visan A, Zgura I, Rasoga O, Breazu CS, Stanculescu A, Chiritoiu M, Sima L, Antohe F, Ivan L, Mihailescu IN, Socol G**
Deposition of degradable polymeric coatings based on lysozyme embedded into poly(ϵ -caprolactone)/poly(lactic acid-co-glycolic acid) blends
E-MRS Spring Meeting, Advanced Materials Synthesis, Processing and Characterization Symposium, Lille, France
11-15 May 2015, Poster
124. **Popescu-Pelin G, Axente E, Sima F, Nita C, Visan A, Zgura I, Rasoga OL, Breazu CS, Stanculescu A, Chiritoiu M, Sima L, Antohe F, Ivan L, Socol G, Mihailescu IN**
Comparative study on the deposition of degradable polymeric coatings based on lysozyme embedded into PCL/PLGA blends
The 8th International Conference on Advanced Materials, Bucharest, Romania
7-10 July 2015, Poster
125. **Popescu-Pelin G, Axente E, Sima F, Nita C, Visan A, Zgura I, Rasoga OL, Breazu CS, Stanculescu A, Chiritoiu M, Sima, Antohe F, Ivan L, Mihailescu IN, Socol G**
Deposition of degradable polymeric coatings based on lysozyme embedded into poly(ϵ -caprolactone)/poly(lactic acid-co-glycolic acid) blends
EMRS 2015 Spring – Symposium CC, Lille, France
11-15 May 2015, Poster
126. **Popescu DG, Ganea CP, Florica C, Anghel I, Husanu M**
Light confinement in a two dimensional ge photonic crystal
The 8th International Conference on Advanced Materials, Bucharest, Romania
7-10 July 2015, Poster
127. **Popescu T, Raditoiu V, Teodorescu VS, Diamandescu L, Purcar V, Vlaicu AM, Tarabasanu-Mihaila D, Lupu AR**
Physicochemical properties and processes relevant for *in vitro* biological studies involving TiO₂ nanoparticles
8th International Conference on Advanced Materials, ROCAM 2015, Bucharest, Romania
7-10 July 2015, Talk
128. **Preda N, Zgura I, Socol M, Evanghelidis A, Florica C, Costas A, Enculescu M, Enculescu I**
Effect of low temperature oxygen plasma treatment on the wetting property of self-assembled polymer spheres
The 8th International Conference on Advanced Materials, Bucharest, Romania
7-10 July 2015, Poster
129. **Preda N, Zgura I, Socol M, Evanghelidis A, Florica C, Costas A, Enculescu M, Enculescu I**
Effect of low temperature oxygen plasma treatment on the wetting property of self-assembled polymer spheres
The 8th International Conference on Advanced Materials, Bucharest, Romania
7-10 July 2015, Poster

130. *Prodan AM, Ciobanu CS, Beuran M, Turculeț C, Teleanu G, Motelica-Heino M, Sizaret S, Predoi D*
Effect of dextran coated superparamagnetic iron oxide nanoparticles during in vivo observation of the rats
20th International Conference on Magnetism, Barcelona, Spain
5-10 July 2015, Poster
131. *Prodan AM, Ciobanu CS, Beuran M, Turculeț C, Pavelescu C, Teleanu G, Chapon P, Predoi D*
Evaluation of dextran coated iron oxide magnetic nanoparticles toxicity after intratracheal instillation
15th European Conference on Solid State Chemistry, Viena, Austria
23-26 August 2015, Poster
132. *Radu R, Pintilie I, Fretwurst E, Lindstroem G*
Study of electron-induced defects in n-type silicon detectors
Third International Conference on Radiation and Dosimetry in Various Fields of Research, Nis, Serbia
8-12 June 2015, Talk
133. *Radu R, Galca AC, Trinca LM, Besleaga C, Pintilie I, Socol G, Craciun V*
On the electrical and optical properties of amorphous oxide semiconductors
8th International Conference on Advanced Materials, ROCAM 2015, Bucharest, Romania
7-10 July 2015, Poster
134. *Rasoga O, Stanculescu A, Breazu C, Socol M, Catargiu AM, Stanculescu F, Girtan M*
Bulk heterojunctions with arylene based polymers donor for solar cells applications
EMRS 2015, Spring-Symposium S,Lille, France
11-15 May 2015, Poster
135. *Sandu V, Greculeasa S, Kuncser V, Kuncser A, Nicolescu S, Ionescu A*
Capital Role of Nanosized Crystallites in Magnetic Response of Glass Ceramics
Int. Workshop "Advances in Nanophysics and Nanophotonics", Magurele, Romania
31 August -2 September 2015, Talk
136. *Sava F, Velea A, Popescu M, Socol G, Vlaicu MA, Pasuk I, Lőrinczi A, Simandan ID*
The local structure of amorphous Ga₂Se₃ thin films
Amorphous and Nanostructured Chalcogenides (ANC-7), Cluj-Napoca (Romania)
5-10 July 2015, Poster
137. *Simion CE, Rusti CF, Florea OG, Sackmann A, Piticescu RM, Osinceanu P and Stanoiu A*
Gas-sensing properties of Cr doped BaSrTiO₃ materials
8th International Conference on Advanced Materials, ROCAM 2015, Bucharest, Romania
7-10 July 2015, Talk
138. *Smaranda I, Scocioreanu M, Baibarac M, Baltog I, Mevellec JY, Lefrant S*
SERS and SEIRA studies of carbon nanotubes electrochemically functionalized with poly(2,2'-bithiophene-co-pyrene)
The 8th International Conference on Advanced Materials, Bucharest, Romania
7-10 July 2015, Poster

139. *Sorescu M, Bushunow V, Diamandescu L, Tolea F, Valeanu M, Xu T*
Nanostructured lithium oxide-hematite magnetic oxide semiconductors
Meeting of the American Physical Society Aps March Meeting 2015, San Antonio, Texas, USA
2–6 March 2015, Talk
140. *Stancu V, Sima M, Besleaga C, Tomulescu A, Sima Ma, Stan G, Pintilie L, Pintilie I*
Efficient perovskite solar cells prepared by solution processed via two step deposition
8th International Conference on Advanced Materials, ROCAM 2015, Bucharest, Romania
7-10 July 2015, Talk
141. *Stanculescu A, Socol G, Vacareanu L, Socol M, Rasoga O, Breazu C, Girtan M, Stanculescu F*
MAPLE preparation and characterization of mixed arylenevinylene based oligomers: C60 layers
EMRS 2015, Spring –Symposium CC, Lille, France
11-15 May 2015, Poster
142. *Socol G, Le Caër S, Craciun D, Galca AC, Martin C, Craciun V*
Gamma irradiation effects of the electrical and optical properties of amorphous indium zinc
oxide thin films
EMRS Spring Meeting, Lille, France
11–15 May 2015, Poster
143. *Socol G, Stefan N, Grumezescu V, Popescu-Pelin G, Craciun V, Craciun D, Socol M, Luculescu CR, Galca AC*
MAPLE deposition of conducting polymers
EMRS Spring Meeting, Lille, France
11–15 May 2015, Poster
144. *Socol G, Stefan N, Grumezescu V, Popescu-Pelin G, Craciun V, Craciun D, Socol M, Luculescu CR, Galca AC*
MAPLE deposition of conducting polymers
EMRS 2015, Spring –Symposium CC, Lille, France
11-15 May 2015, Poster
145. *Socol M, Rasoga O, Breazu C, Preda N, Stanculescu F, Stanculescu A, Socol G, Girtan M*
Normal and inverted organic solar cells based on small molecule compounds
The 8th International Conference on Advanced Materials, Bucharest, Romania
7-10 July 2015, Poster
146. *Socol M, Preda N, Rasoga O, Breazu C, Stanculescu F, Socol G, Gherendi F, Grumezescu V, Stefan N, Girtan M*
Flexible heterostructures based on metal phthalocyanines thin films deposited by MAPLE
EMRS 2015, Spring –Symposium CC, Lille, France
11-15 May 2015, Poster
147. *Sofronie M, Crisan AD, Tolea F, Enculescu M, Valeanu M*
Temperature dependent magnetostrains in Mn and Ga-doped Fe-Pd ferromagnetic shape
memory ribbons
20th International Conference on Magnetism, Barcelona-Spain
5-10 July 2015, Poster

148. **Sofronie M, Tolea F, Crisan AD, Enculescu M, Valeanu M**
Characterization of martensitic transformation in Fe-Pd-X (X= Mn, Ga, Ti) ferromagnetic shape memory ribbons
10th European Symposium on Martensitic Transformations (ESOMAT), Antwerp, Belgium
14-18 September 2015, Poster
149. **Stefan M, Nistor SV, Ghica D**
EPR applications in materials science
CERIC-ERIC New Users Symposium, Krakow, Poland
24-25 June 2015, Poster
150. **Stefan M, Ghica D, Nistor SV**
Probing the Annealing Induced Transformations in Semiconductor Nanostructures by EPR
The 8th International Conference on Advanced Materials ROCAM-2015, Bucharest, Romania
7-10 July 2015, Talk
151. **Stefan M, Ghica D, Nistor SV, Maraloiu AV, Plugaru R**
Manganese ions distribution in doped sol-gel deposited ZnO films
E-MRS Fall Meeting 2015, Symposium V, Warsaw, Poland
15– 18 September 2015, Poster
152. **Stratulat A, Serban B, Cobianu C, Avramescu V, Brezeanu M, Buiu O, Diamandescu L, Feder M, Udrea F, De Luca A, Ali SZ**
Novel sonochemical route for manufacturing O₂ sensitive STFO
NATO ARW Ukraine, Odessa
30 August - 3 Septembrie 2015, Talk
153. **Teodorescu VS, Maraloiu AV, Negrea R, Ghica D, Scarisoreanu ND, Dinescu M, Gartner M, Zaharescu M, Blanchin MG**
High atomic diffusivity during pulsed laser irradiation of TiON quasi-amorphous films
EMRS Spring Meeting 2015, Lille, France
11-15 May 2015, Poster
154. **Teodorescu VS, Maraloiu AV, Negrea R, Slav A, Palade C, Lepadatu AM, Ciurea ML**
Crystallization features of the Ge-HfO₂ amorphous films obtained by magnetron sputtering,
EMRS Spring Meeting 2015, Lille, France
11-15 May 2015, Poster
155. **Teodorescu VS, Ghica C, Maraloiu AV, Kuncser A, Lepadatu AM, Stavarache I, Ciurea ML, Scarisoreanu ND, Andrei A, Dinescu M**
Fast Ge diffusion in amorphous films induced by laser pulse irradiation at fluencies less than the melting threshold
1st International Conference on Applied Surface Science ICASS, Shanghai, China
27-30 July 2015, Talk
156. **Tolea F, Sofronie M, Crisan AD, Valeanu M**
Magnetocaloric effect in Ni-Fe-Ga-Nd Heusler alloys
Energy science Technology International Conference & Exhibition, (EST), Karlsruhe, Germany
20-22 May 2015, Talk

157. **Tolea F, Sofronie M, Crişan AD, Văleanu M**
Magnetocaloric effect in Ni-Fe-Ga-Co-Al Heusler alloys
20-th International Conference on Magnetism, ICM, Barcelona, Spain
5-10 July 2015, Poster
158. **Tolea F, Sofronie M, Crisan AD, Valeanu M**
Magnetocaloric effect in Ni-Fe-Ga Heusler alloys with Co, Al or Nd substitutions
European Symposium on Martensitic Transformations, ESOMAT, Antwerp, Belgium
14-18 September 2015, Talk
159. **Trinca LM, Galca AC, Evanghelidis A, Busuioc C, Matei E, Enculescu I, Pintilie L, Pintilie I**
Flexible transparent electrodes for solar cells
EMRS Spring Meeting, Lille, France
11-15 May 2015, Poster
160. **Trinca LM, Galca AC, Besleaga C, Aldica G, Boni AG, Pintilie L**
Zinc oxide based epilayers and polycrystalline thin films for transparent thin film transistors
EMRS Spring Meeting, Lille, France
11-15 May 2015, Poster
161. **Trinca LM, Galca AC, Besleaga C, Boni AG, Stancu V, Tomulescu AG, Sima M, Pintilie L, Pintilie I**
ZnO-based conductive oxide thin films as transparent contact for photovoltaic cells
8th International Conference on Advanced Materials, ROCAM 2015, Bucharest, Romania
7-10 July 2015, Poster
162. **Trinca LM, Gălcă AC, Besleaga C, Aldica G, Boni AG, Pintilie L**
Zinc oxide based epilayers and polycrystalline thin films for transparent thin film transistors
EMRS Spring Meeting, Lille, France
11-15 May 2015, Poster
163. **Trupina L, Nedelcu L, Banciu MG, Champeaux C, Dumas-Bouchiat F, Marchet P, Huitema L, Madrangeas L, Crunteanu A, Passerieux D**
Growth of highly (110)-, (001)- and (111)-textured iridium thin films on MgO single-crystal substrates
International Balkan Workshop of Applied Physics and Materials Science, IBWAP 2015, Constanta, Romania
2-4 July 2015, Poster
164. **Trupina L, Nedelcu L, Banciu MG, Negrila CC, Champeaux C, Dumas-Bouchiat F, Marchet P, Huitema L, Madrangeas L, Crunteanu A, Passerieux D, Cros D, Monediere T**
Thermal stability of highly textured iridium thin films grown on silicon substrates
8th International Conference on Advanced Materials, ROCAM 2015, Bucharest, Romania
7-10 July 2015, Poster
165. **Veljović D, Mihailescu N, Stefan A, Stan GE, Luculescu C, Janačković D, Đorđević V, Dramićanin MD, Krsmanović Whiffen R, Ristoscu C, Georgescu S, Mihailescu IN**
Fabrication of Y₂O₃ and Y_{1.94}Yb_{0.05}Er_{0.01}O₃ thin films by pulsed laser deposition
ICOM 2015, Budva, Montenegro
31 August – 4 September 2015, Poster

166. *Visan A, Erakovic S, Jankovic A, Ristoscu C, Duta L, Mihailescu N (Serban), Stan GE, Socol M, Iordache O, Dumitrescu I, Luculescu CR., Mihailescu IN, Janackovic D, Miskovic-Stankovic V*
Ag:hydroxyapatite coatings with antifungal activity synthesized by pulsed laser deposition on Ti and Ti modified by TiO₂ nanotubes substrates
EMRS Spring –Symposium S, Lille, France
11-15 May 2015, Poster
167. *Visan A, Miroiu M, Nita C, Socol M, Zgura I, Cristescu R, Chifiriuc MC, Sima L, Antohe F, Mihailescu IN, Socol G*
MAPLE fabrication of antimicrobial coatings for medical
The 8th International Conference on Advanced Materials, , Bucharest, Romania
7-10 July 2015, Talk
168. *Visan A, Stefan N, Miroiu M, Nita C, Dorcioman G, Rasoga O, Zgura I, Breazu C, Stanculescu A, Cristescu R, Chifiriuc MC, Chiritoiu M, Sima L., Antohe F, Ivan L., Mihailescu IN, Socol G*
In vitro evaluation of embedded lysozyme into degradable PEG/PCL coatings
EMRS Spring Meeting, Advanced Materials Synthesis, Processing and Characterization
Symposium, Lille, France
11-15 May 2015, Poster
169. *Vlaicu AM, Mercioniu I, Kuncser AC, Negrea RF, Ghica C, Mihailescu A, Stefan A, Ionescu G, Manoliu V*
Several aspects concerning chemical stability and microstructural effects of thermal treatments on TBCs
European Congress and Exhibition on Advanced Materials and Processes EUROMAT
2015 Warsaw, Poland
20–24 September 2015, Poster

Invited Lectures

1. ***Enculescu M, Evanghelidis A, Enculescu I***
Optical and morphological properties of dye-doped nanostructures
The 15 th International Balkan Workshop on Applied Physics and Materials Science, Constanta, Romania
2-4 July 2015, Invited
2. ***Galca AC***
Errors in X-ray diffraction measurements: case studies on polycrystalline bulk and epitaxial samples
7th International Workshop on “Advanced optical and X-ray characterization techniques of multifunctional materials for information and communication technologies, health and renewable energy applications”, Bucharest, Romania
16–18 September 2015, Invited
3. ***Huitema L, Madrangeas L, Crunteanu A, Passerieux D, Cros D, Monediere T, Champeaux C, Dumas-Bouchiat F, Marchet P, Nedelcu L, Trupina L, Banciu MG, Cernea M***
Tunable ferroelectric materials for RF- microwave applications: high-frequency properties and integration in frequency-agile devices
8th International Conference on Advanced Materials, ROCAM 2015, Bucharest, Romania
7-10 July 2015, Invited
4. ***Kuncser V, Iacob N, Palade P, Kuncser A, Comanescu C, Schinteie G***
Magnetic nanoparticles for bio-medical applications
International Balkan Workshop for Applied Physics, Constanta, Romania
3-6 July 2015, Invited
5. ***Lörinczi A***
Supporting excellent researchers all over Europe" – Regional ERC Workshop, 4 Nov.2015, Hungarian Academy of Sciences
World Science Forum 2015, Budapesta, Ungaria
4-7 November 2015, Invited
6. ***Maraloiu VA, Negrea RF, Mercioniu IF, Ghica C***
Characterization of materials by EPR and SEM - TEM techniques
1st CERIC New Users Symposium, Krakow, Poland
24-25 June 2015, Invited
7. ***Negrea RF, Ghica C***
Advanced characterization of materials by analytical high resolution TEM techniques
1st CERIC New Users Symposium, Krakow, Poland
24-25 June 2015, Invited

8. *Ozawa S, Azuma S, Funkner S, Niehues G, Yamamoto K, Furuya T, Kitahara H, Banciu MG, Nedelcu L, Estacio ES, Kurihara K, Bakunov M, Tani M*
Electro-optic sampling of terahertz pulses using BaTiO₃ in non-collinear Cherenkov phase-matching scheme
40th International Conference on Infrared, Millimeter, and Terahertz Waves, IRMMW-THz 2015, Hong-Kong, China
24-28 August 2015, Invited
9. *Pintilie L, Pintilie I, Teodorescu CM, Ghica C, Pasuk I, Boni AG, Chirila C, Hrib LM, Trupina L, Negrea R, Stefan M, Ghica D, Stancu V*
Polarization controlled phenomena in ferroelectric thin films
2015 Joint IEEE International Symposium on Applications of Ferroelectric (ISAF), International Symposium on Integrated Functionalities (ISIF), and Piezoresponse Force Microscopy Workshop (PFM) (ISAF-ISIF-PFM 2015), Singapore
24-27 May 2015, Invited
10. *Pintilie L*
Polarization driven effects and the role of interfaces in ferroelectric thin films and heterostructures
Conference for Young Scientists in Ceramics, SM-2015, Faculty of Technology, Novi Sad, Serbia
21-24 October 2015, Invited
11. *Popescu M, Sava F, Lőrinczi A, Velea A, Simandan ID, Galca AC, Socol G, Gherendi F, Savastru D, Miclos S*
Amorphous thin films in the system Gallium-Chalcogen
Amorphous and Nanostructured Chalcogenides (ANC-7), Cluj-Napoca, Romania
5-10 July 2015, Invited
12. *Stefan M*
Electron paramagnetic resonance of doped semiconductor nanostructures
CERIC-ERIC New Users Symposium, Krakow, Poland
24-25 June 2015, Invited
13. *Stefan M, Nistor S V, Ghica D*
Size, structure and local strain in nanostructured ZnO probed by electron paramagnetic resonance
E-MRS Fall Meeting 2015, Symposium V, Warsaw, Poland
15–18 September 2015, Invited
14. *Tani M, Banciu MG, Nedelcu L, Ozawa S, Azuma S, Tsuzuki S, Furuya T, Funkner S, Niehues GG, Estacio ES, Kurihara K, Yamamoto K, Bakunov M*
Electro-optic sampling of terahertz pulses using ferroelectric crystal and non-collinear Cherenkov phase-matching
8th International Conference on Advanced Materials, ROCAM 2015, Bucharest, Romania
7-10 July 2015, Invited

Selected Results

Condensed Matter Physics at Mesoscale

Influence of substrate and electrode materials on electrical properties of $\text{Pb}(\text{Zr}_{0.52}\text{Ti}_{0.48})\text{O}_3$ thin films

Andra Georgia Boni, Cristina Chirila, Luminita Hrib, Ioana Pintilie, Lucian Pintilie

Lead titanate–zirconate $\text{Pb}(\text{Zr,Ti})\text{O}_3$ (PZT) thin films are of great interest in many applications such as non-volatile memories, pyroelectric detectors, piezoelectric transducers or micromechanical systems (MEMS). PZT thin films with 52/48 ratio of Zr/Ti are near the morphotropic phase boundary and are characterized by a high electro-mechanical coupling factor due to existence of two phases, rhomboedral and tetragonal. It is well known that thin films properties are influenced by the compositional and structural defects, but they can be minimized using advanced deposition techniques that allow obtaining high quality epitaxial layers. For such systems became interesting to study how the substrate or electrodes interfaces influence the electrical properties, especially from the leakage point of view. Therefore we grew PZT epitaxial thin films on two different substrates Si (001) and SrTiO_3 (001) by pulsed laser deposition (PLD) [1]. In order to acting as barrier for Pb diffusion on Si substrate a STO buffer layer was deposited by molecular beam epitaxy (MBE). On top of each STO film a 20 nm layer of SrRuO_3 (SRO) was grown by PLD in order to act as back electrode for metal-ferroelectric-metal (MFM) capacitors. Final capacitor-like structures were obtained by deposition of several metal contacts (Pt, SRO, Ir and Ru) on top of the PZT layers. It was found that macroscopic properties such as dielectric constant and polarization switching are affected by the electrodes interfaces as well as by the substrate. Thus, the polarization-voltage (P-V) loops for different temperatures revealed that while the remnant polarization (P_r), the coercive field (E_c) and the leakage current (LC) in PZT film grown on single-crystal STO are larger than for the one grown on Si with STO buffer layer, the dielectric constant is smaller (see Fig. 1). These differences could be explained by different stress situations, due to different lattice

parameters of the two substrates, $a=3.905\text{\AA}$ for STO substrate and $a = 5.43\text{\AA}$ for Si substrate. The lower values of P_r , E_c and LC can be seen as an advantage for the PZT films deposited on Si substrate with STO buffer layers if we want to use them for applications, as capacitors (e.g. NVM, IR detectors, etc.).

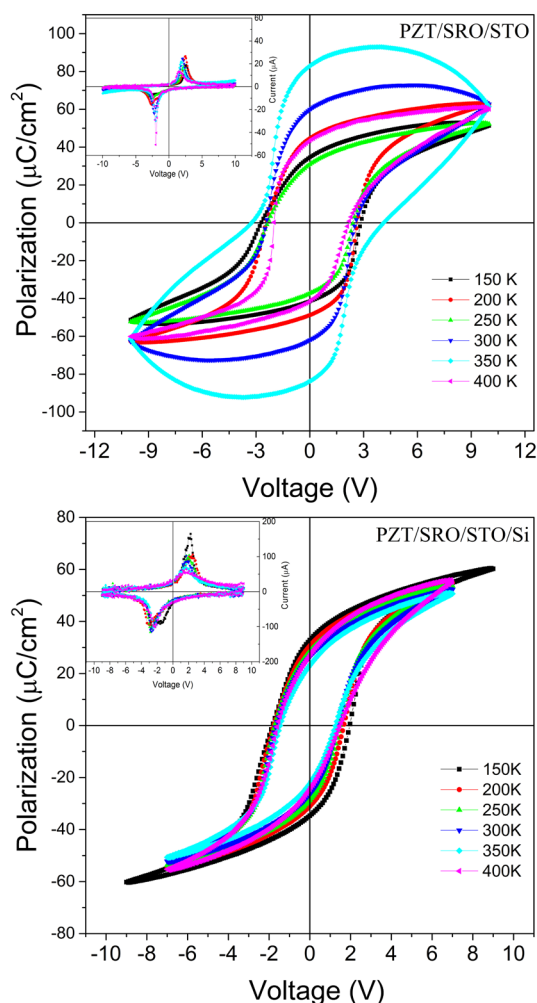


Fig. 1. Hysteresis measured at 1 kHz recorded in the 150–400 K temperature range

The influence of the top electrode (Pt, Ir, Ru and SRO) on the electrical properties of the MFM structures has been investigated using PZT thin films grown on Si substrates with STO buffer layer [2]. Examples of P-V and C-V characteristics, for SRO and Ru contacts, are given in Fig.2. The hysteresis characteristics observed in P-V and C-V, according to various

metals used as top electrode, are interpreted considering both the work function of each metal part and its position in the periodic table. An imprint, attributed to the non-homogeneous distribution of charged defects and to different densities of both interface states, has been observed in the hysteresis loops, Fig.2. The different values obtained for the static dielectric constant of each metal tested as top contact are explained by the variation in the top Schottky contact capacitance when the metal is changed.

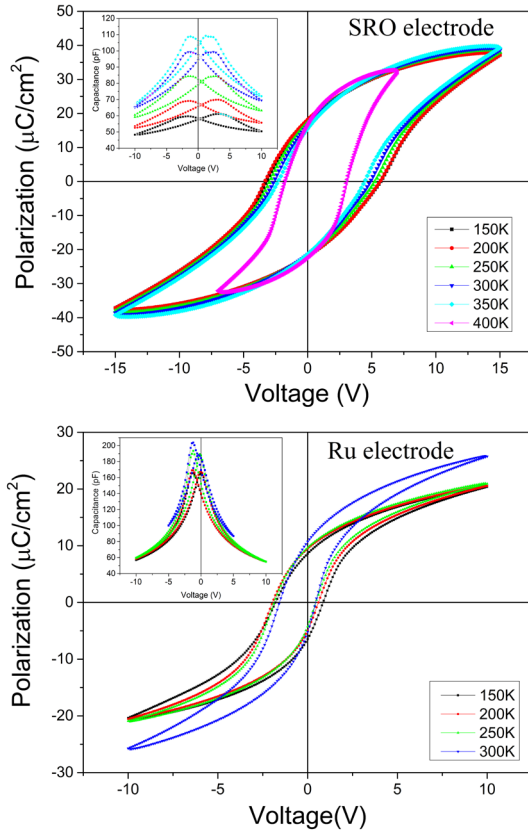


Fig. 2 The voltage dependence of the polarization and capacitance (inset) for epitaxial PZT films deposited on Si substrates with different SRO and Ru electrodes.

The effect of the electrode interfaces on the leakage current was also analyzed. The dominant conduction mechanism was assumed to be Schottky emission, in line with the presence of the Schottky type contacts at the electrode interfaces [3]. The equation that explain the current density behavior is Schottky-Simmons:

$$J = 2q \left(\frac{2\pi m_{eff} kT}{h^2} \right)^{3/2} \mu E \exp \left(-\frac{q}{kT} \left(\phi_B^0 - \sqrt{\frac{qE_m}{4\pi\epsilon_0\epsilon_{op}}} \right) \right)$$

Here J is the current density, q is the electron charge, h is the Planck's constant, m_{eff} is the

effective mass, μ is the mobility, k is the Boltzmann's constant, T is the temperature, E is the electrical field in the film, ϵ_0 is the vacuum permittivity, ϵ_{op} is the optical dielectric constant, ϕ_B^0 is the interfacial potential barrier height at 0V, and E_m is electrical field at the interface.

The analysis of the experimental data has revealed that the potential barriers do not correlate with the work function values of the metals used as top electrodes, table 1.

Table 1. The values of the potential barriers height (ϕ_B^0 (eV)) and dielectric constant calculated for negative and positive polarities of the voltage applied on the top electrodes made from different metals.

Electrode	ϵ_{st}		ϵ_{op}	Φ_B^0 (eV)	
	Positive	Negative		Positive	Negative
SRO	392	367	4.23	0.12	0.11
Pt	523	466	5.58	0.43	0.47
Ir	443	391	5.05	0.42	0.49
Ru	309	335	4.36	-	0.24

It was found that for Pt and Ir top electrodes the potential barriers for positive and negative polarities are about the same although the bottom SRO electrode has a lower work function. For SRO top electrode, the leakage current is higher and potential barrier is lower than for metallic electrodes.

NIMP researchers acknowledge financial support from Romanian Ministry of National through the Idea-Complex Research Grant PN-II-ID-PCCE-2011-2-0006 (contract nr.3/2012)

References

1. C. Chirila, A.G. Boni *et al.* Journal of Materials Science 50, 3883-3894, 2015.
2. A. G. Boni, C. Chirila *et al.* Thin Solid Films 593, 124-130, 2015.
3. A.G. Boni, C. Chirila, L. Hrib *et al.* Digest Journal of Nanomaterials and Biostructures 10, 4, 1257-1265, 2015.

Simulation of the capacitance-voltage and current-voltage characteristics of metal-ferroelectric-metal structures

L. D. Filip, L. Pintilie, V. Stancu and I. Pintilie

Thin film metal-ferroelectric-metal (MFM) structures have great potential in becoming the building blocks for next generation electronic devices such as random access memories (RAM). However, in order to harness this potential, detailed control of their properties must be achieved at least to the same level of their silicon counterparts. This can be done by using specialised experimental techniques coupled with theoretical models that can probe various properties such as: the doping concentration or the nature of the contacts and potential barrier heights at the device interfaces.

One of the most common investigations performed on MFM devices is the C-V measurement which can be theoretically modelled by replacing the structure with an equivalent circuit consisting of two back-to-back Schottky diodes representing the two interfaces of the MFM device [1]. The ferroelectric polarization is taken into account through the dipole moment of two charged sheets (+P and -P) located at some distance X_i in the vicinity of each interface (see Fig.1a).

The capacitance measurement on a MFM structure is performed using a small *ac* voltage. Thus the entire structure is regarded as an impedance and the capacitance is extracted from its imaginary part. The equivalent circuit proposed in Fig. 1b, replaces the two interface regions and the main bulk region with R-C circuits.

The capacitance of the Schottky contacts at the two metal-ferroelectric interfaces can be obtained by modifying the equation for the metal-semiconductor interface to take into account the effects of the ferroelectric polarization on the built-in voltage at each interface. The bulk capacitance is expressed in the classical way, with the exception that the dielectric constant is field dependent.

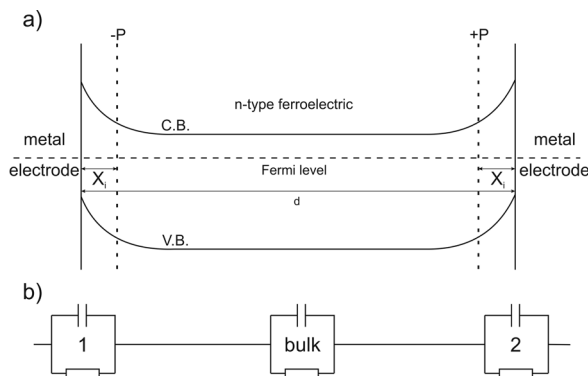


Figure 1: a) proposed band diagram for the MFM device, showing the two charged sheets near each interface and b) the equivalent circuit for the characterization of the MFM device.

Using this framework, the C-V characteristic can be obtained and qualitatively compared to experimental measurements (see Fig.2).

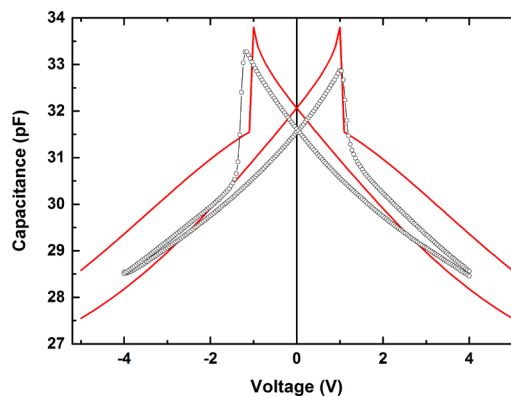


Figure 2: Calculated C-V diagrams (continuous lines) compared to experimental data (hollow symbols).

Another method for investigating MFM devices is the leakage current measurement. Such investigation measures the current when the ferroelectric polarization is saturated and it provides good information about the nature of electrode-ferroelectric contact [2]. Simulations of I-V characteristics have focused on adaptations of the classical metal-semiconductor interface and the results are decidedly one-

sided since the final formula calculates the leakage current at one or the other interface without any connection between the two.

Like the previous theoretical model for C-V characteristics, the ferroelectric polarisation is taken into account as two charged sheets in the vicinity of the two interfaces. The rest of the structure is divided into five different regions where the Poisson equation is solved in order to obtain the potential energy profile of the MFM device. Thus allowing for the calculation of the incoming and outgoing electron currents through both interfaces of the device. By imposing the condition of a local thermodynamic equilibrium in the ferroelectric layer, a balance equation for the incoming and outgoing electron currents (see Fig. 3) such that:

$$I_{in}^b(V, \mu_0) + I_{in}^t(V, \mu_0) = I_{out}^b(V, \mu_0) + I_{out}^t(V, \mu_0),$$

where μ_0 is the chemical potential in the ferroelectric. All the currents involved are obtained from a combination between thermionic and tunnelling mechanisms. It should be noted that for the range of temperatures that are usually used in the measurements, the potential barrier heights at the two interfaces are much higher than $k_B T$, and the contribution of the thermionic current should be minimal.

Using the barrier heights, dielectric constants and the widths of the layers in the vicinity of the two interfaces as parameters, the calculated I-V characteristics can be fitted to similar experimental data (see Fig. 4). As it can be observed, there is very good qualitative agreement with experimental data. Within the confines of this model, it was obtained that the dielectric constant throughout the ferroelectric layer is not uniform.

Only by considering a much smaller value in the two “Transition layers” (see Fig. 3) the experimental data could be fitted with this model. This conclusion is corroborated by independent numerical calculations that can be

found in the literature using ab-initio methods [2].

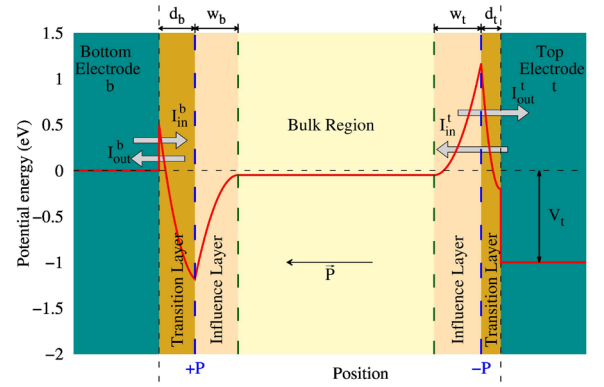


Figure 3: Sketch of the MFM capacitor with all the different regions highlighted. The incoming and outgoing electron currents are marked by arrows and the red line represents the calculated potential energy profile.

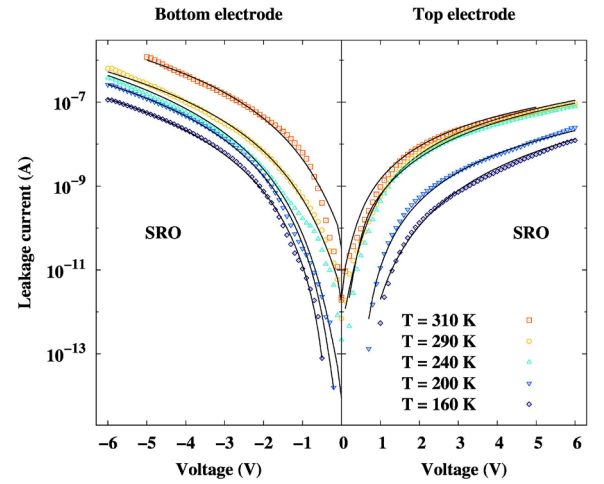


Figure 4: Best fit curves (black lines) for the case of a symmetrical MFM device and experimental I-V data at different system temperatures (symbols).

References

1. L. D. Filip, L. Pintilie, V. Stancu and I. Pintilie, Thin Solid Films 592, p. 200-206 (2015).
2. L. D. Filip and L. Pintilie, European Physics Journal B 89, 44 (2016).

Defect generation in electron irradiated silicon

R. Radu, I. Pintilie, L. C. Nistor

in cooperation with

G. Lindstroem¹, E. Fretwurst¹ and L.F. Makarenko²

¹ Institute for Experimental Physics, University of Hamburg, Hamburg, Germany

² Belarusian State University, Independence Ave. 4, 220030 Minsk, Belarus

Strong efforts is put to into development of silicon sensors with sufficient radiation tolerance for the future Large Hadron Colliders [1,2]. One of the key objectives is the identification of the radiation-induced defects affecting the sensor properties. A complex study, regarding the generation, time evolution and impact on the electrical properties of silicon detectors damaged by irradiation with monoenergetic electrons, with energies ranging from 1.5 MeV to 27 MeV, has been performed on standard float-zone (STFZ) and oxygen-diffused float-zone (DOFZ) materials [3]. It was shown that by increasing the electron irradiation energy the maximum recoil energy increases leading to a stronger increase of the cluster related defects.

Deep Level Transient Spectroscopy (DLTS) measurements have revealed the linear dependence with the irradiation fluence for the VO, V₂ and V₃ (in PHR configuration) defects [3]. Their introduction rates increase with electron energies and seem to have a saturation behavior for energies higher than 15 MeV as can be seen from Fig. 1a). Annealing studies at moderate temperature (80°C) enabled to determine the capture cross section for holes of the V₃^(-/0) acceptor state as $\sigma_p = 2.15 \times 10^{-13}$ cm². Moreover, it was shown that while the contribution of V₃ defect (in PHR configuration) to the leakage current increases with electron energy it decreases with increasing the irradiation fluence. Thermally Stimulated Current (TSC) measurements on samples irradiated with larger fluences demonstrated that the extended defects with strong contribution on the macroscopic properties of the silicon detectors like the E(30K) – shallow donor in the upper part of the silicon badgap and the H(116K), H(140K), H(152K) defects – acceptors in the lower part of the badgap, are generated in concentrations increasing

linearly with the irradiation fluences. The rates for all these clusters start to saturate around 15 MeV electron energy (Fig.1 b)). Comparing the irradiated STFZ and DOFZ materials, it has been proven that the generation of E(30K) defect is influenced by the oxygen content, its introduction rate being 40% larger in DOFZ compared to STFZ. In contrast, the generation rates for the H defects are very similar indicating that oxygen is not directly involved in their formation, thus, one can associate them with higher order of vacancy complexes ($V_n > 3$).

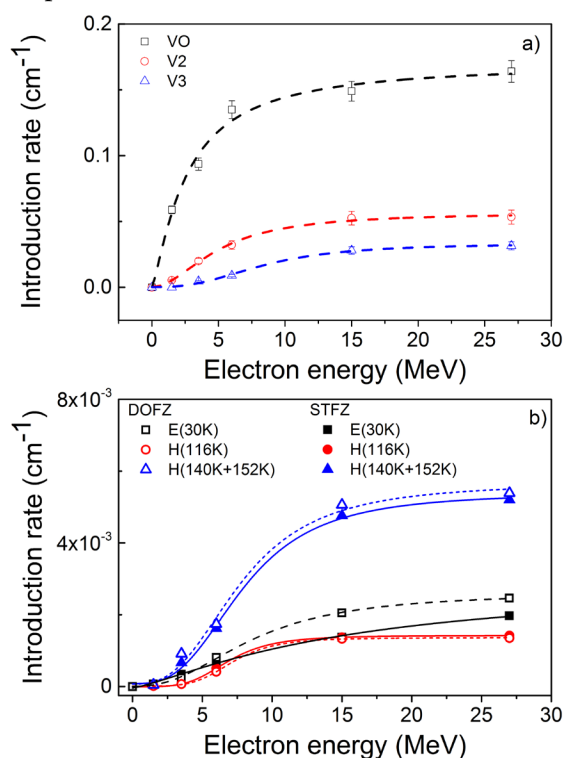


Fig 1. Introduction rates function of electron energy of a) VO, V₂ and V₃ and b) extended defects.

It has also been shown that part of the H defects can change their configuration at RT from an electrically active one giving rise to H(116K) and H(140K+152K) TSC peaks to an electrically inactive one (without energy levels in the bandgap of silicon) undetectable in electrical measurements

(Fig. 2). This change in the defect concentration, reflects fully as a decrease of the depletion voltage V^{dep} [3].

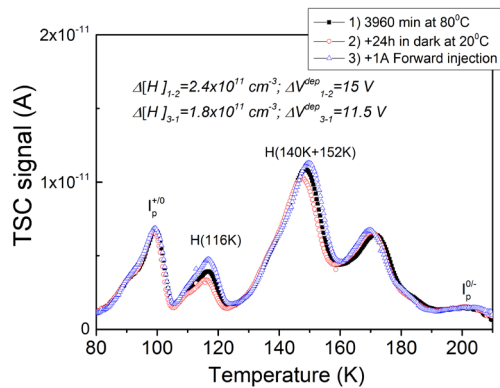


Fig. 2 Bistability of $H(116K)$, $H(140K)$, and $H(152K)$ defects and the corresponding change in the depletion voltage of a STFZ diode irradiated with 27MeV electrons.

In order to describe the generation of point and cluster defects two approaches were used, the classical NIEL – used so far with success for different particles and the effective NIEL. Thus, it was shown [3] that point defects (VO and V_2) are well described with the classical NIEL approach accounting for two body elastic collisions between the PKA's and other secondary recoils in the collision cascade with the lattice atoms (binary calculations), while a linear dependence of introduction rates of the $E(30\text{ K})$ and $H(140\text{ K}+152\text{ K})$ is obtained when molecular dynamics simulations with many body interactions are considered - effective NIEL. Fig. 3 shows an increase of the ratio cluster defects/ point defects by roughly a factor of 10 in the electron energy range between 1.5 and 27 MeV.

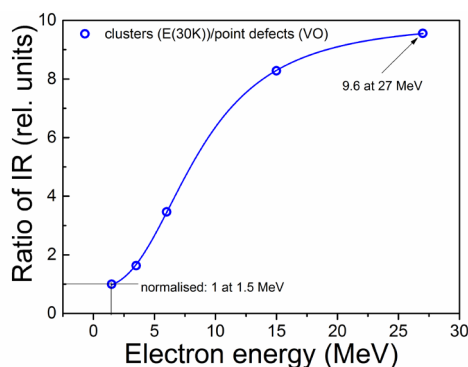


Fig. 3 Normalized ratio of introduction rates (IR) for $E(30K)$ and VO for DOFZ silicon versus electron energy.

HRTEM investigations performed on samples irradiated with high energy electrons revealed the presence of clusters of point defects most of them agglomerated either along the principal crystallographic directions, or randomly, giving rise to dark patches with dimensions in the 3-6 nm range (see Fig. 4). The annealing at 80 °C [3] produces an apparent migration of the defect clusters. The clusters of point defects generated by irradiation with electrons of 15 MeV and 27 MeV in oxygen-lean and oxygen-rich materials, respectively, show similar contrast and distribution along the principal crystallographic directions indicating that the clusters of defects observed by HRTEM are not related to the presence of oxygen in the samples.

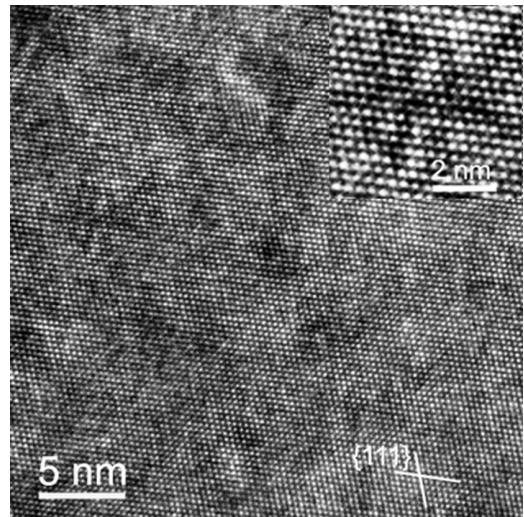


Fig 4. STFZ irradiated with 15 MeV electrons, HRTEM image along the $[110]$ zone axis: clusters of point defects (dotted dark contrast) some agglomerated in dark patches; inset detail of a star-like agglomerate of defect clusters.

Funding from CERN-RD50 collaboration (WODEAN Project) and Romanian Authority for Scientific Research through the Project PCE 72/5.10.2011.

References

1. Peltola T, on behalf of RD50 Collaboration, Nucl. Instrum. Meth. A, 796, 74-79 (2015)
2. G. Casse, on behalf of the RD50 collaboration J. Instrum, 10 (2015)
3. Radu R, Pintilie I, Nistor, LC, Fretwurst E, Lindstroem G, Makarenko LF, J. Appl. Phys., 117, 16503(2015)

Pyroelectricity in polar materials

M. Botea, G.E. Stan, I. Pintilie, G.A. Boni, V. Stancu, A.Iuga and L. Pintilie

Currently, pyroelectric materials are largely used for applications of infrared radiations detectors. The miniaturization of the pyroelectric devices and the integration of the Si-based technology requires thin films deposited on Si substrate. Ferroelectric materials (PZT) or polar wide bandgap (AlN) were deposited on Si substrate by various techniques, such as sol-gel or radio-frequency magnetron sputtering [1].

The pyroelectric measurements on the PZT thin films were performed with modulated light from a 800 nm laser diode coupled with a mechanical chopper having variable frequency. The pyroelectric signal was collected in the voltage mode, with a field effect transistor, and recorded with a lock-in amplifier. The pyroelectric signal generated by the PZT films depends on the substrate. It was demonstrated that the Si substrate amplifies the pyroelectric signal generated by the PZT layer through photogenerated carriers (Fig 1).

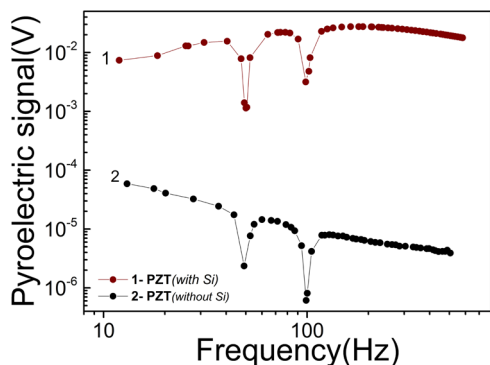


Fig. 1 Frequency dependence of the pyroelectric signal with Si (1) and without Si (2) in the measurement circuit

This effect is only present at wavelengths below 1100nm, when the incident light is absorbed in the substrate, due to the fact that the electric field inside the ferroelectric layer is modulated by the photogenerated carriers. This finding suggests an optical amplification on a specific range of wavelengths corresponding to the semiconductor band gap. The effect was observed not only for PZT thin films, but also for multilayers (PZT/BiFeO₃) or for polar aterials

such as AlN, which has recently attracted the attention due to its properties - the high thermal stability, excellent electrical and optical properties, a wide bandgap, low expansion coefficient and interesting pyroelectric properties [2]. Moreover, it has the advantage that the component elements are fully present in nature and it is a eco-friendly material although it possess a lower pyroelectric coefficients compared with PZT.

Electrical and pyroelectrical properties were studied on AlN thin films with different thickness (600 nm and 1300 nm), deposited by reactive radio-magnetron sputtering on Si substrates with different resistivities. These properties depend on structural quality, which is better for thicker layers.

The surface morphology of films was analyzed by atomic force microscopy (AFM) and the structural quality of the AlN layers was investigated by X-ray diffraction (XRD). For electric and pyroelectric measurements, the top Cu electrodes were deposited by DC magnetron sputtering, using a metal shadow mask. The electrode exposed to the IR beam was blackened for increase the absorption of the incident radiation.

The electric properties of AlN were investigated by capacitance and current measurements. It was found that the structure Cu/AlN/Si⁺⁺ acts as a metal-insulator-semiconductor (MIS) structure, as suggest the S-shaped C-V curve (Fig.2).

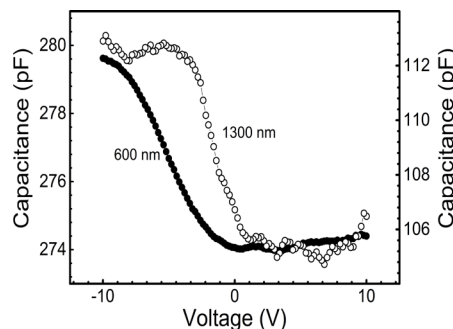


Fig.2 Capacitance-voltage (C-V) characteristics for Cu-AlN-Si⁺⁺ structures, with AlN layers of 600 nm and 1300 nm

Frequency dependence of the pyroelectric signal was measured using two different IR sources of radiation (the same laser diode with wavelength of $\lambda = 800$ nm and the blackbody at 700 °C). The different frequency dependence for the two IR sources is related to different absorption processes: for the black body, the incident radiation is absorbed only by thermal effect and the signal was generated only by the AlN layer through the pyroelectric effect. At 800 nm, the signal can be generated by both of the AlN and Si, with generation of free carriers. These carriers induce a faster response, which is different of the typical pyroelectric detector - doesn't depend on the frequency. Also, the pyroelectric signal is better for the thicker layer, probably due to better structural quality (Fig.3)

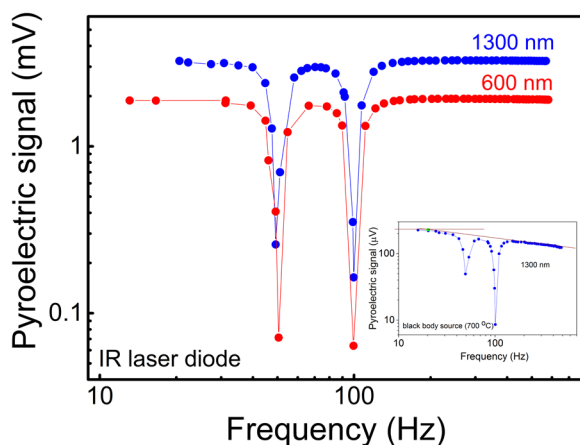


Fig. 3 The pyroelectric response from the IR laser diode for Cu-AlN-Si⁺⁺ samples with different thickness of the AlN layer; in the inset is the pyroelectric signal recorded with black-body at 700 °C for the thicker AlN film.

It has been established that the contribution due to the photogenerated carriers into the Si⁺⁺ substrate was of 10% from the total signal, while the rest of 90% is generated by the AlN layer through pyroelectric effect.

The pyroelectric coefficient was estimated from the pyroelectric signal in the frequency range where the signal is constant. The value obtained was 10 - 12 $\mu\text{C}/\text{m}^2\text{K}$ for the AlN with better structural quality.

The results of the pyroelectric measurements for the AlN layers deposited on the two types of Si substrates are presented comparatively (Fig. 4).

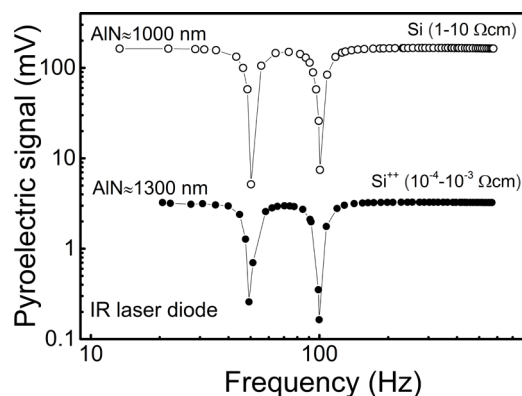


Fig. 4 The signals recorded using the IR laser diode from AlN layers deposited on Si substrate with different resistivities

It can be observed that the resistivity of Si substrate can influence the pyroelectric signal when the radiation source is laser diode. The signal for the AlN deposited on the high resistivity (1 - 10 Ωcm) is with two orders of magnitude higher than for the case of the Si with smaller resistivity was used (5×10^{-4} - 10^{-3} Ωcm). In the first case, the AlN signal generated represents only 1% of the total signal. It shows that the optical amplification can be controlled by the properties of the semiconductor substrate on which is deposited the active pyroelectric element.

NIMP researchers acknowledge financial support from the Core (Nucleus) program of the Nationale Institut of Materials Physics and the IFA (Institute of Atomic Physics, Romania)-CEA (the Commissariat for Atomic Energy, France) cooperation program (Contract no.4/2014).

References:

- [1] M. Botea, L. Pintilie, I. Pintilie, and V. Stancu, *Digest Journal of Nanomaterials and Biostructures*, vol. 10, No.2 (2015) pp. 341-347
- [2] G.E. Stan, M. Botea, G.A. Boni, I. Pintilie, and L. Pintilie, *Applied Surface Science*, 353 (2015), pp. 1195-1202

Polarization induced self-doping in epitaxial $\text{Pb}(\text{Zr},\text{Ti})\text{O}_3$ thin films

L. Pintilie, C. Ghica, C. M. Teodorescu, I. Pintilie, C. Chirila, I. Pasuk, L. Trupina, L. Hrib, A. Boni, N. Apostol, L. Abramiuc, R. Negrea, M. Stefan, D. Ghica

An important step in preserving the polarization direction in a ferroelectric material is represented by the compensation of the depolarization field.

The occurrence of this field is directly related to the polar order, leading to sheets of surface charges having opposite signs on the two faces of the ferroelectric slab. The compensation is performed either with free/trapped charges existing in the volume of the ferroelectric material or with free charges existing in the surrounding atmosphere (including possible electrodes).

The situation changes a little bit in the case of a thin films grown on a conductive substrate because the compensation is favored at the interface between the ferroelectric and the conductive substrate. This may lead to preferential orientation of polarization in the grown film. This type of situation was recently reported in epitaxial $\text{Pb}(\text{Zr},\text{Ti})\text{O}_3$ (PZT) films grown on SrRuO_3 (SRO) electrode [1]. Another experimentally observed phenomena is the increase of the leakage current magnitude as the thickness of the PZT film decreases. The two observations suggest that free carriers are generated in the film during its growth by a kind of self-doping process.

The hypothesis was tested on a set of epitaxial PZT films with different thicknesses grown by pulse laser deposition (PLD) method on SRO electrodes previously deposited with the same method on single crystal SrTiO_3 (STO) substrates with (001) orientation. Details on the growth conditions can be found elsewhere [2,3]. The structural quality of the films was verified by in depth analysis using X-ray diffraction and high resolution transmission electron microscopy (XRD and HR-TEM). It was found that, as the thickness increases, the films have the tendency to relax by forming dislocations and ferroelectric domains (see the figures 1 and 2).

The presence of a mono-domain state in very thin films (usually below 50 nm) was tested with the aid of the piezoelectric force microscopy (PFM). Correlated with the results of the poling test, it was concluded that the dominant polarization in the as

grown films, in atmosphere, without deposited top electrode, is the upward direction from the substrate to the surface (see figure 3).

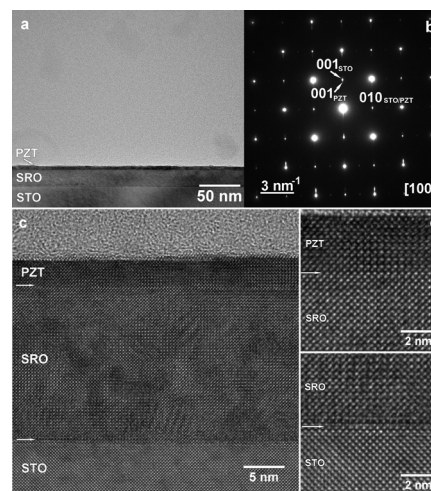


Fig. 1 Low-magnification cross-section TEM image of the PZT/SRO/STO structure (5 nm PZT sample); (b) SAED pattern from the substrate and the deposited layers; (c) low magnification HRTEM image of the PZT/SRO/STO structure; (d) HRTEM images at the PZT-SRO and SRO-STO interfaces (white arrows indicate the SRO-STO and PZT-SRO interfaces).

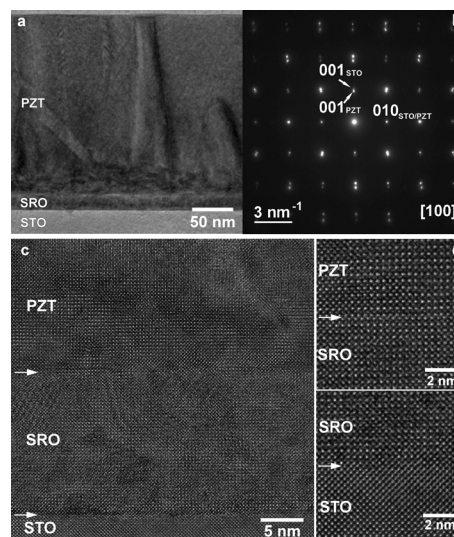


Fig. 2 Low-magnification cross-section TEM image of the PZT/SRO/STO structure (250 nm PZT sample); (b) SAED pattern from the substrate and the deposited layers; (c) low magnification HRTEM image of the PZT/SRO/STO structure; (d) HRTEM images at the PZT-SRO and SRO-STO interfaces (white arrows indicate the SRO-STO and PZT-SRO interfaces).

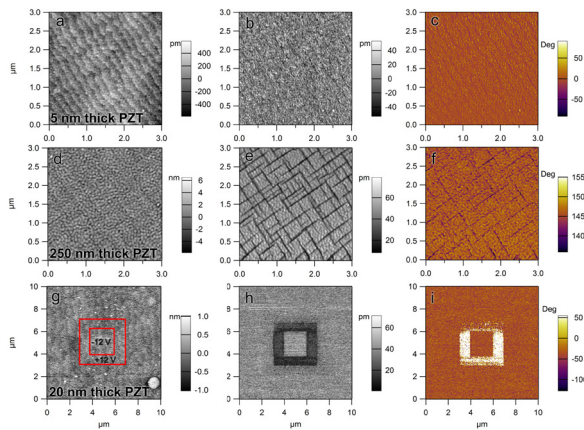


Fig. 3 a) – c) AFM topography, PFM amplitude and phase for the 5 nm thick PZT film - unit cell step terraces can be observed; d) – f) same for the 250 nm thick film - the characteristic grid of 90° domains can be observed; g) – i) poling map, PFM amplitude and phase for a 20 nm thick film - one can observe that the inner square, poled UP (P^+), has the same phase contrast as the unpoled area outside the outer square.

The analysis of the results of the electrical measurements has clearly shown that the concentration of the free carriers in PZT film increases as the thickness decreases (see figure 4). This is a consequence that the polarization value remains approximately constant thus a larger concentration of free carriers is required to compensate the depolarization field as the thickness goes down from 300 nm to 5 nm. It means that structural defects acting as donors or acceptors occur in the film during the growth phase, generating electrons or holes that are involved in the compensation of the depolarization field and in the preservation of the upward direction of polarization. This assumption was verified by performing detailed chemical analysis of the bulk and of the surface of the PZT films using EDS, EELS and XPS techniques. It was found that the $O/(Ti+Zr)$ ratio varies with thickness, suggesting that the amount of vacancies in the films is not similar. Moreover, it was found that for thicknesses over 50 nm the $O/(Ti+Zr)$ ratio has a steady increase with thickness, towards the stoichiometric value of 3, suggesting that oxygen vacancies may be responsible for a higher concentration of free carriers in thinner films (below 300 nm).

An electrostatic model was developed, considering that the polarization charges are partly compensated with electrons provided by oxygen vacancies acting as donors, and partly with free electrons from the electrode. The resulting thickness dependence resembles the empirical $1/d$ relation extracted from figure 4.

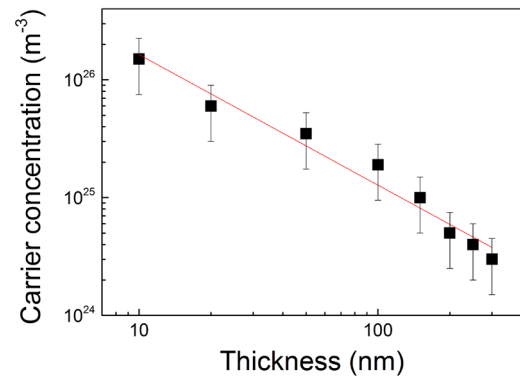


Fig. 4 The thickness dependence of the free carrier concentration in epitaxial PZT thin films.

Funding from Idea-Complex Research Grant PN-II-ID-PCCE-2011-2-0006 (contract nr. 3/2012).

References

- [1] Luo, Y., et al. , Upward ferroelectric self-poling in (001) oriented $PbZr_{0.2}Ti_{0.8}O_3$ epitaxial films with compressive strain, *AIP Advances* **3**, 122101 (2013).
- [2] I. Pintilie, C. M. Teodorescu, C. Ghica, C. Chirila, A. G. Boni, L. Hrib, I. Pasuk, R. Negrea, N. Apostol, and L. Pintilie, Polarization-Control of the Potential Barrier at the Electrode Interfaces in Epitaxial Ferroelectric Thin Films, *ACS Appl. Mater. Interfaces* **6**, 2929–2939 (2014).
- [3] Pintilie, C. Ghica, C. M. Teodorescu, I. Pintilie, C. Chirila, I. Pasuk, L. Trupina, L. Hrib, A. Boni, N. Apostol, L. Abramiuc, R. Negrea, M. Stefan, D. Ghica, Polarization induced self-doping in epitaxial $Pb(Zr,Ti)O_3$ thin films, *Scientific Reports* **5**, 14974 (2015).

FeSe_{0.3}Te_{0.7} single crystals: superconductivity and Mössbauer spectroscopy aspects

Simona Greculeasa, Lucica Miu, Petre Badica, Mugurel Tolea, Victor Kuncser

in cooperation with

Jiacai Nie

Department of Physics, Beijing Normal University, Beijing 100875, People's Republic of China

The occurrence of superconductivity in iron-based chalcogenides attracted special interest for a possible interplay between superconductivity and magnetism. The FeSe superconducting transition (ST) temperature of 8 K can be increased up to 36.7 or 14 K by high external pressure or by substitutions in Se sites [1], respectively. Given the easy way of tuning their magnetic, structural, and superconducting properties, $FeSe_{1-x}Te_x$ compounds may be good candidates for studying the relationships among structure, magnetism, and superconductivity. The interplay among structure, superconductivity, and electron configuration of Fe in the FeSe_{0.3}Te_{0.7} single crystal prepared by the Bridgman method was studied by Mössbauer spectroscopy and SQUID magnetometry [2]. The behavior of the hyperfine parameters is explained in terms of lattice distortion, enhanced phonon excitation, and electron reconfiguration accompanying the ST.

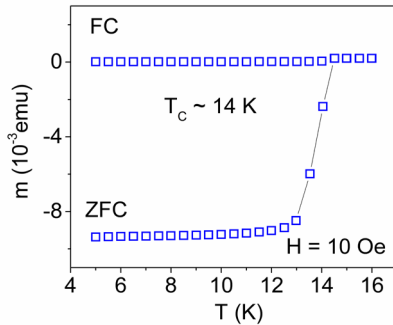


Figure 1 Magnetic moment vs temperature T for the investigated FeSe_{0.3}Te_{0.7} single crystal in the low- T range for an external magnetic field H of 10 Oe.

The ST is evidenced in Fig. 1 at ~ 14 K, and the transition width is of ~ 1 K. An enhanced structural texture is considered, and accordingly the fitting procedure used for the Mössbauer spectra (Fig. 2) consisted in the full Hamiltonian method, evidencing the presence of the FeSe_{0.3}Te_{0.7} phase, with no effective magnetic moment down to 5 K. The fitting parameters

evidence abnormal temperature variations of both the isomer shift IS and the total absorption area (related to the recoil free f factor), as well as of the quadrupole splitting.

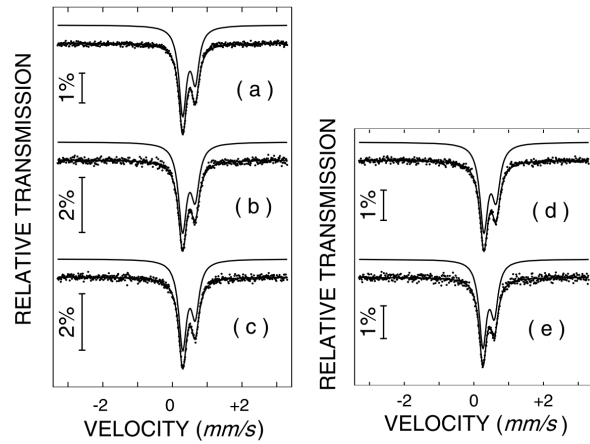


Figure 2 Mössbauer spectra of FeSe_{0.3}Te_{0.7} acquired at 5 (a), 17 (b), 50 (c), 100 (d), and 200 (e) K.

An extensive analysis of the evolution of the hyperfine parameters in a wide T range across the ST can be performed. As it is known, by taking into account the effect of the lattice dynamics, the general expression of IS [3] is:

$$IS = IS_{CH}(T) + IS_{SOD}(T), \quad (1)$$

where IS_{CH} is the chemical IS, while IS_{SOD} is the second-order Doppler shift. IS_{CH} is weakly temperature dependent (unless a T -dependent electron reconfiguration takes place), while IS_{SOD} is strongly affected by T .

In the frame of the Debye model, it results:

$$IS = IS_{CH} - \frac{3kT}{2mc} \left[\frac{3\theta_D}{8T} + 3 \left(\frac{T}{\theta_D} \right)^3 \int_0^{\theta_D/T} \frac{x^3}{e^x - 1} dx \right], \quad (2)$$

and

$$f = \exp \left\{ - \frac{6 \left(\frac{E_\gamma^2}{2mc^2} \right)}{k\theta_D} \left[\frac{1}{4} + \left(\frac{T}{\theta_D} \right)^2 \int_0^{\theta_D/T} \frac{x dx}{e^x - 1} \right] \right\}. \quad (3)$$

In Eqs. (2) and (3), the mass is the effective mass m_{eff} , taking into consideration the effect of bonding the nucleus in the solid state through the surrounding ligands. The best fit for IS and total

absorption area was obtained for m_{eff} of 95(5) Da. The evolution of the Debye temperature relative to the effective mass is also shown in Fig. 3 (up), converging to 250(10)K for m_{eff} of 95(+5) Da. Once the two parameters θ_D and m_{eff} are extracted, one can precisely determine both IS_{SOD} and IS_{CH} (related to electron configuration effects). First, a direct correlation between the second-order Doppler shift and the total absorption area was obtained (Fig. 3 (down)), and, assuming no structural transition, this correlation can be extrapolated to the low-T range. According to such a correlation, the decrease in f in the low-T domain is accompanied by a corresponding decrease of IS_{SOD} . This behaviour is related to phonon softening, which can start to set in at $T \leq T_C$.

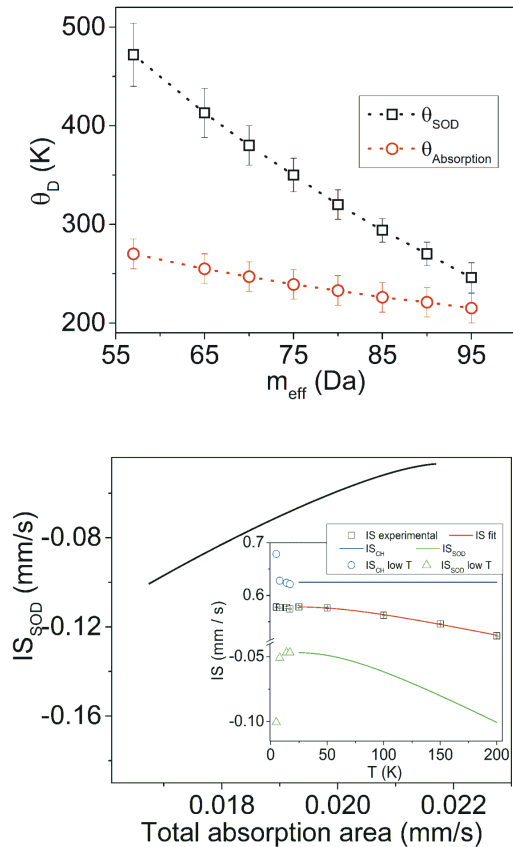


Figure 3. Debye temperatures θ_D as obtained from the T dependence of IS_{SOD} (θ_{SOD}) and $f(\theta_{\text{Absorption}})$ for different values of m_{eff} (up). Temperature evolution of IS , IS_{SOD} , and chemical IS , IS_{CH} (down).

Taking into account the decrease in IS_{SOD} with decreasing T below 17 K (with the clear indication of an enhanced thermal activation of

the phonons), the behavior of the experimental IS can be explained by a pronounced increase in IS_{CH} in the superconducting state (Fig. 3 (down)), indicating a decreased density of $4s$ electrons at the Fe nucleus. Note that if a $3d^{6-x}4s^x$ configuration is assumed for Fe^{2+} ions, owing to the strong hybridization effects with Te/Se neighbors, such a decrease in the density of $4s$ electrons at the Fe nucleus might be consistent with either a decrease in the density of the outer $4s$ electrons or with an increase in the density of screening inner $3d$ electrons. That is, in the superconducting state, pairs of the most external electrons with opposite spin (overall, the $S = 0$ spin state is preserved) can be released in the structure, leading to weaker Fe–Te/Se bonds and an enhanced vibration of Fe ions. However, abnormal variations of both I_{CH} and QS below ~ 17 K suggest a correlation between tiny structural changes and electronic reconfigurations in the superconducting state.

Hence, an insignificant modification of the energy phonon spectrum is expected below T_C , giving support for the same correlation between IS_{SOD} and f (related only to thermal activation processes) in the entire range of analysed temperatures. In addition, the typical variation of QS suggests that, by lowering the temperature, the distortion of the tetragonal lattice along the c -direction slightly increases, but at approximately T_C its trend is inverted, indirectly supporting the idea of an internal driving force towards a more symmetrical orthorhombic structure in the superconducting state.

References

- [1] K.-W. Yeh et al., Europhys. Lett. 84 (2008) 37002.
- [2] S. Greculeasa, L. Miu, P. Badica, J. Nie, M. Tolea, V. Kuncser, J Phys Soc Jap 84 (2015) 014701.
- [3] J. Cieslak, B.F.O. Costa, S.M. Dubiel, M. Reissner, W. Steiner, J. Phys.: Condens. Matter 16 (2004) L343.

X-ray photoelectron spectro-microscopy of ferroelectric surfaces

D.G. Popescu, M.A. Huşanu, N.G. Apostol, L. Hrib, L. Trupină, L. Pintilie, C.M. Teodorescu

in cooperation with

A. Barinov, S. Lizzit, P. Lacovug

Elettra Sincrotrone Trieste, Area Science Park, 34169 Basovizza-Trieste, Italy

Photoelectron spectroscopy was demonstrated during the last years to be a valuable method for deriving surface band bendings via precise investigation of surface core level shifts [1,2]. This method is particularly appropriated for the investigation of free surfaces of thin ferroelectric films exhibiting out-of-plane polarization [3], owing to band bendings produced by the fixed charges at the surfaces and by the accumulation of mobile charges of opposite sign, to compensate the depolarization field inside the film. For thicker layers, domains are formed (Fig. 1), but for thinner layers quite often the film manifests like a single domain. In such cases, patterned pre-polarization is employed to determine by piezoresponse force microscopy (PFM) the initial polarization [3].

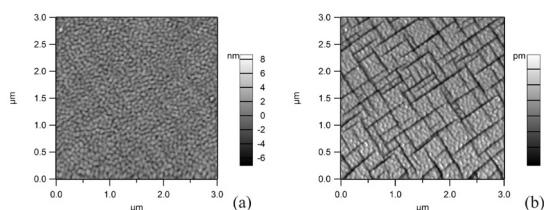


Fig. 1. Images of (a) atomic force microscopy and (b) amplitude signal of piezoresponse force microscopy for a 200 nm PZT(001) thin film.

The actual performances of pulsed laser deposition allows one to prepare high quality ferroelectric thin films, which may be processed in ultrahigh vacuum up to the achievement of perfect surface compositions, absence of contamination and reasonable low energy electron diffraction (LEED) patterns (Fig. 2). On the other hand, synchrotron radiation facilities nowadays include spectromicroscopy beamlines where photoelectron spectroscopy may be achieved with sub-micrometer resolution. This work reports recent studies aiming to combine spectro-microscopic techniques with the new ability of photoelectron spectroscopy to derive surface band bending and thus to visualize direct

domains formed on the surface. Figure 3 presents such an example, obtained on lead zirconate-titanate PZT(111) thin films of 100 nm thickness [4]. The formation of domains is straightforward, however, for practical applications in catalysis, sensors and photovoltaics, (001) surfaces are more appropriated.

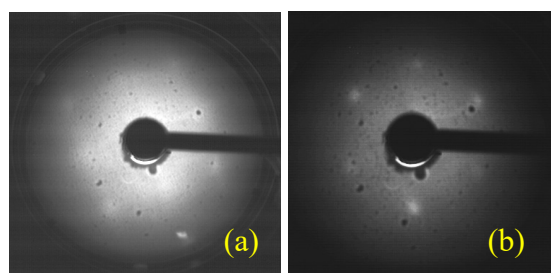


Fig. 2. Low energy electron diffraction (LEED) patterns of (a) PZT(001) and (b) PZT(111). Electron energy: 165-166 eV.

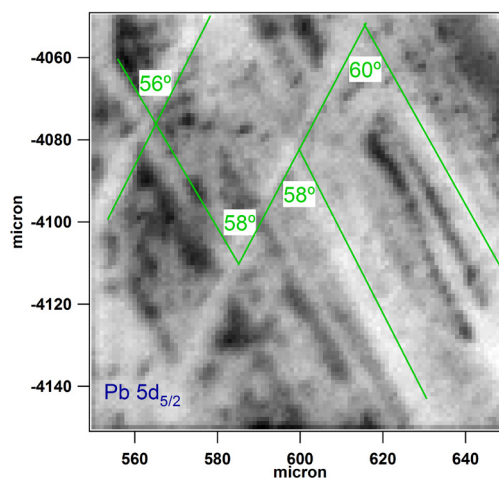


Fig. 3. Total intensities over the Pb 5d_{5/2} core level for a PZT(111) surface.

Spectromicroscopy data in fact consist in data cubes reflecting photoelectron intensities in (width x height x energy) parameter space. Fig. 3 or Fig. 4 for PZT(001) [4] represent maps of total intensities; for each point separate photoemission spectra have been measured.

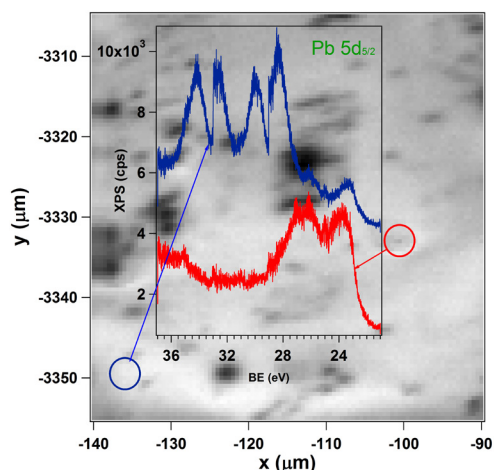


Fig. 4. Total intensities over the Pb 5d_{5/2} core level for a PZT(001) surface. Superposed are separate spectra obtained from the areas highlighted with red and blue circles.

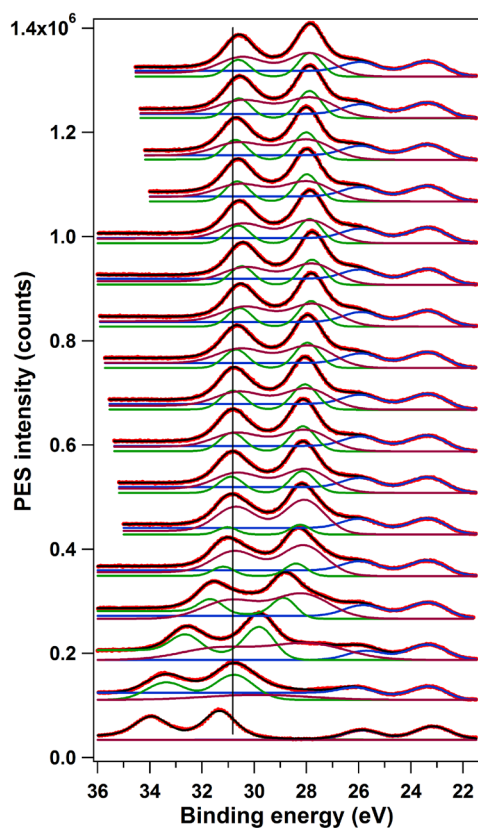


Fig. 5. Time evolution of photoelectron spectra from areas exhibiting components with high binding energy (from bottom to top).

More than 40 data cubes were recorded, each one consisting in average in 100 x 100 spectra. Figure 4 represents photoemission spectra quite position-dependent on PZT(001) surfaces, with sometimes huge shifts (8 – 9 eV). Such shifts cannot be explained by charging due to photoemission processes. Indeed, the time dependence of photoelectron peaks of such areas

(Fig. 5) exhibit a progressive shift of the initial shift towards higher binding energy (HBE). If photoemission charging was responsible by the shift towards HBE, this should increase in time, but actually it decreases. Such behaviour is explained (Fig. 6) by photoemission producing mobile charges into the ferroelectric layer which progressively screen the depolarization field and reduce this shift [5]. Hence, the HBE shift on some areas has the significance that these areas are only partially compensated, thus they present an inner (depolarization) field and are good candidates for charge separation in photovoltaics.

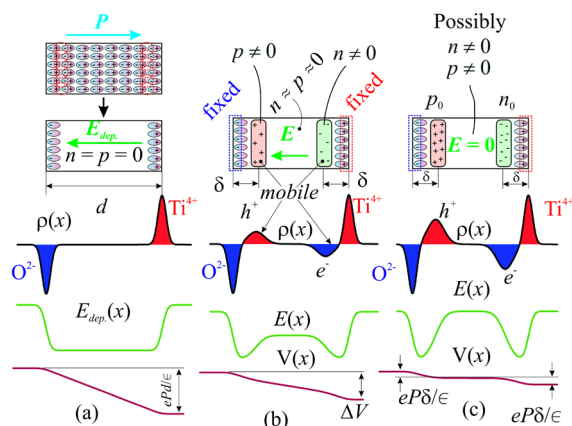


Fig. 6. Charge distributions, fields and potential energies for ferroelectric films with no compensation (a), partial compensation (b), and compensation (c) of the depolarization field.

References

- [1] N.G. Apostol, L.E. Stoflea, G.A. Lungu, C. Chirila, L. Trupina, R.F. Negrea, C. Ghica, L. Pintilie, C.M. Teodorescu, *Appl. Surf. Sci.* **273**, 415-425 (2013).
- [2] L.E. Stoflea, N.G. Apostol, C. Chirila, L. Trupina, R. Negrea, L. Pintilie, C.M. Teodorescu, *J. Mater. Sci.* **49**, 3337-3351 (2014).
- [3] L.E. Ștoflea, N.G. Apostol, L. Trupină, C.M. Teodorescu, *J. Mater. Chem. A* **2**, 14386-14392 (2014).
- [4] M.A. Hușanu, D.G. Popescu, C.A. Tache, N.G. Apostol, A. Barinov, S. Lizzit, P. Lacovig, C.M. Teodorescu, *Appl. Surf. Sci.* **352**, 73-81 (2015).
- [5] D.G. Popescu, M.A. Hușanu, L. Trupină, L. Hrib, L. Pintilie, A. Barinov, S. Lizzit, P. Lacovig, C.M. Teodorescu, *Phys. Chem. Chem. Phys.* **17**(1), 509 - 520 (2015).

Quantitative model for SERS amplification factors

C.M. Teodorescu

Raman spectroscopy is a widely used method for identification of molecular species from their vibrational spectra and, during the last decades, surface enhanced Raman spectroscopy (SERS) has been promoted as method with ultimate sensitivity, owing to amplification factors which may 10^4 - 10^7 in the vicinity of metal substrates [1]. This allows, for example, single molecule detection or ppt range sensitivity. Noble metal surfaces (Au, Ag) are the most widely used SERS substrates; also, surface nanostructuring yields further enhancement [2]. The enhancement is particularly important when the excitation frequency approaches the plasmon frequency in the metal ω_p ; from here, an electromagnetic (EM) theory of the SERS enhancement is nowadays accepted, which basically can be sketched as following: (a) the incoming alternate EM field excites plasmons in the metal; (b) plasmons produce an oscillating EM field in phase with the incoming radiation, thus amplifying it and yielding enhanced scattering.

The present work proposes a different outline: (a) the incoming EM field polarizes the target molecule; (b) the polarized molecule (a dipole) produces an image dipole in the metal; (c) the field produced by the image dipole is added to the incoming EM field; (d) the modified polarizability in presence of the image dipole increases by several orders of magnitude (Fig. 1). One has to figure out that the Raman scattering is proportional to the modulus of the polarizability squared $I_{SERS} \propto |\alpha|^2$. The basic algebra to describe this effect was firstly sketched almost four decades ago [3] and is reconsidered in the actual work [4], as follows. Let d be the distance from the excited molecule to the metal wall, P its dipole moment and E_0 the incoming EM field. It is easy to estimate that the induced electric field at the original molecule by its image is $E_{ind.} = P/[4\pi\epsilon_0(2d)^3]$, ϵ_0 being the vacuum permittivity. Let α_0 be the polarizability of the molecule in absence of the metallic wall. Therefore, the total

dipole moment given by the incident E_0 and the induced $E_{ind.}$ electric fields is given by:

$$P = \alpha_0 (E_0 + E_{ind.}) = \alpha_0 E_0 + \frac{\alpha_0 P}{4\pi\epsilon_0 (2d)^3} \quad (1)$$

The ‘effective’ polarizability near the metal surface is computed from $P = \alpha E_0$, yielding:

$$\alpha = \frac{\alpha_0}{1 - \frac{\alpha_0}{4\pi\epsilon_0 (2d)^3}} = \frac{4\pi\epsilon_0 V_p}{1 - \frac{V_p}{(2d)^3}} \quad (2)$$

where V_p is the ‘polarizable molecular volume’, defined such as $\alpha = 4\pi\epsilon_0 V_p$. A singularity in eq. (2) is obtained when $2d \sim V_p^{1/3}$, i.e. the distance d must be lower than a few Ångstroms for usual molecules.

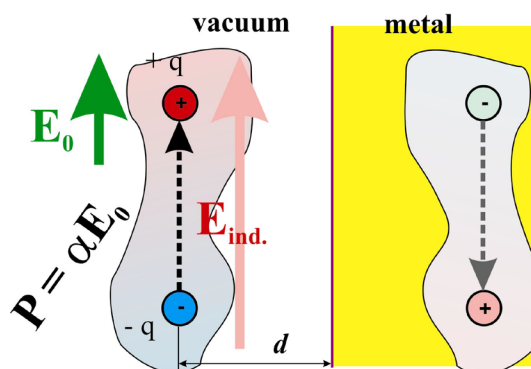


Fig. 1. Image dipole created into a metal surface. E_0 is the external field, $E_{ind.}$ is the induced field by the image dipole at the location of the original dipole.

This model explains why SERS is obtained mostly on noble metals (Au, Ag), since these metals have usually lower inherent contamination as compared with other, more reactive, metals; thus, molecules may be found closer to the metal surface. It is also shown how stronger SERS amplifications may be obtained using nanostructured surfaces, once the excited molecules are localized in concave sites (Fig. 2). A ‘geometric enhancement factor’ f emerges from this study:

$$f = \frac{E_i}{E_i^{(0)}} \approx \left(\frac{2R}{2R-d} \right)^3 \quad (3)$$

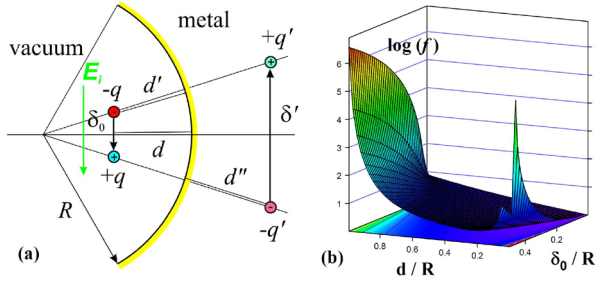


Fig. 2. (a) Image dipole produced by a concave metal surface. (b) Enhancement factor f due to the presence of concavities. δ_0 is the distance between charges in the investigated molecule.

The dependence on the fourth power of the incoming radiation electric field is obtained by taking into account the dynamics of adsorption/desorption processes of molecules [4]. The SERS effect is maximal when the excitation frequency is red-shifted with respect to the bulk plasmon resonance. From a dynamic theory, a frequency dependent amplification factor $g(\omega)$ is derived such as:

$$g(\omega) = \frac{\left(1 - \frac{\omega^2}{\omega_p^2}\right)}{\left(1 - \frac{\omega^2}{\omega_p^2}\right)^2 + \omega^2 \tau_0^2} \approx \frac{1}{1 - \frac{\omega^2}{\omega_p^2}} \quad (4)$$

when $\omega\tau_0 \ll 1$, ω being the frequency of the radiation, τ_0 the relaxation time in the metal and ω_p the bulk plasmon frequency. Taking into account geometry and frequency effects, the SERS polarizability may be written as:

$$\alpha = \frac{4\pi \epsilon_0 V_p}{1 - \frac{V_p \cdot f \cdot g(\omega)}{(2d)^3}} \quad (5)$$

Also, the SERS amplification factor may be dictated by the polarizability of the investigated molecule α_0 in a much more critical way than just a power law α_0^2 or even α_0^4 . By comparing the dipole induced charge density with the amplitudes of plasma waves, the domain of validity of the present theory is derived to be in the low separation regime, where the distance between molecules and metal substrates are below a few

nanometres. Some data from the literature are analyzed in the framework of this model, namely the distance, frequency and temperature dependence of the SERS signal, all confirming the validity of the model. For example, Fig. 3 presents the dependence of the SERS intensity on an insulating (Al_2O_3) interlayer spacing to the metal (Ag) amplification substrate, together with a fit of the actual model.

The result of this work is the endowment of the SERS community with a quantitative formula for the SERS amplification factor, given by eqs (3-5).

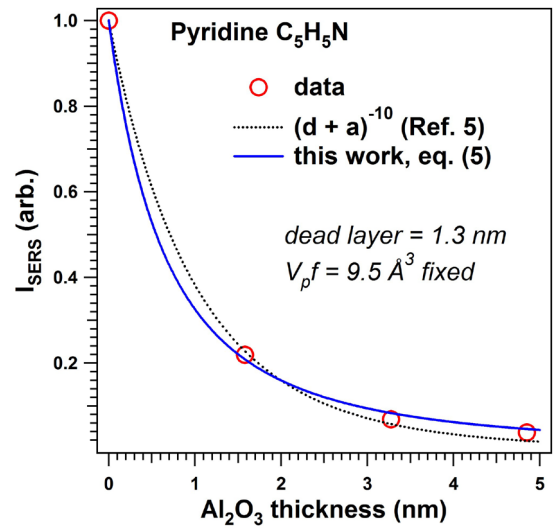


Fig. 3. Fits of the dependence of the SERS signal on the Al_2O_3 spacer to Ag films. Data extracted from Ref. [5].

References

- [1] K. Kneipp, M. Moskovits and M. Kneipp, (Eds.) *Surface-Enhanced Raman Scattering. Physics and Applications*, Top. Appl. Phys. **103**, Springer, Berlin, 2003.
- [2] T. Ignat, M.-A. Husanu, R. Munoz, M. Kusko, M. Danila, C.M. Teodorescu, *Thin Solid Films* **550**, 354-360 (2014).
- [3] G.C. Schatz, R.P. Van Duyne, *Surf. Sci.* **101**, 425-438 (1980).
- [4] C.M. Teodorescu, *Phys. Chem. Chem. Phys.* **17**, 21302-21314 (2015).
- [5] J.A. Dieringer, A.D. McFarland, N.C. Shah, D.A. Stuart, A.V. Whitney, C.R. Yonzon, M.A. Young, X. Zhang, R.P. Van Duyne, *Faraday Discuss.* **132**, 9-26, (2006).

Influence of hole depletion and depolarizing field on a ferroelectric tunnel junction: photoelectron spectroscopy and first principles calculations

D.G. Popescu, N. Barrett, C. Chirila, I. Pasuk, M.A. Huşanu

The effects of the bonding mechanism and band alignment in a ferroelectric (FE) BaTiO₃/ferromagnetic La_{0.6}Sr_{0.4}MnO₃ tunnel junction are revealed in X-ray photoelectron spectroscopy correlated with first principles calculations[1].

The electronic origin of the magnetoelectric coupling at a ferroelectric / ferromagnetic (FE/FM) interface where the bottom FM electrode is a hole doped manganite (Ca, Sr) LaMnO₃ is a hot topic due to applications in, for example, resistive readout in random access memories (RAMs). If one takes into account the electron spin, functionality can be extended to four state memories and to controlled, spin-dependent current injection into an insulating layer sandwiched between the ferromagnetic electrodes. Therefore, combining ferroelectricity with additional degrees of freedom offers opportunities for developing interesting applications in, for example, spin-dependent transport, or devices where magnetocrystalline anisotropy is controlled by electric fields [2].

Our heterostructure prepared by pulsed laser deposition results in smooth surface, with single cell stepping (Figure 1) and abrupt (La,Sr)O|TiO₂ interface.

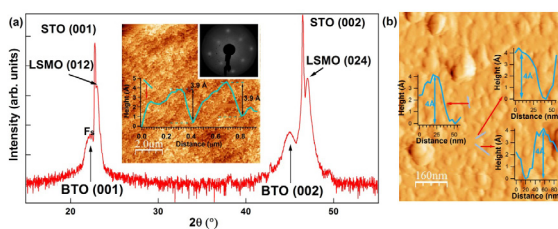


Figure 1 XRD diffraction profile on BTO-covered LSMO crystalline layer and AFM image of both bare LSMO sample BTO-covered LSMO sample showing the uniform character of the surface and the single unit-cell steps between most of the surface features

The band lineup at the interface is determined by a combination of band bending and ferroelectric polarization induced modification of core-hole screening. A Schottky

barrier height for electrons of 1.25 eV is obtained in the case of downwards FE polarization of top layer. The mechanism of band alignment is depicted in Figure 2.

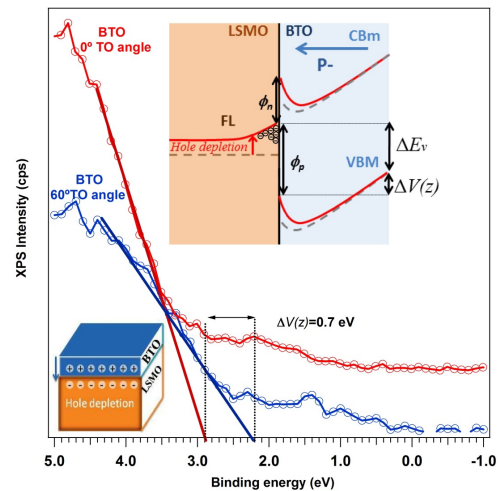


Figure 2 Valence band region of the LSMO/BTO heterostructure recorded at two collection angles in order to infer the effects of the built-in potential in the BTO on the valence band maximum. The inset shows the band alignment and Schottky barrier formation

Moreover, in a ferroelectric heterojunction it is relatively well understood that screening charges are pulled towards interface from the FM layer, leading to hole depletion when the FE polarization points towards and hole accumulation when FE polarization points away from the interface. This, in turn, can reflect in modulation of the electroresistance depending on the FE polarization direction or magnetic phase transition for the bottom electrode in the interface region. In this context we clarify for the first time the signature of hole-depletion state in photoemission as smaller shift towards higher binding energies (0.7 eV) of the interface component in Sr 3d spectrum (Figure 3) with respect bare LSMO case, where the separation between surface and bulk component is of 1.4 eV.

Concerning the electronic properties of the interface, the symmetry of the bonding states are emphasized from integrating the local density of

states ± 0.2 eV around the Fermi level and strong dependence on the FE polarization is found: upwards polarization stabilizes occupation of Ti $t_{2g}(xy)$ orbitals while downwards polarization favors Ti $t_{2g}(yz)$ symmetry as seen in Figure 4.

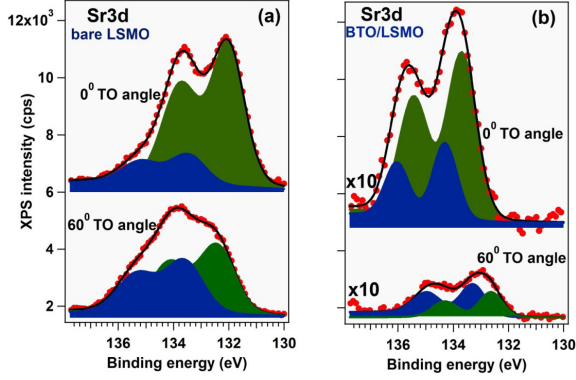


Figure 3 Sr3d XPS spectra recorded on the two samples at normal incidence and at 60° on bare LSMO-(a) and BTO-covered LSMO-(b). Green curves are the bulk components and blue, surface and interface ones

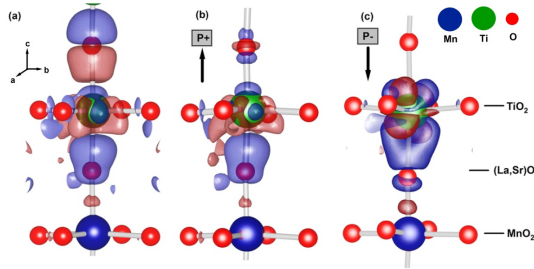


Figure 4 Calculated bonding charge distribution of the LSMO/BTO interface for the paraelectric state, $P=0$ (a), BTO polarization pointing outwards, $P+$ (b) and inwards $P-$ (c). Red color represents the regions with charge depletion and with blue are represented the charge accumulation regions. Isocharge surface 0.5 e.

We predict that the abrupt (La,Sr)O|TiO₂ interface is magnetoelectrically active, leading to a A-type antiferromagnetic (AF) coupling of the first TiO₂ interface layer with the underlying manganite layer through a super exchange mechanism. The spin-dependent orbital polarization and AF coupling visible in Figure 5 indicates that the electronic population at the Fermi level is a combination of spin-up Mn $e_g(3z^2-r^2)$ states and spin-down Ti $t_{2g}(xy)$ ones for $P+$ polarization and spin-up Mn $e_g(3z^2-r^2)$ with Ti $t_{2g}(yz)$ contribution for the opposite FE

polarization of the upper layer. The calculated spin polarization for the interface Ti atoms is $-0.27\mu_B$ in $P+$ case and $-0.78\mu_B$ for $P-$ polarization. The AF magnetic order which stabilizes through a super-exchange mechanism between Mn and Ti atoms adjacent to the interface, mediated by apical oxygens is seen in the peak at -0.3 eV which features the valence region.

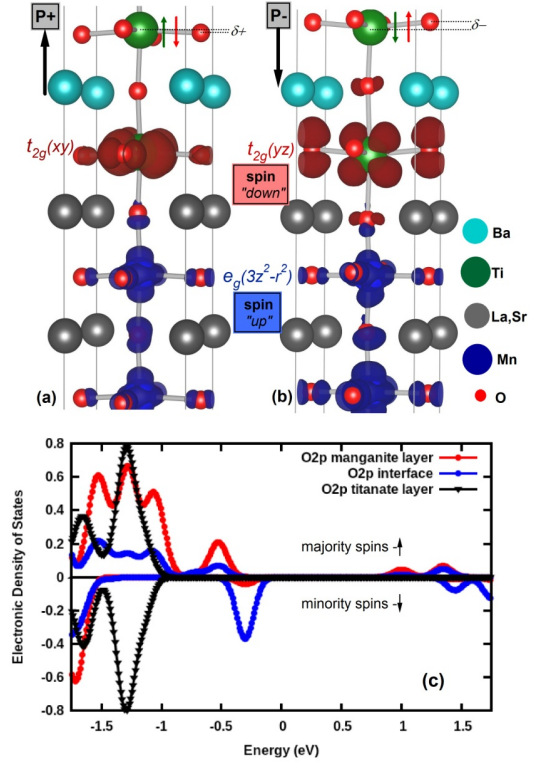


Figure 5 Spin-resolved local density of states integrated ± 0.2 eV around E_F for the BTO layer polarization pointing upwards (a) and downwards (b). Majority, up spins are depicted in blue and minority, down spins in red. Isosurface is 0.004 eV⁻¹. The electronic density of states for O2p states in the manganite environment, at the interface and in the titanate layer are presented in (c).

References

- [1] D.G. Popescu, N. Barrett, C. Chirila, I. Pasuk, M.A. Huşanu, Phys. Rev. B **92**, 235442 (2015).
- [2] A. Mardana, S. Ducharme, S. Adenwalla, Nano Lett. **11**, 3862 (2011).

Surface topography to reflectivity mapping in two-dimensional photonic crystals designed in germanium

M.A. Husanu, C.P. Ganea, I. Anghel, C. Florica, O. Rasoga, D.G. Popescu

In order to achieve a proper manipulation of light in optoelectronic devices routinely used in telecommunication and information technology, extensive efforts are conducted to the development of PhCs and of devices with PhCs. These artificially created periodic dielectric materials possess a photonic bandgap (PBG), preventing light from being transmitted in a range of frequencies, diffract light in UV, visible, and near infrared regions and are associated with photon localization. The PBG width and localization in energy scales depends on the dimensionality of the system (1D-3D), geometry parameters (lattice constant, symmetry) and material used as guiding medium.

A bidimensional photonic crystal has been realized by laser ablation, using a pulsed laser ($\lambda=775\text{ nm}$), perforating an In-doped Ge wafer thus creating a lattice of holes with well-defined symmetry, as seen in Figure 1.

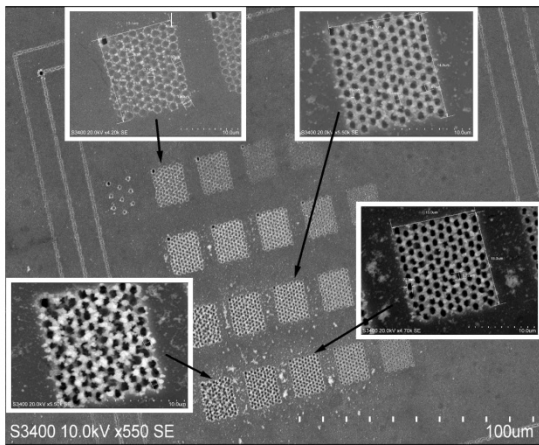


Figure 1 SEM plane-view image of the under test Ge structure.

In particular, using pulses at 2kHz repetition rate, with 200fs pulse duration, 775nm central wavelength, and maximum laser energy of about 0.6mJ per pulse, a impurity-free surface with well-defined triangular symmetry is obtained which we shown that is appropriate for trapping and guiding radiation in telecommunication range.

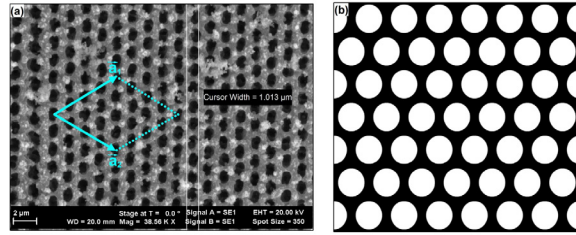


Figure 2 a) SEM top-view image of the prepared 2D PhC structure by drilling Ge sample; b) Calculated schematic diagram of the 2D triangular PhC lattice with a radii cylinders R and lattice constant a .

The region investigated has a filling factor

$$f = \frac{\pi r^2}{a^2} = \frac{\pi (0.375a)^2}{a^2} = (0.375a)^2 \pi \cong 0.442 \quad (1)$$

and the lattice constant $a=1.5\mu\text{m}$ (Fig.2a). A supercell with parameters in accordance with the experimental findings (Fig.2b) has been used for numerical analysis with a dielectric constant $\epsilon=16$. Photonic band structure is computed within finite difference frequency domain framework while the reflection spectra have been obtained using a finite difference time domain formulation as implemented in the open source MIT Photonic Bands (MPB) Package.

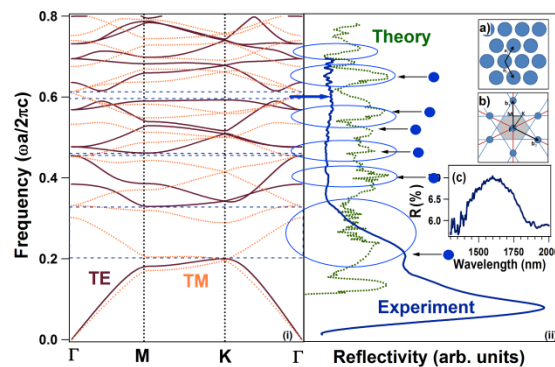


Figure 3 I - Photonic band structure of the triangular PhC lattice that consists of air cylinders in Ge matrix for TE modes (continuous line) and TM modes (dashed line); II - experimental and theoretical reflectivity spectra in the Γ point for the PhC. Insets: unit cells of the PhC structures in direct (a) and reciprocal (b) space and Γ^t Brillouin zone (c).

The resulted band structure is shown in Figure 3(I) and the theoretical one in Figure 3(II), with frequencies expressed in ca units, c – the speed of light and a – the lattice constant. With solid line are depicted the transverse electric (TE) modes and with dashed line the transverse magnetic (TM) ones. The existence of 3 bandgaps for TE modes and 2 gaps for the TM ones is reported. The large TE gap with the central frequency at $\omega_{1e}=0.266$, and bandwidth $\Delta\omega_{1e}=0.133$, is also found in other 2D PhC realized in Si substrate. Additionally, two smaller gaps are identified at $\omega_{2e}=0.458$, $\omega_{3e}=0.602$ with $\Delta\omega_{2e}=0.01$, $\Delta\omega_{3e}=0.025$. TM modes are featured by two smaller gaps located at $\Delta\omega_{1m}=0.543$ and $\Delta\omega_{2m}=0.669$.

By inspecting the calculated band structure around the Γ point, which corresponds to $k_x=k_y=0$ in the reciprocal space (*i.e.* at normal incidence) with the experimental reflectivity spectrum we establish a fair agreement with the reflection experiment, except for a loss of intensity in the region at higher frequencies. We note that measurements have been performed with uniform-polarized light, and this is why the intensity of the photonic bands is seriously attenuated once we record reflected light with no well-defined polarization. A second reason of the intensity drop in the region at higher frequencies is that their localization is within the radiation continuum, falling above the $\omega=ck$ light cone of the ambient air. Thus, inherently they are leaky, radiative modes.

Besides the gap in the low energy range of transversal electric modes, a second one is identified in the telecommunication range, originating in the localization of the leaky modes within the radiation continuum.

In order to achieve spatial resolution of the regions featured by light localization in our photonic structure and assess the efficiency for PhC production, we investigated the prepared sample by Fourier Transform Infrared Imaging. In Figure 4 such maps recorded in different regions are presented. They were obtained by

recording a different spectrum for every scanning point. Thus, the regions featured by intense reflectance associated with photonic gaps are displayed in red and the less intense signal is depicted in violet. The violet regions mark the position where the microscopic-FTIR spectra record no band gap. In this manner, direct visualization of the photonic activity can be obtained. SEM image of these regions under study is presented in Figure 4(g) equivalent to the white square from Figure 4(a).

The dark areas in Fig. 4(a-e) stand for maximum reflectivity originating in photonic gaps and are associated with blocked light propagation.

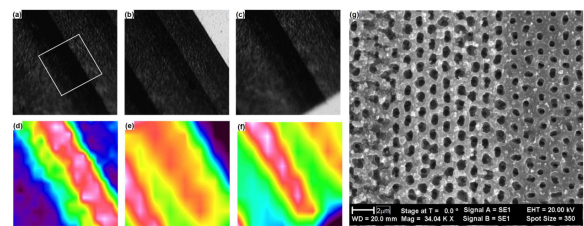


Figure 4 FTIR spectromicroscopic images. (d, e, f) Topography of the photonic structures built in Ge matrix recorded in the areas depicted in (a, b, c), with the white square delimiting the region recorded by SEM (g).

For comparison, regions with different morphology and poor periodicity in which consequently the PBG lacks, are featured by low reflectance.

The emerging picture is of a device with promising characteristics as an alternative to Si-based technology in photonic device fabrication with special emphasize in energy storage and conversion.

References

- [1] M.A. Husanu, C. P. Ganea, I. Anghel, C. Florica, O. Rasoga, D.G. Popescu, Appl. Surf. Sci **355**, 1186-1191 (2015)
- [2] M. A. Husanu, D. G. Popescu, C. P. Ganea, I. Anghel, C. Florica, Eur. Phys. J. D **69**(12), 273 (2015)

Comparison between p- and n-GaAs(100) electrodes covered with L-cystein thiolate self-assembled layers

C.C. Negrila, M.F. Lazarescu

in cooperation with

V. Lazarescu, A.M. Toader M. Enache, L. Preda, M. Anastasescu, G. Dobrescu

Romanian Academy - Institute of Physical Chemistry "Ilie Murgulescu" Bucharest, Romania

L-cysteine, one of the two natural thiol-containing amino acids, has both the ability to build self-assembled layers on solid surfaces and the possibility to exchange protons with the environment. These properties recommend it not only as an excellent bio-linker for various bio-applications (such as preparing new biocompatible materials or exploring biomolecular recognition processes) but also as a very attractive molecule for fundamental studies on the electronic and electrostatic interactions at electrified interfaces (such as the influence of the multifunctionality and field-effects on the molecular self-assembling process). L-cysteine has three potential binding centers represented by the amino, carboxylate and sulfhydryl functional groups, which may be equally involved in a chemisorption bond with a metal or semiconductor substrate. It is reported here the performing of *in-situ* (Electrochemical Impedance Spectroscopy, EIS) and *ex-situ* X-ray Photoelectron Spectroscopy, XPS) data concerning the electrochemical behavior of the L-cysteine covered p- and n-doped GaAs(100) electrodes at low pH (0.45). Density Functional Theory, DFT, calculations have also been performed in order to get a deeper insight into the chemical interaction between this organic molecule and the semiconductor substrate. The working electrodes were prepared from Zn doped GaAs(100) ($p=1.1 \cdot 10^{19} \text{cm}^{-3}$) and Si doped ($n=3.8 \cdot 10^{18} \text{cm}^{-3}$) wafers. Back ohmic contacts to the sample were provided by alloying with Au-Zn alloy (p-doped) and Au-Ge-Ni alloy (n-doped) using the thermal evaporation technique. The L-cysteinethiolate film was formed by immersing the semiconductor substrates in 2.5 mM aqueous solution (pH 4.25) for 20 h. EIS investigations were performed with an IM6

Zahner frequency analyzer. Impedance spectra recorded between 0.3 and $3 \cdot 10^5$ Hz were fitted using the ZView software. A SPECS spectrometer with a monochromatized Al K α -anode radiation source was used for the XPS investigations. The survey and detail spectra were taken for all the samples examined, at pressures lower than $2 \cdot 10^{-9}$ mbar and at a pass energy of 100 eV and 20 eV, respectively. The binding energy scale was referenced to the C1s peak at 285.00 eV. Peaks were resolved with the SDP v7.0 software and assigned by considering literature reports. The spectra were fitted using Voigt peak profiles and either a linear or a Shirley background depending on the background shape. The subsequent XPS analysis of the L-cysteine covered p- and n-GaAs(100) samples exhibited in Fig. 1, evidenced the formation of cysteine-thiolate species both in the S2p (Fig.1a) and the As2p core level regions. Analysis of the S2p core-level region (Fig.1a) proved that L-cysteine is bound to the GaAs surface through the thiol head-group, the doublet with binding energies of 162.20/163.38 \pm 0.2 eV being characteristic for thiolate species. The As2p $^{3/2}$ spectra (Fig.1c) were fitted with 3 peaks assigned to As-S species (BE = 1324.9 \pm 0.2 eV), As-O species (BE = 1326.2 \pm 0.2 eV) and substrate As atoms (BE = 1323.2 \pm 0.2 eV), whereas the Ga2p $^{3/2}$ spectrum (Fig.1d) has only contributions from the substrate Ga atoms (BE = 1117.6 \pm 0.2 eV) and Ga-O species (BE = 1118.9 \pm 0.2 eV).

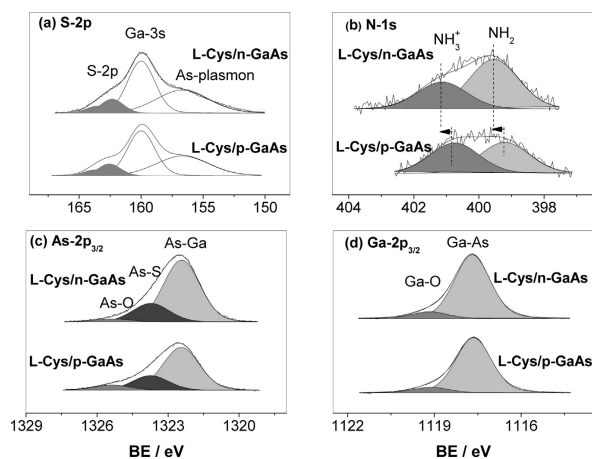


Fig.1 S-2p (a), N-1s (b), As-2p_{3/2} (c) and Ga-2p_{3/2} (d) core-level lines for L-cysteine covered n- and p-GaAs(100).

The two distinct species found in the N1s spectral region (Fig. 1b) with binding energies typical for amino (BE = 399.2±0.2eV) and protonated amino (BE= 400.7±0.2eV) groups point to the coexistence of the neutral and zwitterion species in the cysteine-thiolate overlayer. The profile of the surface / interface state density at the Fermi level, $N_{SS}(\epsilon_F)$, within the semiconductor band gap, estimated from the EIS investigations on the bare electrodes and shown in Fig. 2, evidences higher densities of the surface/interface states associated to As_{Ga} antisite defects at p-GaAs(100) than at n-GaAs (100) electrode, in good agreement with the results of the fractal analysis of the AFM images of the two bare substrates. XPS data evidenced preferential chemisorption bonds of L-cysteine thiolate with As sites at the p-doped and with Ga-sites at the n-doped substrates as previously reported[1,2]. They also pointed to different configurations of the adsorbed species at the two types of semiconducting substrate in good agreement with the results of the fractal analysis of the AFM images.

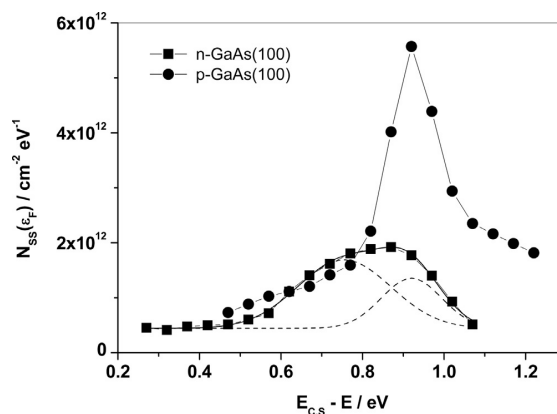


Fig.2 Energetic distribution of surface/interface state densities at Fermi-level, $N_{SS}(\epsilon_F)$ for n-GaAs(100) (■) and p-GaAs(100) (●) under electrochemical bias.

Electrochemical impedance spectroscopy coupled with XPS and AFM investigations on the L-cysteine-thiolate monolayers spontaneously self-assembled on p- and n-GaAs(100) electrodes revealed remarkable effects of the doping type on their electrochemical, chemical, and structural properties. XPS and AFM data brought evidence that, under the cathodic bias, the field-dipole interactions result in replacement of Ga-sites by As-sites in the chemisorption bond at L-cysteine thiolate covered n-GaAs(100), allowing the potential induced internal proton transfer to proceed during the backward potential scan. One may therefore conclude that although the strong affinity of the thiol head to the Ga and As sites is a key factor in the chemisorption process of L-cysteine at GaAs substrates, the adsorption configuration is driven by the field-dipole interaction dependent, in its turn, on the semiconductor space charge both in equilibrium and under polarization conditions.

References:

- [1] V. Lazarescu, M.F. Lazarescu, E. Santos, W. Schmickler, *Electrochim. Acta* **49**, 4231 (2004).
- [2] V. Lazarescu, R. Scurtu, M.F. Lazarescu, E. Santos, H. Jones, W. Schmickler, *Electrochim. Acta* **50**, 4830 (2005).

Strain driven changes of defect parameters in heavy ion implanted Si

*Cătălin Palade, Ana-Maria Lepadatu, Adrian Slav, Ionel Stăvărache,
Magdalena Lidia Ciurea, Sorina Lazanu*

Strain engineering represents a modern field of research. Strain affects the physical, electronic, optical and magnetic properties of crystals and devices from piezoresistive strain sensors up to quantum well lasers with lattice-mismatched heterostructures, strain enhanced MOSFETs and devices which use high atomic mass and size dopants, where the system of electron and nuclear spins of donor atoms in silicon is an excellent qubit candidate for quantum information processing.

We tackled the topic of strain field from the point of view of defects as their presence and behaviour dictate the performance of semiconductor devices. The strain is produced simultaneously with irradiation defects, by implanting I and Bi ions of 28 MeV kinetic energy into high resistivity Si. Both ions have higher atomic size and mass in respect to Si atoms, and consequently produce a local deformation of the lattice. In order to devise the influence of strain on the trapping characteristics of defects, the information obtained from the simulation of the penetration of ions in silicon, *i.e.* distributions of stopped ions and primary defects, is integrated with the results obtained from modelling experimental measurements (parameters of the trapping centres) of thermally stimulated currents without applied bias. The differences found in the characteristics of the trapping centres corresponding to Bi and I implanted Si samples are put in relation and explained using the fields of strain created by the two ions.

We have simulated the penetration of 2000 Bi and 2000 I ions into Si, using the Monte Carlo code *Stopping and Range of Ions in Matter*. The slowing-down of the ions and of all particles set in motion by them is followed until they either leave the target or fall below a selected low kinetic energy. The heavy ions stopped in the lattice, being bigger and heavier than Si ones, produce a local strain. In Figs. 1 and 2 we present the 3D profiles of stopped ions and of their positions in the depth-radius plane, for Bi and I, respectively [1]. The distribution of stopped ions in the depth is a Pearson distribution, which is a nearly Gaussian one with a small tail toward the surface.

From the simulation we obtained for the average range and range straggling the values of 5.09 and 0.42 μm for Bi, and 7.65 and 0.55 μm for I respectively. The corresponding mean radial ranges are 0.49

and 0.77 μm . One can see that the same number of ions is stopped in a narrower region in the case of Bi irradiation, both in depth and radial direction. At the same time, there is a higher difference in size and mass of Bi ions than of I ones in respect to the Si host atoms, so that the strain induced by Bi ions is more intense, but extended on a more limited region than for I irradiated samples.

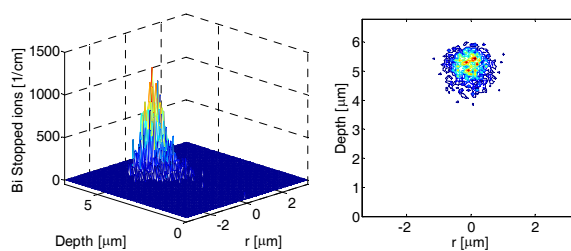


Fig. 1 Distribution of stopped Bi ions: a) 3D profile; b) position in depth-radius plane

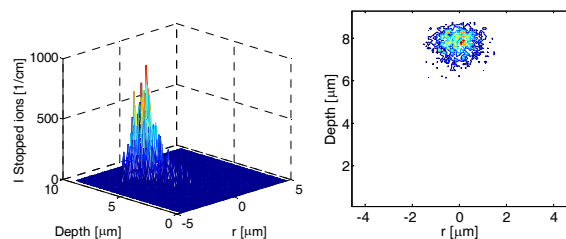


Fig. 2 Distribution of stopped I ions: a) 3D profile; b) position in depth-radius plane

The contour plot in the depth-radius plane for the primary defects produced by Bi and I irradiation obtained from SRIM simulations are presented in Fig. 3. There is an important tail of the vacancy distribution toward the surface, consequence of the process of slowing down, characterized by the cascade of displacements produced by each incoming ion. By comparing the distributions of primary defects with the distribution of ions, one can see that for both Bi and I the maximum of vacancy distribution does not coincide with the maximum of the distribution of stopped ions. Moreover there is an important region under the surface characterized by the presence of primary defects but without stopped ions. In Si both vacancies and interstitials have a high mobility, and consequently during their migration they interact between themselves annihilating or producing V_2 , and interact with the impurities existing in the wafer, as O, C and also doping P, forming the following defects, stable at room temperature: VO, C_i , C_iO_i ,

C_iC_s , and VP. All of them have energy levels in the band gap, and consequently act as traps for the charge carriers.

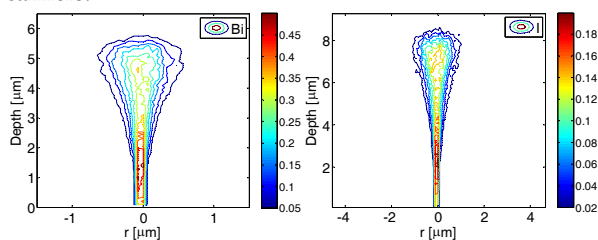


Fig. 3 Contour plot of primary defects in the depth-radius plane for Bi (left) and I irradiation (right)

We calculated the distribution of stable defects starting from the distribution of vacancy-interstitial pairs, using our phenomenological model based on diffusion limited reactions, for the following uniform distribution of impurities in silicon: 4×10^{12} P/cm³, 10^{15} O/cm³ and 5×10^{15} C/cm³. By solving the associated system of differential equations, the time dependence of defect concentrations is found. The distributions of stable defects in the depth of Si, illustrated in Figs. 4 and 5, for the case of Bi and I irradiation respectively, are the asymptotic solutions.

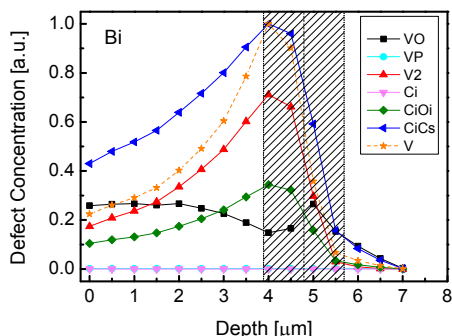


Fig. 4 Depth distributions of defects produced by Bi

In both figures, the depth distributions of defects produced by irradiation with ions of 28 MeV kinetic energy and of 5×10^{11} cm⁻² fluence, normalised to the concentration of C_iC_s , are illustrated together with depth distribution of vacancies, normalised to its maximum. Shaded areas represent regions with stopped ions (one standard deviation). For both Bi and I irradiation, all radiation-induced defects have non-uniform distributions that follow the distribution of vacancies and interstitials (same peak positions, but wider) excepting the VO defect. The superposition between the region with high concentrations of defects and the region with stopped ions is significant, but differs for Bi and I ions. The ratio between the concentration of defects located in the strain region and the total concentration of defects is 33 % for Bi, and 50% for I, respectively.

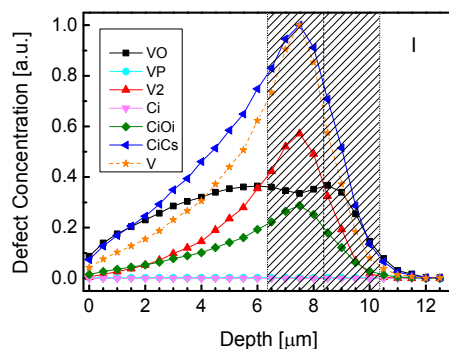


Fig. 5 Depth distributions of defects produced by I

By comparatively analysing the information obtained from modelling experimental curves on Bi and I implanted Si [2, 3] we found that: a) all defects (V_2 , VO, C_iC_s , C_iO_i) are present in both cases as it results by comparing the trap parameters determined by the fitting procedure with those reported in the literature; b) in Bi irradiated samples the energy levels of all traps are broadened with Gaussian distributions (18-30 meV), while in I irradiated samples, for each trap a discrete energy level is determined; c) the capture cross sections of traps in Bi irradiated Si depend on temperature as $1/T^2$, while for I irradiated samples temperature independent capture cross sections were found. The average electric field corresponding to strain is two times more intense in Bi irradiated samples than in I irradiated ones, although the region with stopped ions, i.e. with electric field gradient is narrower.

The only difference between Bi and I irradiated Si is the ion nature, all other characteristics for the irradiation (kinetic energy of the ions, ions charge, fluence, relative orientation beam-Si crystal axes) and the samples used (producer, impurities, resistivity) being similar. Consequently, we can conclude that the strain intensity is the main factor determining the modifications of the parameters of trapping centres, and its spatial superposition on the region with trapping centres is a second order effect.

References

- [1] C. Palade, A.M. Lepadatu, A. Slav, M. L. Ciurea S. Lazanu, Dig. J. Nanomater. Bios. **10**, 1373 (2015).
- [2] M.L. Ciurea, S. Lazanu, A. Slav, C. Palade, EPL **108** 36004 (2014).
- [3] A.M. Lepadatu, C. Palade, A. Slav, S. Lazanu, "Influence of strain field on nanoscale electronic processes in Si-based semiconductors", CAS 2015 IEEE Proc. (2015 International Semiconductor Conference, Oct. 12-14, Sinaia, Romania), pp.41-44, New York (2015).

The effect of in-plane electric field on the Integer Quantum Hall plateaus in grapheme

B. Ostahie and A. Aldea

We investigate the properties of Dirac electrons in a finite graphene sample under a perpendicular magnetic field that emerge when an in-plane electric bias is also applied. The role of electric bias is to act on the spatial position of the channels, with immediate consequences on the quantum Hall effect. Then, having in mind a many-terminal Hall device, it is obvious that the migration of the channels with the electric field affects the electron transmission between different leads, a fact that suffices to change the quantum Hall plateaus. The modified edge states, responsible for this effect, will be called *shortcut edge states*.

The possibility to electrically manipulate the edge states generated by the magnetic field was advanced in [1] for the confined 2D electron gas using the tight-binding approach. We remind that the 2D gas exhibits only conventional Landau bands, which depend linearly on the magnetic field. However, the study of the graphene looks especially promising due to specific aspects such as the relativistic range of the energy spectrum, and the presence of the flat $n = 0$ Landau level at zero energy.

Since the honeycomb lattice arises from the overlapping of two triangular lattices A and B, the tight-binding Hamiltonian can be written in terms of creation and annihilation operators $a_{n,m}^\dagger a_{n,m}$ and $b_{n,m}^\dagger b_{n,m}$, which act on the sites of the two sub-lattices, correspondingly. In accordance with Fig.1, the index n counts the atoms along the horizontal zigzag chains, and m is the chain index. It turns out that for A sites of the blue sub-lattice, one has $n + m = \text{odd}$, while for the red sub-lattice $n + m = \text{even}$. In the presence of a perpendicular magnetic field, the hopping integral t acquires a Peierls phase, which can be calculated by integrating the vector potential along the $A - B$ bonds. Then, the spinless tight-binding Hamiltonian that describes

the π electrons in the graphene lattice in a perpendicular magnetic field has the form:

$$\begin{aligned}
 H = & \sum_{\substack{n,m \\ n+m=\text{odd}}} \varepsilon^a a_{n,m}^\dagger a_{n,m} \\
 & + \sum_{\substack{n,m \\ n+m=\text{even}}} \varepsilon^a b_{n,m}^\dagger b_{n,m} + \\
 & t \sum_{n,m} e^{\pi i \phi (m - \frac{5}{6})} a_{n,m}^\dagger b_{n-1,m} \\
 & + e^{-\pi i \phi (m - \frac{5}{6})} a_{n,m}^\dagger b_{n+1,m} \\
 & + t \sum_{n=\text{odd}} \sum_{m=\text{even}} a_{n,m}^\dagger b_{n,m-1} \\
 & + t \sum_{n=\text{odd}} \sum_{m=\text{even}} b_{n,m}^\dagger a_{n,m+1} \\
 & + H. c., \quad (1)
 \end{aligned}$$

where ϕ is the flux through the hexagonal cell.

The first two terms in Eq.(1) represent the atomic contributions, the next two terms describe the hopping along zigzag chains, while the last ones describe the hopping between neighboring chains.

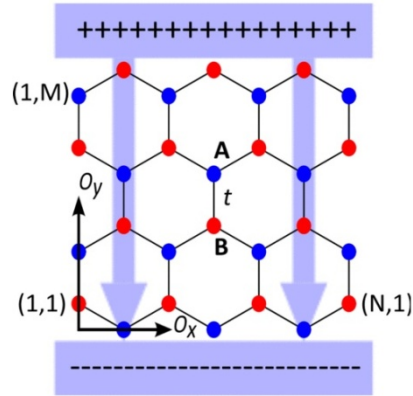


Fig.1: A sketch of graphene lattice with two type of edges: zigzag (O_x direction) and armchair (O_y direction). The blue and red points belong to the sub-lattice A and respectively B, t is the hopping amplitude and the static electric field (blue arrows) is applied parallel to O_y . The number of lattice sites is $N \times M$, in our case 7×4 .

The in-plane electric field is introduced along Oy direction, and it is simulated by replacing in Eq.(1) the on-site energies $\varepsilon^{a,b}$ with $\varepsilon_{n,m}^{a,b} = e\mathcal{E}(y_{n,m} - L_y/2)$, where \mathcal{E} is the electric field, $y_{n,m}$ is the site coordinate and L_y is the length of the honeycomb lattice.

Analyzing the eigenenergies and the charge density $|\psi(\vec{r})|^2$ of the finite graphene system the following aspects can be noticed:

- (i) The energy range occupied by the bulk state at $\mathcal{E} \neq 0$ is more extended than in the case of vanishing electric field. This is understandable since the electric field lifts the quasi-degeneracy of any Landau band, giving rise to a Stark fan with increasing field.
- (ii) The presence among the bulk states at $\mathcal{E} \neq 0$ of several states of reverse chirality indicates that the states are of edge-type, nevertheless, they behave unusually. Indeed, the calculation of the charge density $|\psi(\vec{r})|^2$ proves that all these states keep the localization along the edges, but exhibits also a ridge in the middle of the plaquette, which is perpendicular on the direction of the electric field, and shortcuts two opposite sides. For a given magnetic field, the position of the ridge depends on the energy and can be modified by changing the electric field. Such states generated by the application of the electric field, are shown in Fig. 2 (a, b) and will be called *shortcut edge states*.

The result of the numerical investigation of the Hall resistance as function of the energy in the relativistic range of the spectrum, both in the presence and absence of the applied electric bias, is shown in Fig.2. At vanishing bias, the red curve exhibits the well-known plateaus of the IQHE in graphene at $1, 1/3, 1/5$ (in units h/e^2). However, at $\mathcal{E} \neq 0$, the blue curve shows supplementary unconventional plateaus that appear in-between at $2/3$ and $4/15$, and also a very specific plateau at $R_H = 0$.

In our recent paper [2], we proved the presence of *shortcut edge states* in the relativistic energy range and their influence on the transport

properties denoted by new, unconventional, plateaus of the quantum Hall resistance.

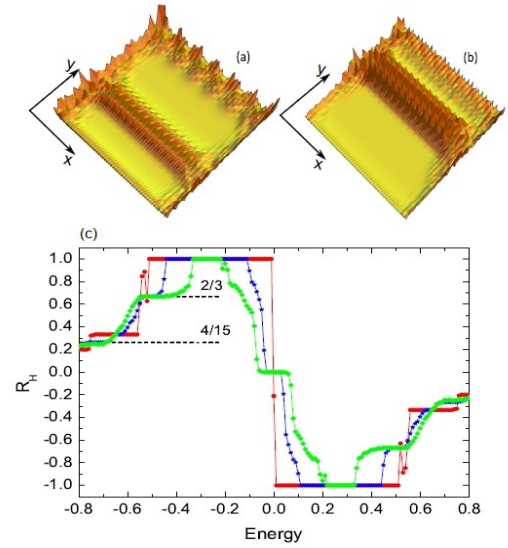


Fig.2: (a, b) $|\psi(\vec{r})|^2$ for two shortcut edge states from the first relativistic Landau band corresponding to the energies $E = 0.5306(a)$ and $0.5786(b)$. The number of lattice sites is 105×40 , $\phi/\phi_0 = 0.03$ and $e\mathcal{E}L_y/t = 0.2$. (c) Hall resistance as a function of energy with no electric field (red curve) and with electric field $e\mathcal{E}L_y/t = 0.25$ (blue) and 0.5 (green). We notice the appearance of the intermediate Hall plateaus in the presence of the electric field. The number of lattice sites 51×100 and $\phi/\phi_0 = 0.03$.

References

- [1] A. Aldea, P. Gartner, A. Manolescu, and M. Nita, Phys. Rev. B **55**, R13389.
- [2] B. Ostahie, M. Nita, and A. Aldea, Phys. Rev. B **91**, 155409.

Ceramics and amorphous thin films based on gallium sulfide and rare-earth sulfides

*M. Popescu, A. Lőrinczi, F. Sava, A. Velea, I. D. Simandan, P. Badica, M. Burdusel,
A. C. Galca, E. Matei, N. Preda, M. Secu,*

in cooperation with

G. Socol, F. Jipa, M. Zamfirescu, A. Balan

National Institute for Laser, Plasma and Radiation Physics, Bucharest-Magurele, Romania

In order to check if gallium sulfide is a good host for accommodating rare-earth ions, we have prepared Ga_2S_3 disc-shaped bulk ceramics doped with 5% EuS , 5% Er_2S_3 and 5% Gd_2S_3 using spark plasma sintering (SPS) [1]. Using the same technique, additional disc-shaped bulk samples of EuS , Er_2S_3 and Gd_2S_3 have been prepared. The sintered ceramic disks of 2 cm in diameter have been used as targets for pulsed laser deposition (PLD) of thin films. All the bulk samples and the thin films have been studied by X-ray diffraction (XRD), scanning electron microscopy (SEM), energy dispersive X-ray spectroscopy (EDX), optical transmission spectroscopy and atomic force microscopy (AFM).

The resulted ceramic based on undoped and doped Ga_2S_3 are polycrystalline and they contain small amounts of base-centered monoclinic Ga_2O_3 . The structure of ceramic Ga_2S_3 is base-centered monoclinic. The doped ceramics Ga_2S_3 contain, besides the base-centered monoclinic Ga_2S_3 , ternary compounds such as face-centered orthorhombic EuGa_2S_4 in $\text{Ga}_2\text{S}_3:\text{EuS}$ or base-centered orthorhombic Er_3GaS_6 in $\text{Ga}_2\text{S}_3:\text{Er}_2\text{S}_3$. The rare-earth sulfides are also polycrystalline in the ceramic disks and they have the following symmetries: face-centered cubic for EuS , monoclinic for Er_2S_3 and orthorhombic for Gd_2S_3 .

The X-ray diffraction patterns of the thin films show that all the PLD prepared films are amorphous. From EDX data we have obtained that the concentration of sulphur in the thin films is lower than in the corresponding bulk samples. Thus, in fact the Ga_2S_3 sample has the formula $\text{Ga}_2\text{S}_{2.27}\text{O}_{0.73}$, EuS is $\text{Eu}_{3.12}\text{S}_{1.88}$, Er_2S_3 is $\text{Er}_{3.46}\text{S}_{1.54}$ and Gd_2S_3 is $\text{Gd}_{3.05}\text{S}_{1.95}$.

The optical band gap for the prepared sulfide amorphous thin films were obtained using the plot $(I_{\text{Abs}})^{1/2} = f[E(\text{eV})]$, where $E(\text{eV})$ is the energy of light quanta expressed in electronvolts and

$I_{\text{Abs}} = \ln(100/I_T)$, $I_T = f(E(\text{eV}))$ is the optical transmission curve measured in the range of 200 ÷ 800 nm. The inferred optical band gaps are: a) a- Ga_2S_3 : 2.17 eV, b) a- $\text{Ga}_2\text{S}_3:\text{EuS}$: 2.16 eV, c) a- EuS : 1.52 eV, d) a- $\text{Ga}_2\text{S}_3:\text{Er}_2\text{S}_3$: 2.06 eV, e) a- Er_2S_3 : 3.64 eV, f) a- $\text{Ga}_2\text{S}_3:\text{Gd}_2\text{S}_3$: 2.12 eV, g) a- Gd_2S_3 : 3.02 eV.

Photoluminescence spectra recorded on undoped and EuS doped Ga_2S_3 bulk polycrystalline samples are presented in the figure 1 a, b. The undoped Ga_2S_3 bulk sample shows a relatively weak and broad peak at about 430 nm, while in the case of EuS doped bulk sample a new broad and strong peak emerges at about 537 nm that was ascribed to the $4f^65d \rightarrow {}^8\text{S}_{7/2}$ transition of Eu^{2+} dopant ions.

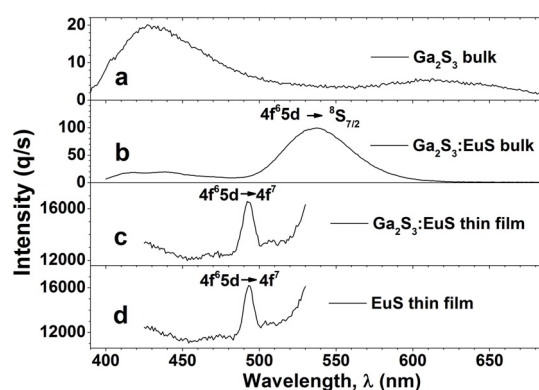


Fig. 1. Luminescence measurements on a) Ga_2S_3 and b) $\text{Ga}_2\text{S}_3:\text{EuS}$ bulk samples (using an excitation radiation with $\lambda = 350$ nm), c) $\text{Ga}_2\text{S}_3:\text{EuS}$ and d) EuS amorphous thin films (using an excitation radiation with $\lambda = 300$ nm).

The very similar shape and intensity in the cases of EuS doped Ga_2S_3 (figure 1 c) and EuS (figure 1 d) amorphous thin films are probably due to the similar cluster formation of the EuS dopant. The peak at 492.9 nm seems to correspond to transition $4f^65d^1 \rightarrow 4f^7$ of Eu^{2+} ions. The luminescence of Er doped Ga_2S_3 and Gd doped Ga_2S_3 has not been possible to be measured.

From the ellipsometric measurements we inferred the refractive index of Ga_2S_3 , EuS , Er_2S_3 and Gd_2S_3 amorphous thin films (figure 2) [2]. The refractive index for the Ga_2S_3 is higher than 3.0 between 308 nm and 378 nm. The extinction coefficient (k) is situated in the range $0 \div 1.5$.

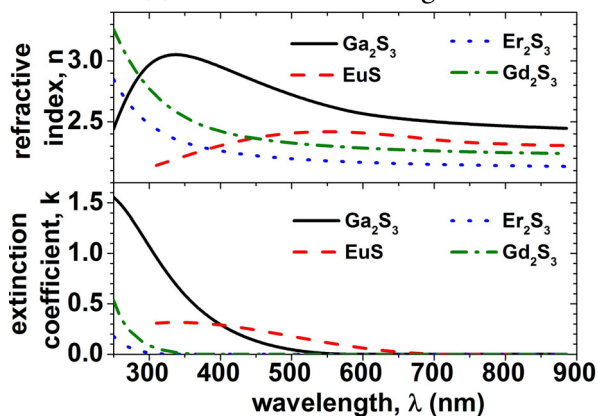


Fig. 2. Refractive index (n) and extinction coefficient (k) for amorphous thin films of Ga_2S_3 , EuS , Er_2S_3 and Gd_2S_3 .

The optical properties of the rare-earth doped gallium sulfide thin films make them promising candidates for planar waveguides and light polarizer applications.

By irradiation of an amorphous Ga_2S_3 thin film ($1.7 \mu\text{m}$ thickness) with a femtosecond laser spot of micrometer size, which has the power between 85 mW and 100 mW, nanostructures in the form of hillock are formed (figure 3), as observed for amorphous As_2S_3 thin films [3]. For the power of 100 mW of the femtosecond laser pulse: $\text{Volume}_{\text{hillock}} = 0.077 \mu\text{m}^3$, the expansion coefficient = 2.45 %.

In figure 4 is shown a comparison between profiles of the hillocks performed with the maximum possible power of femtosecond laser pulses in the case of As_2S_3 [3] (20 mW) and of Ga_2S_3 (100 mW).

Above these thresholds ablation occurs by femtosecond laser irradiation (figure 3).

The authors kindly acknowledge the financial support of the Ministry of National Education (Romania) in the frame of the contract NANOVISMAT PN2-162/2012 and of the Project PN45N/2009.

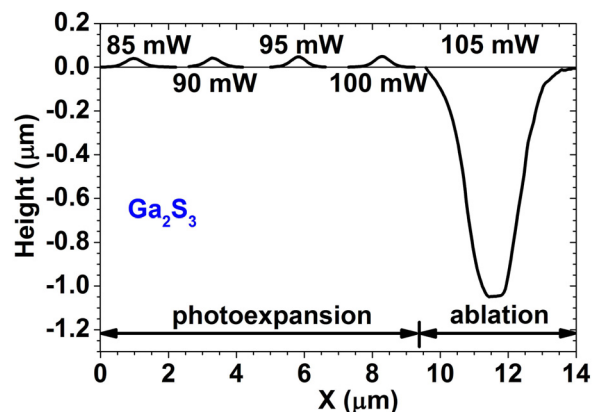


Fig. 3. The profiles of the hillocks performed by irradiation with different power of femtosecond laser pulse (85 mW, 90 mW, 95 mW, 100 mW) and of the hole performed by irradiation with 105 mW.

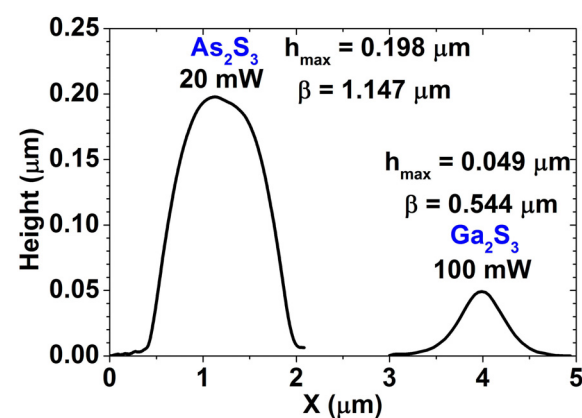


Fig. 4. Comparison between profiles of the hillocks of As_2S_3 [3] and of Ga_2S_3 .

References

- [1] M. Popescu, A. Lőrinczi, F. Sava, A. Velea, I. D. Simandan, P. Badica, M. Burdusel, A. C. Galca, G. Socol, F. Jipa, M. Zamfirescu, *Materials Letters*, 142, 229–231 (2015).
- [2] M. Popescu, F. Sava, A. Lőrinczi, A. Velea, I. D. Simandan, P. Badica, M. Burdusel, A. C. Galca, E. Matei, N. Preda, M. Secu, G. Socol, F. Jipa, M. Zamfirescu, A. Balan, *Semiconductor Science and Technology*, 30, 044001 (2015).
- [3] Velea A, Popescu M, Sava F, Lőrinczi A, Simandan ID, Socol G, Mihailescu IN, Stefan N, Jipa F, Zamfirescu M, Kiss A, Braic V., *Journal of Applied Physics* 2012;112(3);033105-1-033105-4.

Up-conversion luminescence of $\text{Er}^{3+}/\text{Yb}^{3+}$ co-doped sol-gel derived oxyfluoride $\text{SiO}_2\text{-LiYF}_4$ glass-ceramic

C.E. Secu, R.F. Negrea and M. Secu

Rare-earth doped LiYF_4 nanocrystals have received considerable attention in particular for the up-conversion (UC) (i.e. near-infrared (NIR) conversion into the visible or UV spectral range) properties and related applications [1,2], leading to an increased interest for the nanochemistry of this compound. Among the other methods sol-gel method has been proved very useful for obtaining rare-earth-doped nanocrystals embedded in silica glass matrix, i.e. the so called *glass ceramics*.

For the preparation of the oxyfluoride glass-ceramics containing $\text{Yb}^{3+}/\text{Er}^{3+}$ co-doped LiYF_4 nanocrystals we have used the sol-gel route using metal alkoxides [2,3]. Glass ceramization was achieved after subsequently annealing in air at 530 °C [4]. For comparison we prepared $\text{Yb}^{3+}/\text{Er}^{3+}$ co-doped LiYF_4 polycrystalline pellet by using solid state reaction.

The XRD pattern of the glass-ceramic has shown the extra-diffraction peaks due to the LiYF_4 nanocrystals precipitation in the glass matrix (Figure 1)

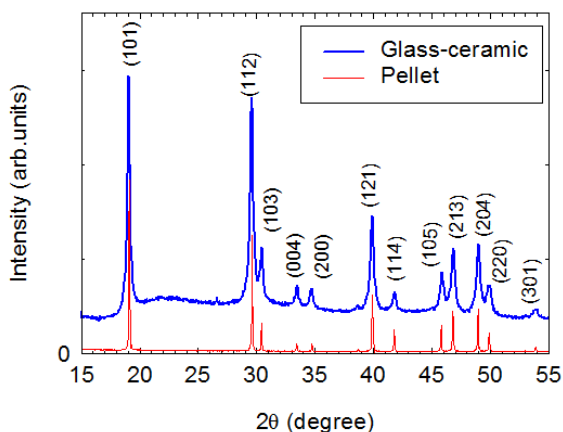


Fig. 1: The XRD patterns of the $\text{Yb}^{3+}/\text{Er}^{3+}$ co-doped $\text{SiO}_2\text{-LiYF}_4$ glass-ceramic and LiYF_4 polycrystalline samples.

Transmission electron microscopy (TEM) image of a glass-ceramic grain showed a distribution of LiYF_4 nanocrystals of about tens of nm size [3,4] (Figure 2).

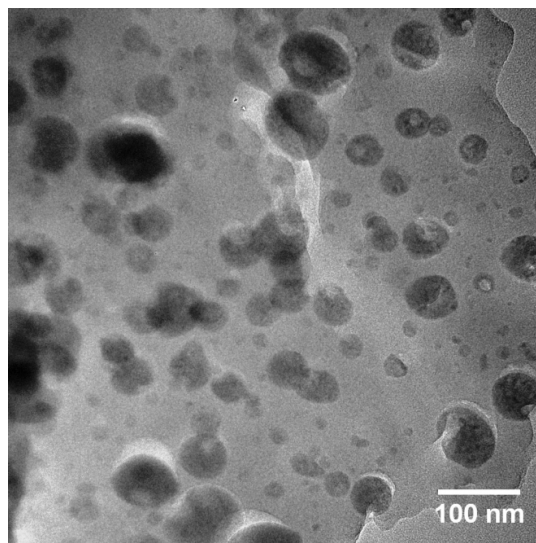


Fig. 2: TEM image of the $\text{Yb}^{3+}/\text{Er}^{3+}$ co-doped $\text{SiO}_2\text{-LiYF}_4$ glass-ceramic grain [3].

Under 980nm laser light pumping, glass-ceramic showed „green” (${}^2H_{11/2}$, ${}^4S_{3/2} \rightarrow {}^4I_{15/2}$) and „red” (${}^4F_{9/2} \rightarrow {}^4I_{15/2}$) Er^{3+} up-conversion luminescences (Figure 3).

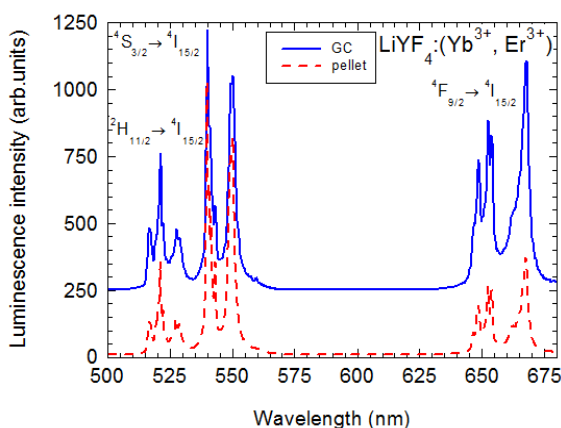


Fig. 3: Up-conversion spectra recorded on $\text{Yb}^{3+}/\text{Er}^{3+}$ co-doped $\text{SiO}_2\text{-LiYF}_4$ glass-ceramic and LiYF_4 polycrystalline samples.

To investigate the UC mechanism for the (${}^2H_{11/2}$, ${}^4S_{3/2}$) \rightarrow ${}^4I_{15/2}$ and (${}^4F_{9/2} \rightarrow {}^4I_{15/2}$) luminescence we measured the pump power dependence of UC intensity (Figure 4); the quadratic dependence indicated a mechanism involving a two-photon process.

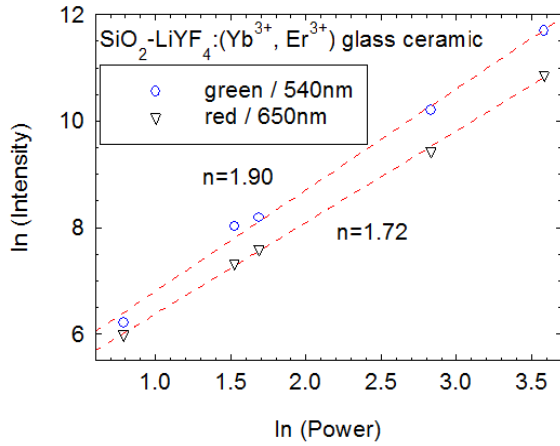


Fig. 4: Double logarithmic plot of UC intensity vs. incident laser power for the „green” and „red” UC luminescences recorded on $\text{Yb}^{3+}/\text{Er}^{3+}$ co-doped $\text{SiO}_2\text{-LiYF}_4$.

Under 980 nm laser light pumping the green emitting levels ($^2\text{H}_{11/2}$, $^4\text{S}_{3/2}$) are populated by the Yb^{3+} - Er^{3+} ET1 [$^2\text{F}_{5/2}(\text{Yb}^{3+}) + ^4\text{I}_{15/2}(\text{Er}^{3+}) \rightarrow ^2\text{F}_{7/2}(\text{Yb}^{3+}) + ^4\text{I}_{11/2}(\text{Er}^{3+})$] and ET2 [$^2\text{F}_{5/2}(\text{Yb}^{3+}) + ^4\text{I}_{11/2}(\text{Er}^{3+}) \rightarrow ^2\text{F}_{7/2}(\text{Yb}^{3+}) + ^4\text{F}_{7/2}(\text{Er}^{3+})$] processes (Figure 5), followed by the rapid multiphonon (MP) transition $^4\text{F}_{7/2} \rightarrow ^2\text{H}_{11/2}$. The lower emitting levels are then populated via multiphonon and cross-relaxation (Yb^{3+} - Er^{3+}) processes followed by the „green” ($^2\text{H}_{11/2}$, $^4\text{S}_{3/2}$) $\rightarrow ^4\text{I}_{15/2}$ and „red” ($^4\text{F}_{9/2} \rightarrow ^4\text{I}_{15/2}$) luminescence emissions (Figure 5).

The „red” emission shows a tendency for a saturation (the slope is smaller than two). This effect is caused by the competition between linear decay and UC processes for the depletion of the $^4\text{I}_{13/2}$ intermediate excited state and is related to the *local* Yb^{3+} concentration [3,4]. Supposing that almost all Yb^{3+} and Er^{3+} ions are embedded in the nanocrystals, their actual concentration might reach 10% (molar) and 3% (molar), respectively. Hence, an energy back transfer (EBT) process [$^4\text{S}_{3/2}(\text{Er}^{3+}) + ^2\text{F}_{7/2}(\text{Yb}^{3+}) \rightarrow ^4\text{I}_{13/2}(\text{Er}^{3+}) + ^2\text{F}_{5/2}(\text{Yb}^{3+})$] (Figure 5) is very efficient [3,5] that results the saturation of the $^4\text{I}_{13/2}$ intermediate state.

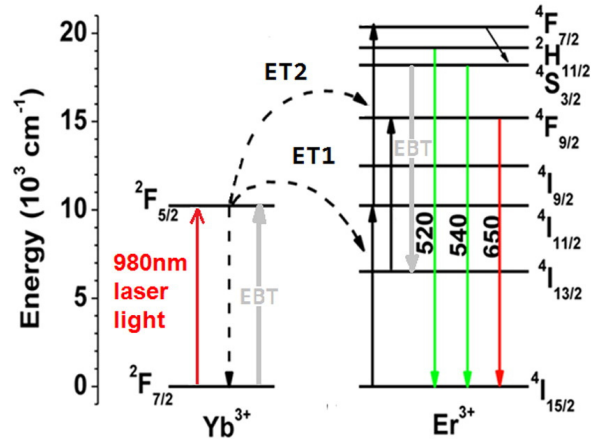


Fig. 5: Energy level schemes of Yb^{3+} and Er^{3+} and the main energy transfer processes (ET) from Yb^{3+} to Er^{3+} represented by curved dashed arrows.

The lifetimes of the „green” and „red” luminescences are 0.015ms and 0.048ms, respectively. The non-radiative relaxation rate is greatly enhanced within the Er^{3+} ions pairs/aggregates [3] that results in a drastically reduction of the luminescence decay times. By using the calculated probabilities of radiative transition we computed the quantum efficiencies in the glass-ceramic ($\eta = 2\%$ and $\eta = 3.5\%$) [3]. The results compare very well with those on other $\text{Yb}^{3+}/\text{Er}^{3+}$ codoped oxyfluoride glass-ceramics.

References

- [1] Xiangyu Zhang, Minqiang Wang, Jijun Ding, Xiaohui Song, Jing Liu, Jinyou Shao, Yajing Li, RSC Adv. 4 (2014) 40223-4023.
- [2] Go Kawamura, Ryota Yoshimura, Kazunari Ota, Song-Yul Oh, Norio Hakiri, Hiroyuki Muto, Tomokatsu Hayakawa, Atsunori Matsuda, J. Am. Ceram. Soc. 96 (2) (2013) 476-480.
- [3] M. Secu and C.E. Secu Journal of Non-Crystalline Solids 426 (2015) 78-82
- [4] C.E. Secu, R.F. Negrea, M. Secu, Opt. Mater. 35 (2013) 2456-2460.
- [5] G. Chen, G. Somesfalean, Y. Liu, Z. Zhang, Q. Sun, F. Wang, Phys. Rev. B 75 (2007) 195204.

Atomic scale elemental mapping using advanced techniques of analytical transmission electron microscopy

R. F. Negrea, V. S. Teodorescu and C. Ghica

The film-substrate or film-film interfaces play a crucial role in the growth mechanisms and in their subsequent physical and functional characteristics. The stress/strain effects induced in epitaxial films by the substrate, the vacancies, dislocations, are responsible for local structural changes which are of paramount importance in complex materials such as the ferroic materials.

Aberration-corrected analytical transmission electron microscopes are nowadays able of unprecedented imaging (point resolution below 1 Angstrom) and spectral capabilities (atomic resolution elemental mapping). Getting structural and chemical information at atomic resolution is nowadays of paramount importance in nanoscience and nanotechnology when analyzing nanometric multilayers, epitaxial heterostructures or core-shell nanoparticles.

The ferroelectric oxide thin films or artificial multiferroics represent typical heterogeneous systems where acquiring structural and compositional information at atomic resolution is crucial for correctly understanding the fine mechanisms controlling phenomena like the electrical polarization switch or the magneto-electric coupling, for applications such as dynamic random access memories, field effect transistors, non-volatile ferroelectric random access memories, micro-electromechanical systems, tunable microwave devices etc.

Barium titanate (BaTiO_3) is among the most studied perovskite systems, being considered as a potential candidate in lead-free ceramic and microelectronic industry. Our study [1] concerns the atomic resolution microstructural characterization of the interfaces between epitaxial BTO layers deposited onto single-crystal (001) SrTiO_3 (or STO) substrates using a SrRuO_3 (SRO) buffer layer, especially regarding the low-Z chemical elements (O in our case). Transmission electron microscopy observations have been performed using a probe-corrected analytical

high-resolution JEM ARM 200F electron microscope provided with a high-brightness Schottky FEG and a Gatan Quantum SE Image Filter for EELS analysis.

Figure 1 presents the dark-field STEM image of the BTO/SRO/STO sample in cross section. The EELS – Spectrum Image acquired from the marked area allows identifying the nature and spatial distribution of the contained chemical elements: Sr, Ru, Ti, B, O.

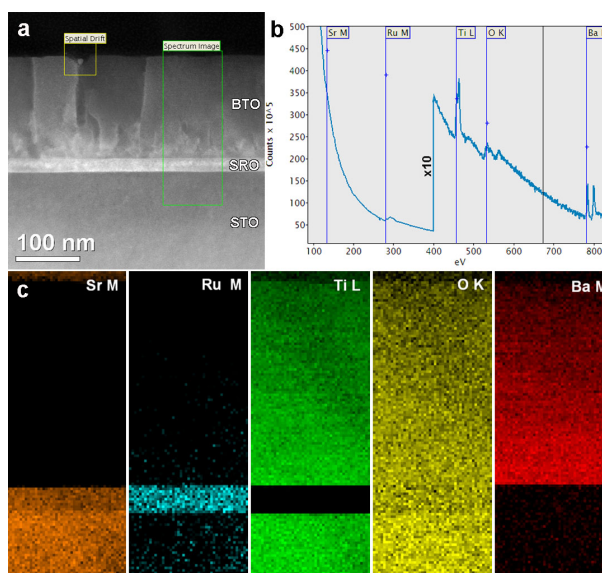


Figure 1. (a) Low-magnification cross-section HAADF-STEM image of the analyzed sample of BTO/SRO/STO; (b) Overall EEL spectrum extracted from the spectrum-image data cube; (c) Elemental maps in false colors for Sr, Ru, Ti, O and Ba extracted from the data cube.

For the atomic-resolution elemental mapping and “visualization” of the oxygen atoms, EELS-SI data has been acquired in the STEM mode at higher magnification at the interface between the single crystal STO substrate and the SRO layer (Figure 2). By subsequent processing of the EELS-SI data cube, we have generated atomic resolution elemental maps corresponding to the Ti $L_{2,3}$ edge at 456-462 eV, Sr $M_{4,5}$ edge at 133 eV and O K edge at 532 eV.

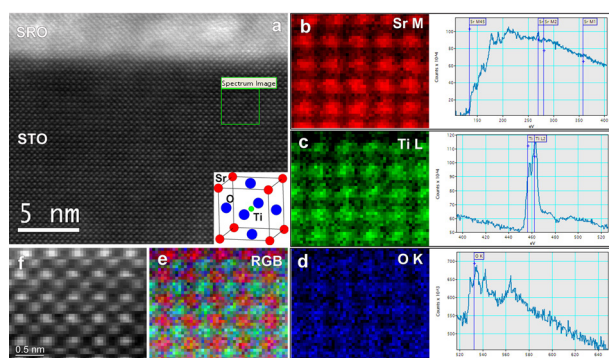


Figure 2. (a) HAADF – STEM image at the STO-SRO interface; (b)-(d) atomic resolution EELS – SI maps showing the elemental distribution in the area marked on the STEM image (a); the O positions are revealed in the spaces between the Sr atoms; EELS spectra containing the Sr, Ti and O absorption edges extracted from the EELS – SI data cube are displayed next to the elemental maps; (e) RGB composed image by overlapping the Sr, Ti and O elemental maps; (f) atomic resolution DF STEM image of the selected area.

For the direct visualization of the oxygen atoms we employed a modified observation technique based on low-angle electron scattering in STEM mode called Annular Bright Field. In figure 3 a and b we present the BF and HAADF STEM images at atomic resolution at the interface between the BTO and SRO layers of our BTO/SRO/STO sample. The complementary contrast of the two types of images allows one to easily identify the nature of the atoms in the BTO and SRO structures, in agreement with the Z^2 dependence. However, the lightest O atoms are not visible on either of the two images, due to their reduced scattering power at the employed scattering angles. In order to image the oxygen atoms, we have modified the acquisition conditions to access the low-angle scattering range. By inspecting figure 3c with respect to the BF and HAADF images one can clearly observe the oxygen atoms imaged as faint dark spots midway between the Ba atoms or between the Sr atoms in BTO and SRO, respectively. The direct interpretation of these images helps identifying the positions of the light atomic species without using any another analytical technique. Such images revealing the exact positions of the oxygen atoms can be further used to directly evidence the structural distortions around

interfaces or defects in strained environments, like tilt/rotation of the BO_6 octahedra in ABO_3 perovskites or Jahn-Teller distortion.

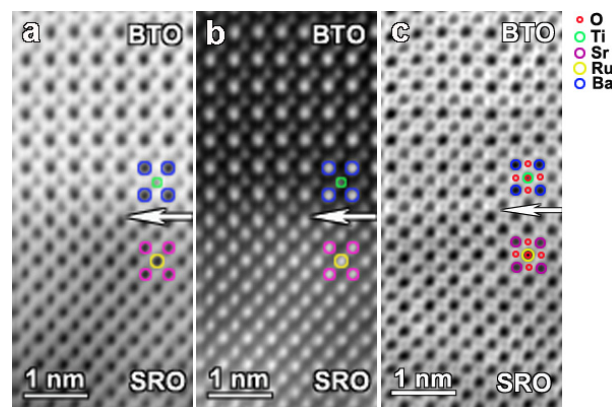


Figure 3. Atomic-resolution STEM images at the SRO – BTO interface: (a) BF image (b) HAADF image and (c) ABF image. The arrow marks the interface.

In conclusion, we have demonstrated that by using the mass-thickness contrast of the STEM images it was possible to quickly identify the heavy atoms from lighter atoms on atomic-resolution micrographs, both in BF and HAADF modes, for BTO/SRO/STO heterostructures. As the oxygen atoms cannot be directly imaged using conventional acquisition conditions (low scattering cross-section), direct imaging of the oxygen atoms in epitaxial perovskite layers was demonstrated by modifying the conventional STEM acquisition parameters using the ABF technique. In addition, combining STEM imaging and EEL spectroscopy in a probe aberration-corrected TEM, atomic resolution mapping for the oxygen atoms was obtained.

References

- [1] R. F. Negrea, V. S. Teodorescu, C. Ghica Appl. Surf. Sci. 315, 250-255 (2015).

Phase evolution in $\text{Eu}_2\text{O}_3 - \alpha\text{-Fe}_2\text{O}_3$ system under high energy ball milling

L. Diamandescu

in cooperation with

M. Sorescu, John DiGnazio

Duquesne University, Department of Physics, Pittsburgh, PA 15282, USA

and

Tianhong Xu

FlexEl, LLC, 387 Technology Drive, College Park, MD20742, USA

High-energy ball milling technique is a well-established method for mechanochemical synthesis of nanostructured materials in which non-equilibrium phases, extended solid solutions or complex structures can be formed at fairly low temperatures [1]. In this work, we report on the synthesis of $x\text{Eu}_2\text{O}_3-(1-x)\alpha\text{-Fe}_2\text{O}_3$ ($x = 0.1, 0.3, 0.5, 0.7$) nanoparticles system by mechanochemical activation method through ball-milling of Eu_2O_3 and $\alpha\text{-Fe}_2\text{O}_3$ mixtures. X-ray powder diffraction (XRD), ^{57}Fe and ^{151}Eu Mössbauer spectroscopy and thermal analysis have been employed to investigate the phase evolution, structural and magnetic properties of ball-milled oxides at different ball-milling times. Powders of hematite and europium oxides were milled in a hardened steel vial with 12 stainless-steel balls (type 440; eight of 0.25 in diameter and four of 0.5 in diameter) in the high energy (SPEX 8000) mixer mill for time periods ranging from 2 to 12 h. The ball/powder mass ratio was 5:1. Fig 1 represents the XRD patterns of europium oxide-doped hematite, $x\text{Eu}_2\text{O}_3-(1-x)\alpha\text{-Fe}_2\text{O}_3$ for $x = 0.1$, corresponding to milling times between 0 and 12 h. The starting materials were pure $\alpha\text{-Fe}_2\text{O}_3$ and Eu_2O_3 phases, where both cubic (C) and monoclinic (M) europium oxide phases were detected after the physically mixing process in air (Fig 1a). For the ball-milled composites (Figure 1b-e), the XRD patterns show progressive peak broadening with milling time. This peak broadening is associated with the decrease in grain sizes for both hematite and europium oxide samples.

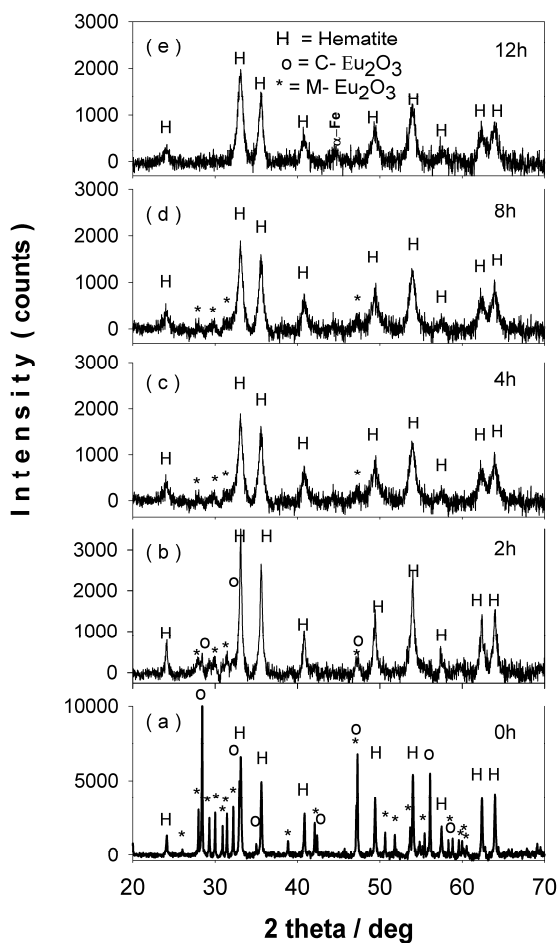


Fig 1. XRD patterns of mechanochemically activated $x\text{Eu}_2\text{O}_3-(1-x)\alpha\text{-Fe}_2\text{O}_3$ ($x = 0.1$) composites at ball milling time of: (a) 0 h; (b) 2 h; (c) 4 h; (d) 8 h; (e) 12 h, respectively.

It can also be seen that the diffraction peak intensities of hematite and europium phases decrease with the increase in ball-milling time, indicating the possible ion substitutions between Eu^{3+} and Fe^{3+} in the corresponding hematite and europium oxide lattices. Europium-doped hematite is the dominant crystalline phase present after 2 hours of milling time, with an average grain size decreased to ~ 28 nm. This grain size

decreases even further, down to ~ 15 nm after 12 hours of mechanochemical activation. Rietveld refinement reveals that lattice parameters c and a of α - Fe_2O_3 increase slightly, supporting the presence of Eu ions in the hematite structure.

In the series at $x=0.3$, after 8h of milling, EuFeO_3 perovskite phase can be identified in the XRD patterns [2, 3]. At $x=0.5$, after 12 hours of milling, the nanoscaled perovskite EuFeO_3 is the unique phase in the XRD pattern (Fig 2).

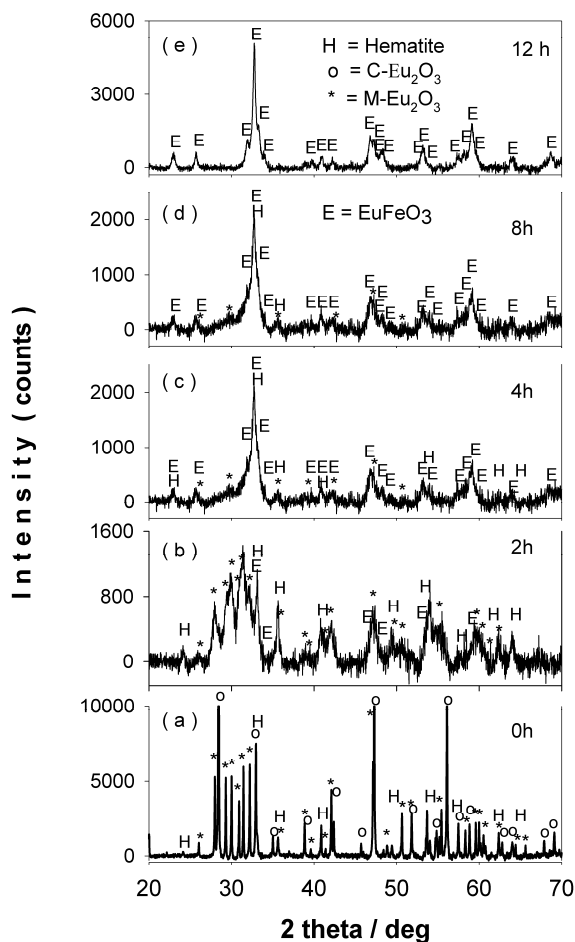


Fig 2. XRD patterns of mechanochemically activated $x\text{Eu}_2\text{O}_3-(1-x)\alpha\text{-Fe}_2\text{O}_3$ ($x = 0.5$) composites at ball milling time of: (a) 0 h; (b) 2 h; (c) 4 h; (d) 8 h; (e) 12h, respectively.

At $x=0.7$, the abundance of EuFeO_3 was ~ 23 % after 8 hours and ~ 51 % after 12 hours.

The amounts of perovskite phase (XRD data), versus ball milling time, for all molar concentration x , are shown in Fig 3.

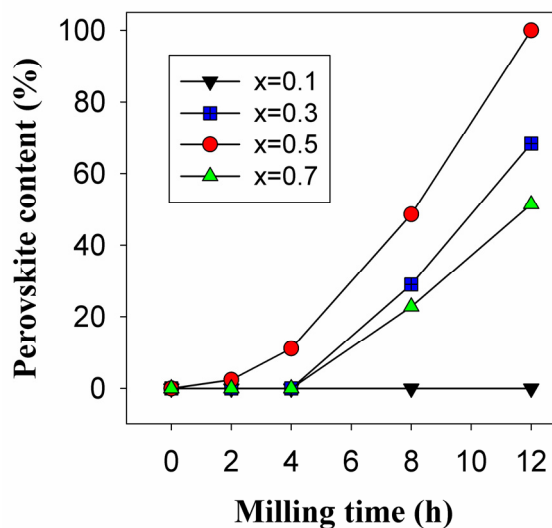


Fig 3. Abundance of perovskite phase EuFeO_3 as function of ball milling time for all molar concentrations x , from XRD patterns.

In this brief report, based on XRD data refinements, the phase evolution in the binary oxide system, $x\text{Eu}_2\text{O}_3-(1-x)\alpha\text{-Fe}_2\text{O}_3$ ($x = 0.1, 0.3, 0.5$, and 0.7) during high energy ball milling, was presented. The most important result is the finding that the nanoscaled EuFeO_3 perovskite, which is an orthoferrite with multiple technological applications, such as solid oxide fuel cells, catalysts, electrodes, chemical sensors, gasoline detectors, magneto-optical devices and microwave guides [4], can be obtained by a simple high energy ball milling route.

References

- [1] T. P. Yadav, R. M. Yadav, D. P. Singh, *Nanoscience and Nanotechnology*, 2 (2012) 22-48.
- [2] Monica Sorescu, Lucian Diamandescu, John DiGnazio, Tianhong Xu, *Ceramics International*, 41 (2015) 1579-1588.
- [3] Monica Sorescu, Lucian Diamandescu, John DiGnazio and Tianhong Xu, *MRS Advances (2015)* DOI:10.1557/adv.2015.16.
- [4] D. Seifu, L. Takacs, A. Kebede, J. Magn. *Magn. Mater* 302 (2006) 479-483.

Nanoscale Physics

Thermal stability studies of the hard magnetic $L1_0$ phase in nanocomposite magnets based on FePt and (Fe,Mn)Pt

Alina Daniela Crisan, Florin Vasiliu, Ionel Mercioniu and Ovidiu Crisan

in cooperation with
R. Nicula, S. Vaucher

Empa, Swiss Federal Laboratories for Materials Science and Technology, Thun, Switzerland

M. Stir

University of Berne, Department of Chemistry and Biochemistry, Berne, Switzerland

D. Pantelica, A. Pantelica

Horia Hulubei National Institute for Physics and Nuclear Engineering, Magurele, Romania

Compared with either Nd-Fe-B or Sm-Co permanent magnets, rare-earth free nanocomposite magnets derived from the FePt binary alloy system [1, 2] exhibit superior corrosion resistance and can operate at significant higher temperatures due to their higher Curie point. A step forward in the development of exchange-spring nanocomposite magnets derived from FePt alloys might be achieved by the controlled addition of Mn to obtain a pseudo-binary alloy of the system $(\text{Fe}_{1-x}\text{Mn}_x)_{50}\text{Pt}_{50}$. In such pseudo-binary alloys the $L1_0$ phase consists of a chemically-modulated superlattice of Pt layers alternating with layers of randomly distributed 3d elements. The unit cell is tetragonally distorted fcc with the c axis lying perpendicularly to the superlattice planes. The extent of this distortion, i.e. the ratio c/a , is one of the important structural parameters that influence both the long-range order parameter and the magnetic performance. Several compositions of the FeMnPt-based systems have been prepared by melt spinning. The atomic structure and morphology of the alloy ribbons were studied using high-resolution (HREM). The chemical composition was determined using energy-dispersive X-ray spectroscopy (EDX) and proton-induced X-ray emission (PIXE) while the magnetic properties were investigated using SQUID magnetometry. PIXE experiments have been carried out using a 3 MeV proton beam at the 3 MV Tandatron of the Horia Hulubei National Institute of Physics and Nuclear Engineering (IFIN-HH). To investigate the temperature evolution of the phase composition and microstructure, temperature synchrotron

radiation powder diffraction (SRPD) experiments were performed *in-situ* at the MSX04 SA beamline of Swiss Light Source. The HREM image of *as-cast* $\text{Fe}_{35}\text{Mn}_{15}\text{Pt}_{50}$ is shown in Fig. 1

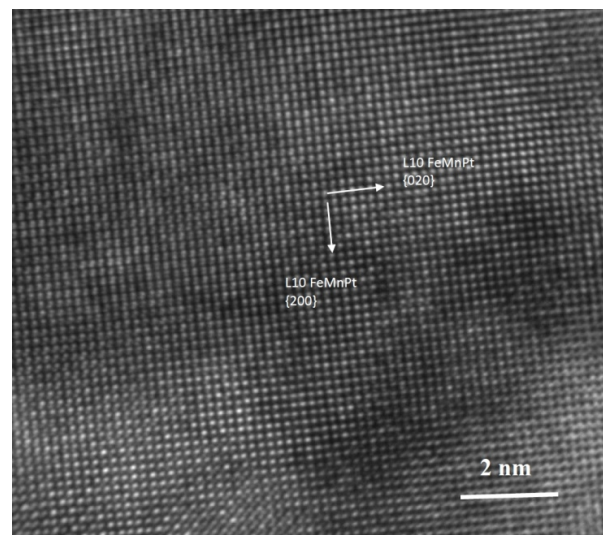


Fig. 1. HREM image of well-ordered region in *as-cast* $\text{Fe}_{35}\text{Mn}_{15}\text{Pt}_{50}$ showing the presence of the ternary $L1_0$ phase.

Large (35 to 60 nm) well-ordered $L1_0$ regions were found to exist in the *as-cast* sample. The (200) and (020) planes ($d = 1.91 \text{ \AA}$) can be easily seen.

The *in-situ* high-temperature SRPD heating experiment revealed that no phase transitions occur during heating and no new phases are formed. The lattice parameter c remains practically unchanged (at $c = 3.7 \text{ \AA}$) up to 540°C .

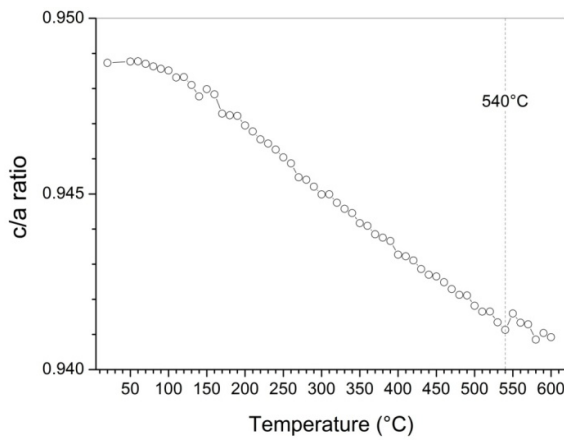


Fig.2 Tetragonal ratio c/a vs. temperature.

Above 540°C, the expansion along the c -axis is more pronounced. The thermal expansion is *in-plane* thus strongly anisotropic. The corresponding tetragonal ratio (c/a) is shown in Fig. 2. It is an important parameter, since it correlates with the degree of magnetocrystalline anisotropy (MCA) of the $L1_0$ phase. The fct $L1_0$ alloy structure thus remains mono-phased and thermally stable up to 600°C.

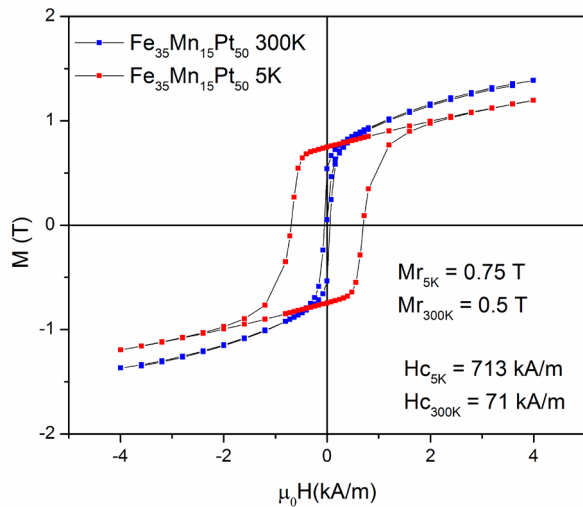


Fig. 3 300K and 5K hysteresis loops in parallel field for the as-cast $Fe_{35}Mn_{15}Pt_{50}$.

The 300K hysteresis loop (Fig. 3) show low coercivity (71 kA/m) and magnetization that does not saturate at 5T. The 5K loop exhibits very large coercivity (around 700 kA/m), very high remanence (0.75 T) and good squareness. This magnetic behavior might be related to the effect the gradual replacement of Fe with Mn which leads to a possible formation of an antiferromagnetic MnPt magnetic sublattice.

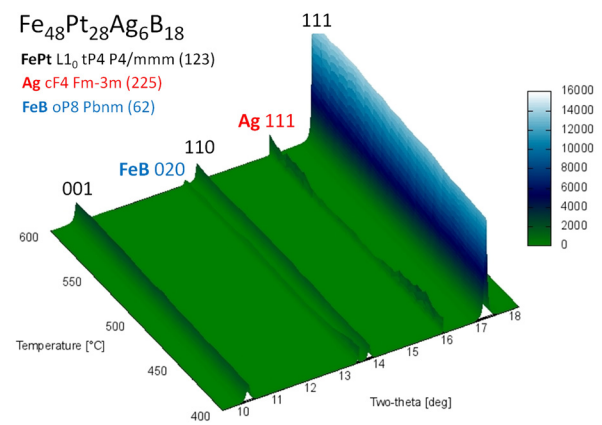


Fig. 4 XRD spectra at temperatures between 400 and 600°C during SRPD experiment

The *in-situ* high-temperature SRPD heating experiment of the $Fe_{48}Pt_{28}Ag_6B_{18}$ melt spun ribbons, a study summarized in Fig. 4 show the occurrence of the superlattice $L1_0$ peaks even at 400°C.

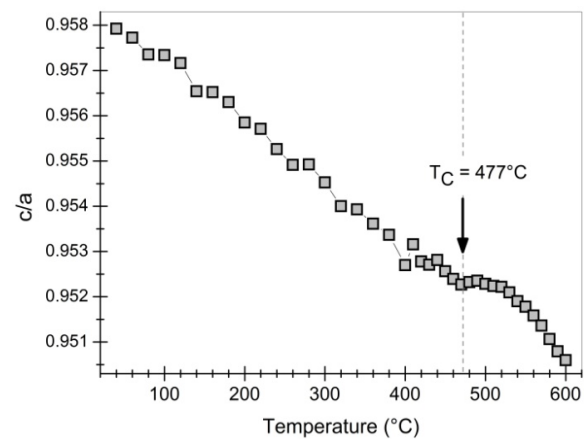


Fig.5. Axial ratio c/a for tetragonal $L1_0$ phase.

The non-linear lattice expansion behavior above T_C show a kink in the T evolution of the c/a ratio (Fig.5) that may be related to Ag diffusion / segregation from FePt grains.

These findings provides good insight for the thermal stability of these alloys in view of using them in industrial environments.

References

- [1] O. Crisan, A.D. Crisan, I. Mercioniu, D. Pantelica, A. Pantelica, S. Vaucher, R. Nicula, M. Stir, F. Vasiliu, *Intermetallics* 65 (2015) 81-87
- [2] R. Nicula, O. Crisan, A.D. Crisan, M. Stir, I. Mercioniu, F. Vasiliu, *Journal of Alloys and Compounds* 622 (2015) 865-870

Magnetic nanoparticles. Relaxation phenomena and applications

V. Kuncser, G. Schintei, P. Palade,

in cooperation with

N. Jacob (National Institute for Lasers, Plasma and Radiation Physics, Bucharest-Magurele)

and

C. Nicula and C. Panaiotu (Faculty of Physics, University of Bucharest)

A continuous growing interest has been manifested during the last decades on magnetic relaxation phenomena of nanoparticulate systems, especially due to their implications in many branches of applications, starting from medicine and ending up with bio-detection and sensoristics, information storage technology and even geology.

New achievements related to implications of magnetic relaxation of nanoparticles (NPs) in bio-medicine, especially connected with the specific absorption rate in magnetic hyperthermia [1,2] as well as in paleogeology, as connected to a subtle derivation of the size/volume distribution of magnetic nanoparticles in loess/paleosol sequences [3] are briefly reported in this work.

An important aspect of the magnetic hyperthermia is related to the efficiency of the magnetic nanoparticles system to transform the energy of the AC magnetic field into a temperature increment of the system (usually consisting in NPs dispersed in an aqueous medium), process which is counted by a power deposition term, q_p , which in turn depends on the volume fraction of nanoparticles, η . The power deposition term, q_p , which characterize the energy transfer, is directly related to the so called specific absorption rate (SAR), with the usual meaning of power absorbed per mass unit of human tissue (W/Kg) embedding the thermally active NPs. Accordingly, $SAR = P/m = c \times \Delta T / \Delta t = q_p / \rho$, with P the power absorbed by the tissue's mass m (the whole absorbed energy is supposed to be transformed in heat, e.g. SAR has to be evaluated for an adiabatic system). Terms c and ρ are the specific heat and the density of the tissue, respectively, and $\Delta T / \Delta t$ represents the rate of the temperature increment. Generally, in laboratory experiments the ferrofluid sample volume is small (a few ml) and therefore, heat losses with the

external environment are significant in comparison to the amount of heat dissipated in the sample. Two specific methodologies for compensating the heating losses along a relatively wide temperature range in respect to hyperthermia applications (providing correct SAR experimental evaluations together with its temperature dependence) have been proposed.

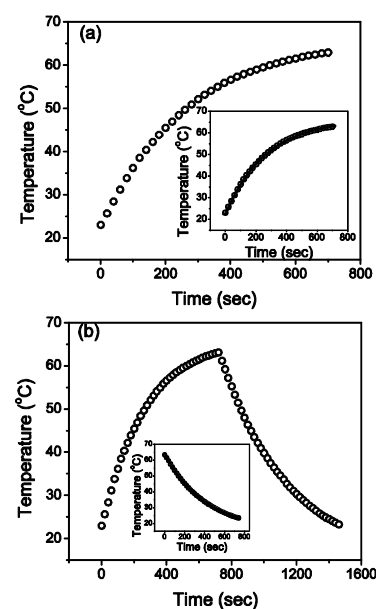


Figure 1. Time dependent experimental heating curve (a), and complete experimental recording of both heating and cooling curves, $T_H(t)$ and $T_C(t)$ (b) for the ferrofluid of given volume fraction ($\eta=0.004$) under an AC magnetic field with amplitude ($H=19\text{kA/m}$). Insets of (a) and (b) show fittings of heating and cooling curves, respectively.

According to the first methodology, besides heating temperature data, also cooling temperature data over a similar temperature range are recorded in order to count for heat losses to each corresponding temperature (Figure 1).

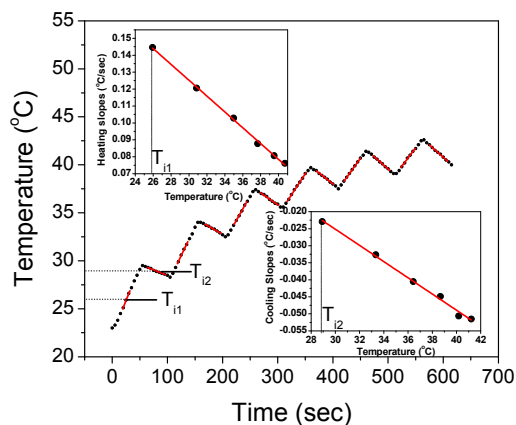


Figure 2. Time dependent experimentally recorded points of heating and cooling steps. Fitting around temperatures of interest T_{i1} , T_{i2} , etc., is represented by straight lines. The insets show the fitting of heating and cooling slopes (speeds $v_C(T)$ and $v_H(T)$).

According to the second methodology, heating and cooling temperature data ($T_H(t)$, $T_C(t)$) have been recorded in appropriate consecutive steps (Figure 2) in order to approach the heating and cooling speeds, dT/dt (noted by $v_H(T)$ and $v_C(T)$), at similar temperature points.

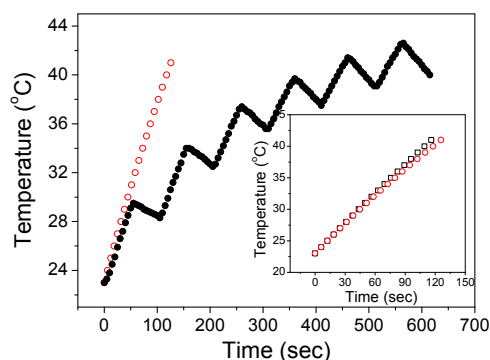


Figure 3. Recorded temperature steps (black circles) and adiabatic heating profile (empty circles). The inset of figure shows the adiabatic heating profile (empty circles) together with a theoretical evaluation from Rosensweig's model (empty squares).

The heating speed of the adiabatic process, at different temperatures, was simply obtained by adding to $v_H(T)$ the absolute value of $v_C(T)$, due to the need to compensate the experimental heat losses accounted via the cooling steps.

Finally, the temporal profile of temperature corresponding to an adiabatic-like heating process is obtained, providing further the correct SAR

determination at different temperatures (Figure 3) which can be compared with theoretical evaluations.

The FSMS method showed that all paleosol samples display relatively narrow, unimodal GSD pattern with maximum probability at the same diameter of about 17 nm in all paleosols. Mössbauer experiments showed GSDs slightly shifted to smaller diameters of NPs (at an average size about 14nm). The results have proved that the degree of pedogenesis influences the paleosol GSDs and the fact that loess GSDs differ from of the paleosols, being broader and with maximum probability shifted to slightly higher diameters. The concentration of NPs in loess is one order of magnitude smaller than in paleosols. All these results suggest also that magnetic relaxation phenomena of NPs are sensitive to pedogenesis aspects of the soils.

References

1. N.Iacob, G.Schinteie, P.Palade, C.M.Ticos, V. Kuncser, Eur. Phys. J.E. (2015) 38 57
2. N. Iacob, G. Schinteie, P.Palade, V. Kuncser, J. Nanopart. Research (2015), DOI 10.1007/s11051-015-2997-2
3. C. Necula, C. Panaiotu, G. Schinteie, P.Palade, V. Kuncser, Global and Planetary Change (2015), doi: 10.1016/j.gloplacha.2015.05.009

Time-dependent transport in single-molecule magnets

V. Moldoveanu, I. V. Dinu

Single-molecule magnets (SMM) are promising candidates for solid state implementation of quantum information protocols in view of technological devices [1]. The main features of a magnetic molecule are its inner magnetic core and the surrounding orbitals which serve to couple the molecule to source and drain probes [2]. Notably, a rather large magnetic anisotropy may affect the transport properties of the nanomagnet and leads to the formation of a magnetic barrier for spins.

We develop a suitable theoretical framework for studying time dependent spin-transport in single-molecule magnets. The transport through a molecular system is typically mediated by its unoccupied orbitals which are coupled to source and drain electrodes. We also allow tunable spin polarizations in the leads. N_{σ}^{α} is the spin density of states in the lead.

The transport properties were investigated using the generalized Master equation approach [3]. Essentially the method provides the reduced density operator (RDO) of the molecule. We calculate the transient currents which develop when the molecule is smoothly coupled to the source and drain electrodes. The transport setting we study relies on the partitioning approach which is suitable for perturbative calculations w.r.t to the lead-molecule tunneling coefficient. The SMM is connected to electrodes at $t = 0$ and a steady state regime establishes after all transients vanish. The spectrum of an $S=2$ SMM is given in Fig. 1.

In the absence of the transverse anisotropy the eigenstates of the molecule are labeled by the eigenvalues m of the total spin operator S_z^t since $[S_z^t, \mathbf{s} \cdot \mathbf{S}] = 0$. Note that $m \pm 1/2$ scans the values of molecular spin projection $S_z = -S, \dots, S$. The one-particle states corresponding to $m = [-S + 1/2, S - 1/2]$ and are given by:

$$|1, m\rangle^{\pm} = C_{m\downarrow}^{\pm} \left| \downarrow, m + \frac{1}{2} \right\rangle + C_{m\uparrow}^{\pm} \left| \uparrow, m - \frac{1}{2} \right\rangle$$

where the coefficients $C_{m\sigma}^{\pm}$ have an explicit form.

Clearly, the magnetic switching cannot start unless the state $|1, S - 1/2\rangle_+$ is populated. In particular this means that if the bias window energetically allows only back-and-forth tunneling between the states $|0, 2\rangle$ and $|1, 5/2\rangle$ the total spin is eventually locked to $5/2$. The time for full switching depends on the transition rates between neighbor states. From the spectrum one infers at once that the depletion of the state $|1, 5/2\rangle$ is quite slow, because electrons have to experience two tunneling processes to access the states $|1, 3/2\rangle_{\pm}$. In contrast, spin down electrons tunnel directly to these states.

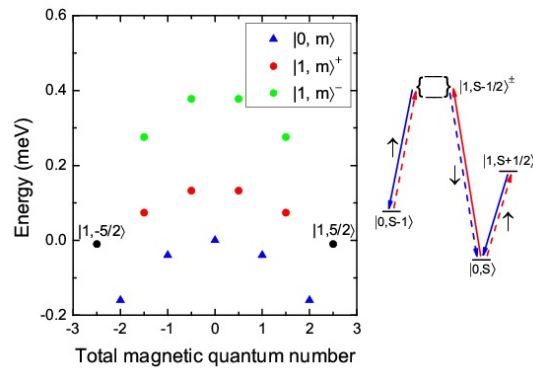


Fig. 1: The spectrum of the SMM, $S=2$.

A sketch of the allowed magnetic transitions is given on the right panel.

Otherwise stated, the magnetic switching slows down if the 'rightmost' state $|1, 5/2\rangle$ is significantly charged in the transient regime. Fig. 2(a) shows the evolution of the total spin for different polarizations of the right lead, while the left lead carries only spin-down electrons. In all cases S_z settles down to -2.5 (which corresponds to the final state $|1, -S - 1/2\rangle$) but the magnetic switching is faster if the right lead is spin polarized. For unpolarized drain electrode the evolution of the total spin S_z^t cannot be traced back from the transient current. As expected J_R increases smoothly when the leads are coupled and then reaches a steady state. Looking at Fig. 2(b) one notices that the onset of a steady state transport regime does not imply neither that all

projections of the total spin S_z^t have been spanned nor that the spin reversal is accomplished.

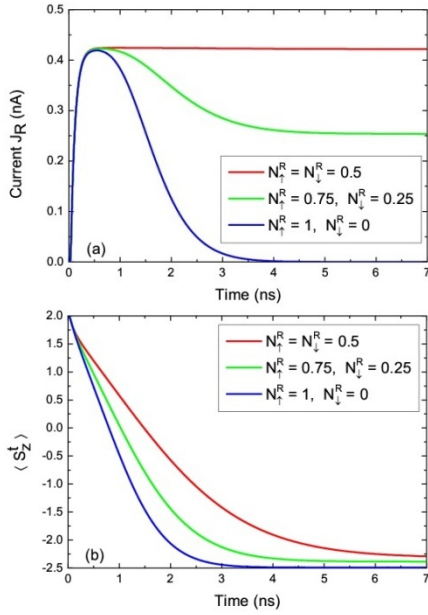


Fig.2 (a) The relevant populations at bias $V=0.125$ meV. (b) The same populations at higher bias $V=0.5$ meV. As expected the steady-state value of the current increases with V . Other parameters: $\varepsilon_0=0.14$ meV, $J=0.1$ meV and $D=0.04$ meV. J is the exchange interaction, D is the easy-axis magnetic anisotropy constant.

The magnetic switching can be read from the transient current in the polarized case. For $N_{\uparrow}^R = 1, N_{\downarrow}^R = 0$ the steady state current vanishes because the orbital is spin-down polarized from the left lead and the drain lead allows only spin-up tunneling.

Consequently, the occupation number of the orbital approaches 1 (not shown). In contrast, a small density of spin-down electrons (e.g $N_{\downarrow}^R = 0.25$) leads to a non vanishing steady-state current. By comparing Figs. 2(a) and 2(b) we observe again that the full magnetic switching coincides with the onset of the steady-state.

Our results show that by measuring the transient current in the antiparallel configuration one can extract the time needed for the system to experience all states $|N, S_z^t\rangle$ and to reach the final state $|N = 1, S = -1/2\rangle$. However, this setup does not provide any information on the intermediate molecular states.

We also investigated the possibility to write and read integer values of S_z (i.e the purely molecular spin). To this end we used the fact that when the orbital is empty S_z^t has only integer values while for full occupation S_z^t becomes half integer.

The results are published in [4, 5].

References

- [1] L. Bogani and W. Wernsdorfer, Nature Mater. 7, 179 (2008).
- [2] D. Gatteschi, R. Sessoli, and J. Villain, Molecular Nanomagnets (Oxford University Press, Oxford, 2006).
- [3] V. Moldoveanu, A. Manolescu, C.-S. Tang, and V. Gudmundsson, Phys. Rev. B 81, 155442 (2010).
- [4] V. Moldoveanu, I. V. Dinu, B. Tanatar, Superlattices and Microstructures 87, 71 (2015).
- [5] V. Moldoveanu, I. V. Dinu, C. P. Moca, B. Tanatar, New Journal of Physics 17, 083020 (2015).

Photochemical processes developed in composite based on highly separated metallic and semiconducting SWCNTs functionalized with polydiphenylamine

M. Baibarac, I. Baltog, I. Smaranda,

in cooperation with

Arnaud Magrez

Ecole Polytechnique Federale Lausanne, Institute of Condensed Matter Physics,
CH-1015 Lausanne, Switzerland

Doping of carbon nanotubes (CNTs) and conjugated polymers (CPs) with heteropolyanions allowed the development of novel composite materials finding applications in the field of electro-catalysis and energy storage. This work reports new results obtained by photoluminescence (PL) and vibrational spectroscopic studies on diphenylamine (DPA) electrochemically polymerized onto electrodes of Pt coated with highly separated metallic (98%) or semiconducting (99%) single-walled carbon nanotubes (SWCNTs). The electrochemical polymerization was performed by cyclic voltammetry from which was obtained a composite materials based on polydiphenyl-amine (PDPA) doped with heteropolyanions of $H_3PW_{12}O_{40}$ (abbreviated PW12) and carbon nanotubes [1]. In this context, the vibration spectroscopic studies have revealed a covalent functionalization of the nanotubes with PDPA in the doped state when a steric hindrance effects are induced to vibrational modes N–H, N,N0-diphenyl benzidine radical cations and C–C stretching (in benzene ring) + C–H bending (in benzene ring). To characterize this new material of high efficiency were PL studies, which revealed the quenching mechanism of SWCNTs. In this context the main question is what type of nanotube play the role of PL quencher, semiconductor or metallic? For this necessary to compare the PL spectra of PDPA doped with PW12 synthesized onto working electrodes as blank Pt support and Pt plate coated with either a metallic SWCNTs (98%) film or a semiconducting SWCNTs (99%). Such a results, obtained under excitation light of 275 nm, are presented in Fig.1.

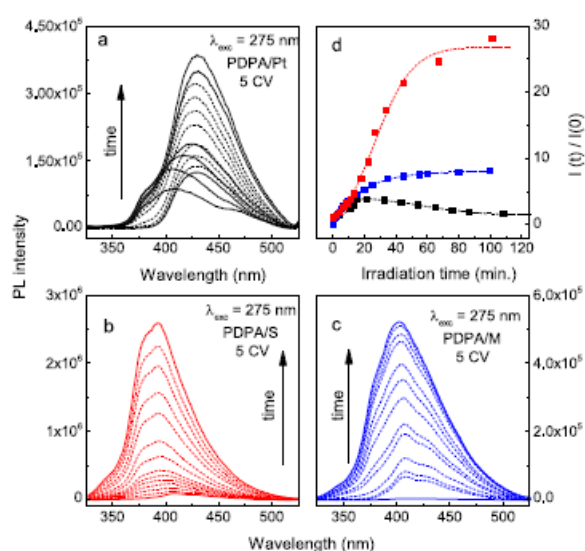


Fig.1 Photoluminescence (PL) spectra of PDPA synthesized by CV using as working electrode a blank Pt electrode (a), a Pt support covered with a semiconducting SWCNTs (99%) film (b) and a Pt plate covered with a metallic SWCNTs (98%) film (c). Panel d shows the variation of the PL intensity of PDPA electrochemical synthesized onto the three supports, depending on the irradiation time at the 275 nm excitation wavelength.

Fig. 1a–c shows that, in the initial state, the PL intensity of the three samples measured in identical experimental conditions, before being submitted to 275 nm light is $\sim 87,960$, ~ 3220 and $\sim 91,450$ counts/s when the PDPA doped with PW12 was electrochemically synthesized onto a blank Pt electrode, the Pt electrode coated with a film of metallic SWCNTs and the Pt electrode coated with a film of semiconducting SWCNTs, respectively. The low intensity of the PL in the case of PDPA doped with PW12 electro-synthesized onto the Pt electrode with a film of metallic SWCNTs, ~ 3220 counts/s, indicates a quenching effect, which is due to a collecting electrical charges mechanism that involves only metallic nanotubes.

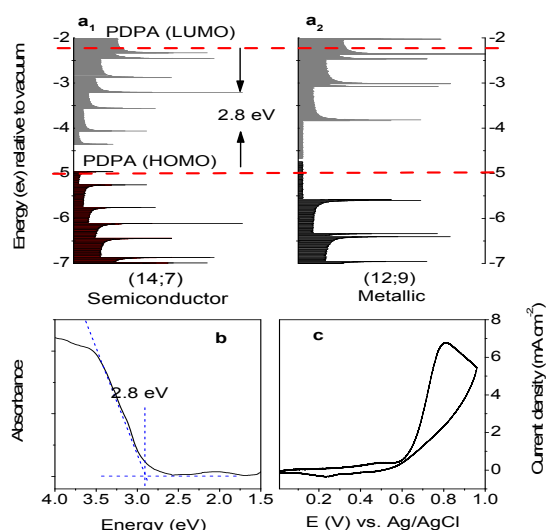


Fig.2 The diagram with electronic energy levels of semi-conducting (a₁) and metallic (a₂) SWCNTs as well as PDPA in the doped state. The highest occupied molecular orbital (HOMO) and the lowest unoccupied molecular orbital (LUMO) of PDPA doped with PW12, were used by cyclic voltammetry and UV-vis absorption spectroscopy. At present, it is well known that the HOMO (related to the ionization potential) and LUMO (related to the electron affinity) energy levels of a conducting polymer can be calculated using the following equations [2]:

$$\text{HOMO} = -e(E_{\text{onset}}^{\text{ox}} + 4.4) \text{ (eV)}$$

$$\text{LUMO} = -e(E_{\text{onset}}^{\text{red}} + 4.4) \text{ (eV)}$$

$$E_{\text{g}}^{\text{opt}} \text{ (eV)} = \text{HOMO} - \text{LUMO}$$

where: $E_{\text{onset}}^{\text{ox}}$ and $E_{\text{onset}}^{\text{red}}$ is the onset potential for the oxidation and the reduction of polymer and $E_{\text{g}}^{\text{opt}}$ is optical band gap of polymer. Using the relationship between the position of the RBM Raman line and the diameter of SWCNTs and the Kataura plots [3] has been determined the chirality (n,m) (12,9) and (14,7) of metallic and semiconducting SWCNTs, respectively. A further detail shown in Fig.3 is that the PL spectrum of the PDPA doped with PW12, electrochemically synthesized on a blank Pt

electrode and covered with semiconducting SWCNTs, can be de-convoluted into three Gaussian components having maxima at 2.65, 2.92 and 3.19 eV.

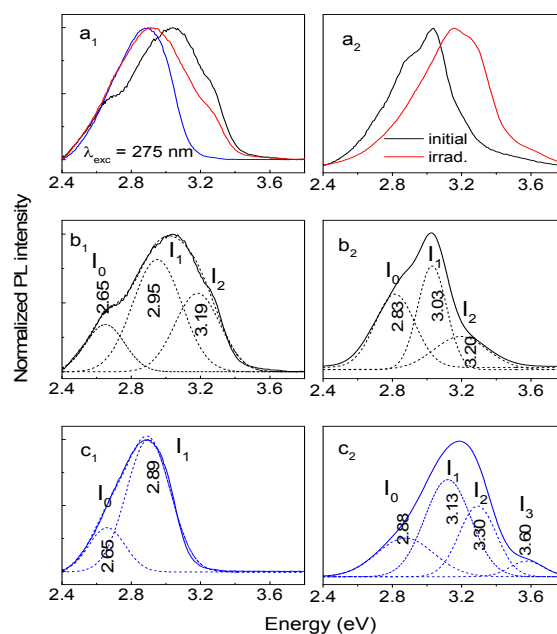


Fig. 3(left) – (a) PL spectra of the PDPA doped with PW12 film, synthesized on the blank Pt electrode by of 5cyclic voltammograms in the potential range (+100;+960) mV vs. Ag/AgCl and stopping at the potential of +960 mV, with a scan rate of 50 mVs⁻¹. Black curve shows the PL spectrum of the initial sample, and the red and blue curves are recorded after 7 and 110 min. of UV-irradiation. (a). Spectral components of the PL spectra in the initial state and after 110 min of UV-irradiation are shown in panels b₁ and c₁. Fig.3 (right) is the same figures obtained with Pt covered with semiconducting nanotubes.

This work reports for the first time new results of PL concerning the influence of highly separated metallic (98%) or semi-conducting (99%) single-walled carbon nanotubes (SWCNTs) on PDPA doped with PW12 heteropolyanions.

References

- [1] M. Baibarac, I. Baltog, I. Smaranda, A. Magrez. Carbon, **81**, 426-438, (2015)
- [2] Q. Liu, J. Mao, Z. Liu, N. Zhang, et al. Nanotechnology; **19**,(11):115601, (2008)
- [3] Kataura H, Kumazawa Y, Maniwa Y, et al. Synth Met; **103**(1–3):2555–8,(1999).

SERS as new spectroscopic method to identify the semiconducting or metallic nature of carbon nanotubes

M. Baibarac, I. Baltog, A. Matea, M. lie,

in cooperation with

S. Lefrant¹ and A. Magrez²

¹Institut des Materiaux “Jean Rouxel”, Nantes, France

²Ecole Polytechnique Federale Lausanne, Lausanne, Switzerland

In the context of Raman spectroscopy, the Surface Enhanced Raman Scattering (SERS) is a powerful technique for studying vibrational states and interface processes. This phenomenon results from a complex interaction between an incident electromagnetic wave (EM) and the molecular or atomic structure of a material. The Raman processes is conditioned of the strength of the polarization, which is induced under the electric field of the incident EM wave. Raman emission consists of two branches, Stokes and anti-Stokes. At thermal equilibrium and under nonresonant optical excitation (OE) the anti-Stokes/Stokes Raman intensity ratio (I_{as}/I_s) is established by the Boltzmann law. In the frame of SERS technique, at resonant OE, the deviations of ratio I_{as}/I_s can indicate the occurrence of a non-linear optical processes as stimulated Raman scattering (SRS) or coherent anti-Stokes Raman scattering (CARS)) [1] as well the identification of semiconducting or metallic structures the latter, with much impact in the study of carbon nanotubes.[2-4].

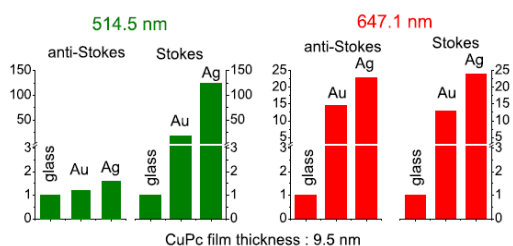


Fig.1 Variations of the anti-Stokes and Stokes Raman line at 1530 cm^{-1} of CuPc at non-resonant (514.5 nm) and resonant (647.1 nm) on 9.5 nm film thickness deposited on glass, Au and Ag substrate.

Fig.1 highlights the main frame for the revealing of SERS technique of two nonlinear optical processes, a stimulated Raman effect observed under non-resonant OE and a reminiscent single-beam CARS effect generated at resonant OE.

Under resonant OE SERS reveals new dependences for the increasing I_{as}/I_s ratio: (i) the intensities of anti-Stokes Raman lines increase as the vibration wavenumber increases; (ii) there is a quadratic dependence on the film thickness; (iii) there is a quadratic dependence on the excitation laser intensity; (iv) there is a linear dependence on the NA of the microscope objective used for the detection of the anti-Stokes emission; and (v) there is a greater polarization ratio on the anti-Stokes side in comparison with that measured for spontaneous Stokes Raman emission.

The asymmetry between the Stokes and anti-Stokes spectra is a general feature generally interpreted as a resonant Raman scattering effect produced by the excitation of different metallic (n, m) carbon nanotubes (CNT). When considering that this conclusion was drawn from Raman studies performed on a mixture CNT containing 2/3 semiconducting (S) and 1/3 metallic (M) species (resulting from synthesis procedures) the question that arises is what the SERS specific anti-Stokes Raman signatures of enriched M (95 %) and S (99%) CNT ? This scenario is highlighted in Fig.2, which illustrates different enhancements in the G Raman band in Stokes and anti-Stokes branches which for CNT reveals a change of I_{as}/I_s ratio compared with the Boltzmann predictions. Regardless of the wavelength of the excitation, the most surprising result is shown in Fig.2 observed on metallic nanotubes for which the gradual increase in the G band in the Stokes branch is not accompanied by a similar variation in the anti-Stokes branch. Contrary to our expectations, although 676.4 nm is resonant for metallic nanotubes, these species do not show any variation in the anti-Stokes branch when the glass substrate is replaced by Au or Ag. However, in the

Stokes branch, an enhancement dependent on the substrate type is observed, which is stronger for Ag than for Au. In this case the Raman enhancement have a plasmonic origin.

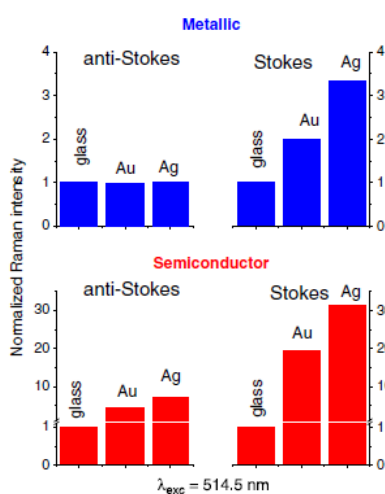


Fig.2. Intensities of the anti-Stokes and Stokes Raman lines at 1595cm^{-1} (G band) under 514.5-nm OE for M, $\sim 98\%$ pure, S, $\sim 99\%$ pure single-walled nanotube thin films deposited on glass, Au and Ag supports.

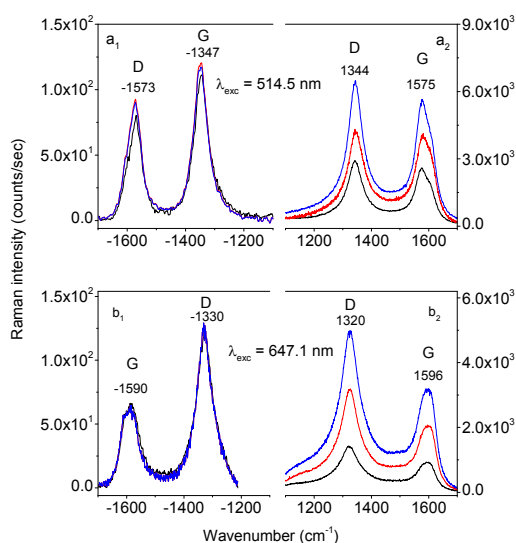


Fig. 3 Anti-Stokes (a_1 , b_1) and Stokes (a_2 , b_2) Raman spectra at $\lambda_{exc} = 514.5 \text{ nm}$ and 647.1 nm of metallic-MWCNTs deposited as thin films on glass (black), Au (red) and Ag (blue) supports.

Generality of this phenomenon is found also in Fig.3 the case of metallic multi-wall carbon nanotubes (MWCNTs) under excitation light of 514.5 nm and 647.1 nm or in Fig.4 for double-wall carbon nanotubes (DWCNTs) for which the SERS technique allows to determine the type the metallic tube in the double-wall configuration.

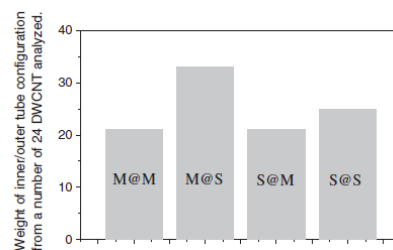


Fig. 4 The percentages of the configurations of the inner/outer tubes of the double-walled carbon nanotubes considered in Table 1. (M) metallic, (S) semiconducting.

The major results of this work show:

- (i) For the Stokes branch, both types of CNT show Raman spectra that increase in intensity with a change of the glass substrate. The SERS enhancement originate in the coupling of plasmons associated with incident excitation light and spontaneous Stokes Raman scattering.
- (ii) For the metallic CNT the invariance of the SERS intensity in the anti-Stokes branch to a change in the substrate results from a Raman light scattering process that takes place only within the skin depth.
- (iii) In this context the anti-Stokes branch can be considered a useful method for identifying metallic or metallic/semiconductor mixtures of MWCNTs or DWCNTs.

References:

- [1] M. Baibarac, I. Baltog, L. Mihut, A. Matea, S. Lefrant; J. Opt. **16**, 035003, (2014)
- [2] M. Baibarac, I. Baltog, L. Mihut, S. Lefrant; J. Raman Spectrosc. **45**, 323–331, (2014)
- [3] M. Baibarac, I. Baltog, A. Matea, L. Mihut, S. Lefrant; J. Raman Spectrosc. **46**, 32, (2015)
- [4] M. Baibarac, A. Matea, M. Ilie, I. Baltog, A. Magrez; Anal. Methods, **7**, 6225, (2015)

Doping ultrasmall cubic ZnS nanocrystals with Mn²⁺ ions over a broad concentration range

S. V. Nistor, M. Stefan, L. C. Nistor, D. Ghica, I. D. Vlaicu and A. C. Joita

Doping II-VI semiconductor nanocrystals (NCs) with transition metal ions (TMIs) is essential for enhancing and controlling the nanoscale induced physical properties for a broad range of applications, *e. g.* light emitting devices, optoelectronics, biological labeling, solar energy harvesting, or spintronics [1,2]. However, the doping of such ultrasmall ($d < 3\text{ nm}$) colloidal NCs in the initial stages of growth is not yet understood. The standing trapped dopant model of incorporation, requiring rather large ($d > 3\text{ nm}$) well faceted NCs, predicts no incorporation for NCs with $d < 2\text{ nm}$, in contradiction with experimental data [1,3].

To elucidate these aspects we investigated by quantitative multifrequency electron paramagnetic resonance (EPR) the variation in the concentration of Mn²⁺ incorporated in the core, on the surface, and as an agglomerated separate phase in cubic ZnS (cZnS) NCs, prepared by surfactant-assisted liquid-liquid synthesis, in the 20 to 20000 ppm nominal impurity concentration range [4,5]. According to our X-ray diffraction (XRD) and high resolution transmission electron microscopy (HRTEM) data (Fig. 1) the cZnS:Mn NCs are self-assembled into a mesoporous structure with nanocrystallites of the same 2.9 nm size in the whole concentration range, reflecting the reproducibility of the synthesis [5].

The variation in the concentration of the Mn²⁺ ions incorporated in the cZnS:Mn NCs is reflected in the changes in the intensity and shape of the EPR spectra (Fig. 2a). The total concentration of incorporated Mn²⁺ ions was determined by double integration of the EPR spectra with the absolute quantitation routine included in the XEPR software (Bruker) [5]. The Mn²⁺ ions separate concentrations in the cZnS:Mn NCs core, on the surface and in a separate aggregated phase was further determined by deconvolution and quantitation routine of the corresponding EPR spectra (Fig. 2b).

According to the results presented in Fig. 3a the total concentration of the incorporated Mn²⁺ ions increases almost linearly with the nominal concentration up to 5000 ppm, slowing down at higher nominal concentrations. The evolutions of the separate concentrations of Mn²⁺ ions incorporated at different sites *vs.* nominal concentration increase, as determined from the deconvoluted spectra, are given in Fig. 3a. It shows that the evolutions of the core and surface incorporated Mn²⁺ ions concentrations are different. Thus, while the concentration of the surface bound Mn²⁺ ions increases almost constantly with the nominal concentration increase, the concentration of the core incorporated Mn²⁺ ions increases much slower, leveling out at the higher nominal concentrations.

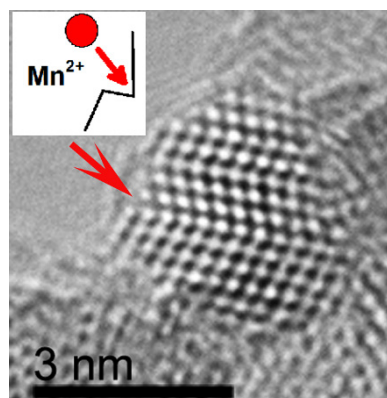


Figure 1. HRTEM image of cZnS:Mn(5000ppm) NCs at high magnification, also illustrating the ELDA mechanism of incorporation [5].

This different behavior is better observed in the evolution of the doping efficiency, defined as the percentage of incorporated/doped Mn²⁺ ions relative to the nominal concentration (Fig. 3b). Thus, while the surface doping efficiency is about 7% for the lower and medium nominal concentrations (up to 5000 ppm), decreasing to 5% at the highest nominal concentration, the core doping efficiency exhibits a strong decrease, from about 9% at the lowest 20 ppm nominal concentration to less than 1% at 20000 ppm nominal concentration.

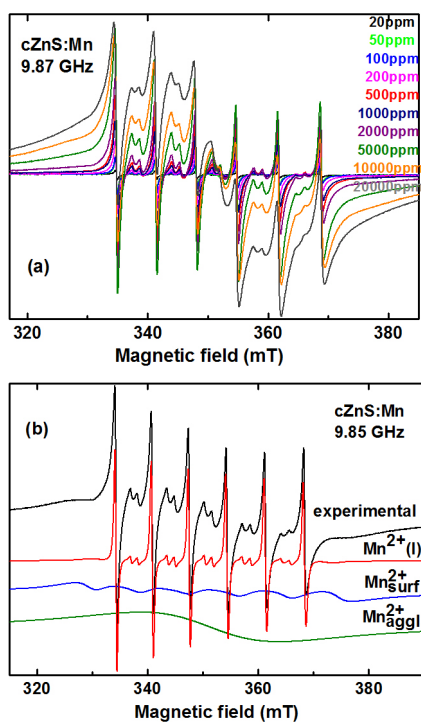


Figure 2. The X-band EPR spectra of the cZnS:Mn NCs. (a) The sequence of spectra at increasing nominal concentrations. (b) The experimental spectrum for 5000ppm nominal concentration (black) and the deconvoluted spectra of the core localized $Mn^{2+}(I)$ (red), surface localized (Mn^{2+}_{surf}) and agglomerated (Mn^{2+}_{aggl}) Mn^{2+} ions [5].

The observed differences in the incorporation of the Mn^{2+} impurity ions at isolated core and surface sites of the cZnS NCs can be explained by the action of different doping mechanisms [5]. Thus while the surface doping follows the predictions of the trapped dopant mechanism [1,3] which predicts a doping efficiency almost constant vs. nominal concentration increase, in good agreement with data from Figs. 3a,b, the core doping efficiency strongly decrease with nominal concentration increase.

The core incorporation properties can be explained based on the results of our previous multifrequency EPR investigations on cZnS:Mn NCs of 2 nm core diameter [3], which have shown that Mn^{2+} ions are preferentially incorporated in the cZnS NCs core at cation sites next to a stacking defect. To explain this preferential localization we suggested the so-called extended lattice defect assisted (ELDA) mechanism of incorporation [3]. According to the ELDA mechanism, the incorporation of the

Mn^{2+} ions takes place mainly by adsorption at the dislocation steps formed by the emerging planar stacking defects at the surface of the NCs. Such a dislocation step, as a possible trapping site of the Mn^{2+} ion, is indicated by a red arrow in the HRTEM image in Fig. 1.

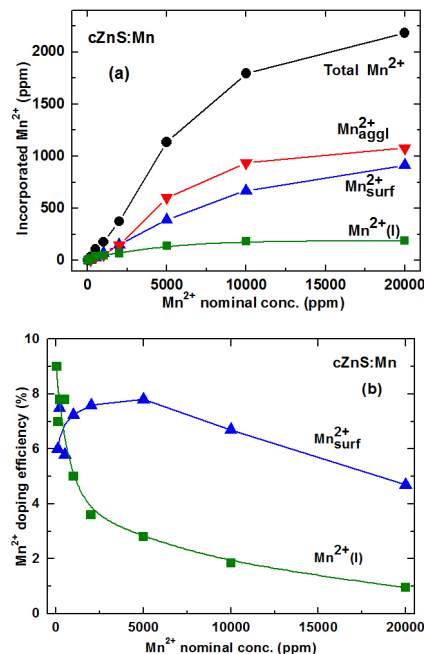


Figure 3. Results of the EPR quantitation of the Mn^{2+} ions incorporated in the 2.9 nm cZnS:Mn NCs as a function of the nominal impurity concentration. The solid lines connecting the data points are guide for the eye only [5].

The ELDA mechanism of incorporation of the Mn^{2+} ions in ultrasmall cZnS NCs is expected to be valid for other II-VI semiconductor NCs and doping TMIs too.

References

- [1] D. J. Norris, A. L. Efros, S. C. Erwin, *Science*, **319**, 1776 (2008).
- [2] X. Fang, T. Zhai, U. K. Gautam, L. Li, L. Wu, Y. Bando, D. Goldberg, *Prog. Mater. Sci.* **56**, 175 (2011).
- [3] S. V. Nistor, M. Stefan, L. C. Nistor, E. Goovaerts, G. Van Tendeloo, *Phys. Rev. B.* **81**, 035336 (2010)
- [4] S. V. Nistor, D. Ghica, M. Stefan L. C. Nistor, *J. Phys. Chem. C.* **117**, 2217 (2013)
- [5] S.V. Nistor, M. Stefan, L. C. Nistor, D. Ghica, I. D. Vlaicu, A. C. Joita, *J. Phys. Chem C* **119**, 23781 (2015)

Study on the photocatalytic reduction of MTT tetrazolium salt on the surface of TiO₂ nanoparticles

T. Popescu, V. S. Teodorescu

in cooperation with

A.R. Lupu

Cantacuzino National Institute for Microbiology and Immunology, Bucharest, Romania

Victor Babes National Institute of Pathology, Bucharest, Romania

V. Raditoiu, V. Purcar

National Research and Development Institute for Chemistry and Petrochemistry-ICECHIM, Bucharest, Romania

The MTT [3-(4,5-Dimethylthiazol-2-yl)-2,5-diphenyltetrazolium-bromide] tetrazolium salt (used as *in vitro* cell cytotoxicity indicator) is photocatalytically reduced on the surface of TiO₂ nanoparticles in phosphate-buffered-saline (PBS) environment (Lupu and Popescu, 2013). We hypothesize that specific phosphate adsorption may be used to modulate the efficiency of the TiO₂-MTT reaction through colloidal and semiconductor-liquid interface processes. The TiO₂-MTT reaction kinetics was studied in PBS, with respect to photocatalyst and MTT concentrations and irradiation wavelength. The effects of PBS and electron scavengers (Fe³⁺ ions) on reaction efficiency and the role of colloidal surface charge in the photocatalytic process were investigated. The structural and spectroscopic characteristics of relevant TiO₂-formazan systems were studied by X-ray diffraction, transmission electron microscopy and IR-spectroscopy.

Formazan production rates were directly proportional to radiation wavelength and TiO₂ concentration (Fig.1) and inversely proportional to the MTT initial concentration [1].

The reaction was pseudo-first order with respect to photocatalyst and showed a negative and fractional partial order with respect to MTT [1]. The addition of Fe³⁺ ions, as well as the absence of PBS, induced strong reaction inhibition (Fig. 2). In the presence of iron nitrate (Fig. 2a), the inhibitory action was attributed to the capacity of Fe³⁺ ions to trap the electrons photogenerated on the surface of TiO₂ nanoparticles, making them unavailable for the MTT reduction process. This process may consist of either a direct electron transfer from the

photocatalyst to the substrate (MTT) or an indirect reaction pathway involving reactive species formed by the photogenerated electrons. After 60 minutes of irradiation (312 nm) in the absence of PBS the amounts of produced formazan were very small, their corresponding absorbance values representing only 5-6% of that of control (Fig. 2b). By showing no significant difference between the two cases tested in this experiment (MTT dissolved in pure deionised water (pH=6.4) and NaOH solution (pH=7.4)), the results indicate that the major decrease in the MTT-TiO₂ reaction efficiency is solely caused by the absence of PBS.

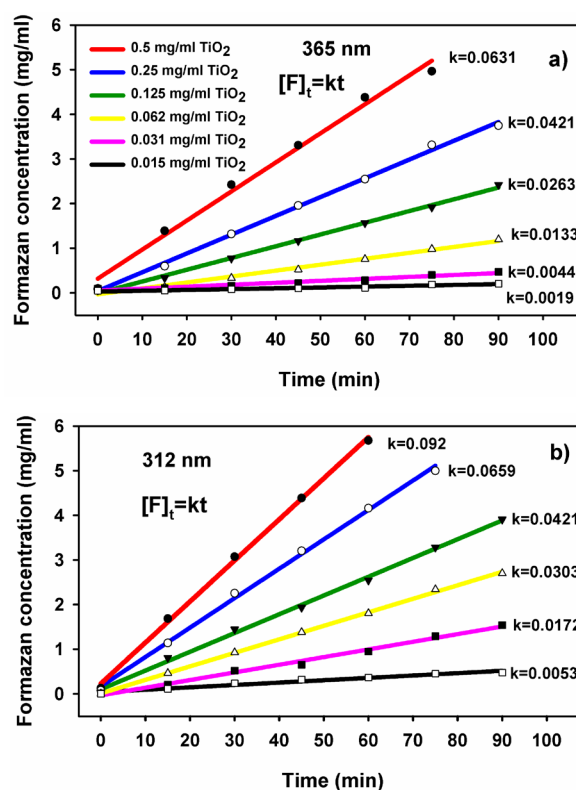


Fig. 1 Kinetics of TiO₂-MTT reaction in type A experiments; a) 365 nm; b) 312 nm.

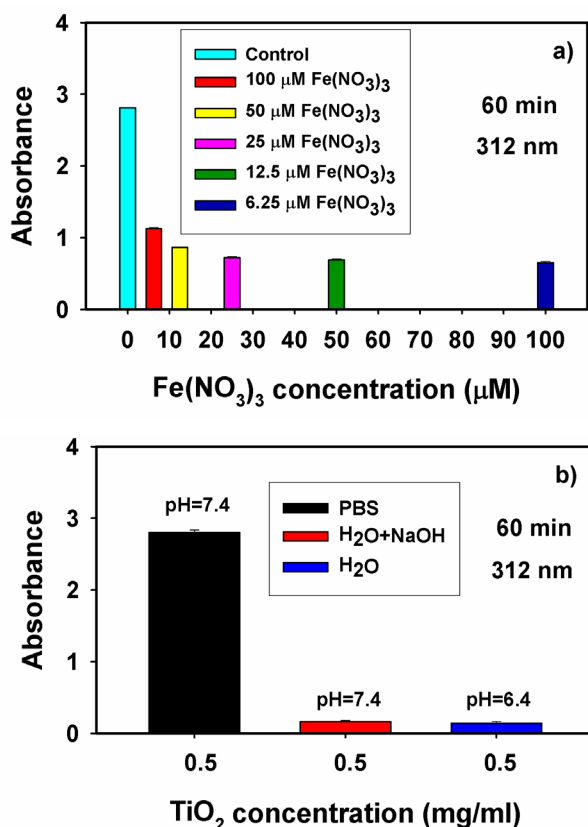


Fig. 2 Effect of ferric ions (a) and PBS absence (b) on the efficiency of the TiO_2 -MTT reaction.

Reaction efficiency (Fig. 3) and catalyst Zeta potential (Fig. 4) were enhanced by Na_2HPO_4 (PBS component) and showed a maximum around the phosphate concentration 0.005 M.

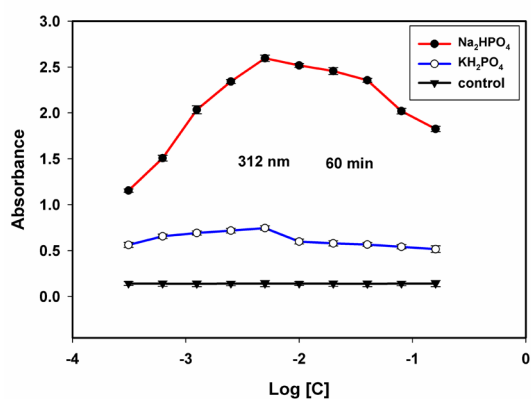


Fig. 3 Efficiency of the TiO_2 -MTT reaction for different phosphate concentrations; the control samples (black line) did not contain phosphate ions

We consider two possible scenarios to account for the strong enhancement of the TiO_2 -MTT reaction in the presence of PBS: (i) the phosphate-mediated MTT adsorption - the reactant molecules (MTT) bind by phosphate

bridges to the surface of the photocatalyst; (ii) the change of redox potentials of the adsorbed MTT molecules partially anchored in the charge layer formed by phosphate and H^+/HO^- ions on the surface of TiO_2 nanoparticles.

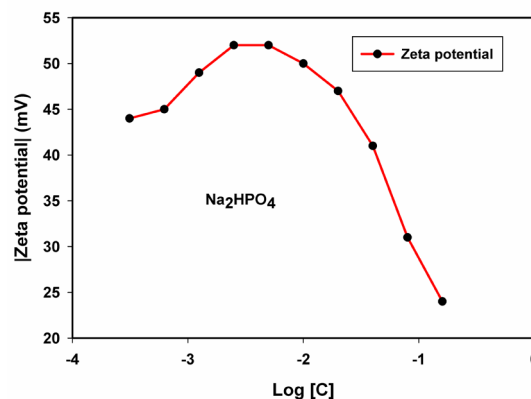


Fig. 4 Zeta potentials of TiO_2 nanoparticles suspended in Na_2HPO_4 solution

Structural and spectroscopic characterization confirmed the formation of amorphous MTT-formazan on the surface of TiO_2 and the TiO_2 -phosphate binding [1].

Acknowledgements

T. Popescu acknowledges support under projects SOPHRD/107/1.5/S/82514 and PN09-450103.

References

- [1] Popescu T, Lupu AR, Raditoiu V, Purcar V, Teodorescu VS, Journal of Colloid and Interface Science, 457, 108–120 (2015)

Potential Applications

Diodes and Field Effect Transistors based on CuO nanowires

C. Florica, A. Costas, A. G. Boni, R. Negrea, L. Ion, N. Preda, L. Pintilie, I. Enculescu

The most attractive class of materials for functional nanodevices is based on semiconductors, in particular metal oxides nanostructures. Among these, CuO is a p-type semiconductor with a narrow band gap (1.2 eV) which has been widely investigated from both fundamental scientific research and practical application points-of-view. CuO nanostructures have been extensively studied taking into account their potential applications in many fields, such as sensors, rechargeable ions batteries, supercapacitors, solar cells, memristors, field emission emitters, etc. Particularly, one dimensional nanostructures, especially nanowires defined by large surface areas (high aspect ratio) have gained considerable research popularity in electronics devices, being the building blocks in the next generation of nanoelectronics. To date, different approaches have been employed for growing CuO nanowires including wet-chemical methods based on solution growth, electrochemical and hydrothermal routes as well as thermal and plasma oxidation techniques.

We have reported on the properties of CuO nanowires, obtained by thermal oxidation in air of Cu foils, a relatively simple and cost efficient preparation method. These CuO nanowires are appropriate for building devices such as diodes and field effect transistors [1]. As illustrated in Fig. 1, the nanowires were obtained by oxidizing in air, at 500°C for 12 hours, a copper foil. The X-ray diffraction (XRD) pattern shown in Figure 2a confirms the presence of three phases: face-centered-cubic for Cu, cubic for Cu₂O and monoclinic for CuO. From reflectance measurements (Figure 2b), a band gap of 1.35 eV was estimated for the CuO nanowires. An assessment of the growth of the CuO nanowires through SEM micrographs can be observed in the insets of Fig. 2a, b. In the cross sectional SEM image one can notice three different areas with specific morphologies which can be attributed as seen in Figure 2a to the bulk Cu coming from the Cu foil, a Cu₂O thin film and CuO nanowires.

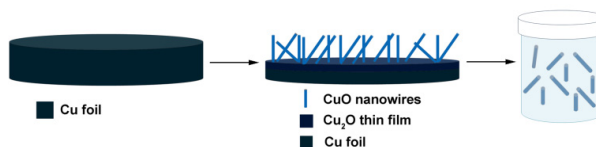


Fig. 1: Illustration of the growth of CuO nanowires by thermal oxidizing in air of a copper foil at 500 °C for 12h and harvesting the nanowires into a solution by sonication.

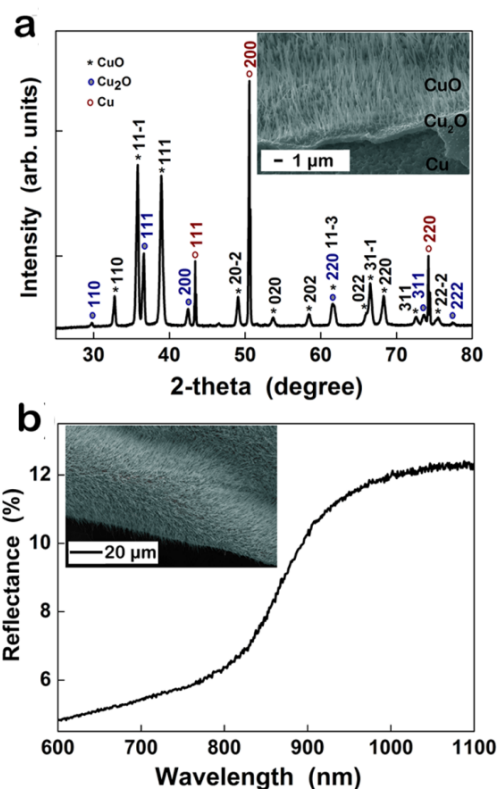


Fig. 2: (a) XRD pattern of the oxidized sample having a cross section SEM image of the synthesized CuO nanowires in the inset; (b) Reflectance spectrum of the CuO nanowires and SEM image having a top view of CuO nanowires in the inset.

The irrefutable proof that the nanowires are formed only by CuO is obtained by the high resolution transmission electron microscopy (HRTEM) and selected area electron diffraction (SAED) analysis (Fig. 3). From the SAED pattern (Fig. 3b), the monoclinic phase with S.G. C2/c of the CuO compound is identified, the directions of the (200) and (1-1-1) planes being presented in the HRTEM image (Fig. 3a).

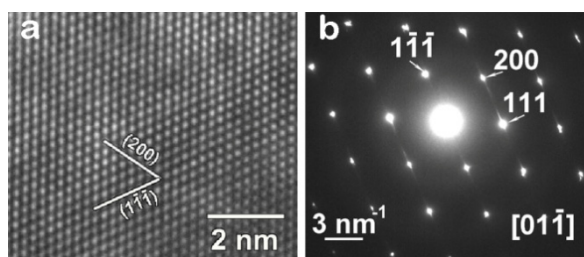


Fig. 3: (a) HRTEM image of CuO nanowire in the [011] zone axis and (b) SAED pattern revealing monoclinic CuO phase.

In order to contact, with different metallic electrodes, single CuO nanowires, a drop of alcohol containing nanowires was placed onto substrates containing interdigitated metallic electrodes prepared by photolithography. We used e-beam lithography (EBL) and focused ion beam induced deposition (FIBID), as depicted in Fig. 4, for contacting the ends of single CuO nanowires.

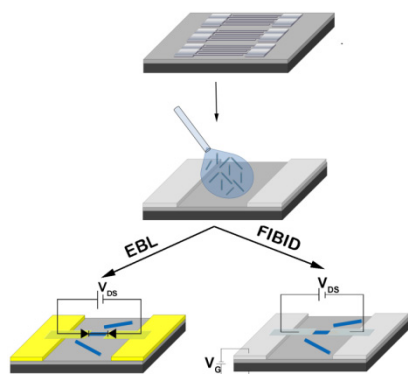


Fig. 4: Representation of the steps for fabricating devices based on single CuO nanowires: placing drops containing nanowires onto electrodes prepared by photolithography followed by contacting single nanowires by EBL and FIBID.

With understanding the Au/CuO nanowire semiconductor Schottky contact and Pt/CuO nanowire ohmic contact, the transport mechanism was found to be an interface dominated one in the Ti-Au/CuO nanowire/Au-Ti structures and an activation mechanism in the Pt/CuO nanowire/Pt structures changing into a nearest neighbor hopping transport one at low temperatures [1]. Considering the metal/semiconductor interfaces and the conduction mechanisms in the CuO nanowires, devices such as diodes based on Ti-Au/CuO nanowire/Pt

structures (Fig. 5a, b) and field effect transistors based on Pt/CuO nanowire/Pt structures (Fig. 5c, d) were fabricated.

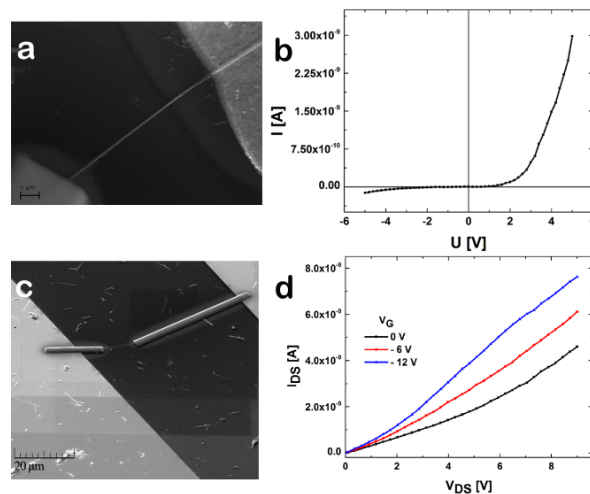


Fig. 5: (a) SEM image of a CuO nanowire contacted at one end of the nanowire by FIBID using Pt and at the other end of the nanowire by EBL using Ti/Au contacts, (b) Current - Voltage characteristics of a Schottky diode based on Au-Ti/CuO nanowire/Pt structure, (c) SEM image of a CuO nanowire contacted at both ends of the nanowire by FIBID using Pt, (d) Output characteristics of a field effect transistor based on the Pt/CuO nanowire/Pt structure.

The fabricated diodes have an ideality factor of 1.83 and on-off current ratios of about 10^3 , while the CuO p-type single nanowire based transistors respond at relatively low applied gate voltages (-12 V) having on-off current ratios also around 10^3 .

References

- [1] C. Florica, A. Costas, A. G. Boni, R. Negrea, L. Ion, N. Preda, L. Pintilie, I. Enculescu, Appl. Phys. Lett. 106, 223501, 2015

Biofunctionalization of dental implants with durable bioglass films by magnetron sputtering

A.C. Popa, G.E. Stan, M. Enculescu

in cooperation with

C. Tanase

“Victor Babes” National Institute of Pathology, Bucharest, Romania

D.U. Tulyaganov

Turin Polytechnic University in Tashkent, Tashkent, Uzbekistan

and

J.M.F. Ferreira

Department of Materials and Ceramics Engineering, CICECO, University of Aveiro, Aveiro, Portugal

The potential of dental implants market is huge, the specialists from reputable economic research agencies forecast that the international dental implants market will continue its strong rise in the coming years.

The worldwide growing demand for dental implants is mandatory to be accompanied not only by an increasing number/capability of manufacturing enterprises, but also by the identification of advanced technological solutions able to facilitate the development of a new generation of implants with superior functionality, and determine both patient comfort and a rapid resumption of his/hers social and professional activities.

A long healing time can be a severe inhibition factor for the future development of this medical branch, affecting both the economic motivation of medical practices for such implant solutions, as well as the patients' psychology and trust.

Bioactive glass (BG) is currently considered the suitable candidate to stir the quest for a new generation of osseous implants with superior biological/functional performance.

In congruence with this vision, we introduce here a reliable technological recipe for coating 3D implants (*i.e.*, dental screws) with uniform and mechanical resistant bioactive glass (of the $\text{SiO}_2\text{-CaO-Na}_2\text{O-P}_2\text{O}_5\text{-MgO-CaF}_2$ compositional system) films by radio-frequency magnetron sputtering (RF-MS) deposition technique (Fig. 1).

The implants were fixed parallel to the BG target surface at a separation distance of 25 mm.

During RF-MS deposition, performed at 0.4 Pa argon pressure, the dental screws were slowly rotated in front of the magnetron plasma with a speed of ~ 10 rpm (Fig. 1a).

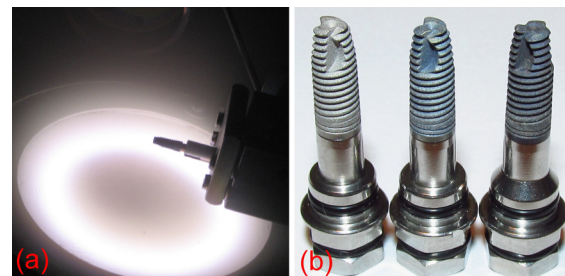


Fig. 1 Snapshot taken during the RF-MS BG coating process of a dental screw (a). Comparative images (left-to-right) of dental screw: simple; functionalized with BG; and functionalized with BG and annealed post-deposition at $630^\circ\text{C}/3\text{h}$ in air (b).

The adhesion of the coating to the metallic surface is of critical importance in view of the successful clinical performance of an implant.

The mechanical reliability of the bioactive glass films applied to real Ti dental implant fixtures has been evaluated with success [1] by a procedure comprised of “cold” implantation in pig mandibular bone from a dead animal, followed by immediate tension-free extraction tests, and analysis by SEM and EDS mapping.

By inserting the dental screws into bone material a far more relevant assessment of how the coating will respond to the complex mechanical stresses taking place upon implantation can be provided [1].

Further, extensive *in vitro* biocompatibility assays – immunofluorescence (Fig. 2) and

Western blot (Fig. 3) – have been performed in human dental pulp stem cells (hDPSC) cultures.

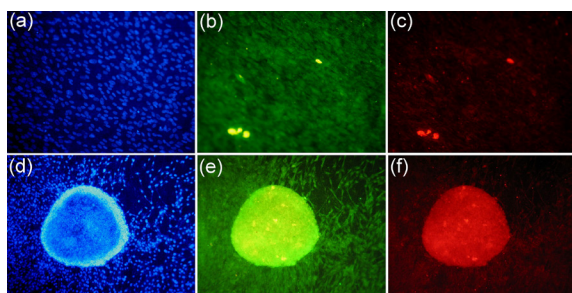


Fig. 2 Indirect immunofluorescence images presenting dental pulp stem cells grown on bare Ti substrates (a,b,c) and as-deposited (d,e,f) BG films, 10 days after seeding: cells nuclei (a,d); CD90 (b,e) and STRO1 expression of cells (c,f). Objective 20X for a,b,c and 10X for d,e,f.

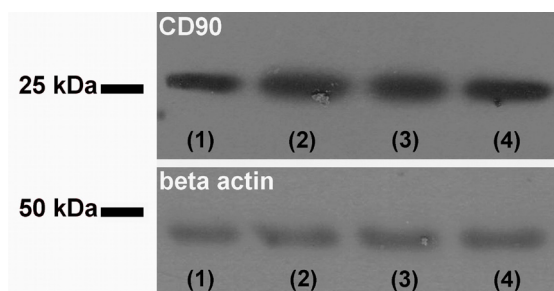


Fig. 3 Western blot analysis of CD90 expression and beta-actin for loading control. Bare Ti substrate (1); as-deposited (2) and annealed (3) BG film; and borosilicate glass control (4).

Presently, the biomaterials scientists rather are inclined to advance implant surfaces capable to induce rapid stem cells differentiation into osteoproliferative cells. Although this may seem at a first glance as a good strategy, it may be disastrous on a long term, since in time all stem cells from the implant vicinity would tend to differentiate quickly to osteoblasts and promote bone formation, conducting to an exhaustion of the stem cell pool.

In our opinion a more favorable situation would be for the BG coatings to allow the optimal growth of stem cells without promoting their differentiation. If the stem cells differentiation control would be reserved to the cell signaling processes, this would lead to a conservation of the stem cell pool, which will provide the timely necessary osteoblast number, and

with that the health of peri-implant structures.

After 10 days of culturing (Fig. 2), we observed in cells grown on bare Ti substrates the progressive decrease of the CD90 and STRO1 stemness markers (Fig. 2-a,b,c) accompanied by a good cell proliferation. On the other hand, the cells grown on BG films presented a conserved stem phenotype as proved by the CD90 and STRO1 expression along with the presence of round spheroid colonies of stem cells that expressed high levels of CD90 and STRO1 (Fig. 2-c,d,e). Thus, it is indicated the capacity of the RF-MS BG films, synthesized under the given deposition conditions, to enable the good adhesion and proliferation of hDPSC, without promoting their differentiation [1].

The Western blot analysis (Fig. 3) further confirmed a decreased expression of CD90 for the cells grown on bare Ti with respect to the BG films and dedicated biological (borosilicate glass) control surfaces.

The goal of this study was to establish a facile way to coat uniformly dental screws with BG films by RF-MS technique, with suitable mechanical resistance and biological behavior, able to sustain the future development of a new generation of implants with superior lifetime and less revision. To our opinion, such an implant design can be achieved only if its surface will be capable to allow good cellular adhesion and proliferation, without intervening in the complex mechanism that is stem cell differentiation.

The promising results warrant the advance of the research towards the in vivo stage testing in animal model, which constitutes a mandatory phase prior to clinical trials.

References

- [1] A. C. Popa, G.E. Stan, M. Enculescu, C. Tanase, D.U. Tulyaganov, J.M.F. Ferreira, Superior biofunctionality of dental implant fixtures uniformly coated with durable bioglass films by magnetron sputtering, *J. Mech. Behav. Biomed. Mater.* 51 (2015) 313–327.

Electrospinning and electro spraying techniques for straightforward fabrication of hierarchical structures

N. Preda, A. Evangelidis, C. Florica, A. Costas, M. Enculescu, I. Enculescu

Electrospinning and electro spraying, two “sister” electrohydrodynamic processes, have recently emerged as powerful, simple and versatile techniques for the fabrication of hierarchical ZnO structures. ZnO has a rich family of structure morphologies [1-4], this being an important aspect which is taken into account in the chemical sensing applications based on it. In our studies, two types of hierarchical structures were prepared: i) hybrid organic core - inorganic shell structures by combining the electrospinning technique with ZnO electroless deposition method [1] and ii) ZnO networks by electro spraying of chemically synthesized ZnO structures on interdigitated metallic electrodes (IME) fabricated by photolithography [4]. In Fig. 1, a schematic illustration of the experimental procedures involved in the preparation of poly(methyl methacrylate) fibers by electrospinning method, further coated with ZnO structures by electroless deposition, it is shown. In Fig. 2, a schematic representation of the experimental procedures involved in the electro spraying of ZnO structures (synthesized by wet chemical precipitation) on IME, it is observed. The samples' morphology was observed by scanning electron microscopy - SEM (Fig. 3 and Fig. 4, respectively). Polymer fibers having a smooth surface are formed by electrospinning. Their surfaces are covered by a continuous, homogeneous and densely packed array of ZnO prisms with the base diameter of 400 nm and height of approximately 500 nm, after the ZnO electroless deposition. For the electro spraying process, ZnO flowers or ZnO snowflakes, formed by assembled leaves or platelets, respectively and having sizes in the 1-2 μm range, form networks covering both the IME and the gaps creating bridges between them.

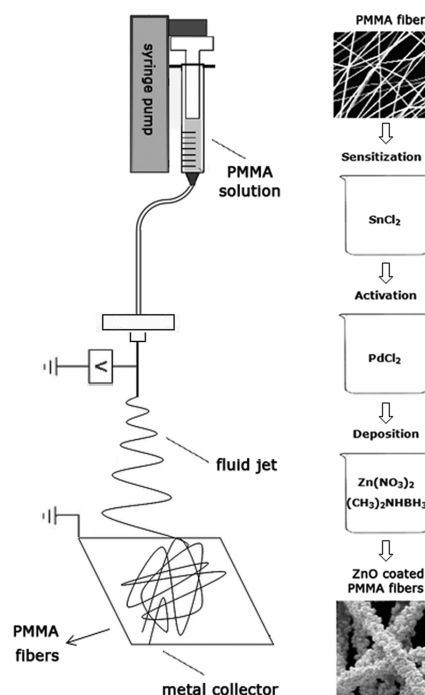


Fig. 1: Electrospinning process and electroless deposition of ZnO structures.

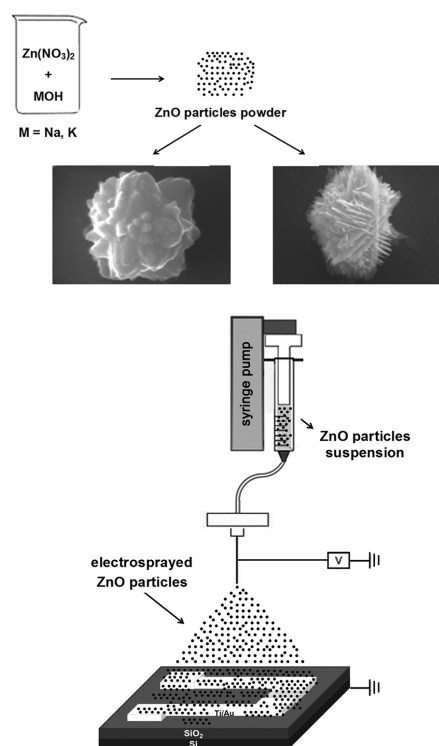


Fig. 2: Chemical synthesis of ZnO structures and electro spraying process.

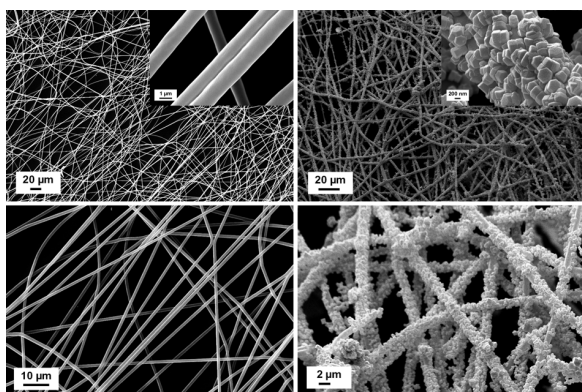


Fig. 3: SEM images at different magnifications of PMMA fibers (left) and PMMA fibers coated with ZnO primers (right).

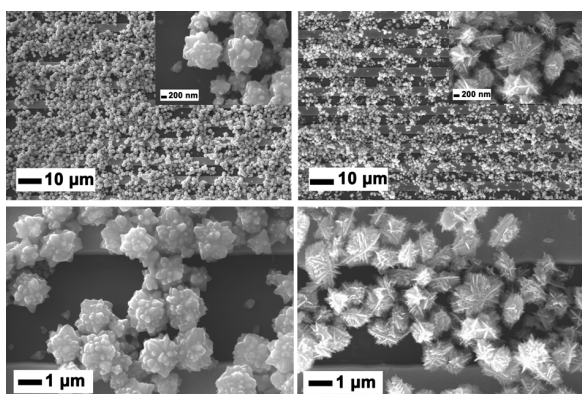


Fig. 4: SEM images at different magnifications of ZnO flowers (left) and ZnO snowflakes (right) on IME.

In fact, the formation of ZnO bridges onto the IME (providing electrical paths between the neighboring grid structures) is the main advantage given by the electrospinning technique in the case of the deposition of different semiconducting structures on IME. Having a large surface to volume ratio, both types of ZnO structures can have perspective chemical sensor applications. Thus, we carried out current-voltage measurements by exposing the samples to ammonia vapors. A decrease in current takes place when exposing to ammonia either ZnO flowers or ZnO snowflakes (Fig. 5). The adsorption of oxygen or water molecules can be enhanced by the presence of ammonia, leading to an increase in resistance up to a saturation point reached when the adsorption processes are also saturated (insets of Fig. 5). A proof-of-concept sensing of ammonia was made.

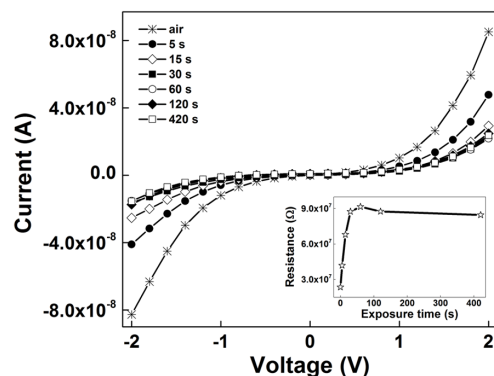
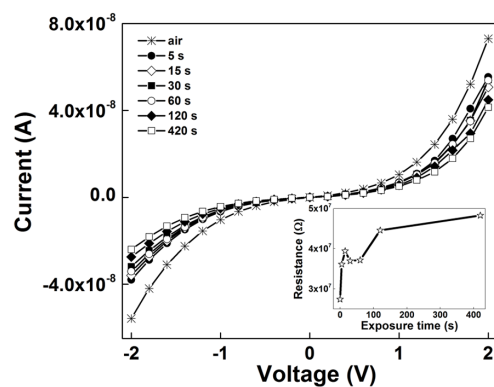


Fig. 5: Changes induced by ammonia vapors in the current–voltage characteristics of ZnO flowers (up) and ZnO snowflakes (bottom) deposited on IME. Insets: resistance variation (2 V) with the time of exposure to ammonia.

Taking into account that in the preparation of ZnO hierarchical structures easily scalable methods such as electrospinning, electrospaying, electroless deposition, wet chemical precipitation and conventional photolithography are used, these techniques are efficient and suitable for industrial processing.

References

- [1] N. Preda, A. Evanghelidis, M. Enculescu, C. Florica, I. Enculescu, *Mater. Lett.* 138, 238, 2015
- [2] N. Preda, M. Enculescu, C. Florica, A. Costas, A. Evanghelidis, E. Matei, I. Enculescu, *Dig. J. Nanomater. Bios.* 8, 1591, 2013
- [3] N. Preda, M. Enculescu, I. Enculescu, *Mater. Lett.* 115, 256, 2014
- [4] A. Costas, C. Florica, A. Evanghelidis, M. Enculescu, N. Preda, I. Enculescu, *Dig. J. Nanomater. Bios.* 10, 1181, 2015

Structural and magnetic transitions in Ferromagnetic Shape Memory Alloys melt spun ribbons

F. Tolea, M. Sofronie, M. Tolea, A. D Crisan, V. Kuncser M. Valeanu, M. Enculescu

Specific to Ferromagnetic Shape Memory Alloys (FSMA) is the so called martensitic transformation (MT), which is a thermoelastic reversible structural phase transition between high and low symmetry phases, transformation which lies in the temperature region of magnetic order.

The prototype ferromagnetic shape-memory material is the Heusler alloy, Ni_2MnGa with a huge magnetic field induced strain of the order of several percents. However, the high fragility of Ni-Mn-Ga, was the main reason to search for new FSMA. Among the potential candidates to replace the brittle Ni-Mn-Ga, a good choice seems to be Ni-Fe-Ga, but also some other non Heusler FSMA like Fe-Pd [1], Fe-Mn-Si or the Fe-Ni-Co-Ti based alloys [2]. All these alloys give rise to a class of active materials with expected potential to produce both the large actuator strain of shape memory alloys and the rapid response of magneto-strictive materials. Rapid solidification using a melt-spinning technique is an effective one-step processing route to produce textured polycrystalline ribbons.

By in situ DSC measurements, the effect of thermal treatments on the MT of two melt spun ribbons of Ni-Fe-Ga-(Co) alloys (with relatively low Ga content and with Co) has been analyzed and compared with the results obtained on ribbons of a more stable alloy (with higher Ga content and without Co addition) [3]. Irrespective of composition, subsequent TTs promote a continuous reduction of the MT temperature. Depending on the main process responsible for the MT temperature reduction, three temperature ranges of the applied thermal treatment may be distinguished (Fig.1): (i) low temperature 200-250°C, the large strains induced by the processing route are relaxed leading to an abrupt decrease of the MT temperature and to an enhancement of the transformation heat; (ii) up to 400-450°C bring no variation or a slow reduction of the MT temperatures, but the heat

of transformation reaches the maximum value due to increased atomic ordering; (iii) higher than -450°C promote the morpho-structural degradation of the ribbons and as consequence, a fast decrease of both the transformation heat and temperature.

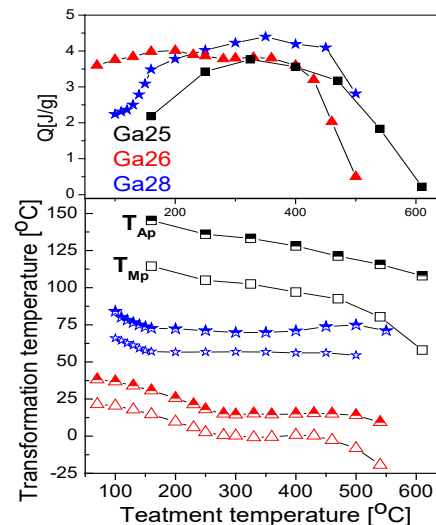


Fig.1. Temperatures corresponding to the direct and reverse martensitic transformations (T_{MP} , T_{AP}) (a) and average heat of transformation (b) as function of the upper limit temperature attained in each cycle for the three alloys.

By applying the melt spinning technique we succeeded to dissolve up to 2at% Nd in the Heusler type alloy $\text{Ni}_{57-x}\text{Nd}_x\text{Fe}_{18}\text{Ga}_{25}$ and to study the influence of rare earth substitution on the MT and magnetic properties [4]. By corroborating DSC and thermo-magnetic results it was revealed that $\text{Ni}_{55}\text{Nd}_2\text{Fe}_{18}\text{Ga}_{25}$, prepared as ribbons, undergoes a magneto-structural transformation, the martensitic and magnetic transformation being concomitant (Fig.2). For higher substitution level ($x \geq 4$) additional occurrence of the secondary R_2Fe_{17} phase was evidenced.

The magnetic and magneto-elastic properties of $\text{Fe}_{69.4}\text{Pd}_{30.6}$ melt-spun ribbons [1] related to different thermal treatments were studied.

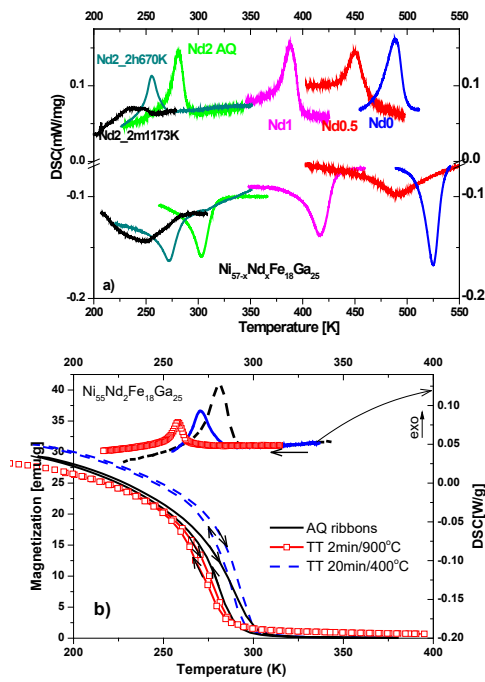


Fig.2. The DSC curves for $Ni_{57-x}Nd_xFe_{18}Ga_{25}$ as prepared ribbons (a) and thermo- magnetic measurements performed in $H=200$ Oe on $x=2$ ribbons (b)

The LTE measurements performed under different magnetic fields in the temperature range of MT indicate that the tetragonal a axis ($a > c$) is the magnetic easy axis (Fig 3).

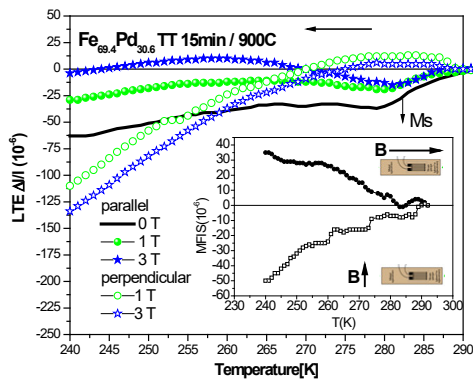


Fig.3. LTE on cooling with magnetic field applied parallel and perpendicular to the ribbon plane. Inset: MFIS in magnetic field ($B = 1$ T), applied parallel and perpendicular to the ribbon.

Do to the high ribbons texture and large magnetic anisotropy of the martensite phase, the magnetic field-induced strain (MFIS) values are strongly dependent on the direction of the applied magnetic field with respect to the ribbon surface. Being inspired by some experimentally observed features of the martensitic transfor-

mation, it was propose a simple phenomenological model for a solid state phase transition [5]. We assume that the direct phase transition takes place by formation of finite plates (Fig.4), geometrically restricted by existing surrounding plates puzzle. This assumption is supported by a numerical simulations transformation. Based on the described model, if a reverse transformation is incomplete (arrested), the larger plates will remain untransformed and a subsequent direct transformation will show an anomalously large number of big size plates, consisting of the untransformed ones plus the newly formed.

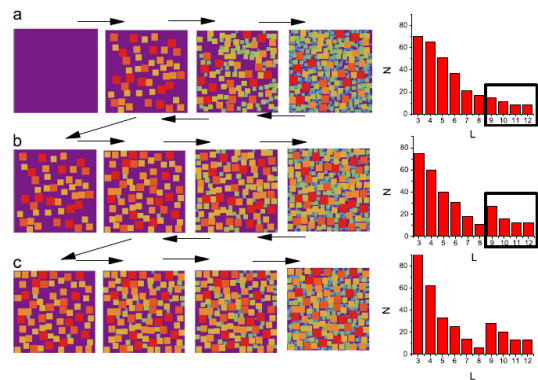


Fig.4. The plates distribution sizes during sequential incomplete reverse transformations.

As temperature is further decreased, intermediate size plates may encounter difficulties to geometrically fit – which results in them growing to a smaller final size and a general depletion of the sample of intermediate sizes. The effect is accentuated if the arrest scheme is repeated.

References

1. Sofronie M, Ţolea F, Kuncser V, Valeanu M, Filoti G, IEEE Transaction on Magnetics, **51**(1), 2500404, 2015;
2. Tolea F, Sofronie M, Tolea M, Kuncser V, Valeanu M, Digest Journal of Nanomaterials and Biostructures, **10** (2), 567-575, 2015;
3. Tolea F, Sofronie M, Crisan A D, Enculescu M, Kuncser V, Valeanu M; J. All.Comp. **650**, 664-670, 2015;
4. Ţolea F, Crişan A D, Sofronie M, Ţolea M, Văleanu M, Materials Today Proceedings, **2S**, S875 – S878,2015;
5. Tolea F, Tolea M, Sofronie M, Valeanu M, Solid State Communications, **213**, 37-41, 2015.

Recent developments of Spark Plasma Sintered MgB₂

*P. Badica, G. Aldica, L. Miu, S. Popa, M. Burdusel, V. Mihalache, I. Pasuk, M. Enculescu,
A. Kuncser, V. Mihalache*

in cooperation with

D. Batalu ('Politehnica' University of Bucharest)

The MgB₂ is a light weight, layered hexagonal, available, relatively cheap, and non-toxic compound. It shows superconductivity below a critical temperature of 39 K. Remarkable is that grain boundaries are efficient pinning centers [1], while the current can pass across them which is contrary to high temperature superconductors that are sensitive in this respect and, thus, it is necessary to produce epitaxial materials at higher costs. All presented advantages recommend MgB₂ as a candidate for practical applications, especially for portable ones.

Further developments through technology optimization or through the use of wisely selected additives are of great interest. The aim is enhancement of the critical current density, J_c and of the irreversibility field, H_{irr} while T_c is preserved at high values.

Additives promote a double action: (i) they can substitute in the crystal lattice of MgB₂ or (ii) they can modify grain boundaries, induce defects or stress. The consequences can be enhancement of flux pinning leading to higher J_c and H_{irr} . Pinning and connectivity details are also influenced through technology leading to specific structural and microstructural aspects.

In our work we use spark plasma sintering (SPS) applied on pristine and added powder of MgB₂. We investigate the influence of heating rate [2] during SPS on superconducting characteristics of pristine samples. Samples with additives such as B₄C [3], Ge [4] and GeO₂ [5] are obtained and characterized. The optimum amount of the additive is revealed. We note that B₄C has a double action, i.e. it produces substitution of B by C in the crystal lattice of MgB₂ and it influences microstructure. Literature indicates that C-based compounds [6] are very effective additions, especially SiC, to improve the functional characteristics of MgB₂ supercon-

ductors. Ge and GeO₂ show no substitution effects, but they lead to formation of Mg₂Ge phase. In the samples the other secondary phases are MgO, MgB₄ and higher Mg-borides or boron oxides (often containing some Mg). The last two phases are present at nanoscale and are not detectable by x-ray diffraction.

Different heating rates of 20, 100, 235, 355, and 475 °C/min were used. Samples have high density, above 95 %. The onset critical temperature T_c , is about 38.8 K. There is an optimum heating rate of ~100 °C/min to maximize J_c (Fig. 1a), H_{irr} , the product ($J_{c0} \times \mu_0 H_{irr}$), and to partially avoid formation of undesirable flux jumps at low temperatures. Significant microstructure differences were revealed for samples processed with low and high heating rates in respect to grain boundaries.

Powder mixtures of MgB₂ and B₄C with composition ((MgB₂)+(B₄C)_x, $x = 0.005, 0.01, 0.03$) were consolidated by SPS. The average particle size of B₄C raw powder was relatively high of 4 μm. Despite this, it is shown that processing processes are fast and carbon substitutes for the boron in the crystal lattice of MgB₂. Carbon substitution and microstructure contribute to enhancement of J_c at high magnetic fields and of H_{irr} (Fig. 1b). Samples are shown to be in the point pinning limit with some tendency toward the grain boundary pinning depending on B₄C doping amount and temperature. An optimum composition is found for $x = 0.01$: for this sample, at 20 K, a J_c of 100 A/cm² is obtained at 5.35 T. This H_{irr} value is higher than for the pristine MgB₂ sample. Furthermore, it is also higher than for an optimum nano-SiC-doped sample obtained for the same SPS processing conditions.

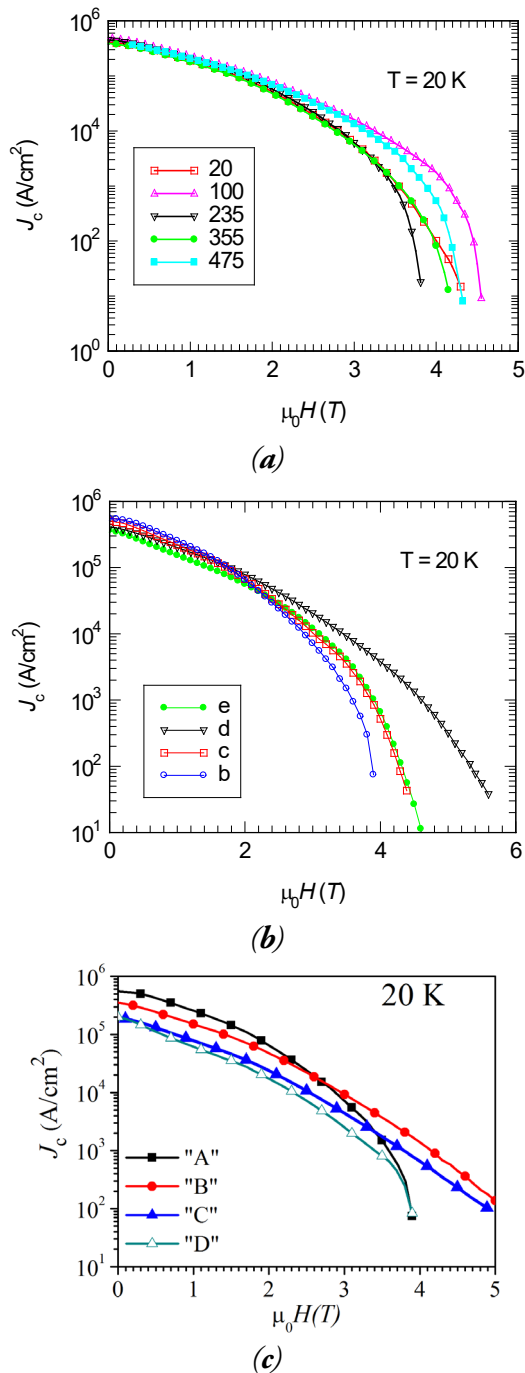


Fig. 1 Curves of J_c - μ_0H at 20 K for: (a)- samples obtained for different heating rates ($^{\circ}\text{C}/\text{min}$); (b)- samples b-e corresponding to $((\text{MgB}_2)+(\text{B}_4\text{C}))_x$, $x = 0, 0.005, 0.01, 0.03$); (c)- samples A-D corresponding to $((\text{MgB}_2)+(\text{GeO}_2))_x$, $x = 0, 0.005, 0.01, 0.03$).

Dense samples ($> 93\%$) of bulk MgB_2 with Ge or GeO_2 additions (G) were obtained by SPS $((\text{MgB}_2)+(\text{G}))_x$, $x = 0.005, 0.01, 0.03$. The J_c of the added samples is improved (Fig. 1c) at high magnetic fields when compared to the pristine sample. The optimum composition is for $\text{MgB}_2(\text{G})_{0.005}$. For these samples, a $J_c(20\text{ K}) = 10^2$

A/cm^2 is obtained at 5 or $\sim 5.1\text{ T}$ for Ge or GeO_2 , respectively, vs. 3.9 T for the pristine sample. The $T_{c,\text{onset}}$ and $T_{c,\text{midpoint}}$ from magnetization measurements scatter within 0.15 and 0.3 K for Ge and 0.2 and 0.6 K for GeO_2 . TEM investigations show some tendency to form secondary phases (20-100 nm) with sphere-like or irregular shapes. Samples are composites and the residual strain of MgB_2 is constant for pristine and G-added samples. Therefore, pinning enhancement leading to improvement of J_c is purely a ‘microstructure’ effect due to the presence of secondary nano phases. The analysis of the pinning force related parameters shows that the point pinning is the predominant mechanism. Addition of a higher amount of G is shifting the pinning mechanism toward a grain boundary pinning.

Authors acknowledge “Nucleu” PN09-2015, PCCE 7/2012 and 214/2014.

References

- [1] D.C. Larbalestier et al, NATURE 410 (2001) 186.
- [2] G. Aldica, M. Burdusel, S. Popa, M. Enculescu, I. Pasuk, P. Badica, PHYSICA C 519 (2015) 184.
- [3] M. Burdusel, G. Aldica, S. Popa, M. Enculescu, V. Mihalache, A. Kuncser, I. Pasuk, P. Badica, CURRENT APPL. PHYS. 15 (2015) 1262.
- [4] D. Batalu, G. Aldica, M. Burdusel, S. Popa, M. Enculescu, I. Pasuk, D. Miu, P. Badica, J. SUPERCOND. & NOVEL MAG. 28 (2015) 531.
- [5] D. Batalu, G. Aldica, S. Popa, A. Kuncser, V. Mihalache, P. Badica, SOLID STATE SCI., Vol. 48, Pages 23-30 2015
- [6] Kim JH et al. NPG ASIA MATER. 4 (2012) 1.

New aspects of diluted magnetic systems with possible catalytic applications

F. Tolea, N. Grecu, S. Constantinescu, D. Ghica, C. Teodorescu, V. Kuncser,

in cooperation with

S. Coman and V. Parvulescu

University of Bucharest, Faculty of Chemistry, Department of Organic Chemistry, Biochemistry and Catalysis

Dilute magnetic oxides (DMO) like ZnO, TiO₂, SnO₂, in which a fraction of nonmagnetic ions is substituted by magnetic transition-metal (TM) ions, have attracted extensive attention in the last decade due to their inter-related and unusual optical, magnetic, and electron transport properties, of potential interest for novel devices in spintronics and related fields. Also, there is currently a growing interest related to oxide/semiconductor catalysts (e.g. nanosized rare-earth ferrites belonging to the class of distorted perovskites with orthorhombic symmetry) which may also present the DMO-like behaviour. The insufficient correlation between the magnetic properties and the local structure of samples gives rise to inherent difficulties in detecting the origin of the room temperature ferromagnetism (RTFM) observed in such samples. Our goal was to understand how the TM local structure and related defects influence the magnetic properties of Fe-doped nano-TiO₂ anatase or how is induced the RTFM in defected perovskites with non-magnetic ions for catalytic applications.

Using superconducting quantum interference device (SQUID) combined with Mössbauer (MS) and electron paramagnetic resonance (EPR) spectroscopies, as methods-of-choice for their remarkable sensitivity and selectivity, was performed a systematic analysis of iron local structure and defects in the doped (0 – 1 at.%) TiO₂ anatase nanoparticles, as-grown via hydrothermal route and further thermally treated at T=650°C for 2 hours, in reduced atmosphere [1]. Also, two types of magnetic nanocomposite catalytic systems, Ru@MNP and Nb@AlF₃, allowing synthesis of sorbitol/glycerol and of lactic acid, respectively, were prepared and characterized as reported in [2, 3].

Thermomagnetic curves and magnetic hysteresis loops at different temperatures between 5 K and 380 K were measured with a SQUID magnetometer. An exemplification of hysteresis loops at different temperatures is presented in Fig. 1a for 1 at.% Fe as doped TiO₂ sample (denoted S2). The raw data are shown in the down-right inset. Accordingly, a linear variation of the magnetic moment of the sample versus applied field is observed at higher fields, with a temperature decreasing slope reaching at 380 K a negative value (of about $-2.4 \cdot 10^{-6}$ emu/g/Oe), common to all Fe doped investigated samples. Certainly, this high temperature negative slope is due to the diamagnetic signal of the oxide matrix, whereas the positive slope observed at lower temperatures is due to a superposed paramagnetic component, related to localized magnetic moments in the samples. By simply subtracting both the paramagnetic and diamagnetic contributions from the hysteresis loop raw data, the ferromagnetic contribution is evidenced. The temperature dependence of coercive fields for 1 at.% Fe thermally annealed sample (denoted S2T) is shown in Fig. 1c. The presence of coercive fields of 40-70 Oe even at 380 K, suggests a magnetically ordered state consisting of either magnetic clusters in the blocked magnetic regime, or a long range interaction ferromagnetic phase. To get more information about the involved magnetic regimes of the samples, typical field cooled (FC) magnetization curves have been collected on temperature lowering from 380 K down to 5 K, in a field of 100 Oe (Fig. 1b). The overall behaviour of the samples FC curves also suggests the existence of two superposed magnetic phases, namely the paramagnetic one, predominating at lower temperatures, and a magnetic ordered phase leading to a finite magnetization at higher temperatures.

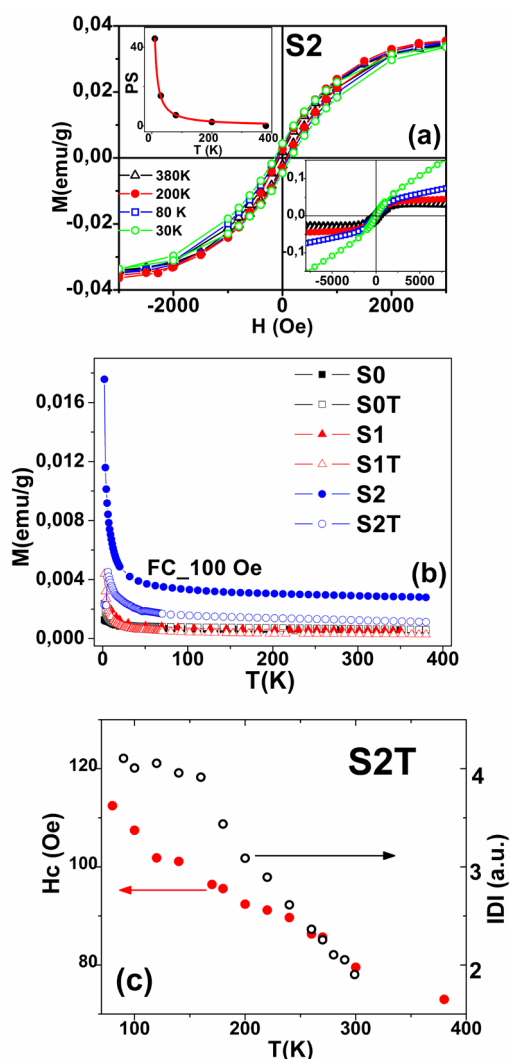


Fig.1.(a). Hysteresis loops at different temperatures for S2 samples. The raw data are shown in down-right insets, and the temperature dependent paramagnetic susceptibility (PS, in 10^{-6} emu/g/Oe) on upper-left.

(b) The overall behavior of the FC curves measured in 100 Oe for undoped samples (S0 and S0T), 0,1 at. % Fe doped (S1 and S1T) and for 1 at. % Fe (S2 and S2T).

(c) Temperature dependent coercivity of annealed sample in comparison with a relative number of defects in the same sample, as obtained from double integrated intensity (IDI) via ESR spectroscopy.

To correlate the above magnetic data with the local configuration state of iron in TiO_2 , Mössbauer spectra at different temperatures between 5 K and RT have been acquired in transmission geometry. Two components were assigned at 5K to Fe^{3+} ions in the highest spin state ($S=5/2$) corresponding to a central doublet

(due to paramagnetic Fe^{3+} ions) and an additional sextet-like pattern. This magnetic sextet (with a magnetic hyperfine field of 51.8T, characteristic to iron oxide compounds) presenting a strong collapsing behaviour at RT, is assigned to iron oxide nanoclusters with blocking temperatures below RT. While blocking temperatures of dc magnetic measurements are even lower than the ones estimated via Mössbauer spectroscopy, such clusters should be in the superparamagnetic state already well below RT. Hence, they cannot be responsible for coercive fields obtained at RT and above. According to MS data, Fe ions seem to contribute only to the sample paramagnetism, but not to their observed RTFM which was finally correlated to oxygen vacancies. A higher iron content increases the concentration of oxygen vacancies and enhances the ferromagnetic saturation magnetization [1].

For Ru@MNP magnetic nanocomposite catalytic systems, the magnetic response is generated using magnetic nanoparticle (MNP) supported catalysts while in Nb@AlF₃, the much weaker magnetic response associated to the RTFM (due to oxygen vacancies accompanying changes in the oxidation state of the Nb ions) might be exploited in this respect [2, 3]. While the observed behavior is similar to the one presented by other DMO systems, a mechanism related to was tentatively assumed as respond for the ferromagnetic ordered phase[2, 3].

Authors acknowledge “Core Program”-PN09-450103/2014.

References

- [1] F. Tolea, M.N. Grecu, V. Kuncser, S.G. Constantinescu, D. Ghica, Applied Physics Letters Vol. 106, 142404 (2015)
- [2] V. Kuncser, S. Coman, E. Kemnitz and V. Parvulescu, J. Appl. Phys. 117 17D724 (2015)
- [3] S. Coman, M. Verziu, A. Tirsoaga, B. Kurca, C. Teodorescu, V. Kuncser, V. Parvulescu, G. Scholz and E. Kemnitz, ACS Catalysis, 2015, 5, 3013-3026

Organic heterostructures for photovoltaic applications

A. Stanculescu, M. Socol, O. Rasoga, C. Breazu, N. Preda, I. Pasuk, I. Stavarache

in cooperation with

F. Stanculescu

University of Bucharest, Faculty of Physics, Magurele, Romania

A. M. Catargiu, L. Vacareanu

“P. Poni” Institute of Macromolecular Chemistry, Iasi, Romania

G. Socol, D. Visan, F. Gherendi

National Institute for Laser, Plasma and Radiation Physics, Magurele, Romania

M. Girtan

University Angers, Lab Photon, Angers, France

U. Sidwaba

University of Western Cape, Dept Chem, Cape Town, South Africa

Organic Solar Cells (OSC) offer an attractive research direction in the field of solar energy conversion because of the special photo-excitation and electron transfer phenomena hosted by the organic molecules. The main challenges are related to the optimization of the organic materials (small molecule, polymers) with the purpose to obtain an efficient generation of excitons by light absorption and control the processes at the organic/organic and organic/metal interfaces. To improve the performances of the bi-layer organic solar cell it is necessary to balance between the low exciton diffusion length and the thickness of the active layer [1]. This limitations can be surpassed by using a mixed active layer, a blend of two components, a donor conjugated polymer and an acceptor fullerene derivative, the separation at the nanometer scale creating donor/acceptor interfaces for exciton dissociation. The performances of polymer solar cells could be improved by the identification of new polymeric material and optimization of the active layer preparation method [1]. Interest was also focused on the study of OSC based on small molecules because they are easier to fabricate and show a better chemical stability [2]. Two types of organic heterostructures (OH) have been investigated: 1. OH with active layer obtained either from an arylene based polymer (with improved charge carrier mobility determined by the extended delocalization of the π electrons) or from a mixture of the same polymer acting as donor and fullerene/ C_{60} (characterized by a high electron

mobility determined by the highly conjugated nature of fullerene molecules) acting as acceptor; 2. multilayer OH based on ZnPc, C_{60} and NTCDA, in standard and inverted configurations.

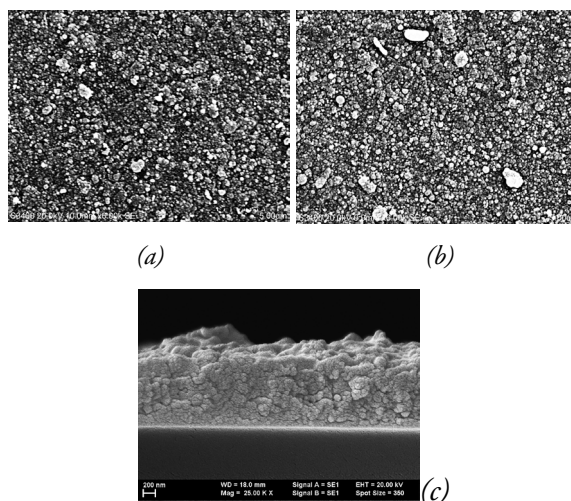


Fig. 1: SEM images: AMC16: C_{60} (a); AMC22: C_{60} (b); AMC22: C_{60} cross-section (c) [1].

New arylene based polymers poly[N-(2-ethylhexyl)2,7-carbazolyl vinylene]/AMC16 and poly[N-(2-ethylhexyl)2,7-carbazolyl 1,4-phenylene ethynylene]/AMC22 layers and AMC16/AMC22: C_{60} mixed active layers have been prepared by MAPLE on glass/ITO and glass/ITO/PEDOT-PSS substrates showing a large globules morphology (Fig.1), emphasizing the effect of the molecular particularities related to conjugation length and configuration on the molecular arrangement in these films [1].

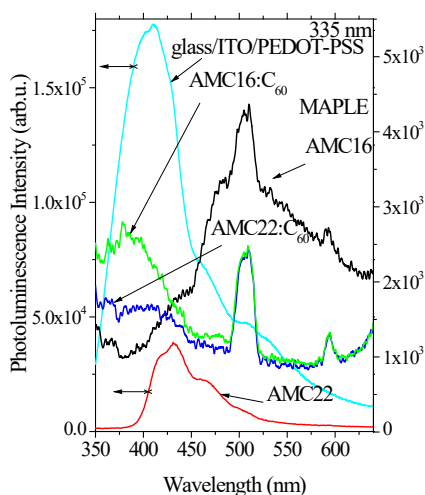


Fig. 2: PL spectra of the single/mixed layers on glass/ITO/PEDOT-PSS substrates [1].

The both polymers films show good absorption in the blue-green region with the fundamental absorption edge of the mixed layers slightly shifted through red. The PL peaks are situated in the absorption region of the active layer favoring the generation of an increased number of charge carriers by absorption of radiation (Fig.2).

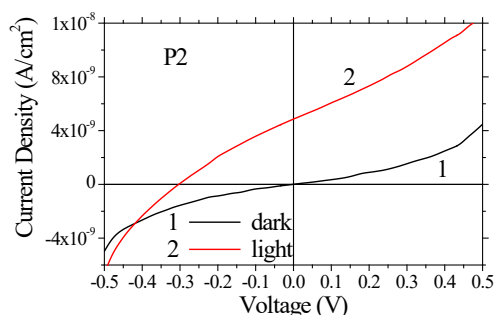


Fig.3: I-V characteristics for ITO/PEDOT-PSS/AMC16/Al solar cell structure [1].

The presence of the photovoltaic effect has been evidenced in the sample realized with AMC16 (P2) and AMC 22 layer and AMC22: C₆₀ mixed layer deposited on PEDOT-PSS favoring the charge carrier collection (Fig.3). The P2 solar cell structure shown the best parameters: $V_{OC}=0.303$ V; $I_{sc}=12.7 \times 10^{-9}$ A, $FF=0.29$.

The component layers of the multilayer OH have been deposited by vacuum evaporation and are characterised by a low roughness and polycrystalline structure. They show absorption peaks in UV-Vis range [2].

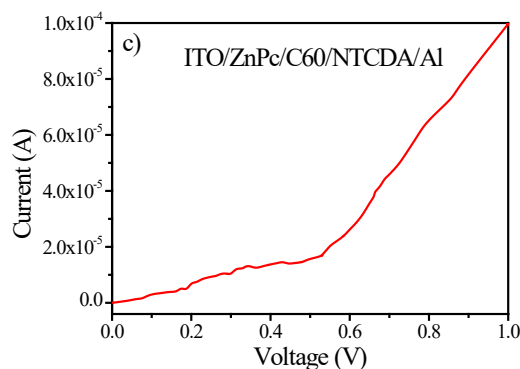


Fig.4: I-V plot for inverted multilayer OH [2].

The layer of PEDOT:PSS has improved with ~one order of magnitude the current in the standard structure. An increase in current has been achieved in the inverted structure, which avoids the chemical interaction between the Al atoms and organic layer (Fig.4).

References

- [1] F. Stanculescu, O. Rasoga, A. M. Catargiu, L. Vacareanu, M. Socol, C. Breazu, N. Preda, G. Socol, A. Stanculescu, *MAPLE prepared heterostructures with arylene based polymer active layer for photovoltaic applications*, Appl. Surf. Sci. 336, 240-248 (2015)
- [2] M. Socol, O. Rasoga, C. Breazu, G. Socol, N. Preda, I. Pasuk, D. Visan, I. Stavarache, F. Gherendi, M. Girtan, U. Sidwaba, "Heterostructures based on small molecules organic compounds", Dig. J. Nanomater. Bios. 10 (4) 1383-1392 (2015)

Semiconductor oxide particles deposited at low temperature upon fabrics and other network materials

I. Zgura, S. Frunza, C.P. Ganea, V.F. Cotorobai, L. Frunza, M. Enculescu, C. Florica, C.C. Negrila and L. Diamandescu

Surface of some polyester (PES) fabrics was functionalized by covering with semiconductor oxides like TiO_2 [1-3]. Other network materials from the class of layered double hydroxides (LDHs) were modified with zinc ions [4]. As deposition methods, sol-gel or vacuum deposition were applied for fabrics and ionic exchange, for LDHs. These works of functionalization continue the results found previously for ZnO deposition upon hemp [5], polyamide (PA), poly(lactic acid) (PLA) and hemp (H) [6] or for SiO_x deposition [7]. Low temperature deposition was asked by the low thermal stability of the fabrics due to their chemical composition. A complex characterization was performed before and after deposition, including XRD, SEM, EDX, XPS, FTIR, optical microscopy, thermal analysis [1-4,6,7]; dielectric properties [4,6] were also pursued and photocatalytic properties [1] as well.

In this presentation we focus on two topics: a) assessing the surface properties by the wetting properties and b) the behavior of the functionalized samples to UV/vis irradiation.

We have applied the two deposition methods at temperatures close to ambient conditions. Thus, sputtering (SP) deposition used a Sputter-Coater installation (Tectra GmbH) and a TiO_2 target (99.9% oxide, K.J. Lesker), at pressure of 4×10^{-3} - 4×10^{-2} bar. Sol-gel (SG) deposition was performed by dip coating the textile samples from a TiO_2 sol in a homemade installation, the precursor being used titanium (IV) tetraiso-propoxide.

A highly polar liquid (water) was used as testing liquid in contact angle measurements, for estimating the wettability properties of polar solids as polyester materials. We measured static (equilibrium) contact angles (Fig. 1) at room temperature with Drop Shape Analyzer DSA 100 (Krüss, Germany). A fixed steel needle supplied a water drop of 3 μL onto the surface of the solid

sample to be investigated. The image of the sessile (static) drops was captured; the data resulted from processing the images using specific programs to fit the profile with the Young-Laplace equation, polynomial of 2nd degree, etc. Finally, one obtains the value of the equilibrium contact angles (CAs). At least five different points on each sample were thus considered.

Higher CA might be due to the droplet on the surface of a composite surface, formed among air, water droplet and the fabric, in presence of nano-roughness. The behavior might be approximated by the Cassie-Baxter (C-B) equation in the form $\cos\theta_c = f\cos\theta_0 - (1-f)$, where θ_c is the composite contact angle formed on the treated fabric and θ_0 is the contact angle formed on untreated fabric. The f parameter is the fraction of the surface contacting the water droplet. The values of f can be then calculated for each pair raw-treated samples by knowing the corresponding CAs.

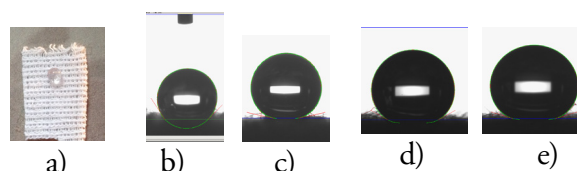


Fig. 1. Water droplets in contact with the surface of PES2 deposited samples for different irradiation times: a) photograph of $\text{TiO}_2\text{SG}/\text{PES2}$ original form; b) $\text{TiO}_2\text{SP4}/\text{PES2}$ original form, $CA(L)=133.2$, $CA(R)=134.4^\circ$; c) $\text{TiO}_2\text{SG}/\text{PES2}$ original form, $CA(L)=133.2$, $CA(R)=134.4^\circ$; d) $\text{TiO}_2\text{SG}/\text{PES2}$ after 90 min irradiation $CA(L)=CA(R)=151.4^\circ$; e) $\text{TiO}_2\text{SG}/\text{PES2}$ after 255 min irradiation $CA(L)=CA(R)=163.0^\circ$ [1].

Changes in the wetting properties were induced in the TiO_2 functionalized samples by exposure to illumination alternating with darkening conditions as follows: Irradiation with white light was performed for 210/255 min using a solar simulator (Lot Oriel) with collimated output beam, an integrated electrical shutter with

controller and a Xe lamp (300 W). UV irradiation was performed with different illumination times with a free ozone lamp (Lot Oriol) in a geometry allowing a short distance to the tissue. Darkening conditions were ensured in a specially designed black box.

Thus, the values found for some of studied fabrics are collected in Table 1 along with the factors resulted by applying C-B equation.

Table 1.

Sample	CA /degree	C-B parameter f^*	CA _{irrad} /degree
PES2	136.9	0.244	
PES3	138.1	0.231	
PLA	129.6	0.328	
TiO ₂ SG/PES2	169.3	0.017	154.8
TiO ₂ SG/PES3	169.7	0.016	
TiO ₂ SG/PLA	140.6	0.225	143.0
TiO ₂ SP4/PES2	133.8	0.209	Hydrophilic
TiO ₂ SP4/PES3	166.0	0.020	
TiO ₂ SP4/PLA	150.3	0.089	117.7

* θ_0 was taken as 84° for the raw samples, 89.4° for the sol-gel samples and 62.1° for the sputtered ones.

All the raw materials are hydrophobic, with $CA > 90^\circ$. Since extruded polymer shows CA of 84° , one can say that the fabrics have larger contact angles. CA increases more by titania deposition. Some samples having $CA > 150^\circ$, can be considered super-hydrophobic. One sample is hydrophilic meaning that water passes through it: it has large voids. The CA measurements can be then used for a primary evaluation of the coating morphology. In addition to the roughness increase by deposition, when more air is trapped in-between the structures, the voids (pores) are smaller for deposited samples than for original samples, a fact which tends to slow down the diffusion. The phenomena are complex and it is rather difficult to separate them.

Although bulk polyester is hydrophobic, the textile contact with water droplets shows the disappearance of water droplets due to high porosity (void areas) of the material allowing for water penetration through the microstructure. The void areas are reduced by the addition of TiO₂. These particles decrease the voids and concomitantly increase the sample hydrophobicity. Under these complex conditions one cannot use the traditional equations like C-B or Wenzel to model the wettability behavior of the heterogeneous and rough samples. However, C-B (or even Wenzel) equation should be applied to superhydrophobic surfaces with caution: TiO₂ can be utilized to lead hydrophobic surfaces by creating artificial roughness via microstructuring.

The sensitivity of the layers coated by sputtering to the UV illumination higher than for those coated by sol-gel clearly resulted from the irradiation experiments as function of the time. This might indicate that the nanoparticle agglomerates randomly distributed on the substrate interact easier with the photons than the uniform mosaic-like structure coated by sol-gel.

References

1. I. Zgura, S. Frunza, L. Frunza, M. Enculescu et al., J. Optoelectron. Adv. Mater. 17, 1055-1063 (2015).
2. I. Zgura, S. Frunza, M. Enculescu, C. Florica et al., Rom. J. Phys. 60 (3-4) 488-494 (2015).
3. I. Zgura, S. Frunza, L. Frunza, M. Enculescu et al., Rom. Rep. Phys. accepted (2015).
4. L. Frunza, P. Ganea, I. Zgura, S. Frunza et al., Semiconductor Conference (CAS), IEEE Proceedings DOI: 10.1109/SMICND.2015.7355162, pp. 67-70 (2015).
5. L. Frunza, N. Preda, E. Matei, S. Frunza et al., J. Polym. Sci. B: Polym. Phys., 51, 1427-1437, (2013).
6. C.P. Ganea, L. Frunza, I. Zgura, N. Preda et al., Digest J. Nanomater. Biostr. 9 (4) 1493 - 1503 (2014).
7. L. Frunza, I. Zgura, M. Enculescu, S. Frunza et al. J. Optoelectron. Adv. Mater. 16, 176-181 (2014).

Room temperature ammonia sensing with barium strontium titanate under humid air background

C.E. Simion, V. S. Teodorescu, A. Stănoiu

in cooperation with

A. Sackmann¹, C.F. Ruști²

¹AG Weimar, Institute of Physical Chemistry, University of Tübingen, Germany

²National R&D Institute for Non-ferrous and Rare Metals, Ilfov-Romania

In this report thick films of $\text{Ba}_{0.75}\text{Sr}_{0.25}\text{TiO}_3$ (BST) have been investigated for their NH_3 detection potential at 23°C , under humid air background. The BST materials were synthesized using a hydrothermal method starting from soluble salts of Ti (TiCl_4), Sr ($\text{Sr}(\text{NO}_3)_2$), $\text{Ba}(\text{OH})_2 \cdot 8\text{H}_2\text{O}$ and mineralizing agent [1].

In order to acquire the gas sensing performance the as-prepared materials were deposited onto commercial Al_2O_3 substrates provided with interdigitated Pt electrodes and heater, via screen-printing technique. The chemical composition indicated the presence of: 41.9%Ba, 8.67% Sr and 19.6 % Ti. The measured surface area was $57.33 \text{ m}^2/\text{g}$ and the mean pore size was 10.71 nm. Transmission Electron Microscopy (TEM) revealed the presence of two components (A and B) in the as-prepared BST materials (Figure 1).

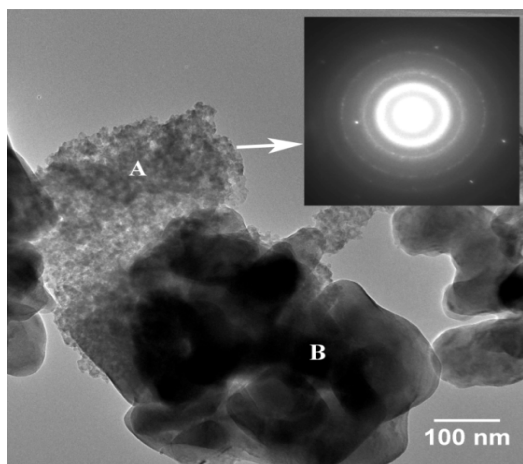


Fig. 1 TEM image and SAED pattern of as-prepared materials.

Selected Area Electron Diffraction (SAED) analysis shows that the B-type component (500-1000 nm), exhibit a monocrystalline structure with complex morphology resulted out of the hydrothermal crystal growth process. The small particles (A) (10-20nm) form a minority quasi-

amorphous component with mainly barium carbonate and titanium oxide, whereas the main component (B) have a cubic like structure. When exposed to humidity the associated dependencies of the electrical resistance R and capacitance C achieve changes within two orders of magnitude as can be seen in Figure 2.

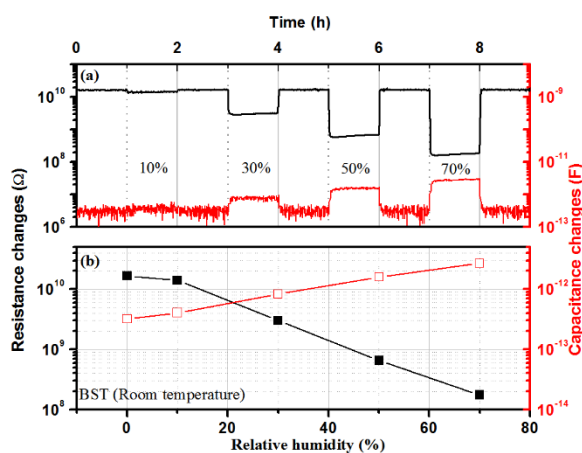


Fig. 2 R and C dependences (a) and semi-log plot (b) with respect to the RH level.

The recorded fast response and recovery times are associated to the high mobility of H_3O^+ and HO^- ions, through the liquid like network of condensed water inside the BST pores. The exponentially increases in capacitance with respect to the RH level can be related to the increase in the dielectric constant as more water is physisorbed inside the pores. The exponential decrease of the electrical resistance with the increase in RH might be due to both ionic and electronic conduction [2].

The optimum NH_3 detection and the best response/recovery times were obtained for 30 and 50% RH at room temperature (Figure 3).

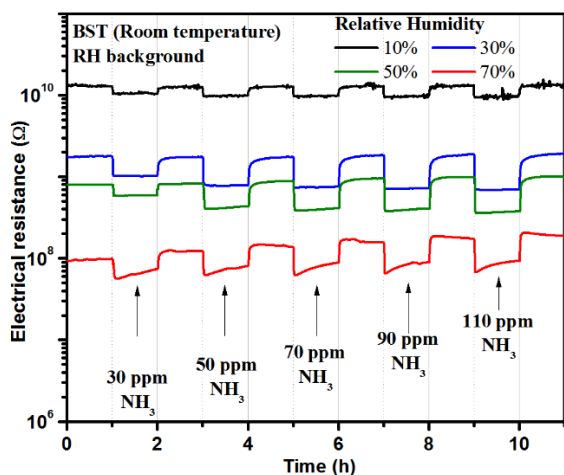


Fig. 3 Electrical resistance dependence with respect to the NH_3 concentrations under different RH levels.

The sensor signal S ($R_{\text{air}}/R_{\text{gas}}$) shows a linear dependence for 50% RH since a power law occurs under 70% RH (Figure 4a). Such mixed dependences can be attributed to different condition mechanisms based Schottky barriers superimposed on proton-assisted exchange [3]. The capacitance changes show a linear dependence with respect to the NH_3 concentration, independent on the RH level (Figure 4b).

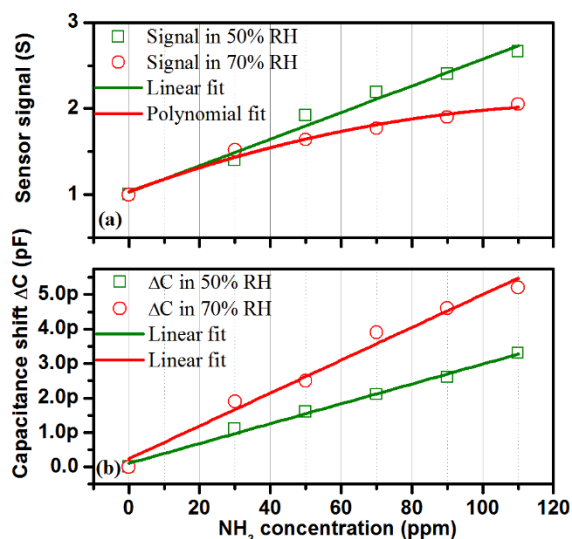


Fig. 4 Sensor signal (a) and capacitance shift dependence (b) with respect to the NH_3 concentrations under different RH levels

An associated cartoon is shown in Figure 5, aiming to describe the enhanced ammonia detection by the presence of water, when operated at room temperature.

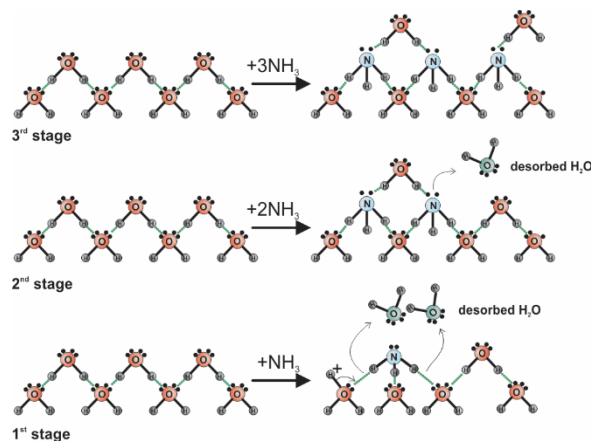


Fig. 5 Intuitive cartoon representing the interaction of NH_3 with water.

As such, in stage 1, single NH_3 molecule may break two hydrogen bonds of physisorbed water leading to a subsequent desorption process. Additionally, the pathway for the H^+ ion is thereby supported by the hydronium ion NH_4^+ . As one can see in stage 2, a solitary H_2O molecule is getting attached to the NH_3 due to the strong electrostatic attraction exhibited by the non-bonding lone pair of electrons available at the N atom. Since the NH_3 concentration increases, stronger attraction towards free H_2O molecules is exerted establishing newer hydrogen bonds $\text{NH}_3\text{-H}_2\text{O}$. Consequently, H_2O recondensation occurs, leading to the formation of water clusters inside the material and respectively to the enriching of the proton transport. This is mirrored by an increase in the overall conductivity (decreasing the electrical resistance).

From the gas sensing performance investigations, the BST thick films were found to be sensitive to NH_3 at room temperature in the presence of humidity. The possible interaction mechanism is based on the $\text{NH}_3\text{-H}_2\text{O}$ proton exchange.

References

- [1] C.E. Simion, A. Sackmann, V.S. Teodorescu, C.F. Rusti, A. Stanoiu, *Sens. Actuators B Chem.* 220, 1241-1246, (2015).
- [2] E. Traversa, *Sens. Actuators B Chem.* 23, 135-156, (1995).
- [3] N. Yamazoe, K. Shimano, *Sens. Actuators B Chem.* 128, 566-573 (2008).

BNT-BTCe@SiO₂ composite material with core-shell structure

M. Cernea, A. Iuga and L. Trupina

in cooperation with

B. S. Vasile,

University POLITEHNICA of Bucharest, Romania

I. V. Ciuchi and C. Galassi,

CNR - Institute of Science and Technology for Ceramics, Faenza, Italy

E. Alexandrescu,

COMOTI, Romanian Research and Development Institute for Gas Turbines, Bucharest, Romania

and

J. Pinte

National Institute for Electrical Engineering ICPE-CA, Bucharest, Romania

The aim of our study is to understand the influence of SiO₂ layer of a core-shell BNT-BTCe@SiO₂ heterostructure on electrical properties of BNT-BTCe ceramic [1]. BNT-BTCe represents (Bi_{0.5}Na_{0.5})TiO₃ (BNT) doped with Ba_{0.95}Ce_{0.05}TiO₃ (BTCe) in molar ratio 92:8. The composite core-shell BNT-BTCe@SiO₂ was prepared from grains of BNT-BTCe powder by chemical coating process with silica layer [1-3]. The core-shell grains show BNT-BTCe core-grains of 200-300 nm size and 128 nm thickness of SiO₂ shell (Fig.1).

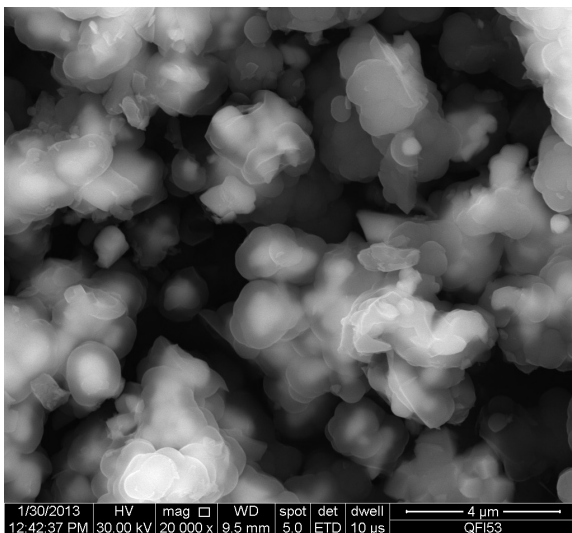


Fig.1. SEM photomicrographs of the core-shell composites BNT-BTCe@SiO₂ powder, dried at 100 °C.

Dielectric and piezoelectric properties of BNT-BTCe@SiO₂ sintered ceramic were investigated and compared with those of the base material BNT-BTCe (not shown here).

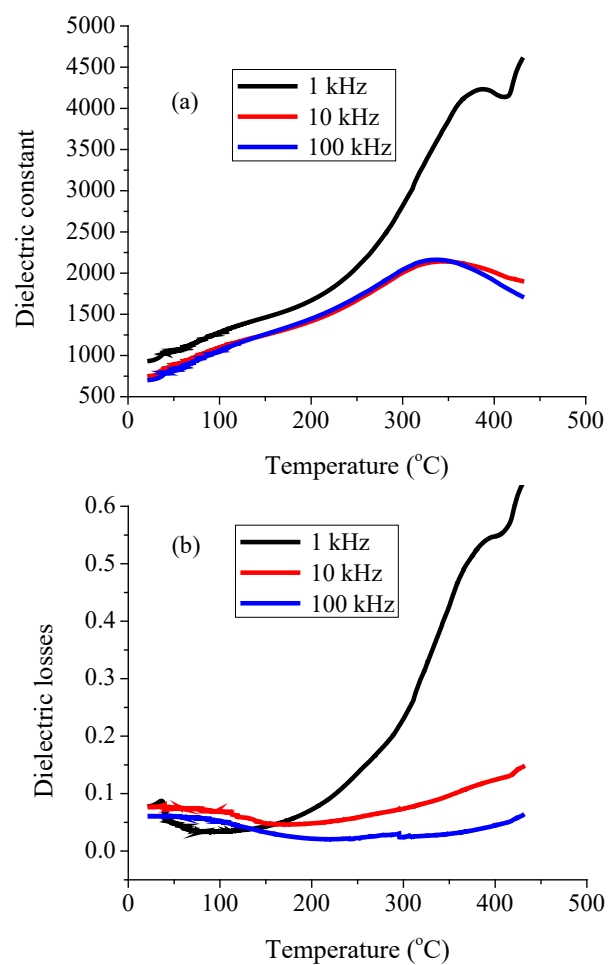


Fig.2. (a) Temperature dependence of dielectric permittivity (a) and dielectric losses (b) for BNT-BTCe@SiO₂ ceramic.

We found that the values of ϵ_r and dielectric losses of core-shell ceramic (Fig. 2) are lower and higher, respectively, than those of BNT-BTCe ceramic indicating that the SiO₂ does not improve the dielectric properties of BNT-BTCe

ceramic. For BNT-BTCe@SiO₂ composite, the silica layer leads to the increase of diffuseness degree of the phase transition and to a better ferroelectric relaxor.

The sintered heterostructure BNT-BTCe@SiO₂ shows higher remnant polarization P_r , higher coercive field E_c (Fig.3) and higher piezoelectric properties than BNT-BTCe ceramic (Tab.1).

Tab.1. Piezoelectric coefficients of BNT-BTCe@SiO₂ sintered core-shell ceramic

Electromechanical coupling factors	k_p	0.186	
	k_{31}	-0.122	
	k_t	0.527	
Piezoelectric charge coefficient	d_{31}	-37.62	pm/V
	d_{33}	18.8	pm/V
Piezoelectric voltage coefficient	g_{31}	-4.91	10 ⁻³ Vm/N
	g_{33}	2.453	10 ⁻³ Vm/N
Dielectric constants	ϵ_{33}^T	865	
	ϵ_{33}^S	604	
Mechanical quality factor	Q_m	32.6	

The results showed that the silica shell contributes to the improvement of some properties of the core material BNT-BTCe and could be interesting for applications in the ferroelectric and piezoelectric domains.

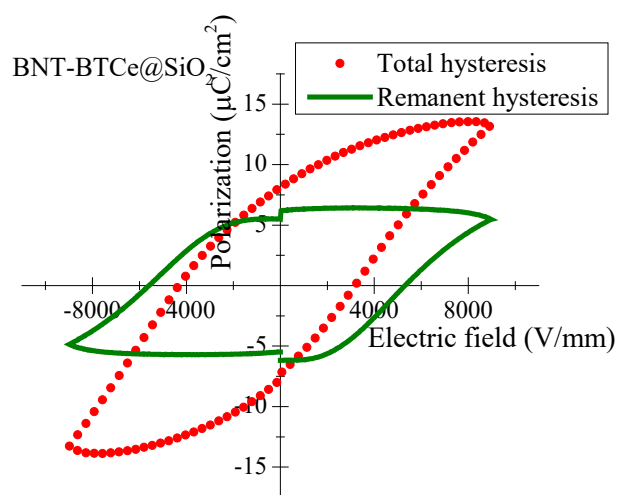


Fig.3. Core-shell BNT-BTCe@SiO₂ ceramic, in the proximity of the break down voltage.

References

- [1] M. Cernea, B. S. Vasile, I. V. Ciuchi, A. Iuga, E. Alexandrescu, J. Pintea, C. Galassi, Synthesis, Structural and Electrical Properties of BNT-BTCe@SiO₂ Core-Shell Heterostructure, *Sci. Adv. Mater.*, **7** (2015) 2297-2305.
- [2] M. Cernea, B. S. Vasile, A. Boni, A. Iuga, Synthesis, structural characterization, and dielectric properties of Nb doped BaTiO₃/SiO₂ core-shell heterostructure, *J. Alloy. Compd.*, **587** (2014) 553-559.
- [3] M. Secu, M. Cernea, C. E. Secu, B. S. Vasile, Structural and optical properties of fluorescent BaFBr-Eu²⁺@SiO₂ core/shell phosphor heterostructure, *Mat. Chem. Phys.*, **151** (2015) 81-86.

Patents and Patent Requests

PATENTS

1. **Cernea Marin, Ghita Rodica, Negrila Catalin**
Method for preparing a photosensitive structure of TiO₂/GaAs.
Patent Number RO123 630 (2015).
2. **Niciu Horatiu, Niciu Daniela, Popescu Mihai, Lorinczi Adam, Velea Alin, Manea Adrian, Lazarescu Mihai**
Procedure for preparation of optical glass microelements for infrared light
Patent Number RO127642 (30.06.2015)
3. **Evanghelidis Alexandru Ionut, Busuioc Cristina, Matei Elena, Enculescu Maria Monica, Preda Nicoleta Roxana, Florica Camelia Florina, Costas Andreea Liliana, Oancea Mihaela, Enculescu Ionut Marius**
Preparation procedure of some conducting, transparent and flexible electrodes by electrospinning
Patent Number RO129633 (30.10.2015)

PATENT REQUESTS

1. **Cotirlan Costel Simioniuc, Manea Adrian Stefan, Logofatu Constantin**
Electrooptical superlens structure obtained with micro- and nanostructured plasmonic guide for imagistics having a resolution under diffraction limit
A/00050 (23.01.2015)
2. **Predoi Daniela, Ciobanu Carmen Steluta, Ghita Rodica, Popa Cristina Liliana, Iconaru Simona Liliana**
Preparation of nanohydroxyapatite in silicon matrix for environment applications
A/00070 (02.02.2015)
3. **Predoi Daniela, Ciobanu Carmen Steluta, Ghita Rodica, Popa Cristina Liliana.**
Bioactive hydroxyapatite glass for applications in depollution of Pb ion contaminated waters
A/00390 (10.06.2015)
4. **Iuga Alin Romulus**
Measurement method of quasi-static ferroelectric hysteresis
A/00483 (08.07.2015)
5. **Gavrila-Florescu Carmen Lavinia, Popovici Ernest, Morjan Ion, Lucian Constantin Diamandescu, Raditoiu Valentin, Raditoiu Alina, Wagner Luminita Eugenia, Badoi Anca Daniela, Miron Dan**
Preparation procedure of titan dioxide by laser pyrolysis for photocatalytic applications
A/00534 (23.07.2015)
6. **Polosan Silviu, Pacala Ovidiu, Pacala Mirela**
Preparation method of scintillator material and scintillator material
A/00995 (30-09-2015)

7. **Popescu Dana Georgeta, Husanu Marius Adrian**
Preparation procedure of photonic bidimensional crystals by laser ablation
A/00731 (13.10.2015)
8. **Aldica Gheorghe Virgil, Burdusel Mihail, Badica Petre**
Superconducting material machinable by cutting tools and a magnetic field concentrator/storage device
A/00748 (21.10.2015)
9. **Ghita Rodica, Frumosu Florica, Logofatu Constantin, Predoi Daniela, Negrila Constantin, Trupina Lucian**
Passivation procedure of III-V semiconductor surfaces and preparation of sensitive structures of GaCl₃-Sb₂S₃/GaSb type
A/00793 (05.11.2015)
10. **Ciurea Lidia Magdalena, Stavarache Ionel, Teodorescu Valentin Serban**
Capacitor structure for nonvolatile memory based on Ge nanocrystals immersed in SiO₂
A/00869 (19.11.2015)
11. **Nedelcu Liviu, Banciu Marian Gabriel, Geambasu Cezar Dragos**
Nb-based ceramic materials with weak absorption in the THz range
A/00898 (26.11.2015)
12. **Apostol Nicoleta Georgiana, Popescu Dana Georgeta, Teodorescu Cristian Mihail**
Graphite sublimator with resistive heating
A/00958 (03.12.2015)

Events

NIMP was in 2015 co-organizer of conferences:

7th International Conference on Amorphous and Nanostructured Chalcogenides,

Cluj-Napoca, 5-10 of July, 2015

<http://www.infim.ro/events/amorphous-and-nanostructured-chalcogenides-anc-7-conference>

8th International Conference on Advanced Materials (ROCAM), Bucharest, 7-10 of July, 2015

<http://rocam.unibuc.ro/rocam2015/>

Workshop “Advances in Nanophysics and Nanophotonics”, Bucharest, 31.08.-2.09.2015

<http://www.infim.ro/nanophysics-solar/>

“Lights of the World” Conference – Bucharest, House of Parliament, 30.10-1.11.2015

<http://iyl2015.infim.ro/>

7th International Conference on Amorphous and Nanostructured Chalcogenides (ANC 7)

Between 5th and 10th of July 2015, NIMP organized in Cluj-Napoca, the 7th Edition of the Amorphous and Nanostructured Chalcogenides Conference, ANC-7. The purpose of the conference was the presentation of the latest results in the field and to promote the exchange of ideas in associated topics, including applications of the chalcogenides materials.

There were organized the following sections:

1. State of the art in physics and chemistry of non-crystalline chalcogenides;
2. Nanostructured chalcogenides;
3. Intermediate phases;
4. Nanocrystalline chalcogenides;
5. Switching (Ovonic) materials;
6. Complex chalcogenide glasses;
7. Applications of chalcogenides.

Prof. Dr. Mihai Popescu (NIMP) was ANC 7 chair.

A partial list of specialists who were invited speakers is given below:

- Punit Boolchand, **University of Cincinnati, USA;**
- Matthieu Micoulaut, **Pierre and Marie Curie University, France;**
- Marcel Poulain, **Université de Rennes 1, France;**
- Jong Heo, **Pohang University of Science and Technology, South Korea;**
- Shinya Hosokawa, **Graduate School of Science and Technology, Kumamoto University, Japan;**
- Maria Mitkova, **Boise State University, USA;**
- Mathieu Bauchy, **University of California, Los Angeles, USA;**
- Andriy Kryuchyn, **Institute for Information Recording of the National Academy of Sciences of Ukraine, Ukraine;**
- Oleh Shpotyuk, **Scientific Research Company “Carat”, Ukraine;**
- Sandor Kokenyesi, **University of Debrecen, Hungary;**
- Victor Minaev, **National Research University of Electronic Technology, Russia;**
- Xiang - Hua Zhang, **Institut des Sciences Chimiques de Rennes, Université de Rennes I, France;**

8th International Conference on Advanced Materials

The 8th edition of the International Conference on Advanced Materials took place in Bucharest between 7th to 10th of July 2015. The purpose of the conference was to present a synthesis of the latest developments in some areas of advanced materials theory, modeling, processing, characterization and applications. The scientific works were conducted in eight sections, as follows:

1. Advanced Materials for solar energy conversion
2. Carbon-based Nanomaterials and Applications
3. Thin films and nanostructures of functional materials
4. Advanced Biomaterials, Bio-devices and Biotechnology
5. Advances in surface science and engineering
6. Advanced ceramics: synthesis, properties, and applications
7. Ferroelectrics, Nonlinear Optical and Luminescent Materials, Properties and Application
8. Advanced Materials Characterization and Modeling

NIMP was co-organizer and one of the chairmen of the Organizing Committee was Dr. Lucian Pintilie. The Romanian Scientific Committee counted six researchers from NIMP. M. L. Ciurea and C. M. Teodorescu held presentations as Key Speakers.

A large number of highly prestigious professors and researchers from around the world have participated with invited lectures and oral presentation:

- Jean-Louis Bobet, **Institut de Chimie de la Matiere Condense de Bordeaux, Universite Bordeaux 1, France**
- Davide Bonifazi, Department of Chemistry, **University of NAMUR, Belgium**
- Gabriel Caruntu, Colege of Science and Technology, **Central Michigan University, USA**
- Floriana Craciun, **Istituto dei Sistemi Complessi, CNR, Roma**
- Jose Maria da Fonte Ferreira, Department of Materials and Ceramic Engineering, Centre for Research in Ceramics and Composite Materials (CICECO), **University of Aveiro, Portugal**
- Emmanuel Defay, **Centre de Recherche Public Gabriel Lippmann, Belvaux, Luxembourg**
- Fabio Di Pietrantonio, **Institute of Acoustic and Sensors “Orso Mario Corbino”, Italy**
- Wolfgang Diehl, **Fraunhofer Institute for Surface Engineering and Thin Films, Germany**
- Thierry Duffar, **Grenoble Polytechnic Institute, Grenoble, France**
- Cathetine Elissalde1CNRS, **ICMCB, Univ. Bordeaux, France**
- Klaus Ellmer Institute Solar Fuels, **Helmholtz Zentrum, Berlin, Germany**
- Claude Estourne, Interuniversity Center for Materials Research and Engineering (CIRIMAT), Institut Carnot, **Universite Toulouse III - Paul Sabatier, France**
- Elvira Fortunato, Centre for Materials Research (CENIMAT), Universidade Nova de Lisboa, **New University of Lisbon, Portugal**
- Mihaela Girtan, LPHIA: Laboratoire de Photonique d' Angers, **Universite d'Angers, France**
- Eric Glowacki, Linz Institute for Organic Solar Cells (LIOS), Physical Chemistry, **Johannes Kepler University, Linz Austria**
- Pedro Gomez-Romero, **Institut Catala de Nanociencia I Nanotecnologia, ICN2 (CSIC-CERCA), Barcelona, Spain**
- Grzegorz Greczynski, **Linkoping University, Sweden**
- Joseph Greene, **University of Illinois, Urbana, Illinois, USA**
- Duncan Gregory, School of Chemistry, **University of Glasgow, Great Britain**

- Maryline Guilloux, Viry Institute des Sciences Chimiques de Rennes, **Universite de Rennes 1, France**
- Laure Huitema, Xlim Laboratory UMR 7252 CNRS/University of Limoges, 87060, **Limoges, France**
- Bernard Humbert, Institute des Matériaux Jean Rouxel (IMN), **Université de Nantes, CNRS, France**
- John Irvine, School of Chemistry, **University of St Andrews, Scotland, United Kingdom**
- Yoji Koike, Department of Applied Physics, **Tohoku University, Japan**
- Thomas Kuech, **University of Wisconsin-** Madison Department of Chemical and Biological Engineering, **USA**
- Rodrigo Martins, Center of Excellence in Microelectronics Optoelectronics and Processes, **UNINOVA, Portugal**
- Hiroaki Minamide, RIKEN Center for Advanced Photonics (RAP), **RIKEN, Japan**
- Xavier Moya, Department of Materials Science & Metallurgy, **University of Cambridge, England**
- Tatau Nishinaga, **The University of Tokyo (Japan)**,
Former President of the International Organization for Crystal Growth
- Aleksandar Ostrogorsky, **Illinois Institute of Technology, Chicago, IL, USA**
- Deepak Pant, **Flemish Institute for Technological Research, Belgium**
- Theo Rasing, Institute of Molecules and Materials, **Radboud University Nijmegen, Netherlands**
- Florencio Sanchez, **Institut de Ciencia de Materials de Barcelona (ICMAB-CSIC), Spain**
- Shashi Paul, Emerging Technologies Research Centre, **De Montfort University, United Kingdom**
- Liliana Stan, **Argonne National Laboratory, USA**
- Marius Stan, **Argonne National Laboratory, USA**
- Alessandro Stroppa, **CNR-SPIN, L'Aquila, Italy**
- Hendrik Swart, Department of Physics, **University of the Free State, South Africa**
- Masahiko Tani, Research Center for Development of Far-Infrared Region, **University of Fukui, Japan**
- Magdalena Titirici, School of Eng. and Mater. Science, **Queen Mary University of London, United Kingdom**
- Elizabeth von Hauff, Department of Physics and Astronomy, **Vrije Universiteit Amsterdam, Netherlands**

Workshop “Advances in Nanophysics and Nanophotonics”

Between 31.08- 2.09.2015, NIMP was the host for the “Advances in Nanophysics and Nanophotonics” workshop, which is the 4 fourth event of this type, organized in cooperation with the UNESCO Department of the Horia Hulubei Foundation and with the scientific and financial support of the International Center for Theoretical Physics “ Abdus Salam “ from Trieste.

This workshop dedicated to nanophysics focused on recent achievement in the field of nanomaterials and nanophotonics, including the vast research domain of solar energy conversion. Nanophysics and solar energy conversion are priorities for modern physics thanks to the rapid development of atomic scale devices but also because of the vital need of development of new renewable energy sources.

There were also organized sessions dedicated to different themes from the nanomaterials and nanophotonics fields. Within the workshop, there were presented a few interdisciplinary contributions, based on applied, computational and theoretical physics, chemistry and electrochemistry.

We consider that this workshop managed to contribute to the strengthening of the regional scientific collaboration, with the participation of active researchers from Central and Eastern Europe.

“Lights of the World” Conference

Conference "Lights of the World" Conference was held in Bucharest at the Parliament Palace, between 30.10-1.11.2015 and was part of a series of events that promote science, culture and education in the context of the International Year of Light in 2015, marking the 70th anniversary of UNESCO.

NIMP was one of the organizers, along with prestigious institutions such as ICR, Bucharest University, ROSA, INFLPR, The Parliamentary Commission for UNESCO, etc. In the organizing committee there were researchers and specialists included, Dr. Victor Kuncser (NIMP) being among them.

The objectives of this conference were:

- Development of the “light (of the world)” concept from a transdisciplinary perspective, highlighting its multiple facets and symbols in science, education, space and culture, as a vector for sustainable development in the XXI century society
- To promote representative scientific and cultural values of Romania, in a creative and fruitful dialogue with similar European and universal values

The conference brought together about 400 participants from around the world, including outstanding figures of science, culture and education, as well as researchers, teachers, managers, artists, policy makers and opinion leaders.

Representing NIMP, Dr. C. Ghica, Dr. I. Pintilie and Dr. C. Teodorescu held interesting and adequate presentations.

The conclusion of the project “Centre for Research, Innovation and Technologies for New Materials” Conference

On 4th of December, at 10:30, NIMP held the conclusion of the project “Centre for Research, Innovation and Technologies for New Materials” Conference, SMIS-CSNR 49185 code, co-financed by the European Regional Development Fund, based on the financing contract no. 654/07.08.2014, signed with the Ministry of National Education (MEN), as Intermediate Body (IB) in the name and for the Ministry of European funds, as Managing Authority (MA) for the Sectoral Operational Programme “Increase of Economic Competitiveness” (SOP). The total value of the project was 43.248.955,84 lei, from which 35 000000,00 lei were nonrefundable financial assistance.

The conference was started by an overview presentation of the General Director, Dr. Ionut Enculescu, followed by the presentations of the three laboratories of the Centre.

RITecC Laboratory 01 (Laboratory for production, processing, and analyzing of functional materials for high technology applications) and RITecC Laboratory 02 (Laboratory for production, processing and analyzing materials for increasing life quality) were presented by Dr. Lucian Pintilie, and RITecC Laboratory 03 (Laboratory for production, processing and analyzing materials for extreme conditions) by Dr. Andrei Galatanu.

International Cooperation

INTERNATIONAL COOPERATION PROJECTS

Pintilie I

CERN RD50 “Radiation hard semiconductor devices for very high luminosity colliders”

[\(http://rd50.web.cern.ch/rd50/\)](http://rd50.web.cern.ch/rd50/): 48 research institutions from 27 countries around the world

Scientific coordinator of the workpackage “Defect/Material Characterization”

Pintilie I

Project funds SEE (EEA Grants) “Perovskites for Photovoltaic Efficient Conversion Technology” (PERPHECT)

Partners: NIMP (INCDFM) , Physics Faculty U.Bocharest , Optoelectronics 2000 SA (Romania); U. Iceland, U. Reykjavik (Iceland); U. Oslo (Norway)

2014-2017

Pintilie L

Project M-ERA NET

NOPYDET (Novel generation of pyroelectric detectors based on polar semiconductors)

Partners from Romania (microelectronics) and France (CEA, YZATEC)

2015-2018

2 FP7 projects

Pintilie L

FP7 project Large-scale integrating project Interfacing Oxides (IFOX) NMP-2009-2.2-1

Coordinator: Theo Rasing (Radboud University, Nijmegen)

Scientific coordinator: Georg Schmidt (Martin-Luther-Universität, Halle-Wittenberg)

Partners: Radboud University Nijmegen (NL), Martin-Luther-Universität Halle Wittenberg (DE), Max Planck Gesellschaft zur Foerderung der Wissenschaften E.V. (MPI-HALLE) (DE), University of Glasgow (UK), Centro Ricerche Fiat SCPA (IT), Universiteit Antwerpen (BE), Paul Scherrer Institut (CH), National Institute of Materials Physics (NIMP) (RO), IBM Research GMBH (CH), Universitat Konstanz (DE), Institute for Nanostructured Materials Bologna (IT), Intel Performance Learning Solutions Limited (IE), Forschungszentrum Jülich GmbH (DE), Twente Solid State Technology (NL), Georg August Universitaet Goettingen (DE) ,Holy Trinity College Dublin (IE), Organic Spintronics srl (IT), Universiteit Twente (NL)

<http://www.ifox-project.eu>

2010-2015

Mercioniu I

Development of a sintering centre and know-how exchange for non-equilibrium sintering methods of advanced ceramic composite materials (SINTERCER)

FP7 EU-Research Potential – Capacities – REGPOT-CT-2013-316232-SINTERCER

Coordinator: The Institute of Advanced Manufacturing Technology, Krakow, Poland

Partners: Politecnico di Torino (POLITO), Torino, Italy, Institute of Ceramics and Glass (ICV-CSIC), Madrid, Spain, University of Rostock (UR), Rostock, Germany, National Institute of Materials Physics (NIMP), Bucharest – Magurele, Romania, Aalto University School of Chemical

Technology, Espoo, Finland, RHP-Technology GmbH & Co. KG (RHP), Seibersdorf, Austria, Universidade de Aveiro(UA), Aveiro, Portugal, University of Science and Technology (AGH), Cracow, Poland, Institute of Metallurgy and Materials Science of Polish Academy of Sciences (IMIM), Cracow, Poland
<http://www.ios.krakow.pl/sintercer>

2 Romanian-Swiss Research Program RSRP projects

Baibarac M

Electrochemical functionalization of carbon nanotubes with heteropolyanions and conjugated polymers and the elucidation of interactions at the carbon nanotubes/ heteropolyacid/ conjugated polymer interface

Partners: Ecole Polytechnique Fédérale de Lausanne, Switzerland and Institute for Problems of Materials Science of National Academy of Science of Ukraine

Crisan O

Novel FePt-based hard magnetic materials for sustainable energy applications

Project RO-CH RSRP 142256 / 6 / 2012-2015

Partner: Swiss Federal Laboratories for Materials Science and Technology, EMPA Thun, Switzerland

C-ERIC

Teodorescu CM

CERIC Project ID: 20142030 Combined studies on magnetism, electronic structure, morphology and spin configuration in Ge(001) and Si(001) -based diluted magnetic semiconductors

2014-2015

2 IFA-CEA projects

Pintilie L

Pyroelectricity in PZT thin films and multilayers

Partner: Laboratory of components for microactuators, CEA Grenoble, France

2014-2016

Predoi D

New bioceramic nanocomposites with antibacterian activity for biomedical applications

Partner Franta: Laboratory of Chemistry and Biology of Metals (LCBM), Grenoble, France

2014-2016

OTHER EUROPEAN PROJECTS

Baibarac M

SCOPES project

Implementation in East Europe of new methods of synthesis and functionalization of carbon nanotubes for applications in the energy storage and sensors field

Partners: Ecole Polytechnique Federal de Lausanne, Switzerland and Institute for Problems of Materials Science of National Academy of Science of Ukraine

2011 - 2015

Baibarac M

Programme Hubert Curien PHC Brancusi

Optical properties of SWNTs highly separated in metallic (98%) and semiconducting (99%) functionalized with conjugated polymers

Partner: Institut des Materiaux Jean Rouxell, Nantes, France

2015-2016

Crisan O

Programme Hubert Curien PHC Brancusi: ANCS-CNRS

Hard magnetic nanocrystalline materials obtained from amorphous precursors

Partner: Universite du Maine, Le Mans, Franta

2013-2015

Nedelcu L

Project ANR-ANCS (RO-FR) PN-II-ID-JRP-RO-FR-2012-0160

Compact and integrated agile antennas based on tunable ferroelectric materials

Coordinator: XLIM UMR 7252 CNRS, University of Limoges

Partners: SPCTS UMR 7315 CNRS, University of Limoges; National Institute of Materials Physics, Romania

2014-2016

Socol M

Programme Hubert Curien PHC Brancusi

Metallic electrode with 2D photonic crystal architecture for multilayer (bio) organic structures

Partner: University Angers, France

2015-2016

Teodorescu CM

Project ANR-ANCS (RO-FR) PN-II-ID-JRP-2011- 2

Chemical switching of surface ferroelectric topology

Partner: Service de Physique et Chimie des Surfaces et Interfaces, Institut Rayonnement Matière Saclay, Commissariat à l'Energie Atomique, France

2013-2015

EURATOM*Galatanu A***EUROfusion Consortium, Grant agreement No. 633053**

2014-2018

2 COST projects*Banciu MG***COST action VISTA (IC1102) “Versatile, Integrated, and Signal-aware Technologies for Antennas (VISTA)”**http://www.cost.eu/COST_Actions/ict/Actions/IC1102

Coordinator: Chair: Dr. Marta Martinez Vazquez, Germania

2011-2015

*Pintilie L***COST actiunea MP1308 “Towards Oxide-Based Electronics (TO-BE)”**http://www.cost.eu/COST_Actions/mpns/Actions/MP1308

Coordinator: Dr Fabio Miletto Granozio (IT)

2014-2018

ELETTRA (Trieste) Synchrotron projects*Apostol NG*

Elettra Project ID: 20145226

Adsorption, desorption and molecular reactions at ferroelectric surfaces

2014-2015

Husanu MA

Elettra Project ID: 20140319

Reactivity and electronic properties of ferroelectric-ferromagnetic interfaces

2014-2015

Pintilie L

Elettra Project ID: 20130333

High-speed field effect devices based on graphene on epitaxial ferroelectric oxides: in-situ investigation of ferroelectric-graphene interface formation and properties by XPS and XAS combined with STM.

2013-2015

Teodorescu CM

Elettra Project ID: 20145462

Photoelectron spectromicroscopic imaging of surface reactions on ferroelectrics with binding energy contrast

2014-2015

Bilateral cooperation projects (Agreements)

Baibarac M

Institut des Materiaux Jean Rouxell, Strasbourg, France

Scientific Cooperation Agreement on optical and electrical properties of composite nanomaterials based on carbon nanotubes and conjugated polymers

Banciu MG

Collaboration project Romania-Japan JSPS 4903, 13039901-000203, Research Center for Development of Far-Infrared Region, University of Fukui (FIR-UF)

Research on EO sampling devices for ultra-high sensitive detection of THz waves using ferroelectric materials

Cernea M

Joint Research Project CNR Italy– Romanian Academy

Study and Development of Single-Phase Multiferroic Perovskite Ceramic and Thin Films for Multifunctional Devices

2014-2016

Ghica C

Departament Surfaces-Interfaces, Institut of Materials Physics and Chemistry, Strasbourg, France

Effet de la réduction de taille, de la forme et des caractéristiques des interfaces sur la structure et les propriétés des matériaux nanostructurés

2012-2016

Stanculescu A

University of Western Cape, Department of Chemistry, SensoLab , South Africa

Polymeric single/multilayer heterostructures for photovoltaic and electronic applications; polymeric field effect transistors for sensing applications; organic and hybrid devices (realisation, characterisation)

Cooperation projects with foreign institutes and universities

Badica P

Tohoku University, Japonia

Joints of superconducting tapes: fabrication and characterization

Project: ICC-IMR Visiting Prof. , collaboration and exchange of researchers/students INCDFM-HFSLM-Tohoku University

Ciurea ML

School of Science and Engineering, Reykjavik University , Reykjavik, Iceland

Nanostructures based on Ge nanoparticles immersed in oxidic matrices for optical sensors applications

Ciurea ML, Lepadatu AM

Istituto Nazionale di Fisica Nucleare-Laboratori Nazionali di Frascati , Frascati, Italy

Nanostructures based on Ge nanoparticles immersed in oxidic matrices for optical sensors applications

Ciurea ML, Lepadatu AM

National Academy of Sciences of Ukraine, V. Lashkaryov Institute of Semiconductor Physics , Kiev, Ukraine

Study of electrical and optical properties correlated with morphology and structure of films based on Ge nanoparticles immersed in oxidic matrices

Maraloiu VA / Teodorescu VS

Institut Lumière Matière – Université Claude Bernard, Lyon, France

Biocalisation et biotransformation de nanoparticules à coeur d'oxydes magnétiques.

Fonctionnalisation des substrats par irradiation laser à faible fluence

Convention Bilatérale de Coopération et d'Echange

2013-2014

Miclea CF

Los Alamos National Laboratory, Los Alamos, NM. USA.

Measurements, co-publication, specimen exchange

Miclea CF

Max Planck Institute for Chemical Physics of Solids, Dresden, Germany

Measurements, co-publication, specimen exchange

Nedelcu L

Research Center for Development of Far-Infrared Region, University of Fukui, Japan

Measurements, specimen exchange

Nistor SV

Institute of Physics, Czech Academy, Prague

Investigation by magnetic electronic resonance techniques and optical spectroscopy of the semiconducting II-VI materials optically activated with transitional ions

Nistor SV

Physics Department, Antwerp University , Belgium

Development of new advanced multifunctional materials containing defects

Pintilie L

UMP CNRS-Thales, Palaiseau, France and Université Paris-Sud

Measurements, specimen exchange

Pintilie L, Pintilie I

University of Oulu, Finland

Ferroelectric measurements

Pintilie L

Universitatea Tehnica Darmstadt, Germany

Specimen exchange, co-publication

Pintilie I

Universitatea din Oslo, Norway

Specimen exchange, working stages

Pintilie L

UMP CNRS-Thales, 1 Av. Fresnel, Palaiseau, 91767, France and Université Paris-Sud

Specimen exchange, common measurements

Preda N

Yildiz Technical University, Turkey

Learning Agreement for Traineeships within the **ERASMUS Program**

Predoi D

Institut de Chimie de la Matière Condensée de Bordeaux CNRS-UPR 9048 France

Elemental analysis, hydrogen storage

Predoi D

Universite Bordeaux, EA 4592 Géoresources&Environnement, ENSEGID, France

Collaboration project IFA CEA C2-06, TEM, environment tests

Predoi D

Marcoule Institute for Separative Chemistry, France

Predoi D

Institute of Life Sciences Research and Technologies: Laboratory of Chemistry and Biology of Metals (LCBM) Grenoble, France

Collaboration project IFA CEA C4-05- biological tests

Predoi D

Institut des Sciences de la Terre d'Orléans, France

Raman, ICP, magnetic measurements

Predoi D

Université du Havre, France

Ultrasound studies

Predoi D

Horiba Jobin Yvon S.A., France

Zeta potential, DLS, photoluminescence

Predoi D

University of Dayton, Research Institute, USA

Carbon nanotubes

Stoica T

Peter Grünberg Institute , Forschungszentrum Jülich, Germany

Studies of epitaxial films of GeSn on Ge substrates aiming to preparation of semiconductors based on IV group elements with direct energy gap for optoelectronic applications

Teodorescu CM

Elettra Trieste (Italia)

CoSMoS -Combined Spectroscopy and Microscopy operating at SuperESCA

Teodorescu CM

IRAMIS CEA Saclay (France)

Chemical switching of ferroelectric surface topology (proiect RO-FR PN-II-ID-JRP-2011-2)

Funding

NIMP Funding

Core Programme	4.476.083 Euro
Ideas	698.965 Euro
Partnerships	582.120 Euro
International Projects	587.347 Euro
Human Ressources	288.628 Euro
Complex Ideas	314.960 Euro
ROSA	188.308 Euro
Euratom	61.867 Euro
Economic Contracts	47.741 Euro
POS-CCE	7.066.871 Euro
TOTAL	14.368.165 Euro

